Philipps Universität Marburg

Structural and Mechanistic Analysis of (p)ppGpp Synthetases

DOCTORAL THESIS

Submitted in Fulfillment of the Requirements

of a Doctoral Degree in Chemistry

(Dr. rer nat.)

to the Department of Chemistry,

Philipps-Universität Marburg

by Manfred Wieland Steinchen, Diploma (Pharmacy),

born in Zwickau.

Marburg an der Lahn, February 2017

Vom Fachbereich Chemie

der Philipps-Universität Marburg (Hochschulkennziffer 1180)

als Dissertation am _____angenommen.

Erstgutachter: Dr. Gert Bange

(Fachbereich Chemie der Philipps-Universität Marburg)

Zweitgutachter: Prof. Dr. Mohamed A. Marahiel

(Fachbereich Chemie der Philipps-Universität Marburg)

Tag der Einreichung: 09. Februar 2017

Tag der Disputation: 07. März 2017

Statutory Declaration

I hereby declare that this work is entirely of my own except where due to acknowledgement explicitly stated and to the best of my knowledge has not been submitted, either in part of as a whole, to this or any other educational institution in fulfilment of an academic degree. I declare that no other sources or references except those stated were used in this work.

Manfred Wieland Steinchen Marburg, 6th February 2017

Eidesstattliche Erklärung

Ich erkläre, dass eine Promotion noch an keiner anderen Hochschule als der Philipps-Universität Marburg, Fachbereich Chemie, versucht wurde.

Ich versiche, dass ich die hier vorgelegte Dissertation selbst und ohne fremde Hilfe verfasst, keine anderen als die angegebenen Quellen oder Hilfsmittel benutzt, alle vollständig oder sinngemäß übernommenen Zitate als solche gekennzeichnet sowie die Dissertation in der vorliegenden oder einer ähnlichen Form noch bei keiner anderen in- oder ausländischen Hochschule im Rahmen eines Promotionsgesuches oder zu anderen Prüfungszwekchen eingereicht habe.

Manfred Wieland Steinchen Marburg, 6th February 2017

Acknowledgements

First and foremost, I would like to express my deepest gratitude to Dr. Gert Bange for providing me the opportunity to conduct my doctoral studies in his laboratory. Through many inspiring discussion, he gave me many insights into science and beyond.

I would like to thank Prof. Mohamed A. Marahiel for the opportunity to perform this work under his and Gert Banges shared guidance and for many fruitful discussion on various parts of this work.

I would like to express my gratitude to Dr. Uwe Linne who introduced me to manifold analytical aspects of HPLC and HDXMS and many nice conversations.

Moreover, I am grateful to all former and present members of the Bange laboratory. Mainly, I would like to thank Florian Altegoer, Jan Schuhmacher, Carina Knauer, Magdalena Rakwalska-Bange and Patrick Pausch for the collaborative atmosphere over the last three years and many happy hours in the lab and outside.

I am thankful to Florian Altegoer and Jan Schuhmacher for their contributions during the studies of SAS1. Moreover, I am indebted to Florian for determination of crystal structures in the course of the preparation of various manuscripts.

I appreciate the great work done by Marian Vogt during his Master thesis on SAS2 and Laura Werel for her contribution during HDX experiments on Rel.

I would like to thank all members of the group of Prof. Peter Graumann, mainly Patricia Bedrunka, Stephan Altenburger and Felix Dempwolff for many nice conversations and their support during *in vivo* studies.

I also would like to thank Elizaveta Krol for her help at the initial determination of SAS1 activity.

My deepest gratitude belongs to my parents who always supported me.

Abstract

The ability of microorganisms to survive under a large variety and rapidly changing environmental conditions is one of their most outstanding features and allowed them to establish within all niches of our planet. To do so, microorganisms have developed a mechanism called the stringent response (SR). The SR relies on the presence of the nucleotide second-messengers (p)ppGpp that contribute to reallocation of resources during stressful environmental conditions. Understanding the broad variety of adaptation processes mediated by the SR therefore necessitates to decipher the metabolism of (p)ppGpp.

The stringent factor RelA was long thought to solely account for synthesis and degradation of (p)ppGpp. However, two additional (p)ppGpp synthesizing enzymes, SAS1 and SAS2, were discovered recently. This work presents an in-depth structural and mechanistic characterization of SAS1 and SAS2. Both proteins are subject to allosteric regulation allowing them to integrate different environmental stress stimuli into the framework of the SR. However, SAS1 and SAS2 also mediate adaptation of the microorganism in the absence of environmental stress stimuli, e.g. lack of nutrients. By this, they provide promising targets for the development of future antibiotics guided by the elucidation of their structure and mechanism present in this work.

Analysis of (p)ppGpp effecting various cellular targets reveals that the SR confers adaptation processes in a wide intracellular concentration range. This sheds new light on the SR as a mechanism of gradual response to subtle changes in the environment rather than following an ‘all or nothing’ paradigm.

Zusammenfassung

Eines der herausragenden Merkmale von Mikroorganismen ist ihre Fähigkeit, unter einer Vielzahl und sich schnell ändernden Umweltbedingungen zu überleben. Diese Eigenschaft erlaubt es ihnen eine Vielzahl von verschiedensten Habitaten unseres Planeten zu besiedeln. Die Toleranz von Mikroorganismen gegen sich schnell ändernde Umweltbedingungen wird dabei durch einen adaptiven Mechanismus, die sogenannte *stringent response*, gewährt. Während der *stringent response*, mediiert durch Interaktionen des second-messengers (p)ppGpp mit diversen Zielproteinen, werden die zellulären Resourcen umverteilt und verleihen dem Mikroorganismus eine erhöhte Stresstoleranz. Ein umfassendes Verständnis dieser Adaptationsprozesse setzt eine genaue Einsicht in den Stoffwechsel von (p)ppGpp vorraus.

Lange Zeit wurde der ‘stringent factor’ RelA als einziges Enzym fähig zur Synthese und Degradation von (p)ppGpp wahrgenommen. Jedoch wurden kürzlich zwei zusätzliche Enzyme, SAS1 und SAS2, entdeckt, die effektiv (p)ppGpp produzieren. Diese Arbeit beinhaltet eine tiefgründige Analyse der Struktur und Funktion von SAS1 und SAS2. Beide Proteine sind das Ziel von allosterischer Regulation, was die Implementierung verschiedener Stressstimuli in das Netzwerk der *stringent response* erlaubt. Dennoch sind SAS1 und SAS2 bereits in Abwesenheit eines umweltbedingten Stressors, z.B. Nährstoffmangel, essentiell zur Anpassung des zelllulären Stoffwechsels und stellen daher vielversprechende Zielstrukturen zukünftiger Antibiotikatherapien dar.

Die genaue Analyse des Effektes von (p)ppGpp auf seine zellulären Zielproteine zeigt auf, dass die *stringent response* nicht nach dem Alles-oder-Nichts-Prinzip verläuft, sondern vielmehr eine fein abgestimmte, graduelle Stressantwort darstellt. Dies wirft ein neues Licht auf die *stringent response* als adaptiven Mechanismus in Mikroorganismen.

Publications

Parts of the work presented here are published or are in the process of publishing:

Steinchen W & Bange G (2016) The magic dance of the alarmones (p)ppGpp. *Molecular microbiology* 101(4):531-544

Steinchen W, Schuhmacher JS, Altegoer F, Fage CD, Srinivasan, V, Linne U, Marahiel MA & Bange *G* (2015). Catalytic mechanism and allosteric regulation of an oligomeric (p)ppGpp synthetase by an alarmone. *Proceedings of the National Academy of Sciences of the United States of America* 112(43):13348-13353. Equally contributing authors.

Schuhmacher JS, Rossmann F, Dempwolff F, Knauer C, Altegoer F, **Steinchen W**, Dörrich A, Klingl A, Stephan M, Linne U, Thormann KM & Bange *G* (2015). The MinD-like ATPase FlhG effects location and number of bacterial flagella during C-ring assembly. *Proceedings of the National Academy of Sciences of the United States of America* 112(43):13348-13353.

Steinchen W, Vogt M, Altegoer F, Marahiel MA & Bange G. The (p)ppGpp synthetase SAS2 senses intracellular zinc levels. *In preparation*.

Steinchen W, Altegoer F, Marahiel MA & Bange G. Mechanism of allosteric regulation of the (p)ppGpp synthetase SAS1. *In preparation*.

Schäper S, **Steinchen W**, Krol E, Altegoer F, Skotnicka D, Søgaard-Andersen L, Bange G & Becker A. The AraC-like transcriptional activator CuxR binds c-di-GMP by a PilZ-like mechanism to regulate extracellular polysaccharide production. *Submitted.* Equally contributing authors.

Gessner C, **Steinchen W**, Bénard S, Skinner J, Woods VL, Walsh TJ, Bange G & Pantazatos P. Computational method allowing Hydrogen Deuterium Exchange Mass Spectrometry at single amide Resolution. *Under Revision.*

Abdelshahid M, Beckert B, Schäfer H, **Steinchen W**, Arenz S, Berninghausen O, Beckmann R, Bange G, Turgay K, Wilson DN. Structure of the *Bacillus subtilis* hibernating 100S ribosome reveals the basis for 70S dimerization. *Under Revision.*

Table of Contents

List of Figures

Abbreviations

Standardized abbreviations for chemical symbols, SI units and one- or three-letter codes for amino acids are used without further reference. Abbreviations for bacterial species are given in the text. All other abbreviations employed in this work are listed:

Å	Ångström (10^{-10} m)
ADP	Adenosine diphosphate
AMP	Adenosine monophosphate
AMPCPP	α,β-methyleneadenosine 5'-triphosphate
APS	Ammonium persulfate
ATP	Adenosine triphosphate
AU	Absorption unit
AX	Anion-exchange
bp	Base pairs
CHES	*N*-Cyclohexyl-2-aminoethanesulfonic acid
Cryo-EM	Cryo-electron microscopy
CV	Column volume
Da	Dalton (1.660538 x 10^{-27} kg)
DNA	Desoxyribonucleic acid
dNTP	Desoxynucleoside triphosphate
EDTA	Ethylenediaminetetraacetic acid
ESI	eEectrospray ionization
ESRF	European Synchrotron Radiation Facility
GDP	Guanosine diphosphate
GMP	Guanosine monophosphate
GMPPCP	Guanosine-5'-[(β,γ)-methyleno]triphosphate
GMPPNP	Guanosine-5'-[(β,γ)-imido]triphosphate
GPX	Guanosine 5'-diphosphate 2':3'-cyclic monophosphate
GTP	Guanosine triphosphate
h	Hours
HDX	$^{1}H/^{2}H$ exchange
HDXMS	$^{1}H/^{2}H$ exchange mass spectrometry

HEPES	4-(2-hydroxyethyl)-1-piperazineethanesulfonic acid
HPLC	High-performance liquid chromatography
HPRT	Hypoxanthine-guanine-phosphoribosyltransferase
IMP	Inosine monophosphate
LB	Lysogeny broth
M	mol/litre
min	Minute
MOPS	3-(N-morpholino)propanesulfonic acid
MR	Molecular replacement
MS	Mass spectrometry
MW	Molecular weight
NTA	Nitrilotriacetic acid
NTP	Nucleoside triphosphate
OD	Optical density
pGpp	Guanosine-3'-diphosphate-5'-monophosphate
ppGpp	Guanosine-3',5'-bisdiphosphate
pppGpp	Guanosine-3'-diphosphate-5'-triphosphate
PCR	Polymerase chain reaction
PDB	Protein data bank
PEG	Polyethylene glycol
PGE	Triethylene glycol
PMSF	Phenylmethylsulfonyl fluoride
rRNA	Ribosomal RNA
RNA	Ribonucleic acid
RSH	RelA/SpoT-homolog
s	seconds
SAS	Small alarmone synthetase
SDS	Sodium dodecyl sulfate
SDS-PAGE	Sodium dodecyl sulfate polyacrylamide gel electrophoresis
SEC	Size exclusion chromatography
SR	Stringent response
TBE	Tris/Borate/EDTA
TEMED	Tetramethylethylenediamine

TRIS	Tris(hydroxymethyl)aminomethane
TPAB	Tetrapentylammonium bromide
tRNA	Transfer RNA
XMP	Xanthosine monophosphate

Introduction

1.1 Bacterial stringent response

The ability of microorganisms to survive under a large variety of environmental conditions is one of their most outstanding features and allowed them to establish within all niches of our planet. These long-term adaptations to temperature, pH, salt conditions, availability of oxygen and different sources of carbon and nitrogen or resistance to all kinds of noxa have been subject to steady evolution. However, adapting to rapidly changing conditions requires concise sensory and regulatory circuits allowing microorganisms to cope with short-term unfavorable conditions.

To do so, microorganisms have developed a mechanism called the stringent response (SR). The SR is a broadly conserved process among all bacterial species (1-3) and is also present in plant chloroplasts (4-7). Historically, the SR was identified as an adaptational mechanism of *Escherichia coli* in response to amino acid starvation (8, 9). However, in recent years the definition of the SR was broadened to many different stresses and environmental conditions.

Upon exposure to nutrient deprivation, pH shifts or heat shock, the intracellular concentrations of the two second messengers ppGpp and pppGpp (collectively: (p)ppGpp or the ‘alarmones’) rapidly increases. Both alarmones adapt the microorganism to the stress condition by affecting DNA replication (10, 11), globally reprogramming transcription and translation (12, 13), interfering with the biogenesis of ribosomal subunits (14), amino acid-/nucleotide metabolism (15-18) and altering a variety of other cellular processes (3, 19-22). As a general theme of (p)ppGpp’s action, energy consuming processes are downregulated to a minimum and only very few processes upregulated depending on the stress condition. For example, the production of chaperones is elevated during heat stress (23, 24) and amino acid uptake and synthesis increased during amino acid starvation (13, 25-28). The decrease in metabolism and growth rate, together with a rewiring of resources subsequently increases the stress resistance of the organism. Recent studies

provide evidence that (p)ppGpp also affects non-stringent response related processes (i.e. not induced by a concise stress) such as virulence (29-31), biolfim and persister cell formation (32-37) and development of cell heterogeneity (38, 39). This highlights the importance of the SR for shape and alterations in the lifestyle of microorganisms in general.

Understanding the broad variety of adaptation processes mediated by the SR and their role in ensuring the survival of the microorganism under stress can only be achieved by decoding the following aspects: *i.)* Biochemical properties of all enzymes involved in (p)ppGpp metabolism *ii.)* Regulation of these enzymes on the genetic and/or protein level *iii.)* Effects of (p)ppGpp on its cellular targets.

1.2 Overview of the (p)ppGpp metabolism

The SR relies on the presence of the nucleotide second-messengers (p)ppGpp (**Fig. 1A**) that contribute to reallocation of resources during stressful environmental conditions. In order to almost instantly adapt the microorganism to stress, alarmones must be produced rapidly, but all the same should be degraded at high rate afterwards. In this respect, microorganisms with the most effective alarmone metabolism should possess an advantage over those that do not - simply because they would survive harsher or prolonged stressful conditions better and outgrow their 'poorly' responding competitors. Nevertheless, synthesis and degradation of (p)ppGpp also have to be properly balanced in the absence of a stress stimulus.

Three different types of enzymes are involved in (p)ppGpp metabolism: (p)ppGpp synthetases, (p)ppGpp hydrolases and proteins capable of converting pppGpp to ppGpp (**Fig. 1B**). Enzymes of the RelA/SpoT homology (RSH)-type carry out the synthesis of alarmones by catalyzing the transfer of pyrophosphate originating from ATP (i.e. the β- and γ-phosphates) onto the 3'-OH group of GDP or GTP yielding ppGpp or pppGpp, respectively (**Fig. 1B, step I**). For a long time, these two compounds were regarded as the only alarmones mediating the SR through interaction with various cellular targets (chapter 1.3 and **Fig. 1B**). However, a recent study indicates that also GMP can be utilized as substrate for alarmone synthesis by the small RSH-type synthetase RelQ from *Enterococcus faecalis* efficiently producing pGpp (**Fig. 1B, step II**) (40). In some bacteria (e.g. *Escherichia coli*), enzymes exist

that convert pppGpp into ppGpp through the removal of the 5'-OH γ-phosphate of pppGpp (**Fig. 1A** and **Fig. 1B, step III**) (41-43). It is unclear so far, whether pGpp can also be produced from ppGpp by a similar reaction and whether pGpp-synthesis from ATP and GMP (see above) is the only source of this 'third' alarmone. All three alarmones are degraded by removal of the 3'-OH pyrophosphate by RSH-type hydrolases (**Fig. 1B, step IV**) releasing PPi and generating GMP, GDP or GTP. Degradation of (p)ppGpp also occurs through some members of the Nudix (nucleoside diphosphates linked to some moiety X) hydrolase family omnipresent in bacteria (44) and plants (45, 46). Nudix-type hydrolases do not share any structural similarities with RSH-type hydrolases and can degrade many other organic pyrophosphates besides (p)ppGpp (47). All enzymes involved in (p)ppGpp metabolism are subject to tight regulation on the genetic and/or protein level (see below).

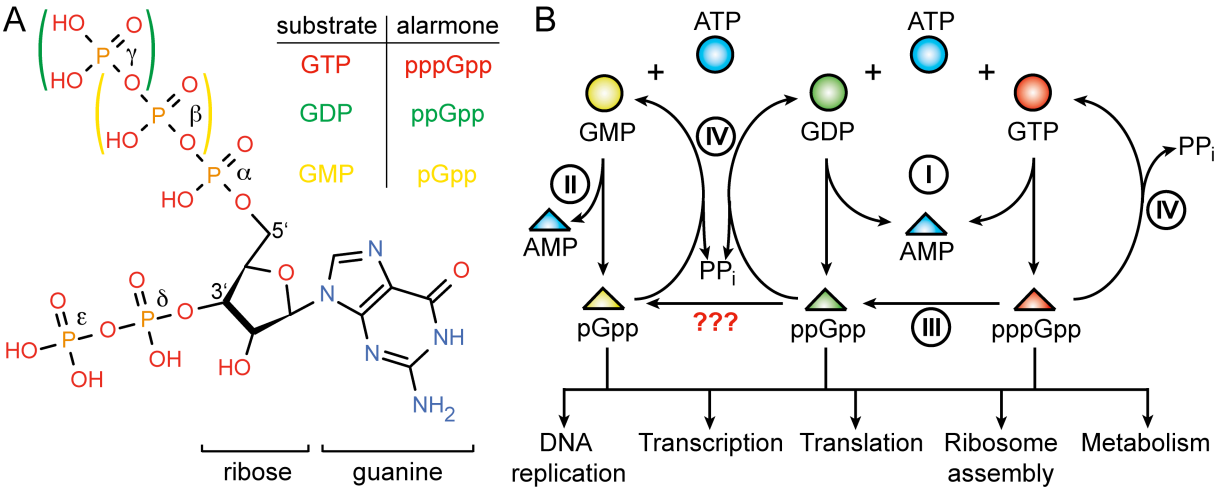

Figure 1. (p)ppGpp structure and metabolism. **A.** Chemical structure of alarmones. The three possible guanosine acceptor substrates and the resulting alarmones are indicated in the inset. 5'-phosphate moieties absent in ppGpp and pGpp are indicated by green and yellow brackets, respectively. **B.** The nucleotide substrates ATP, GMP, GDP and GTP are shown as blue, yellow, green and red spheres, respectively. The products of (p)ppGpp synthesis AMP, pGpp, ppGpp and pppGpp are shown as blue, yellow, green and red triangles corresponding to their substrates. PPi stands for pyrophosphate. Roman numbers are explained in the text. The figure originates from ref. (48).

1.2.1 (p)ppGpp synthesis

Alarmone synthetases of the RSH-type are conserved in bacteria, plants and algae (49, 50) and catalyze the transfer of pyrophosphate from ATP (i.e. the β- and γ-phosphates) onto the 3'-OH group of GMP, GDP or GTP yielding pGpp, ppGpp or pppGpp, respectively. The precise catalytic mechanism of (p)ppGpp synthesis by RSH proteins is far from being understood, however, essential catalytic residues could be identified (51-55). RSH-type enzymes share a highly conserved (p)ppGpp synthetase domain, but otherwise greatly differ in the length of their amino acid sequence and molecular weight. RSH enzymes can be classified as 'long' and 'short' RSH-type enzymes based on their size. Being discovered first, the long RSH-type (p)ppGpp synthetases were thought to solely account for alarmone synthesis. The recent discovery of short RSH-type (p)ppGpp synthetases (56, 57) enlarged the spectrum of this important class of enzymes.

1.2.1.1 Long RSH-type (p)ppGpp synthetases (Rel/RelA/plant RSH)

Long RSH-type synthetases are multi-domain proteins that can be divided into an N-terminal catalytic domain (NTD) and a C-terminal domain (CTD) (**Fig. 2A**). The NTD always harbors a (p)ppGpp hydrolase (HD) followed by a (p)ppGpp synthetase (Syn) domain and is present in all long RSH-type proteins. The CTD mediates binding of Rel/RelA to stalled ribosomes and is supposed to reciprocally couple the antagonistic (p)ppGpp degrading and synthesizing activities of long RSH enzymes (51-53, 58).

While the NTD is present in all long RSH-type proteins, major discrepancies exist in the composition of their CTDs (**Fig. 2A**). In bacterial RSH-type (p)ppGpp synthetases (Rel/RelA), the CTD is composed of a TGS domain (abbreviated for threonyl-tRNA-synthetase, GTPase and SpoT-like), an α-helical domain, a putative zinc-finger domain and the ACT domain (abbreviated for aspartate kinase, chorismate mutase and TyrA). Regulation of the activities of long RSH-type proteins through the CTD is urther described in chapter **1.2.3**.

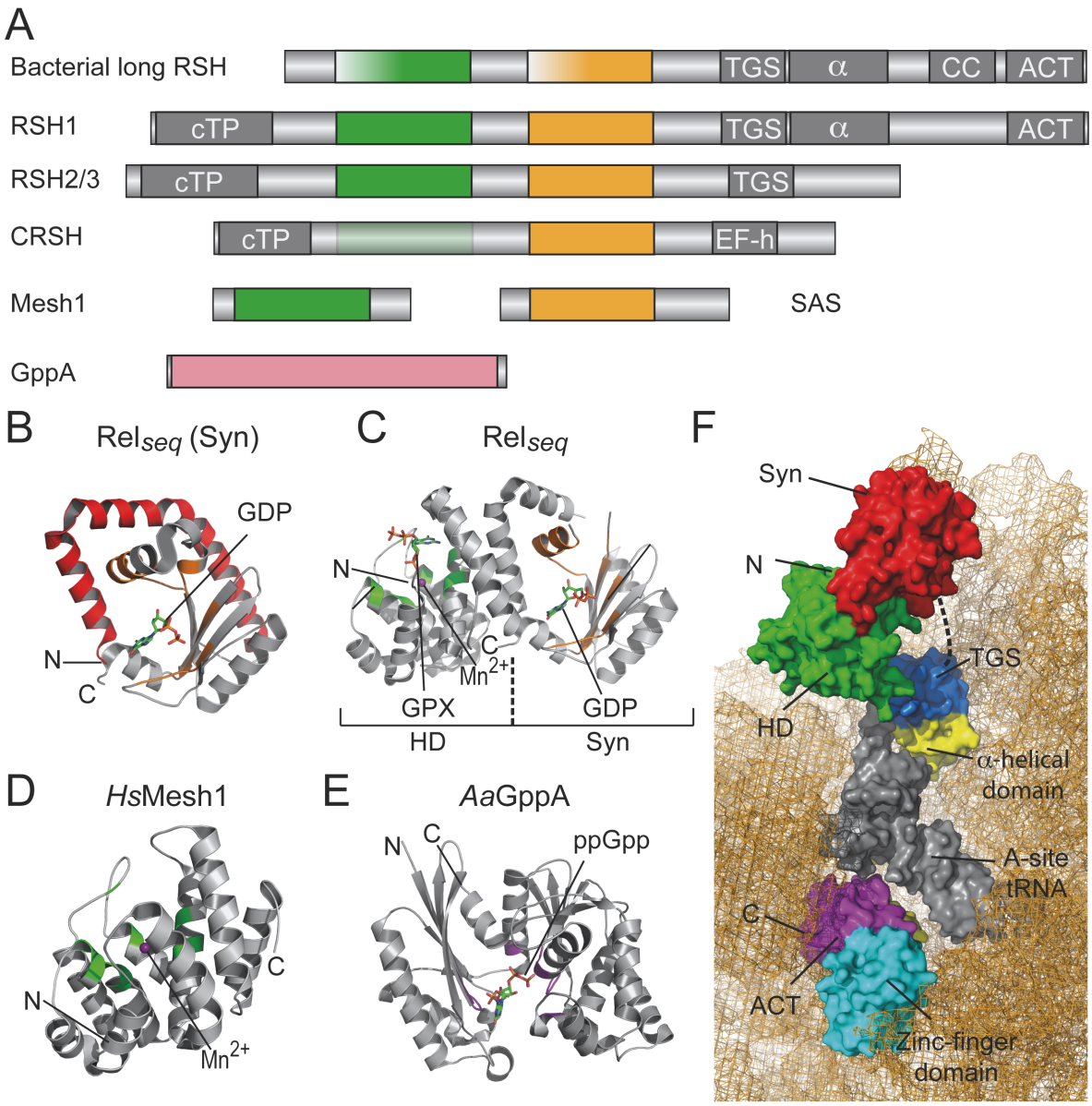

Figure 2. Enzymes involved in (p)ppGpp metabolism. **A.** Domain architecture of enzymes responsible for (p)ppGpp synthesis, degradation and interconversion. Details are given in the text. **B-E.** Crystal structures of enzymes involved in (p)ppGpp metabolism are shown in cartoon representation. Catalytic motifs are colored as in A. Details are given in the text. Ligands are shown as sticks and colored by element. Manganese is shown as violet sphere. N- and C-termini are indicated by 'N' and 'C', respectively. **B.** Syn domain of Rel$_{seq}$ bound to GDP (PDB: 1VJ7 chain A, (54)). The helices involved in reciprocal regulation of Rel's activities are colored in red. **C.** HD and Syn domains of Rel$_{seq}$ bound to GPX and GDP, respectively (PDB: 1VJ7 chain B, (54)). **D.** *Hs*Mesh1 (PDB: 3NRI, (60)). **E.** *Aa*GppA bound to ppGpp (PDB: 2J4R, (43)). **F.** *Ec*RelA bound to the ribosome (orange mesh) and A-site tRNA (grey) (PDB: 5IQR, (61)). Domains are shown in surface representation and further explained in the text. 'N' and 'C' indicate the N- and C-terminus of RelA, respectively. The figure was modified from ref. (48).

The only published crystal structure of an NTD of a long RSH-type (p)ppGpp synthetase comprises the HD and Syn domains of Rel from *Streptococcus equisimilis* ($Rel_{seq,}$ PDB: 1VJ7 (54)). The asymmetric unit of the structure contains two different monomers of the protein: Monomer 1 (chain A of 1VJ7) does only contain GDP bound within the Syn domain and represents the synthetically active state of Rel_{seq} (**Fig. 2B**). Monomer 2 (chain B of 1VJ7) contains the rather unusual nucleotide guanosine 5'-diphosphate 2':3'-cyclic monophosphate (GPX) residing in the HD domain and GDP within the Syn domain of Rel_{seq} and was therefore suggested by Hilgenfeld and coworkers to represent the hydrolytically active state (**Fig. 2C** and chapter **1.2.2.1**). The Syn domain of Rel_{seq} consists of five antiparallel β-strands surrounded by four α-helices (**Fig. 2B**). The GDP resides in a pocket with its guanine base stacking face-to-face against the phenolic ring of a tyrosine moiety (i.e. Y108) strictly conserved among bacterial long RSH (50, 55). The 3'-OH group of GDP points towards the center of the active site and does not establish any contacts to the protein. The presence of two negatively charged residues (i.e. D264 and E323) in close proximity might indicate the binding site of a magnesium cofactor often involved in catalysis in the superfamily of nucleotidyltransferases (59). Although the position of the ATP-substrate might be suggested by the presence of three conserved basic residues (i.e. R241, K243 and K251) potentially involved in coordination of the ATP-substrate, the given structure does not allow a reconstruction of the catalytic mechanism of (p)ppGpp synthesis (54).

Although all bacterial RSH proteins (Rel/RelA/SpoT) possess the above-mentioned conserved residues in their Syn domains, the synthetic activity of SpoT is much less pronounced than for Rel/RelA *in vitro* for so far unknown reasons (53). Nevertheless, SpoT seems to integrate various stress signals including fatty acid (62), iron (63) and carbon source (64) starvation into the framework of the stringent response. Moreover, SpoT seems to be subject to regulation. Interaction of SpoT with the the acyl carrier protein (ACP) during fatty acid starvation has been suggested to activate the (p)ppGpp synthetic activity of SpoT (65-67), while interaction of SpoT with the GTPase Obg under nutrient rich conditions is considered to repress (p)ppGpp synthesis (68). Noteworthy, Obg from *B. subtilis* is a target of inhibition by ppGpp (PDB: 1LNZ, (69)).

1.2.1.2 Short RSH-type synthetases/Small alarmone synthetases (SAS)

Short RSH-type (p)ppGpp synthetases only harbour the Syn domain and lack any obvious regulatory domains found among the long RSH-type proteins (**Fig. 2A**). Therefore, they are also referred to as small alarmone synthetases (SAS). They have been discovered just recently in strains that lacked a functional long RSH protein, but still produced (p)ppGpp (56, 57, 70). The presence of SAS enzymes seems to be restricted to the firmicutes phylum (22, 50). Orthologues of the small alarmone synthetases SAS1 (also: YjbM, RelQ) and SAS2 (also: YwaC, RelP) have been identified and studied in *Bacillus subtilis* (*Bs*) (57), *Staphylococcus aureus* (*Sa*) (71) and *Streptococcus mutans* (*Sm*) (56). *Bs*SAS1 and *Bs*SAS2 exhibit pronounced similarities with the Syn domain of Rel_{seq} (see above) on the amino acid level (57). Despite amino acid identities of 30 - 40% between SAS1 and SAS2 homologues, SAS proteins seem to exhibit different functional roles (71). Transcripts of *Bs*SAS1 peak during logarithmic growth in rich medium, while the transcript of *Bs*SAS2 is mainly observed at the transition from logarithmic to stationary phase (57, 72). These data suggest a close link between cell cycle and appearance of the SAS enzymes in *B. subtilis*, although a functional understanding remains mysterious. Moreover, transcription of SAS2 from *B. subtilis* and *S. aureus* was shown to be upregulated by the σ^M-regulon upon various stress conditions including ethanol, high salt, acidic or alkalic pH and cell wall antibiotics (57, 71, 73-75). Consistently, SAS2 has been reported to accumulate at the cytoplasmic membrane of *B. subtilis* after ethanol and acidic pH stress (76). The activity of SAS2 - but not SAS1 - seems to be tightly linked with increased ribosome hibernation in both *B. subtilis* and *S. aureus* (72).

Recent studies have reported the presence of the small RSH-type enzyme RelV in the γ-proteobacterium *Vibrio cholera* (77). RelV synthesizes (p)ppGpp in a ΔrelAΔspoT mutant background under glucose and fatty acid starvation conditions (77, 78). Mutational analysis of RelV suggests that most of the catalytic motifs required for (p)ppGpp synthesis are overally conserved to other well characterized RSH-type synthetases (77, 79). No further evidence has been provided so far hinting additional members of this RelV-like subtype of SAS proteins.

While it is believed that small alarmone synthetases are solely subjected to transcriptional control, little to nothing is known about their (p)ppGpp synthetic

properties or regulation on the protein level. SAS1 and SAS2 from *B. subtilis* and *S. aureus* were shown to synthesize ppGpp more efficiently than pppGpp *in vitro* (57, 71). This stands in contrast to the long RSH-type synthetase Rel from *Mycobacterium tuberculosis* mainly producing pppGpp (80, 81). Moreover, a stimulation of (p)ppGpp synthesis by SAS1 from *Enterococcus faecalis* in the presence of ppGpp by approximately 3-fold was observed similar to earlier reports on RelA from *E. coli* (40, 82). Taken together, these studies indicate that although being overally conserved, RSH-type enzymes can exhibit different catalytic properties towards the different alarmones and are subject to allosteric regulation. Nevertheless, a precise molecular understanding of these differing properties is lacking to date.

1.2.2 (p)ppGpp degradation

The alarmones (p)ppGpp are degraded by removal of the pyrophosphate from the 3'-OH group of the ribose moiety (**Fig. 1A**). This reaction is executed by (p)ppGpp hydrolases which regenerate the respective guanosine nucleotides by a yet poorly understood catalytic mechanism (**Fig. 1B, step IV**). The (p)ppGpp hydrolases are characterized by a hydrolase domain (HD) and rely on a manganese ion cofactor. The manganese cofactor has been suspected to arrange the 3'-OH phosphate moieties of the (p)ppGpp in a way that allows hydrolysis (53, 54, 60). Structural knowledge on bacterial (p)ppGpp hydrolases is so far restricted to the NTD of the bifunctional (p)ppGpp synthetase/hydrolase Rel_{seq} (see above). In addition, two structures of the (p)ppGpp hydrolase Mesh1 are avalaible from the eukaryotes *Homo sapiens* and *Drosophila melanogaster* (PDBs: 3NR1 and 3NQW, (60)). However, why eukaryotes contain a (p)ppGpp hydrolase, while (p)ppGpp synthetases are not existing, is not known.

1.2.2.1 Long RSH-type (p)ppGpp hydrolases (Rel/SpoT/plant RSH)

The NTD of long RSH-type proteins harbors the hydrolase domain (HD) at its N-terminus (**Fig. 2A**). The HD domain consists of 10 α-helices and 2 β-strands creating an active site with a binding pocket for (p)ppGpp and a binding site for a manganese ion crucial for catalysis. The crystal structure of the NTD of Rel_{seq} (PDB: 1VJ7 chain B; (54)) contains the rather unusual nucleotide guanosine 5'-diphosphate 2':3'-cyclic

monophosphate (GPX) residing within the HD domain and GDP within the Syn domain (**Fig. 2C**). This state was suggested to represent the hydrolytically active state of long RSH-type enzymes (54). The guanine base of GPX is mainly coordinated by π-stacking interactions with the arginine 44 and the formation of a hydrogen bond between the main chain carbonyl of N148 and the N-2 of the guanine base. Both residues are strictly conserved among the HD domains found in long RSHs and variation of either residue ablates (p)ppGpp hydrolysis by Rel_{seq} (54). This suggests that the position of the GPX closely resembles the position of a prototypic alarmone substrate. The manganese ion cofactor that is not essential for but drastically increases (p)ppGpp hydrolysis (53, 60), is hexacoordinated in a distorted octahedral arrangement by two histidines and two aspartates (i.e. H53, H77 and D78, D144, respectively). These manganese-coordinating residues are highly conserved among the (p)ppGpp hydrolases (50, 54, 60). The 3'-OH pyrophosphate moiety of the substrates ppGpp and pppGpp are thought to be coordinated by the manganese ion cofactor. By this, the δ-phosphate at the 3'-OH group of (p)ppGpp (**Fig. 1A**) would come into close proximity to the carboxylate side chains of the highly conserved E81 and D82 residues either of them being involved in activating a water molecule for nucleophilic attack on the δ-phosphate (54).

The bacterial RSH proteins SpoT and the bifunctional Rel comprise all conserved residues for (p)ppGpp degradation (see above). Although the HD domain is present in RelA, all catalytic residues are replaced rendering it incapable of (p)ppGpp hydrolysis (50, 83). In plants, the RSH-type enzymes 1 to 3 contain all conserved residues, while CRSH does not. However, their (p)ppGpp degrading activity has never been tested (84).

The HD and Syn domains in long RSH-type enzymes are separated by approximately 30 Å and are connected by an mainly α-helical linker region including α-helices α8 - α11 in Rel_{seq} (54). Structural rearrangements of this linker region upon substrate binding into the HD or the Syn domain are thought to negatively affect the activity of the corresponding antagonistic catalytic site. This notion is supported by the observation that addition of the ATP-analog AMPCPP (i.e. α,β-methyleneadenosine 5'-triphosphate) that binds into the Syn domain renders Rel_{seq}

hydrolytically less active (54). Therefore, HD and Syn domains seem to be reciprocally regulated.

1.2.2.2 Short RSH-type hydrolase in metazoa (Mesh1)

While it is generally believed that (p)ppGpp is not present in eukaryotes with the exception of plants and green algae (85), functional orthologues of RSH-type (p)ppGpp hydrolases termed Mesh1 are reported for *H. sapiens* (**Fig. 2D**, PDB: 3NR1) and *D. melanogaster* (PDB: 3NQW) (60). Although the crystal structures of Mesh1 from both organisms are obtained without any ligand, the protein has an almost identical topology as the HD domain found in Rel_{seq} (see above) and degrades ppGpp at similar rates as its bacterial counterpart (60). Although the functional role of Mesh1 is unclear, deletion of the encoding gene leads to retarded body formation and impaired resistance to starvation of *D. melanogaster* (60). This obscures the functional role of Mesh1 as no concurrent evidence is provided so far for the existence of (p)ppGpp synthetases metazoan. Small alarmone hydrolases of the Mesh1-type also seem to be present in bacteria. However they are rather rare and distributed without clear phylogenetical clustering (50).

1.2.3 Regulation of the opposing activities of long RSH-type (p)ppGpp synthetases/hydrolases upon binding to stalled ribosomes

In the current model, amino acid starvation of a bacterial cell leads to an increase of uncharged tRNAs from 20% to 80% of the total tRNA pool (86) leading to entering of uncharged tRNAs into the aminoacyl-acceptor site (A-site) of ribosomes (87). Rel/RelA can then bind to the so-stalled ribosome and sense the unoccupied 3'-OH group of the terminal adenosine of the uncharged tRNA (58) upon which the (p)ppGpp synthetic activity of Rel and RelA is drastically stimulated (87-91). Extensive biochemical studies revealed that the CTD of RSH proteins is essential for the ribosome-dependent stimulation by regulating the activities of the HD and Syn domains residing within the NTD (53, 92, 93). Recent cryo-electron microscopy (cryo-EM) structures provide new insights into the conformation of RelA bound to the ribosome ((**Fig. 2F**), (61, 94-96)). RelA adopts an open conformation in which the CTD is intertwined around the A-site tRNA within the intersubunit cavity of the ribosome while the NTD is exposed to the solvent (61, 95, 96). The A-site tRNA is

locked in an A-/T-tRNA like conformation similar but distinct from that observed during decoding when EF-Tu delivers aminoacyl-tRNA to the ribosomal A-site (95, 97-99). The TGS domain of RelA interacts with the unoccupied 3'-OH group of the terminal adenosine of the uncharged tRNA in a way that aminoacyl-tRNA would sterically preclude RelA-binding consistent with earlier reports that only uncharged tRNA stimulated RelA's activity (58, 82, 91). The α-helical domain wraps around the acceptor arm of the A-site tRNA but also provides a bridge between the TGS domain and the zinc-finger/ACT domains of RelA (95). The both C-terminal domains of RelA establish multiple contacts with ribosomal proteins and rRNA (95, 96) while the ACT domain additionally contacts the elbow arm of the A-site tRNA. Although RelA binds close to the N-terminal part of ribosomal protein L11 consistent with earlier observations that L11 is necessary for stimulation of RelA's (p)ppGpp synthetic activity by the ribosome (82, 91, 100), no interaction interface between RelA and L11 is established (96). In contrast, multiple interactions between L11 and the A-site tRNA rather explain the strict dependence on L11 for stimulation of RelA (58, 82, 91). Unfortunately, the recent cryo-EM structures of RelA bound to the ribosome do not cover all aspects of RelA's actions. Cryo-EM structures of the ribosome typically possess good local resolution in the ribosomal centre while the outer parts or ribosome-bound proteins are only poorly resolved. This impedes an exact positioning of RelA-NTD in all three recent RelA-ribosome structures (see above), yet make a precise understanding of atomic rearrangements within the NTD impossible. Moreover, conformation and topology of the CTD in the absence of the ribosome is not known. Only two crystal structures present isolated fragments of the TGS and ACT domains (PDBs: 3HVZ and 3IBW). Some studies evidenced a possible oligomerization of Rel/RelA in the absence of the ribosome and suggested that this oligomerization could be mediated by the CTD (24, 52, 101).

Multiple models were derived for the subsequent actions of RelA after binding to stalled ribosomes. Initially, (p)ppGpp synthesis by RelA was proposed to dislodge the uncharged A-site tRNA from the ribosome, thereby efficiently rescuing the blockade (88). A more recent study does not confirm this dislocation of tRNA from the ribosome and instead proposes a 'hopping model' in which RelA gets detached from the ribosome upon (p)ppGpp synthesis and subsequently 'hops' between stalled ribosomes, thereby measuring the translational fidelity of the cell (91). One controversely discussed report employing single-molecule studies claims that after

binding of RelA to stalled ribosomes its (p)ppGpp synthetic activity is stimulated, however multiple rounds of (p)ppGpp synthesis shall occur off the ribosome (102, 103).

Long RSH-type proteins from plants differ from their bacterial counterparts in the composition of their CTDs. In higher plants such as *Arabidopsis thaliana* (*At*), four long RSH-type enzymes are present. *At*RSH1 harbors all domains that are present in RelA/SpoT homologs from bacteria. *At*RSH2 and *At*RSH3 lack domains within their CTDs and *At*CRSH possess an additional calcium-binding EF-hand motif (**Fig. 2A,** (50, 104)). These differences show that long-RSH enzymes were subject to intricate molecular evolution likely through the need adapt to specific environments. The long RSH-type enzymes found in *A. thaliana* are important for development and reproduction of chloroplasts/plastids and their transcription follows the diurnal rhythm ((105), reviewed in: (84)). Based on their ancestry from the bacterial kingdom, one should also expect RSH-type enzyme within the mitochondria. However, there is no evidence for their existence. Moreover, our structural and functional knowledge on this interesting class of enzymes is poor.

1.2.4 (p)ppGpp interconversion

The metabolism of inorganic polyphosphate (polyP) is intimately linked to the stringent response (106, 107). The exopolyphosphatase (PPX) GppA from *E. coli* was shown to possess pppGpp-hydrolytic activity in that it removes the 5'-OH γ-phosphate of pppGpp yielding ppGpp (**Fig. 1B, step III**, (41, 42)). This interconversion is of great relevance as ppGpp has a stronger effect on growth rate reduction, repression of rRNA transcription or induction of RpoS in *E. coli* than pppGpp (2, 108-112).

1.2.4.1 PPX/GppA phosphatases

While E. coli harbors two PPX proteins one of which is able to convert pppGpp to ppGpp (GppA) (42), the thermophilic organism *Aquifex aeolicus* harbors one bifunctional PPX/GppA protein (113). The crystal structure of PPX/GppA from *A. aeolicus* (PDB: 1T6, (43)) comprises two domains that arrange in a butterfly-like manner, a topology that closely resembles GppA from *E. coli* (43, 114, 115). The

alarmone ppGpp binds into an extended groove formed by the two domains of GppA (**Fig. 2E**, PDB: 2J4R, (43)). By this, pppGpp interconversion and polyP degradation share the same active site on the enzyme explaining the inhibitory effects of pppGpp and ppGpp, exemplified by their inhibitory constants of 10 and 200 µM respectively, on polyP degradation by *E. coli* GppA (106). Coordination of the guanine base of ppGpp is established by π-stacking with R266 and interaction of N19 of GppA with N7 of the base. The 3'- and 5'-OH pyrophosphate moieties are caged between arginines R22 and R266 as well as backbone amides from three conserved regions (amino acids 17-19, 143-147 and 210-211). Although the product of the interconversion reaction, ppGpp, is found in the structure, the position of the 5'-OH γ-phosphate of the substrate pppGpp might be inferred from the position of a sulfate ion in the crystal structure of *E. coli* GppA (PDB: 1U6Z, (114)). If true, the 5'-OH γ-phosphate of pppGpp would be located in close proximity to a strictly conserved glutamate residue (E119) that would either directly or via water molecules perform the hydrolytic reaction (43). GppA from *A. aeolicus* lacks additional domains found in *E. coli* GppA (i.e. domains III and IV). Domain III is structurally similar to metal-dependent phosphohydrolases yet lacks conserved catalytic motifs and activity (115, 116). However, it appears to be involved in dimerization of GppA (117-119) and polyP channeling (Rangarajan 2006). Domain IV has structural counterparts in cold-shock associated RNA-binding proteins, but is of unknown function in GppA (115).

1.3 Cellular targets of (p)ppGpp

Alarmones affect many cellular targets allowing (p)ppGpp to mediate a plethora of processes to adapt bacteria to given environmental conditions (reviewed in: (3, 21, 83, 120)). In general, binding of (p)ppGpp modulates the activity of its target mainly in inhibitory fashion (see below). In recent years, an increasing number of structures of (p)ppGpp-bound target proteins has deepened our understanding of (p)ppGpp's actions complementing the biochemical knowledge. Nevertheless, some adaptational processes are either mediated indirectly by (p)ppGpp or their underlying regulatory mechanisms are unknown so far.

1.3.1 DNA replication

Initiation of DNA replication is coordinated with cell growth (121, 122). During chromosome replication, short RNA primers are synthesized by a specialized DNA-dependent RNA polymerase (named primase or DnaG). These primers serve as indispensible starting points for DNA replication (123, 124). During the SR, DNA elongation is inhibited by binding of (p)ppGpp to the primase DnaG in *B. subtilis* and *E. coli* (**Fig. 3,** (10, 11, 125, 126)). In this case, (p)ppGpp binds into the active site of the RNA-polymerase domain of DnaG and prevents the entrance of NTP substrates needed for primer synthesis (127). Moreover, (p)ppGpp interferes with the binding of either an initiating 5' NTP or the 3' extensible end of an RNA-DNA heteroduplex (127). DnaG from *E. coli* (*Ec*DnaG) and *B. subtilis* (*Bs*DnaG) are efficiently inhibited by (p)ppGpp at concentrations of 200 - 500 µM *in vitro*. However, pppGpp seems to be the stronger inhibitor for *Bs*DnaG, while ppGpp is more potent in inhibition of *Ec*DnaG (10, 125).

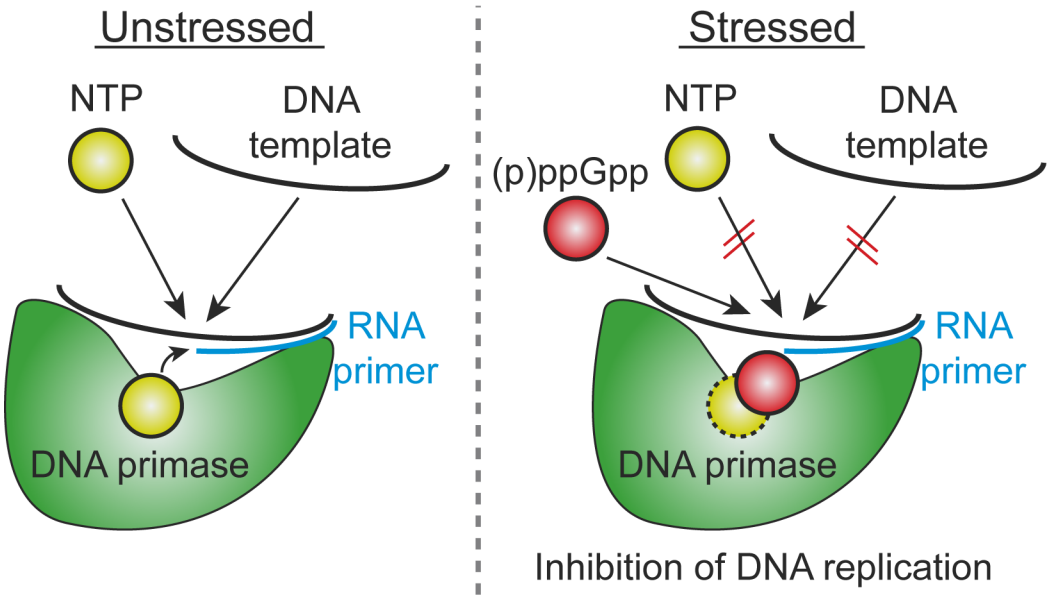

Figure 3. Scheme depicting the mechanism of DNA replication inhibition by (p)ppGpp. DNA primase (DnaG, green) synthesizes short RNA primers (blue) on a template DNA (black). Under stress, (p)ppGpp (red balls) bind within the active site of DNA primase close to the NTP (yellow balls) binding site of the protein thereby inhibiting DNA primase activity.

1.3.2 Transcription

A drop of stable RNA-synthesis in amino acid starved *E. coli* cells was one of the first observations made for the SR (8, 9). Later on, it was recognized that accumulation of (p)ppGpp leads to a drastically altered transcription profile owing to changes in the activity of RNA polymerase (RNAP). While transcription from promotors for ribosomal RNAs (rRNAs) and ribosomal proteins (r-proteins) is decreased, increased transcription from promotors for amino acid synthesis occurs (13, 128, 129). In the crystal structure of RNAP from *Thermus thermophilus* in complex with ppGpp (PDB: 1SMY, (130)), the alarmone is bound close to the active site of the protein and interferes with NTP coordination (130, 131). For the RNAP from *E. coli* however, biochemical data indicated that the binding site for alarmones should be located close to the ω-subunit of RNAP (132), which was recently verified by crystal structures of *E.coli* RNAP-(p)ppGpp complexes (PDBs: 4JKR, 4JK1 and 4JK2 (112, 133)). (p)ppGpp is bound in a small positively charged pocket between the β'- and ω-subunits of RNAP and ~ 25 Å away from the active site. This binding site would allow (p)ppGpp to indirectly control RNAP activity as it would restrain the ratcheting movement between the core and shelf subunits of RNAP (i.e. β' and ω, respectively) essential for RNAP activity (133, 134). Phylogenetic analysis reveals that the N-terminus of RNAP's ω-subunit shows species-specific differences in that a conserved motif facilitating (p)ppGpp-binding to *E. coli* RNAP is present in α-, β- and γ-proteobacteria, but lacking in *T. thermophilus* and the firmicutes phylum (83). Moreover, the activity of *E. coli* RNAP was shown to be efficiently regulated by a concerted action of the protein DksA, a transcription factor that modulates RNAP by binding into the secondary channel, and (p)ppGpp binding to a second site at the RNAP-DksA interface (27, 28, 135-139). However, also DksA seems to be restricted to α-, β- and γ-proteobacteria (137, 140). Taken together, it appears that regulation of transcription during the SR is implemented via different mechanisms. In *E. coli*, rRNA synthesis is downregulated by (p)ppGpp-dependent inhibition of RNAP, while in *B. subtilis* (p)ppGpp-dependent changes in the NTP pools (see below) might indirectly alter transcription by RNAP depending on the promotor (141, 142). The different control of transcription found in *E. coli* and *B. subtilis* is shown in **Fig. 4**.

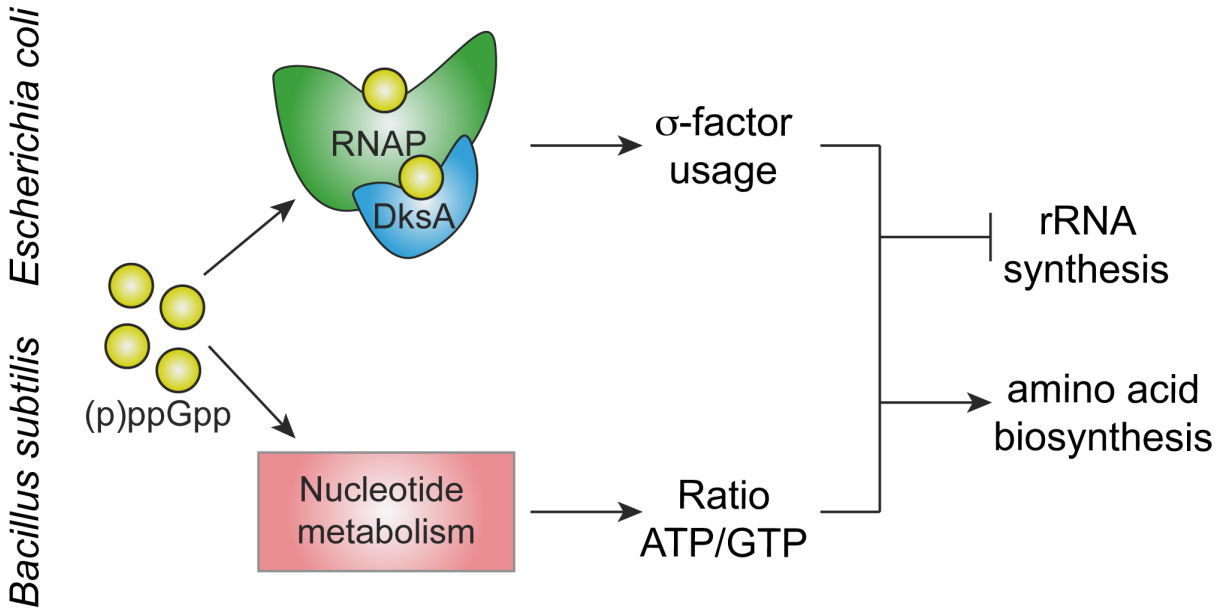

Figure 4. Scheme depicting the mechanism of transcription inhibition by (p)ppGpp. Under stress, increased alarmone levels (yellow balls) lead to a decrease in rRNA synthesis and increased amino acid uptake and biosynthesis. In E. coli, inhibition of RNAP-DksA (green and blue, respectively) alters the affinity of RNAP to promotors located on the DNA augmented by an altered σ-factor usage. In. B. subtilis, inhibition of enzymes involved in nucleotide metabolism (red) alters the ratio of intracellular ATP/GTP indirectly altering transcription.

1.3.3 GTPases involved in translation or ribosomal biogenesis

The alarmones (p)ppGpp are highly similar to GDP/GTP in that they only differ in the presence of a pyrophosphate moiety at the 3'-OH group of the ribose (**Fig. 1A**). Alarmones affect a high number of GTPases involved in the assembly of the ribosomal subunits or the initiation, elongation and termination of translation (reviewed in: (120)). The mechanism by which (p)ppGpp binds to these targets appears to be highly similar: The guanosine moiety of (p)ppGpp binds in the same way to the GTPase as GTP while the 3'-OH pyrophosphate moiety protrudes from the active site without establishing further contacts to the protein (**Fig. 5**, *left*). However, the pyrophosphate moiety can provoke steric clashes that inactivate the cellular function of the GTPase in the assembly of the ribosome/ribosomal subunits (**Fig. 5**, *middle*). Nevertheless, translation is also directly inhibited by interference of (p)ppGpp with GTPases involved in initiation (IF2), elongation (EF-Tu and EF-G) and termination (RF3) at the mature ribosome (**Fig. 5**, *right*).

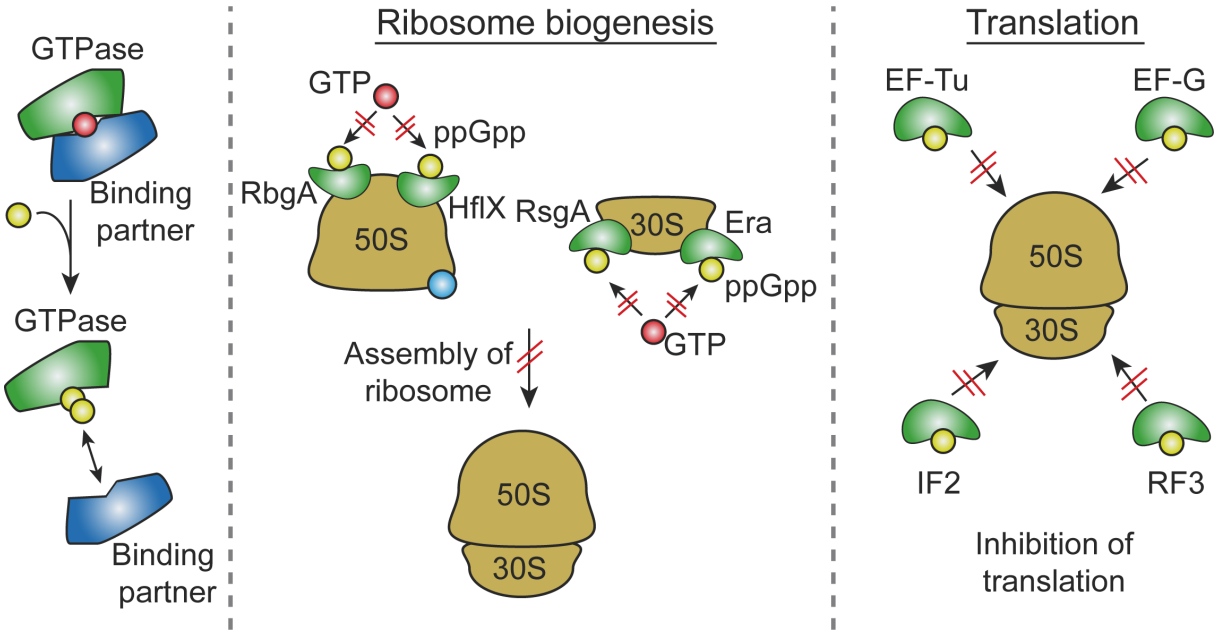

Figure 5. Scheme depicting the mechanism of translation inhibition by (p)ppGpp. Alarmones inhibit translational GTPases by a common mode: The 3' OH moiety of (p)ppGpp prevents binding of the binding partner of the GTPase by steric preclusion (*left*). Ribosomal biogenesis is inhibited by interaction of (p)ppGpp with GTPases involved in assembly of the 50S and 30S ribosomal subunits (*middle*). Translation at mature ribosomes is inhibited by interference of (p)ppGpp with GTPases involved in initiation (IF2), elongation (EF-Tu and EF-G) and termination (RF3) of translation (*right*).

1.3.4 Nucleotide metabolism

The three enzymes GuaB, HPRT and GMK, which are involved in the synthesis of GTP, are subject to regulation by (p)ppGpp (**Fig. 6,** (3, 143)). IMP dehydrogenase (IMPDH or also GuaB) catalyzes the formation of XMP (xanthosine monophosphate) from IMP (inosine monophosphate), the product of *de novo* purine biosynthesis. XMP can be further utilized for the production of AMP by adenolylsuccinate-synthetase and adenolylsuccinate-lyase or production of GMP through GuaA. GMP is also yielded by transfer of a phosphoribosyl-group onto guanine catalyzed by the hypoxanthine-guanine-phosphoribosyltransferase (HPRT). GMP is phosphorylated by guanylate kinase (GMK) yielding GDP, which can be further phosphorylated to GTP by nucleoside-diphosphate kinases. HPRT and GMK from *B. subtilis* are efficiently inhibited by (p)ppGpp with K_i-values of 11 µM (16) and 10-20 µM (18), respectively (**Fig. 6**). However, GuaB retains 50% of its activity even in the presence of 300-500 µM (p)ppGpp. In *E. coli*, GuaB and HPRT are inhibited with K_i-values of

30-48 µM (143, 144) and 85 µM (145) while conversely GMK is no subject to inhibition by (p)ppGpp (18). Moreover, the adenine phosphoribosyltransferase APRT from *E. coli* is inhibited by (p)ppGpp (143-147), which has not been shown for *B. subtilis* so far. These observations imply that (p)ppGpp does not only affect the total nucleotide pool within the microorganism but also effectuates a shift in the balance between nucleotides, most importantly adenosine and guanosine nucleotides (16). Proper balancing of nucleotide levels through (p)ppGpp is essential for survival of *B. subtilis* exemplified by the observation that strains of *B. subtilis* incapable of (p)ppGpp-synthesis are characterized by elevated GTP levels (16) accompanied with reduced survival rates upon sudden amino acid downshift (17).

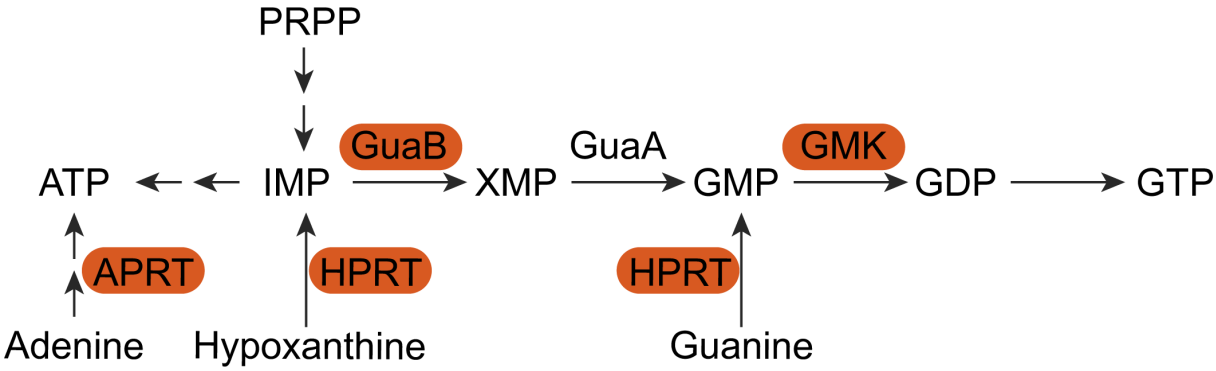

Figure 6. Scheme depicting the interference of (p)ppGpp with nucleotide metabolism. Enzymes inhibited by (p)ppGpp are indicated in orange. The abbreviations are explained in the text.

1.3.5 Other targets

Alarmones inhibit amino acid decarboxylases faciliting adaptation to changing intracellular pH values (148, 149). The biological role of the interaction of (p)ppGpp with the eukaryotic N-acetyl transferase NatA (PDB: 4HNX, unpublished) is unclear so far. The Inhibition of the c-di-AMP degrading phosphodiesterase YybT (150) provides evidence for cross-talk between the regulatory circuits of these two nucleotide second messengers yet again an in-depth biological understanding is lacking.

Aim of the work

This work aims at the biochemical, structural and functional understanding of enzymes involved in the synthesis of (p)ppGpp during the SR in *B. subtilis* and *S. aureus*. A particular focus should be on the recently identified small alarmone synthetases SAS1 and SAS2. Comparison of their structure, mechanism and function with the well-known bifunctional protein Rel should uncover differences and similarities between both prototypic subclasses of RSH-type (p)ppGpp synthetases. These results shall be put in a biological context by investigating the role of SAS proteins and (p)ppGpp on the lifestyle of *Bacillus subtilis.*

Results

3.1 Structural analysis of SAS1

3.1.1 SAS1 forms homotetramers

SAS1 from *B. subtilis* carrying an N-terminal hexa-histidine tag was heterologously produced in *E. coli* BL21 (DE3) using auto-induction medium. Subsequently, SAS1 was purified by a two-step protocol employing Ni-NTA affinity chromatography and size-exclusion chromatography (SEC) as detailed in chapter **5.2.2**. On SEC, SAS1 had an apparent molecular mass of approximately 100 kDa (**Fig. 7A**). Given the molecular mass of ~ 25 kDa of a SAS1 monomer, this suggests a homotetrameric assembly of SAS1.

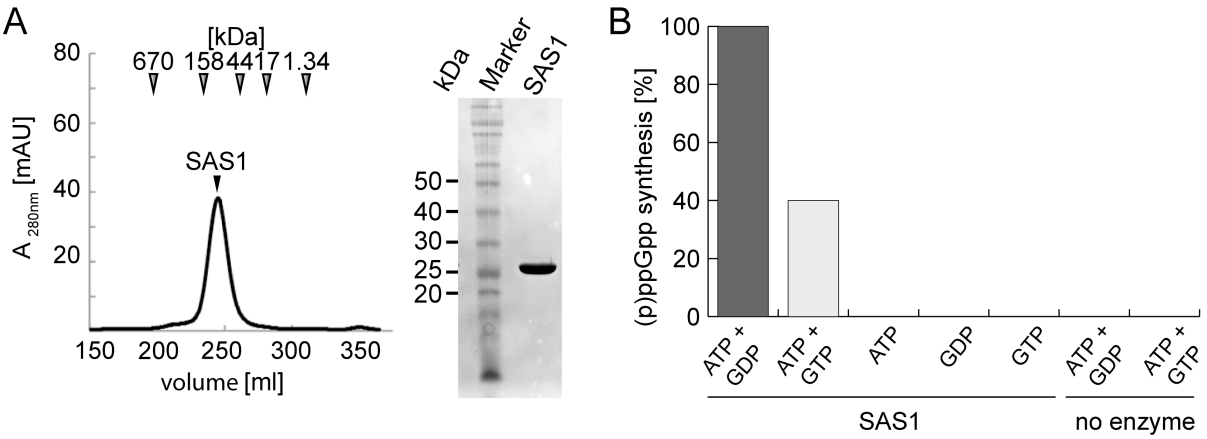

Figure 7. SAS1 forms homotetramers that possess (p)ppGpp synthetic activity. **A.** Left: Size-exclusion chromatography profile of SAS1. Arrows indicate the molecular mass of the size standard. Right: Coomassie-stained SDS-PAGE of the peak fraction containing SAS1. **B.** (p)ppGpp synthetic activity of SAS1 in presence of different nucleotides. (p)ppGpp synthesis in presence of ATP and GDP was set to 100%. Dark and light grey bars show ppGpp and pppGpp, respectively. Figure 7A originates from ref. (151).

3.1.2 SAS1 is an active (p)ppGpp synthetase

The activity of SAS1 was probed by measuring its (p)ppGpp synthetic activity in the presence of different nucleotides. In brief, 2 µM SAS1 were incubated with 1 mM of different nucleotides for five minutes at 37 °C and subjected to anion-exchange chromatography as described by Traxler *et al.* (152) with help from Elizaveta Krol (AG Becker). SAS1 produces ppGpp and pppGpp when incubated with the corresponding substrates ATP and GDP or ATP and GTP, respectively (**Fig. 7B**). However, SAS1 seems less efficient in synthesizing pppGpp than ppGpp. No production of (p)ppGpp is observed in the absence of SAS1. Incubation of SAS1 with ATP, GDP or GTP leads to no observable amount of (p)ppGpp. This indicates that the purified SAS1 protein is an active (p)ppGpp synthetase but also suggests that the protein does not retain any nucleotide during the protein purification. This notion is supported by the ratio of A_{280nm}/A_{260nm} of ~1.6 for all preparations of SAS1 typical for protein preparations that are devoid of nucleotide or nucleic acid contaminations.

3.1.3 Crystal structure of SAS1 in the apo-state

Bioinformatic analysis of the domain architectures of Rel_{seq}-NTD and SAS1 using the Basic Local Alignment Search Tool (BLAST) indicates that both proteins contain the conserved Syn domain (**Fig. 8A**). However, while the Syn domain of Rel_{seq} is embedded between the HD domain and the C-terminal regulatory part of Rel (Rel-CTD, compare to **Fig. 2A**), SAS1 lacks any obvious regulatory domains. To gain a deeper insight into the architecture of the SAS1 homotetrameric complex and to compare it with the long RSH protein Rel, the crystal structure of SAS1 was determined at 1.86 Å resolution using Rel_{seq}-NTD as a search model for molecular replacement (MR; **Table S1**). SAS1 crystallizes as a symmetric, oval shaped homotetramer containing four subunits of SAS1 (α-δ) consistent with its behaviour on SEC (**Fig. 8B,** compare to **Fig. 7A**). The medial sides of the tetramer are stabilized by interactions between helices α1 from the α/β– and γ/δ–subunits forming an interface of ~1100 $Å^2$ primarily stabilized by hydrogen bonds and salt bridges. The lateral sides of the tetramer are exclusively formed by helices α4 and α5 between the α/δ– and δ/γ –subunits in an interface of ~1220 $Å^2$, consisting chiefly of polar contacts. Strikingly, the tetrameric complex of SAS1 contains a prominent central cleft of unknown functional role (**Fig. 8B**).

3.1.4 Structural comparison of SAS1 and Rel

SAS1 and the Syn domain of Rel_{seq} (PDB: 1VJ7; residues 197-371, (54)) share an amino acid sequence identity of ~ 23 percent and their structures superimpose well with an RMSD of 1.6 Å over 78 Cα atoms (**Fig. 8C**). The Syn domain of SAS1 is composed of five antiparallel β-strands β1 - β5 surrounded by α-helices α1 – α4 (named β3 - β7 and α12 – α15 in Rel_{seq}) (**Fig. 8C**). Conserved amino acid residues involved in (p)ppGpp synthesis, are present in both SAS1 and Rel_{seq} (**Fig. 8D**). However, significant differences in the structure of both proteins can be observed. Helix α1 of SAS1 important for the formation of the medial interface of the tetrameric complex is slightly elongated compared to its counterpart α12 of Rel_{seq} (**Fig. 8C**). In Rel_{seq}, α12 together with its preceding helices α10 and α11 is bridging the HD and Syn domains and mediates intra-domain signaling (54). Notably, helix α13 of Rel_{seq} implicated to contribute to substrate-binding (54) is buried between α10 and α11 and its orientation differs by ~30° from its counterpart α2 found in SAS1 (**Fig. 8C**). This indicates that if α2 from SAS1 is involved in substrate-binding, differences between both proteins might exist. Close inspection of the antiparallel β-strand core of the Syn domain reveals that the loop region connecting β3 and β4 (G-loop for guanosine-binding loop) is disordered in SAS1 but ordered in Rel_{seq} (β5 and β6, respectively). This loop contains a conserved tyrosine moiety essential for GDP-binding to Rel_{seq} (i.e. Tyr308 in motif E3, **Fig. 8D**) again implying differences in the substrate-binding mode between SAS and long RSH proteins. Another major difference between SAS1 and Rel_{seq} pertains to the C-terminal helices α4 and α5 of SAS1 mediating oligomerization on the lateral side of the complex. Rel_{seq} harbors an equivalent to the N-terminal part of α4 (α15 in Rel_{seq}), however α4 of SAS1 is elongated by two turns and forms a helical hairpin with α5 which is absent in Rel_{seq}. This is in agreement with reports that Rel_{seq}-NTD predominantly occurs as a monomer in solution (52, 101), while SAS1 forms stable homotetramers (**Fig. 8B**).

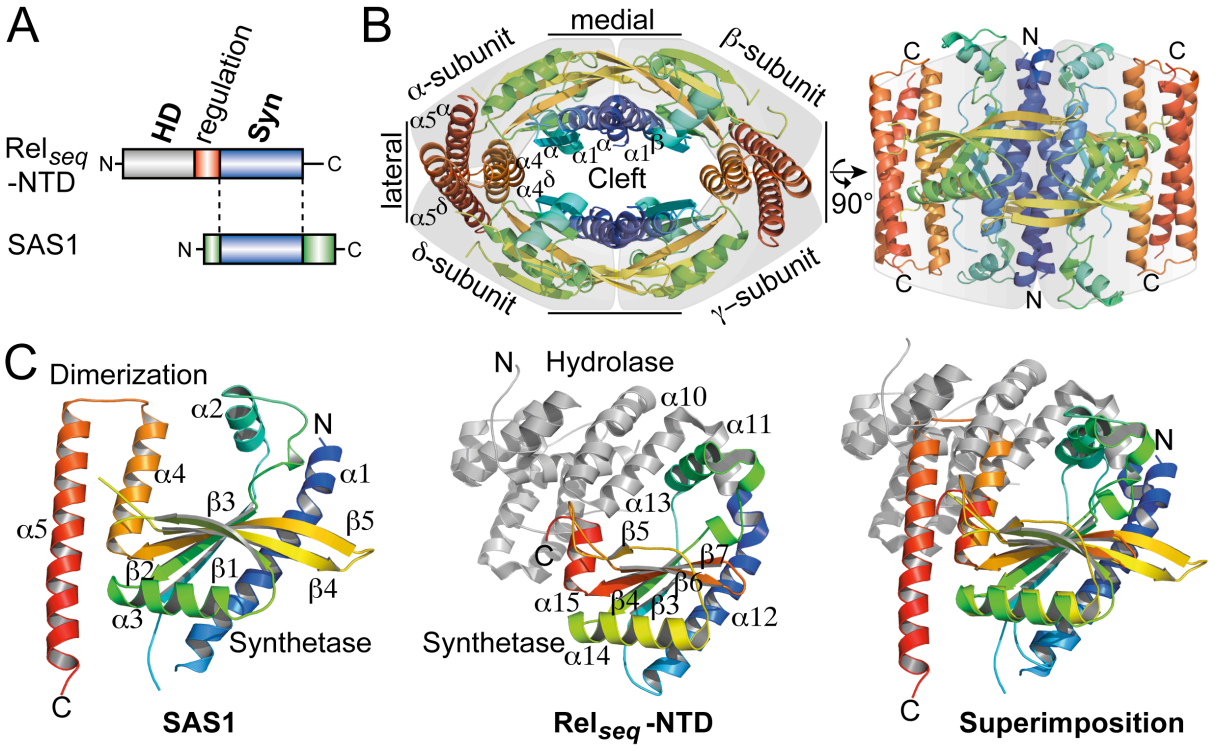

D

Figure 8. Crystal structure of the tetrameric alarmone synthetase SAS1 in the apo-state. **A.** Domain architecture of the alarmone synthetases RelA and SAS1. **B.** Crystal structure of the SAS1 tetramer. Each monomer (α to δ, indicated by a grey shadow) of SAS1 is shown in cartoon representation colored in rainbow from N- to C-terminus, indicated by 'N' and 'C', respectively. Interfaces on the lateral and medial sides of the complex are indicated by brackets. **C.** Cartoon representation of the crystal structures of an SAS1 monomer (left), Rel$_{seq}$-NTD (middle, PDB: 1VJ7; (54)) and the superimposition of their synthetase domains (right). The Syn domains of Rel$_{seq}$-NTD and SAS1 are shown in rainbow colors from N- to C-termini, indicated by 'N' and 'C', respectively. Structural elements in the Syn domain of Rel$_{seq}$ are labelled according to ref. (54). The equivalent elements in SAS1 are labelled and described in the text. **D.** Amino acid sequence alignment of *Bs*SAS1 and RelA from *B. subtilis* (*Bs*) and *S. equisimilis* (*Se*). Important motifs E1-E4 of the (p)ppGpp synthetase active site are indicated. The figure was modified from ref. (151).

3.1.5 Crystal structure of SAS1 in the ATP-bound state

Comparison of the crystal structures of apo-SAS1 and Rel_{seq} informed about the conserved fold of the Syn domain. Nevertheless, subtle differences between both proteins do exist (see above). To further elucidate the properties of SAS1, the crystal structures of SAS1 in different substrate-bound states were determined. To do so, crystallization experiments were carried out in the presence of 1 mM GDP, GTP or the non-hydrolysable ATP analog AMPCPP (i.e. α, β-methyleneadenosine 5′ -triphosphate) and combinations thereof. AMPCPP was used in order to prevent pyrophosphate transfer from ATP onto GDP or GTP through substitution of the oxygen atom linking the α- and β-phosphates of ATP by methylene. Although crystals could be obtained for all nucleotide-bound states, putative GDP- or GTP-containing crystals only allowed for structure solution of SAS1 in its apo-state while only AMPCPP could be undoubtedly identified in structures of SAS1 crystallized in the presence of AMPCPP or AMPCPP plus GDP or GTP. This might also indicate that (under the given conditions) binding of GDP and GTP to SAS1 in the absence of ATP is not possible.

The crystal structure of SAS1-AMPCPP was solved by MR using apo-SAS1 as search model at 2.8 Å resolution (**Table S1**). The crystal structure of SAS1-AMPCPP reveals the same homotetrameric assembly as observed for apo-SAS1 and contains AMPCPP in the active site of each subunit of the complex (**Fig. 9A**). Comparison of the Syn domain uncovers no major conformational changes between both states of SAS1 (**Fig. 9B**). However, while β3 was at least partially resolved in the structure of apo-SAS1, it is completely unresolved in SAS1-AMPCPP. The reason for this was not entirely clear at this point of the study, because β3 should be highly ordered due to interactions of the backbone amide hydrogens between β3 and β4. Remarkably, clear density corresponding to a magnesium ion could be identified in SAS1-AMPCPP when compared to the structure of apo-SAS1 (**Figs. 9B** and **10B**). The magnesium ion contributes to coordination of the 5' phosphate moieties of AMPCPP (see below). Although no further biochemical or biophysical experiments were conducted to probe this phenomenon, this observation might indicate that magnesium is not stable bound as a cofactor to SAS1, but binds concomitantly with the substrate ATP.

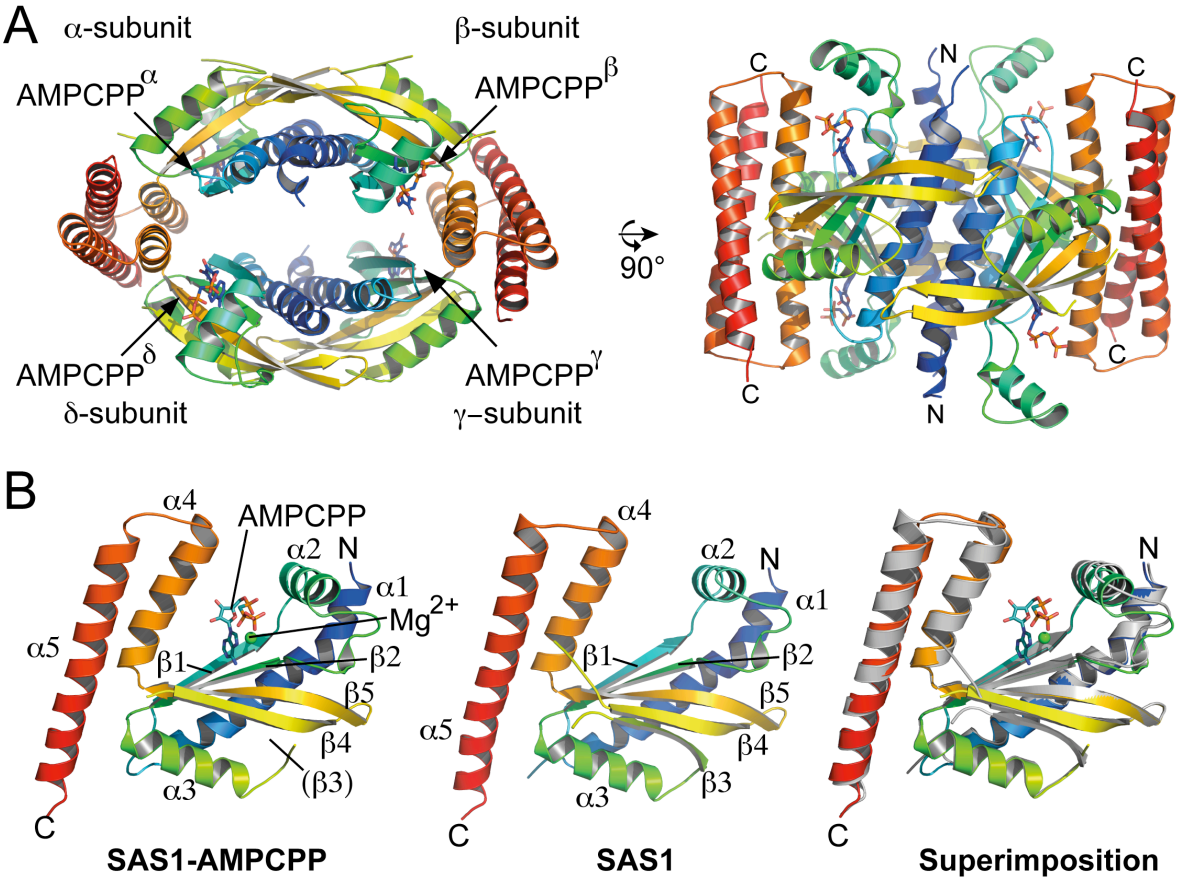

Figure 9. Crystal structure of SAS1 in the ATP-bound state. **A.** Crystal structure of SAS1-AMPCPP. Each monomer (α to δ) of SAS1 is shown in cartoon representation colored in rainbow from N- to C-terminus, indicated by 'N' and 'C', respectively. AMPCPP is shown as sticks. Magnesium is shown as sphere. **B.** Cartoon representation of the crystal structures of SAS1-AMPCPP (left), apo-SAS1 (middle) and their superimposition (right) colored in rainbow from N- to C-terminus indicated by 'N' and 'C', respectively. In the superimposition, apo-SAS1 is colored in grey. Figure 9A originates from ref. (151).

Helix α13 of Rel_{seq} thought to mediate ATP-binding to the Syn domain (54), differs in its relative orientation from its counterpart α2 of SAS1. Conversely, the β5-β6 (β3-β4 in SAS1) linker region involved in GDP-binding is resolved in the structure of Rel_{seq} but not SAS1 (compare to **3.1.4** and **Fig. 8C**). This suggests a disparity in substrate-binding between both proteins and is in agreement with the fact that a crystal structure of SAS1 could only be obtained with the ATP-substrate while the structure of Rel_{seq} contains GDP. A comparative structural analysis of SAS1-AMPCPP and Rel_{seq}-NTD-GDP highlights subtle differences between both proteins in regard to substrate-binding (**Fig. 10A**) and allows to deduce the following aspects: *i.*

Positioning of the ATP- and GDP-substrate in the (p)ppGpp synthetase active site of SAS1, *ii*. ATP-binding through helix α2/α13, and *iii*. GDP-binding by the β3 - β4/β5 - β6 loops.

ATP (mimicked by AMPCPP) is tightly coordinated to SAS1 mainly through interactions with residues from the conserved Syn domain motifs E1 and E2 (**Fig. 8D**). The nucleotide is located in the inner part of the active site pointing inwards of the tetrameric complex. The adenine base of AMPCPP is sandwiched between Arg46 and Arg77 through π-stacking interactions (**Fig. 10B**). The ribose moiety is coordinated by His155 via hydrogen-bonding. The phosphate moieties of AMPCPP are found in an unusually tense conformation bent towards the adenine base aided by the position of the magnesium ion cofactor between the β- and γ-phosphate. Asp72 and Glu139 provide further coordination for the magnesium ion and might be involved in catalysis (54). The positive charge of the γ-phosphate is neutralized by a positively charged pocket formed by Lys48, Lys56 and Arg59 located in helix α2. Arg46 appears to be a highly critical residue as it contributes to substrate-binding not only by caging the adenine base (see above), but also by interacting with the ribose oxygen and the α-phosphate of AMPCPP (**Fig. 10B**). The approximate position of GDP in the active site of SAS1 and the location of the G-loop can be inferred based on the superimposition with Rel_{seq}-NTD-GDP. In this, GDP would be located in the part of the active site pointing outwards of the SAS1 tetramer (**Fig. 10C**). GDP would establish fewer contacts to SAS1 than AMPCPP. The guanine base could be coordinated by hydrogen bonds from Glu154 and π-stacking interactions with Tyr116 (Tyr308 in Rel_{seq}). The ribose oxygen would establish contacts with Gln141. Arg105 and Lys112 might coordinate the α- and β-phosphate moieties of GDP. In this configuration, the 3'-OH ribose moiety of GDP would be located in close proximity to the β-phosphate of ATP allowing pyrophosphate transfer (**Fig. 10C**). However, the unstructured nature of the G-loop raises the question when GDP-binding to SAS1 takes place.

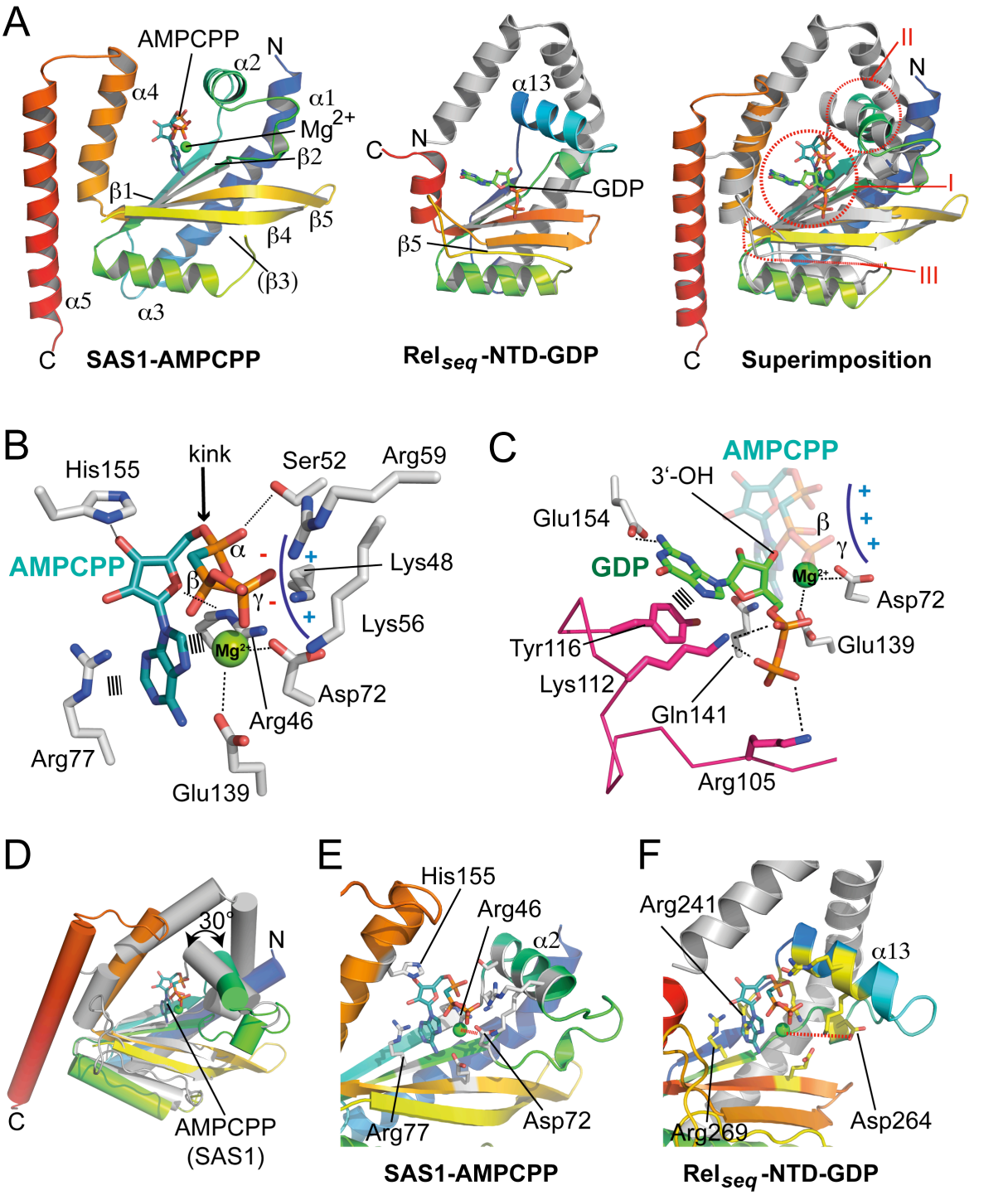

Figure 10. Structural basis for differences in substrate-binding between SAS1 and Rel$_{seq}$. **A.** Cartoon representation of the crystal structures of SAS1-AMPCPP (*l*eft), Rel$_{seq}$-NTD-GDP (middle, PDB: 1VJ7; (54)) and the superimposition of their synthetase domains (right). The Syn domains of Rel$_{seq}$-NTD and SAS1 are shown in rainbow colors from N- to C-termini, indicated by 'N' and 'C', respectively. Roman numbers are explained in the text. **B.** ATP (mimicked by AMPCPP, deep teal) binds in a tense, U-shaped conformation in the active site of SAS1. Interactions between residues of SAS1 and AMPCPP are indicated by dashed lines. The magnesium ion is shown as a green sphere. **C.** Spatial arrangement of ATP and

GDP in the active site of SAS1 based on the superimposition of SAS1 bound to AMPCPP (deep teal) and Rel_{seq} bound to GDP (green). The linker between β5 and β6 of Rel_{seq} is shown in magenta and residues labeled according to their corresponding position in SAS1. The pyrophosphate-accepting 3'-OH group of GDP is indicated. **D.** Cylindrical model of the superimposition of SAS1-AMPCPP colored in rainbow from N- to C-terminus and Rel_{seq} colored in grey. **E-F.** The differing orientation of α2 in SAS1-AMPCPP (**E**) and α13 in Rel_{seq} (**F**) affects ATP-binding. The Syn domains are colored in rainbow from N- to C-terminus. Essential residues are shown as sticks and colored in white (SAS1-AMPCPP) or yellow (Rel_{seq}). AMPCPP (deep teal) is shown as sticks. Magnesium is shown as a green sphere. The red dashed line indicates the distance between magnesium and Asp72/Asp264.

A similar binding of ATP to Rel_{seq} as observed for SAS1-AMPCPP seems rather unlikely based on the differences between both proteins (**Figs. 10D-F**). The position of ATP in the active site of Rel_{seq} seems valid because π-stacking interactions could be established between the adenine base and Arg269 (Arg77 in SAS1, **Figs. 10E** and **F**). However, steric clashes seem to occur between Arg241 (Arg46 in SAS1) and AMPCPP (**Fig. 10F**). Also, a residue corresponding to His155 from SAS1 does not exist in Rel_{seq} (compare to **Fig. 8D**). The orientation of α13 in Rel_{seq} slightly changes the distance between the phosphate moieties of AMPCPP and positively charged amino acid residues located in α13 yet these differences are only ranging from 0.5 to 1 Å. Most importantly, Asp264 (Asp72 in SAS1) is ~8 Å away from the magnesium ion while a distance of ~2 Å is observed in the structure of SAS1. This would render coordination of this essential cofactor for (p)ppGpp synthesis (53) by Asp264 unlikely. However, it might well be that the position of the ATP-substrate within the active site of Rel slightly differs from the one observed for SAS1-AMPCPP.

3.1.6 Crystal structure of SAS1 in the pppGpp-bound state

Initial biochemical evaluation of the (p)ppGpp synthetic activity of SAS1 suggested a different efficiency in the synthesis of the two alarmones ppGpp and pppGpp. To further elaborate this observation, the crystal structure of SAS1 either in the presence of ppGpp or pppGpp was determined. To do so, 1 mM each of the substrates ATP and GDP (for ppGpp) or ATP and GTP (for pppGpp) were added to an approximately 11.5 mg/ml concentrated solution of SAS1 and incubated for 1 h on ice prior to crystallization. Although crystals of SAS1 could be obtained and crystallographic datasets be successfully collected at the ESRF Grenoble, the structure of SAS1-

ppGpp could not be determined due to an excessive degree of twinning within the crystal (not shown). Nevertheless, un-twinned crystals could be obtained for SAS1 containing pppGpp that belonged to the space group C2 in contrast to space group $P2_1$ of apo-SAS1 and SAS1-AMPCPP (**Table S1**). The crystal structure of SAS1-pppGpp could be solved by MR employing apo-SAS1 as search model at 2.94 Å resolution (**Table S1**). Binding of pppGpp to SAS1 does not alter the oligomerization state of SAS1, which still appears in stable homotetramers (**Fig. 11**). The alarmone product pppGpp could be undoubtedly modelled into electron density present within all four active sites of SAS1 (**Figs. 11A** and **B**). Additional cryptic electron density was visible within the central cleft formed by the SAS1 homotetramer that could not be attributed to neither the nucleotides ATP or GTP nor citric acid or PEG6000 both present in the crystallization mother liquor. However, the pppGpp nucleotide in conjunction with a magnesium ion perfectly fitted into this additional density resulting in two additional pppGpp molecules bound per SAS1 homotetramer residing between the α-/δ- and β-/γ- subunits of SAS1, respectively (**Figs. 11A** and **C**).

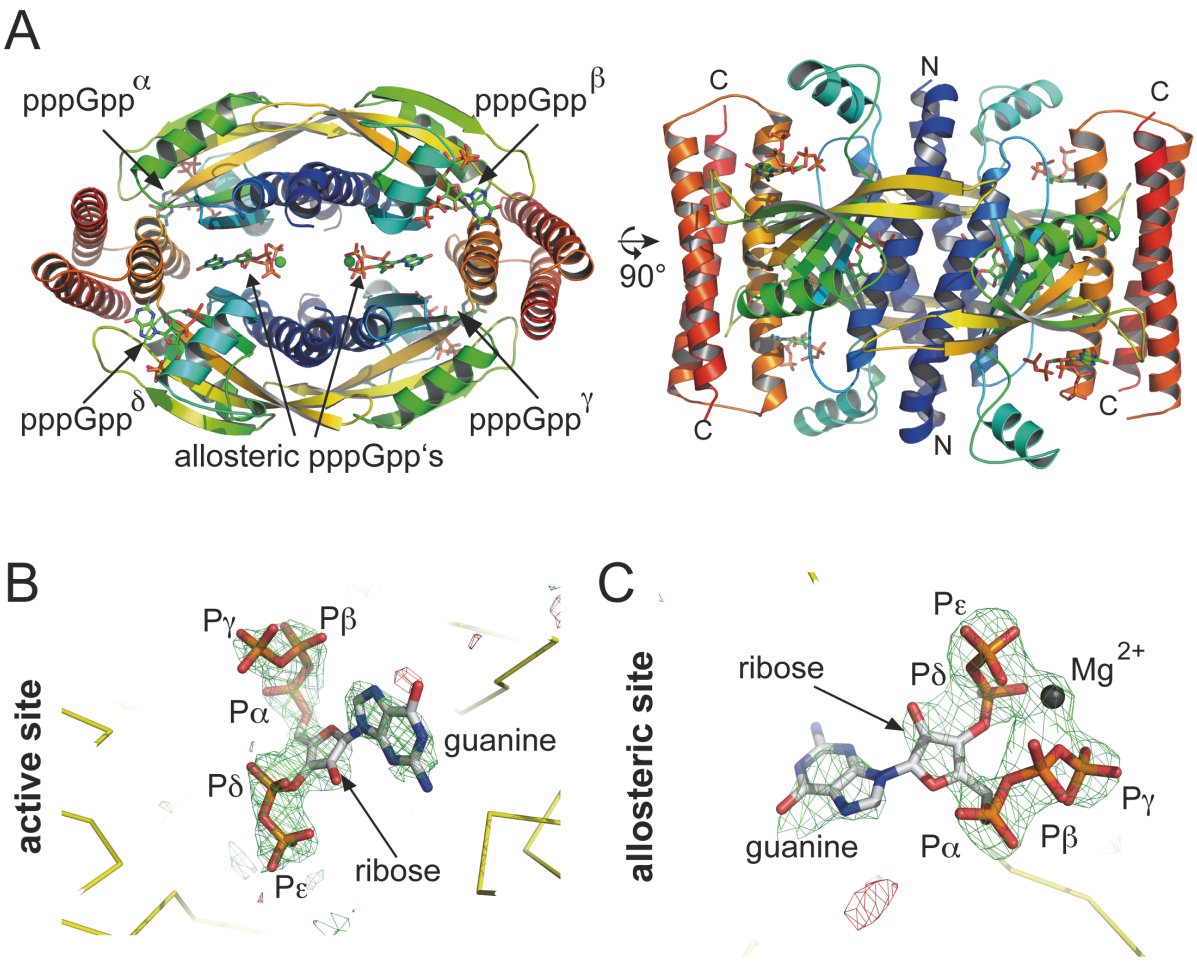

Figure 11. Crystal structure of SAS1 in the pppGpp-bound state. **A.** Crystal structure of SAS1-pppGpp. Each monomer (α to δ) of SAS1 is shown in cartoon representation colored in rainbow from N- to C-terminus, indicated by 'N' and 'C', respectively. Magnesium ions are shown as green spheres and pppGpp is shown as sticks. **B-C.** Electron density present within the active sites (**B**) and allosteric site (**C**) of SAS1 could be unambiguously assigned to pppGpp and pppGpp-magnesium, respectively. The unbiased Fobs-Fcalc difference electron density of pppGpp contoured at 2.5 σ is shown as green and red mesh for positive and negative difference, respectively. The pppGpp molecule (sticks) and magnesium ion (grey sphere) were not present during refinement and are only placed for reasons of illustration. Yellow ribbons indicate the backbone of SAS1. The figure originates from ref. (151).

Comparison of the active sites of SAS1 bound to pppGpp and Rel_{seq}-NTD bound to GDP reveals that the substrate (i.e. GDP) and product (i.e. pppGpp) of (p)ppGpp synthesis reside in the same location within the enzymes active sites (**Fig. 12A**). However, pppGpp seems to establish more contacts to amino acid residues within the active site of SAS1 than GDP (**Figs. 12B** and **C**). The guanine base of pppGpp is coordinated by π-stacking interactions with Tyr116 and a hydrogen bond provided by Glu154 (**Fig. 12B**). The ribose oxygen of pppGpp establishes contacts with Gln141. The 5'-OH phosphates of pppGpp (i.e. α-, β- and γ-phosphates) are coordinated by basic amino acids Arg105, Lys112 and His120 located in the G-loop of SAS1, which is ordered in SAS1-pppGpp in contrast to apo-SAS1 and SAS1-AMPCPP where the approximate position of these residues could only be inferred based on a superimposition of SAS1 with Rel_{seq}-NTD-GDP (compare to **Fig. 10C**). Lys56, Arg59 and Lys60 provide further contacts to the 5'-OH phosphates of pppGpp (**Fig. 12B**). Noteworthy, Lys56 and Arg59 also contribute to coordination of the ATP substrate to SAS1 while Lys60 seems to be uninvolved in ATP coordination (compare to **Fig. 10B**). Strikingly, residues Arg46, Lys48 and His155 provide contacts to the 3'-OH phosphates of pppGpp (i.e. δ- and ε-phosphates), which are not established in the presence of the substrate GDP lacking the δ- and ε-phosphates (**Figs. 12B** and **C**). All three residues majorly contributed to coordination of ATP to SAS1 (compare to **Fig. 10B**). It might be suggested that this 'shared use' of amino acids for coordination of the ATP substrate and (p)ppGpp product raises the efficiency of (p)ppGpp synthesis. In this regard, transfer of pyrophosphate from ATP onto GDP (GTP) would render the product AMP less affine to SAS1 because of the lack of its β- and γ-phosphates. Moreover, the (p)ppGpp product would contribute to expulsion of AMP

as it is able to establish contacts with amino acids formerly coordinating the ATP substrate via its 3'-OH δ- and ε-phosphates.

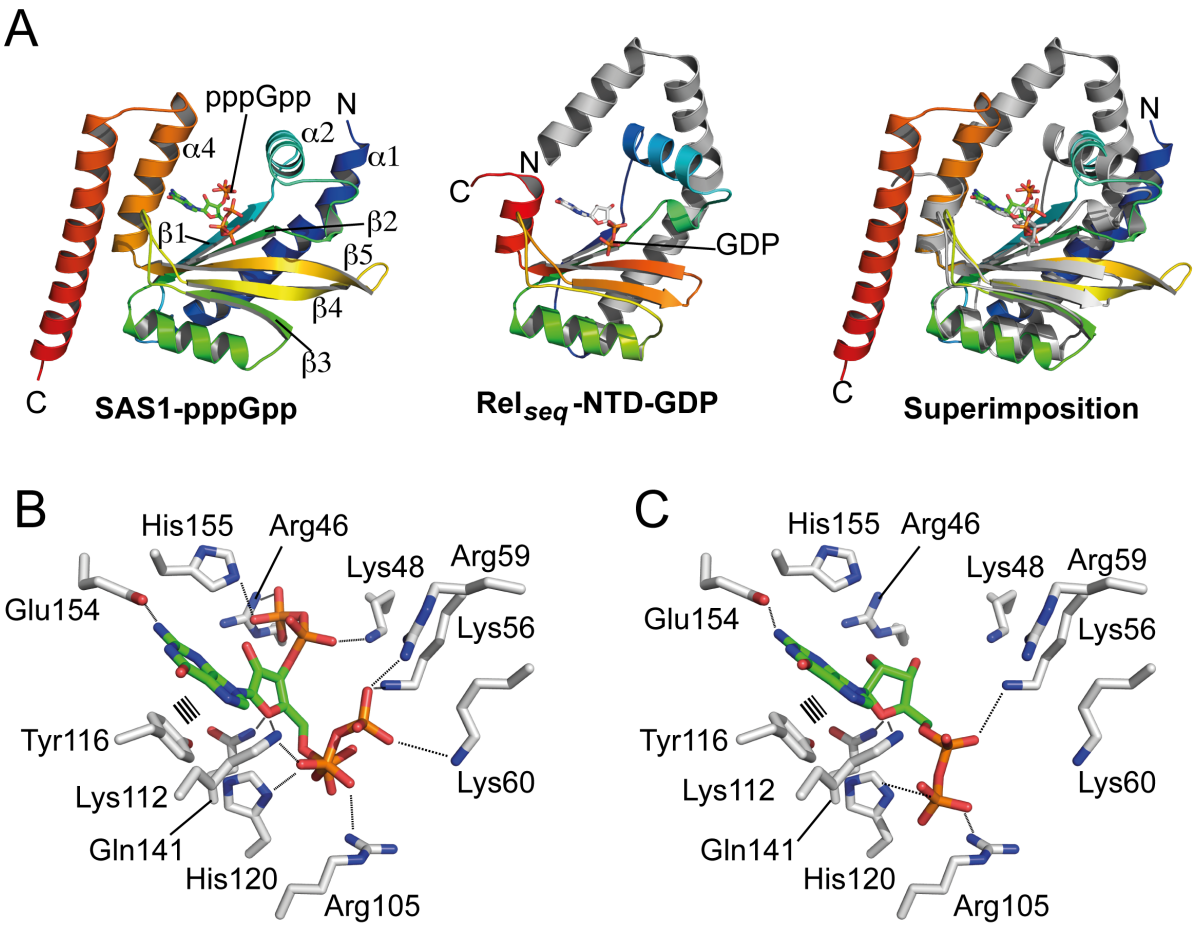

Figure 12. Binding of pppGpp to the (p)ppGpp synthetase active site of SAS1. **A.** Cartoon representation of the crystal structures of SAS1-pppGpp (*l*eft), Rel$_{seq}$-NTD-GDP (middle, PDB: 1VJ7; (54)) and the superimposition of their synthetase domains (right). The Syn domains of Rel$_{seq}$-NTD and SAS1 are shown in rainbow colors from N- to C-termini, indicated by 'N' and 'C', respectively. **B.** Coordination of pppGpp within the active site of SAS1. Dashed lines indicate interactions between residues of SAS1 and pppGpp. **C.** Coordination of GDP within the active site of SAS1. Dashed lines indicate interactions between residues of SAS1 and GDP.

Apart from pppGpp residing within all four active sites of SAS1, two additional pppGpp molecules could be identified within the central cleft of the homotetramer, which was unoccupied in the apo-state of SAS1 (**Figs. 11A** and **4B**). Each of the pppGpp's resides at the interface between two subunits of SAS1 denoted as subunit

and subunit' both contributing to pppGpp coordination. The α-ε phosphates of pppGpp are sequestered in a positively charged cage comprised by Lys21, Lys25 and Arg28 from both subunits (**Fig. 13A**). Furthermore, the β-ε phosphate moieties are arranged in a crab-like manner enforced by a magnesium ion. Specificity for the guanine base is conferred by interactions of Glu41 and Asn148 from two different subunits with the N2 amino- and O6 keto groups, respectively. The guanosine is further stabilized by π-stacking interactions of the guanine base with Phe42 and hydrogen bonding between Thr44 and the 2'-OH group of the ribose. As two subunits heavily contribute to pppGpp coordination, allosteric binding of pppGpp to SAS1 only seems possible in the context of the SAS1 homotetrameric assembly (**Fig. 13A**).

Amino acid sequence alignments of SAS1 and SAS2 proteins from various bacterial species shows that residues conferring pppGpp binding to *Bs*SAS1 are conserved among SAS1 orthologs and differ from SAS2 (**Fig. 13B**). The three allosteric motifs (R1 - R3) are: R1 'KxxxK/RxxR', R2: 'EFVT' and R3: 'LAMNFWAT'. Although only one study reports an influence of pppGpp on the enzymatic activity of SAS1 from *E. faecalis* (40), the high degree of conservation of the allosteric motifs makes a similar mechanism for SAS1 from various species highly likely. Moreover, the presence or absence of the allosteric motifs allows for an accurate classification of small alarmone synthetase proteins to the SAS1- or SAS2 subfamily of SAS proteins.

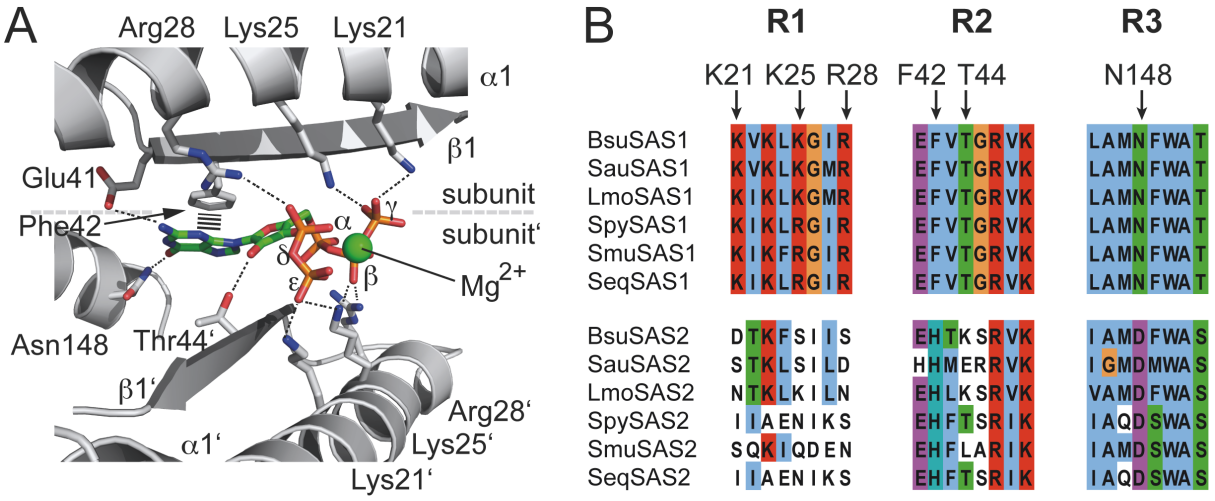

Figure 13. Binding of pppGpp to the allosteric site of SAS1. **A.** Residues from two opposing monomers (denoted as subunit and subunit') of the SAS1 homotetramer coordinate each of the allosteric pppGpp molecules. **B.** Amino acid sequence alignment of SAS1 and SAS2 orthologs from *B. subtilis* (Bs), *S. aureus* (Sau), *L. monocytogenes* (Lmo), *Streptococcus*

pyogenes (Spy), *Streptococcus mutans* (Smu) and *Streptococcus dysgalactiae ssp. equisimilis* (Seq). R1, R2 and R3 indicate motifs conferring binding of pppGpp to the allosteric site of SAS1. Amino acids above the alignment are numbered according to their position in *Bs*SAS1. Figure 13A originates from ref. (151).

Binding of pppGpp does not alter the oligomeric state of SAS1, however the topology of the homotetramer differs significantly between the apo- and pppGpp-bound states of SAS1 (**Figs. 14** and **15A**). The location of helices α1 and α4 as well as β1 differs significantly between both states. This is however not surprising as amino acids located within these secondary structure elements mediate binding of pppGpp to SAS1 (**Fig. 13A**). Nevertheless, also helices α2 and α5 of SAS1 are rearranged although they are far away from the allosteric pppGpp-binding site. Moreover, the G-loop containing residues essential for coordination of the guanosine substrate is ordered in SAS1-pppGpp (**Fig. 12B**). This implies that allosteric binding of pppGpp might alter also alter the function of SAS1.

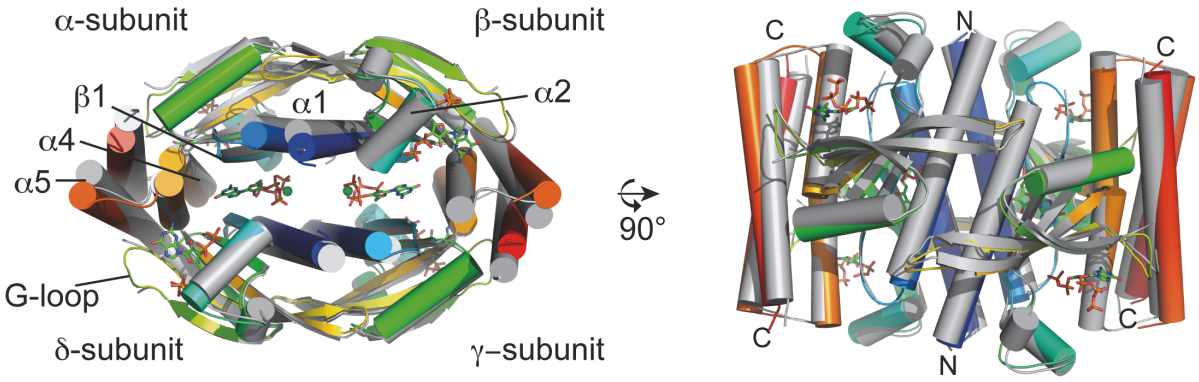

Figure 14. Comparison of the pppGpp-bound state and apo-state of SAS1. SAS1-pppGpp is colored in rainbow from N- to C-terminus, indicated by 'N' and 'C', respectively. The apo-state of SAS1 is colored in grey. Secondary structure elements that differ significantly between both states are indicated.

Conformational changes of pppGpp-bound SAS1 compared to the apo-state are schematically illustrated in **Fig. 15A** and further detailed in **Figs. 15B-G**. Side chains of lysine and arginine residues located in helix α1 provide a positively charged cage for binding of the allosteric pppGpp's. Binding of pppGpp into this cage pulls α1 by 1-2 Å into SAS1's central cleft (**Fig. 15A**, I and **Fig. 15B**). Coordination of allosteric

pppGpp by Glu41, Phe42 and Thr44 located within β1 results in a longitudinal movement of β1 by ~ 1.5 Å (**Fig. 15A**, II and **Fig. 15C**). Helix α2 protrudes ~ 3 Å into the active site of SAS1 in the presence of pppGpp than in its absence (**Fig. 15A**, III and **Fig. 15D**). This movement might at least be partially mediated by rearrangement of the adjacent elements α1 and β1. Noteworthy, α2 comprises the residues Lys48, Lys56, Arg59 and Lys60 which mediate coordination of the ATP substrate but also the pppGpp product within SAS1's (p)ppGpp synthetase active site (**Fig. 15D**). However, it is not clear at this point whether the altered location of α2 is mediated by the allosterically-bound pppGpp molecules or simply because pppGpp is also bound within the active site in the SAS1-pppGpp structure. Further changes of SAS1-pppGpp relate to Asn148 residing in helix α4, which established specificity for the guanine base of allosteric pppGpp by hydrogen bonding with its O6 keto group (compare to **Fig. 13A**). This interaction induces displacement of Asn148 by ~1 Å and rotation of α4 by approximately 15° (**Fig. 15A**, IV and V and **Figs. 15E** and **F**). Through this rotational movement, Phe149 located nearby to Asn148 within α4 extends into the hydrophobic core between helices α4 and α5 resulting in displacement of Leu183 and Met187 residing in α5. Noteworthy, based on the symmetry of the SAS1 homotetramer, helices α4 and α5 from two monomers of the complex undergo the same conformational rearrangement although Asn148 from only one monomer establishes contacts to the allosteric pppGpp. A direct consequence of the altered topology of the lateral interface of the SAS1 homotetramer is displayed in the interface between α5 and the G-loop close to SAS1's active site (**Fig. 15A**, VI and **Fig. 15G**). Through rotation of α5, interactions might be established by Gln174 and Glu178 (both in α5) with Glu113, His111 and Arg117 located in the G-loop. These contacts seem to be impossible in the apo-state of SAS1. To this effect, these interactions might help structuring the G-loop to facilitate binding of the guanosine substrate mediated by Tyr116 (see above). Noteworthy, the G-loop of SAS1 is ordered in SAS1-pppGpp but not in SAS1-AMPCPP or the apo-state of SAS1. However, it is unclear whether this event is goverened by the allosteric pppGpp or simply by pppGpp bound to the active site of SAS1. Nevertheless, it is apparent that binding of two pppGpp molecules within the central cleft of SAS1 results in major topological changes of the SAS1 homotetramer.

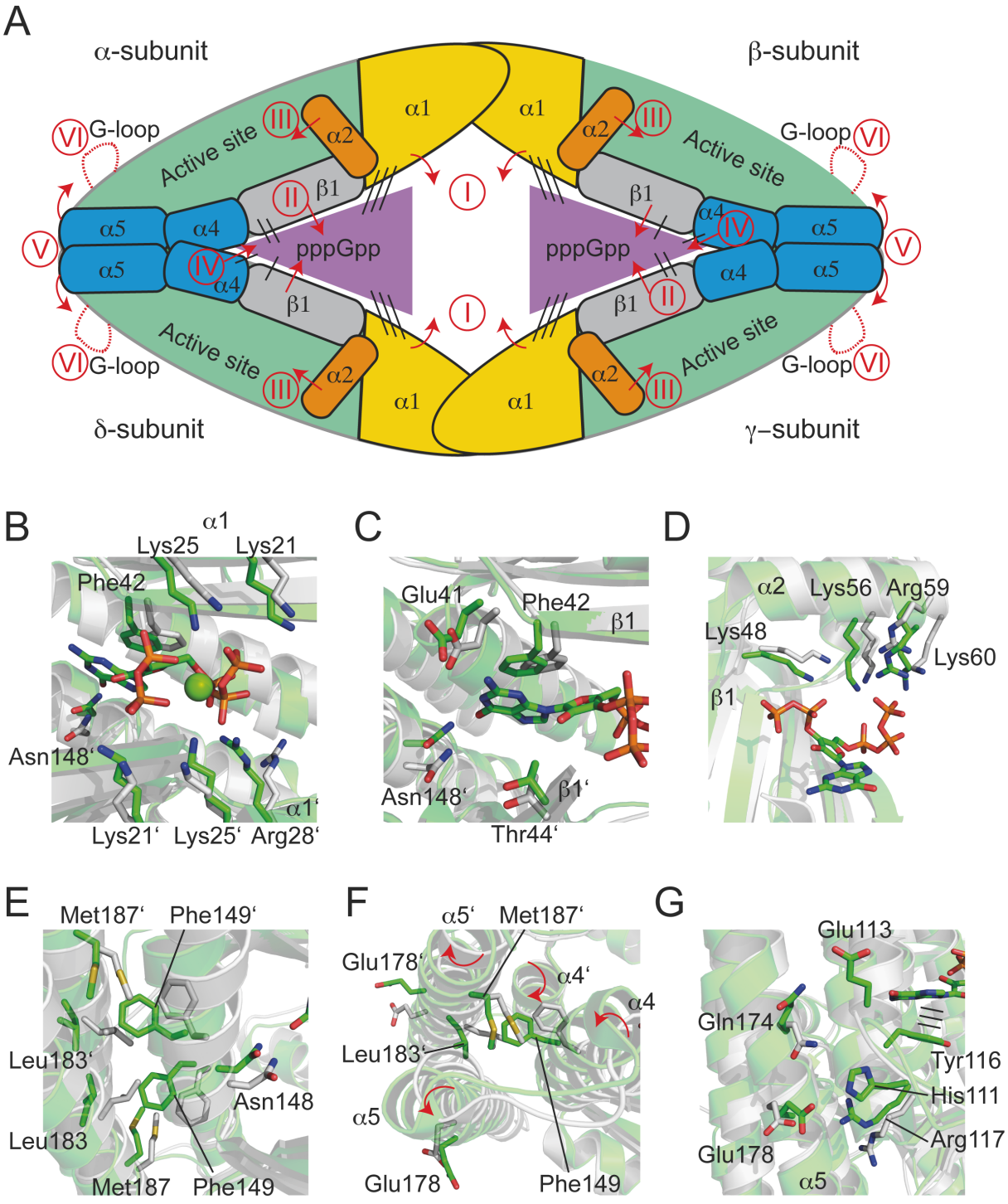

Figure 15. Conformational changes of SAS1 upon binding of pppGpp. **A.** Scheme of the SAS1 homotetramer depicting differences between SAS1-pppGpp and the apo-state of SAS1 (compare to Fig. 10). Black lines indicate the number of interactions established between SAS1 and allosteric pppGpp. Red arrows indicate conformational changes of secondary structure elements of SAS1. Roman numbers are explained in the text. **B-G.** Detailed differences between the apo-state (grey) and pppGpp-bound state (green) of SAS1. **B.** α1 (I). **C.** β1 (100). **D.** α2 (III). **E-F.** α4 and α5 (IV+V). **G.** α5 and G-loop (V+VI).

3.2 Catalytic mechanism and regulation of SAS1

3.2.1 Sequentially ordered substrate-binding mechanism of SAS1

Despite intensive research on (p)ppGpp synthetases over the last decades, the catalytic mechanism of (p)ppGpp synthesis and its structural basis remained widely unadressed so far. In order to gain a better understanding how alarmone synthesis proceeds, I aimed at determining the order of substrate-binding to SAS1. For this purpose SAS1 was subjected to hydrogen-deuterium exchange (HDX) mass spectrometry in the presence of different nucleotides. In brief, SAS1 was incubated with different combinations of GDP, GTP and AMPCPP (see **Fig. 16A**) in D_2O-containing SEC buffer. After completion of the HDX reaction, SAS1 was digested with pepsin and the resulting peptides analyzed by electrospray ionization mass spectrometry. Data analysis was carried out using PLGS and DynamX 3.0 softwares (both from Waters) as further detailed in chapter **5.2.8.**

Two regions of SAS1 (R2 and R3) located within its active site showed significant stabilization in the presence of AMPCPP after 30 s of deuteration (**Figs. 16A** and **B**). However, no effects could be detected in the presence of either GDP or GTP alone. The validity of this observation is supported by the exemplary time course of HDX of the R2 region in which no difference in relative HDX can be observed between the apo- and GDP-state of SAS1 while HDX of AMPCPP-SAS1 is ~20% decreased after 15/30/60 s and only levels up after 10 min of deuteration (**Fig. 18B**). These results suggest that ATP must bind before GDP or GTP can enter SAS1. To support this finding, the experiment was repeated employing combinations of AMPCPP and either GDP or GTP. The presence of both substrates (i.e. AMPCPP and GDP (GTP)) induced an even stronger stabilization of R2 and R3 than AMPCPP alone (**Fig. 16A**). A similar behaviour could be observed, although not as pronounced, for region R1. This is not surprising as coordination of the GDP (GTP) substrate does not require residues found in R1 (compare to **Fig. 10A**). Taken together, these data show that SAS1 binds its substrates in an ordered sequence (**Fig. 16C**).

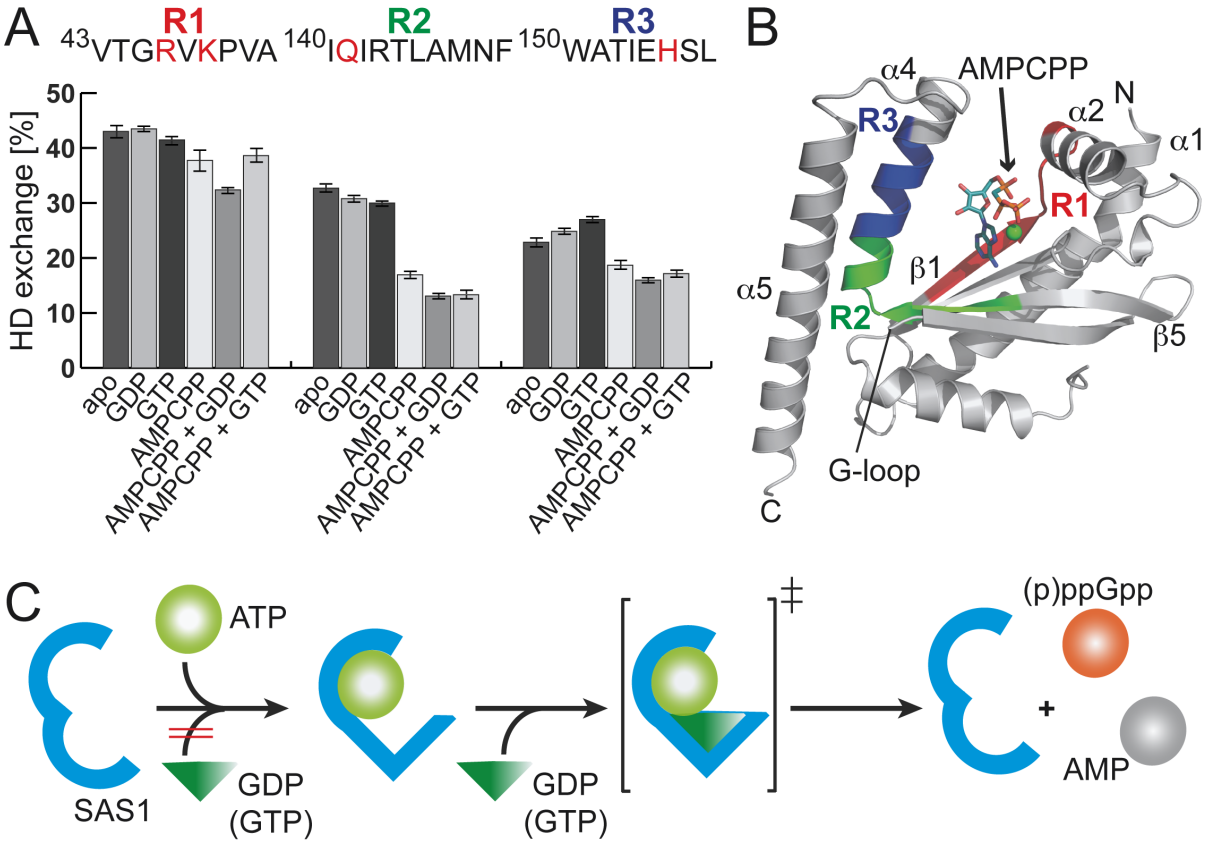

Figure 16. Sequential-ordered substrate binding to SAS1. **A.** Three regions of SAS1 (R1-R3) show different responses to the presence of nucleotides in HDX experiments after 30 s of deuteration. Residues involved in coordination of the ATP substrate are labelled in red. Data represent the mean ± standard deviation of three independent measurements. **B.** Location of the peptides R1 (red), R2 (green) and R3 (blue) in the crystal structure of an SAS1-AMPCPP monomer. An arrow indicates the location of AMPCPP within the active site of SAS1. **C.** The substrates ATP (pale green ball) and GDP/GTP (dark green triangle) bind to SAS1 (blue) in sequential order. Binding of the first substrate ATP leads to a conformational change within SAS1 allowing binding of the second substrate GDP/GTP. The transition state of catalysis in indicated by a double dagger (‡). The reaction products (p)ppGpp and AMP are shown as orange and grey balls, respectively. The figure was adapted from ref. (151).

3.2.2. Catalytic mechanism of (p)ppGpp synthesis by SAS1

With the availability of the crystal structure of an alarmone synthetase in the ATP-bound state (i.e. SAS1-AMPCPP) and the knowledge about the sequential substrate-binding mode, a detailed model of the catalytic mechanism of (p)ppGpp synthesis by SAS1 could be derived (**Fig. 17**). ATP binds to the active site of SAS1 and is held in position by π-stacking interactions with Arg46 and Arg77. The phosphate moieties of

ATP protrude in an unusual angle from the ribose of ATP mainly mediated through coordination by Arg46 and a magnesium ion. The guanosine substrate GDP or GTP enters the active site locating its 3'-OH group in close proximity to Glu139, magnesium and the β-phosphate of ATP. At least partial deprotonation of the 3'-OH group results from its close proximity to magnesium. Furthermore, Glu139 might serve as a general base. The so-activated 3'-O^- group can attack the β-phosphate of ATP via a second-order nucleophilic substitution (S_N2) resulting in the transfer of the β- and γ-phosphates of ATP onto the 3'-OH moiety of GDP (GTP). The AMP product ripped of its tight coordination to SAS1 via the β- and γ-phosphates as well as steric clashes with the (p)ppGpp product should then readily leave SAS1's active site. The (p)ppGpp product does not establish a significantly higher number of interactions than the GDP (GTP) substrate and might as well readily leave SAS1's active site upon reversion of SAS1 into the apo-state conformation.

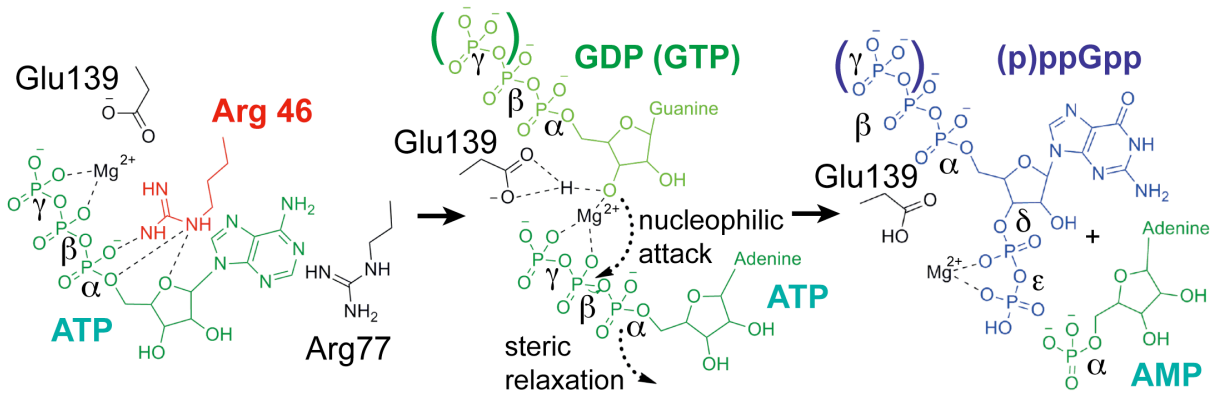

Figure 17. Catalytic mechanism of alarmone synthesis by SAS1. ATP and AMP are shown in dark green. GDP (GTP) is shown in bright green. (p)ppGpp is shown in blue. Further details are given in the text. The model was deployed by Jan Schuhmacher and the figure originates from ref. (151).

To solidify the findings on the catalytic mechanism of alarmone synthesis by SAS1, point mutations were generated within SAS1 resulting in substitution of Arg46 and Glu139 by Gly and Val, respectively. Both variants were purified as described before (**3.1.1** and **6.2.3**) and appeared as a stable homotetramer on SEC (not shown). Both variants were devoid of alarmone product formation (**Fig. 18A**) highlighting their crucial role in (p)ppGpp synthesis (see above). To elucidate the reason for their catalytic inactivity, both SAS1 variants were subjected to HDX in the absence or presence of AMPCPP and treated as the native protein (see **3.2.1** and **6.2.7**).

Although slightly different peptides were generated in this experiment, direct comparison of the apo- and AMPCPP-state of both variants still allows for conclusive data interpretation (**Figs. 18B** - **D**). Evidently, no difference between the two states of both variants over the whole time course of HDX (i.e. 15/30/60/600 s deuteration) does exist (**Figs. 18C** and **D**). This stands in contrast to the previously observed decrease in HDX of SAS1 in the presence of AMPCPP (**Fig. 18B,** compare to **Fig. 16A** region R2). This experiment demonstrates that variation of Arg46 and Glu139 leads to a catalytically inactive protein because ATP-binding to SAS1 is ablated. It seems obvious that removal of Arg46 by mutation does diminish ATP-binding as Arg46 establishes ATP coordination by π-stacking interactions and coordination of the phosphate moieties. However, Glu139 is not involved in coordination of ATP *per se* but aids in arranging the magnesium ion cofactor between ATP's β- and γ-phosphates (**Fig. 10B**). This suggests that magnesium is needed for proper coordination of ATP within the active site of SAS1 and is in agreement with the observation that magnesium was not found in the crystal structure of apo-SAS1 but in the structure of SAS1-AMPCPP (see **3.1.5** and **Fig. 9B**).

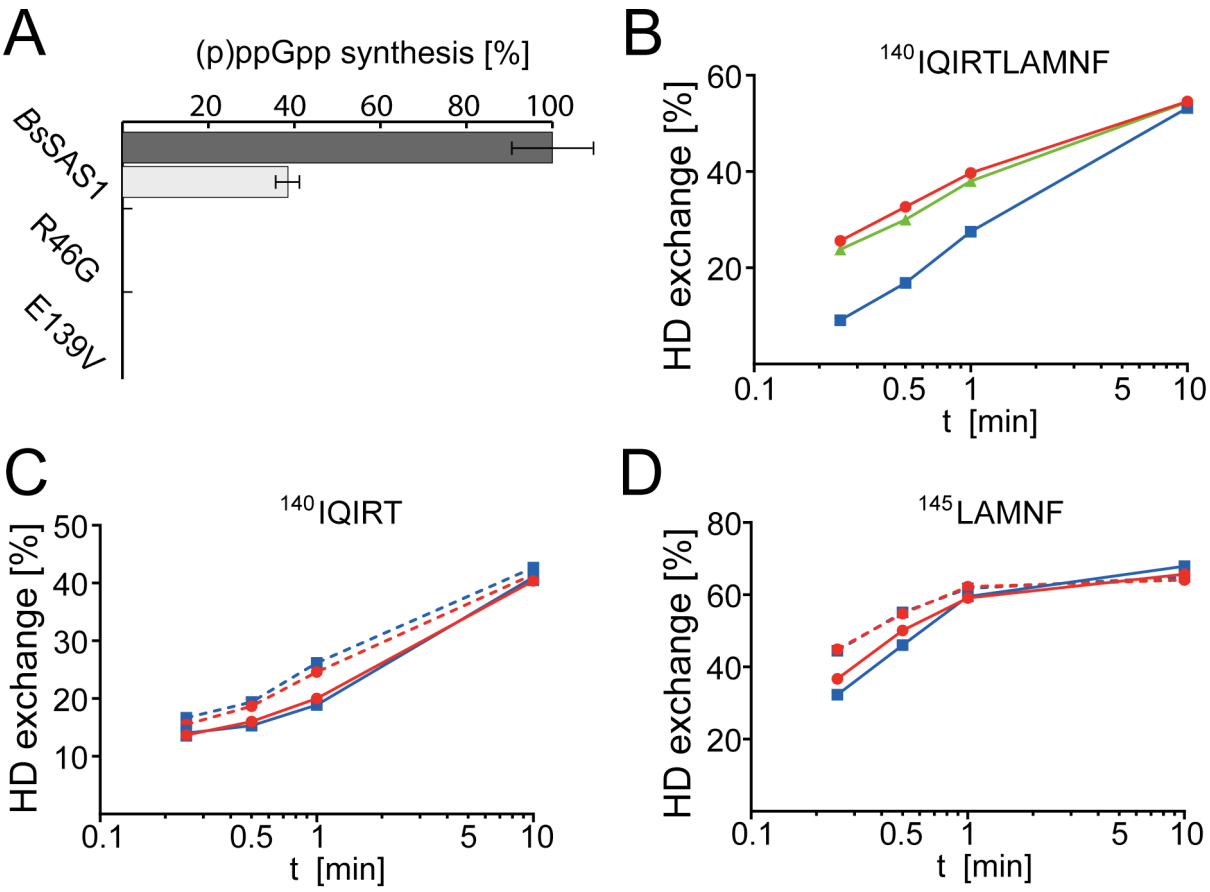

Figure 18. Analysis of variations within SAS1's active site. **A.** Synthesis of ppGpp (black) and pppGpp (grey) by SAS1 and its variants R46G and E139V. 2 µM SAS1 were incubated with 5 mM ATP and 5 mM GDP/GTP for 10 min at 37 °C. Synthesis of ppGpp by SAS1 is set to 100%. Data represent the mean ± standard deviation of three independent measurements. **B.** HDX time course of SAS1 without nucleotides (red) and in presence of AMPCPP (blue) or GDP (green). **C-D.** HDX time course of SAS1 variants R46G (solid line) and E139V (dashed line) without nucleotide (red) or in the presence of AMPCPP (blue). Data represent the mean ± standard deviation of three independent measurements.

3.2.3. Development of a HPLC-based assay for kinetic analysis of (p)ppGpp synthetases and hydrolases

Several methods for measuring the activity of (p)ppGpp synthetases are described. The classical 'magic spot' experiment is based on the formation of ^{32}P-labeled (p)ppGpp either by transfer of ^{32}P-phosphate from radioactive-labeled ATP or by employing radioactive-labeled GDP or GTP as substrate. The reaction mixture is then separated by thin-layer chromatography and (p)ppGpp quantified by illumination and read out of a photo film (153). Recently used instrumental methods are based on the quantification of (p)ppGpp by anion-exchange chromatography (152) or ion-pair reversed-phase high performance liquid chromatography (IP-RP-HPLC) coupled to a UV-detection unit (154, 155). The latter one is also regularly used for separation of various nucleotides. As experiments with ^{32}P-labeled nucleotides require an isotope laboratory and RP-HPLC offers the advantage of greater reproducibility compared to AX-chromatography, I opted for the implementation of a method suitable for quantification of (p)ppGpp based on ion-pair RP-HPLC.

Separation of the negatively charged nucleotide analytes necessitates the inclusion of a positively charged ion-pairing reagent in the running buffer. Commonly used reagents for this purpose are the volatile trimethylammonium bicarbonate (156), tetrabutylammonium dihydrogenphosphate (157, 158) tetraethylammonium bromide or tetrapentylammonium bromide. The retention of the analytes heavily depends on the chain length of the alkyl groups of the ion-pairing reagent (159). Therefore, tetrapentylammonium bromide (TPAB) was used in this work.

HPLC measurements were carried out on an Agilent 1100 Series system (Agilent Technologies) equipped with a variable wavelength detector (Agilent Technologies).

A C18 column (EC 250/4.6 Nucleodur HTec 3 µm; Macherey-Nagel) kept at 25 °C was used for separation of the analyte mixtures. Buffer A contained 50 mM KH_2PO_4, 50 mM K_2HPO_4, 15% (v/v) acetonitrile and 10 mM TPAB, buffer B was acetonitrile. After 30 min running with buffer A at 0.8 ml/min flow rate, a linear gradient up to 90% B was applied over 20 min and subsequently hold for 10 min. Nucleotides elute in order of their number of phosphate moieties (**Fig. 19A**) and guanosine nucleotides elute earlier than adenosine nucleotides when harboring the same number of phosphates. Nucleotides were typically detected at a wavelength of 260.8 nm and quantified using Agilent ChemStation (version: B.04.03, Agilent Technologies). The identity of the nucleotide was determined by comparison of their retention time with standards.

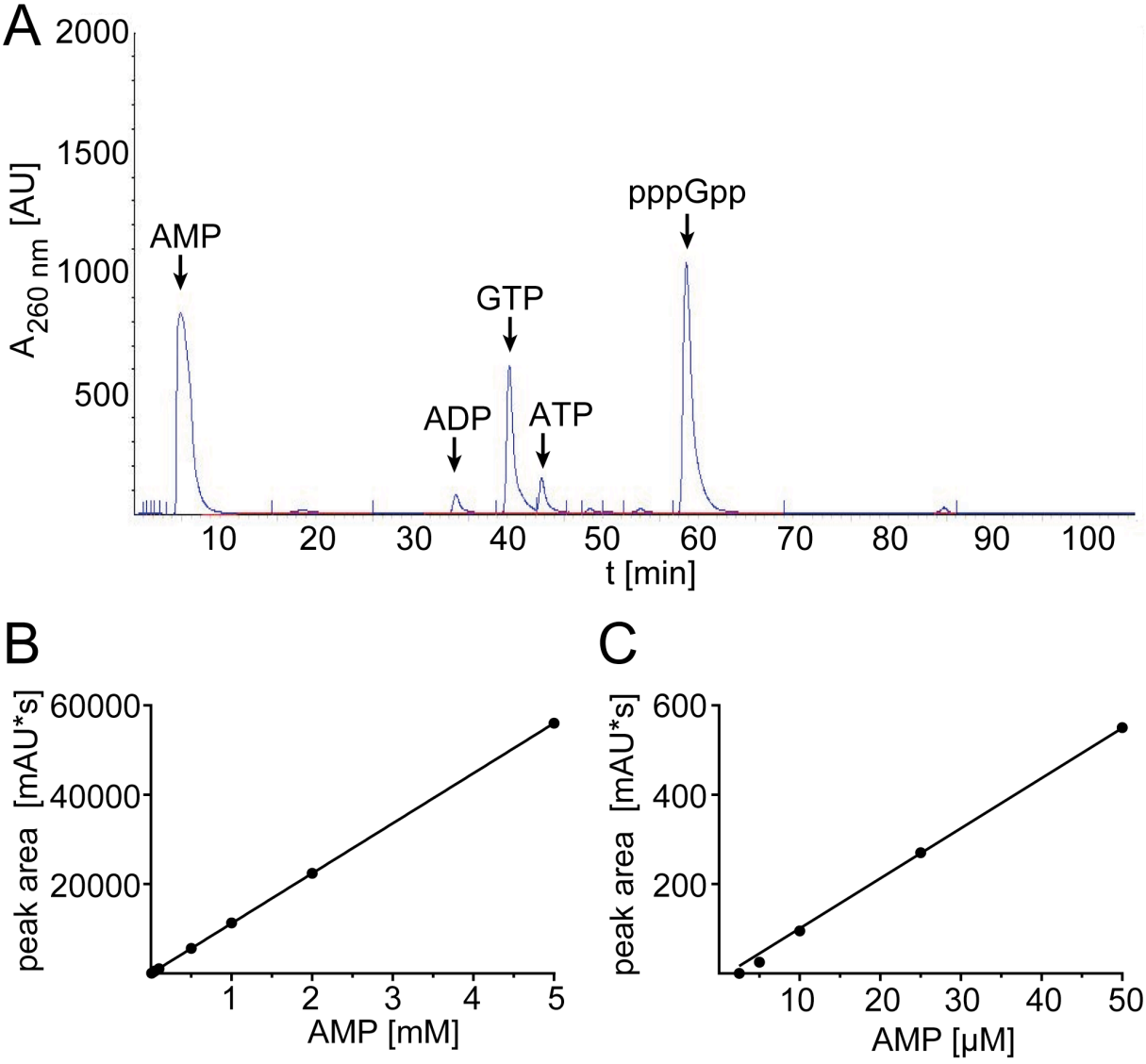

Figure 19. HPLC-based method for quantification of nucleotides and (p)ppGpp. **A.** Exemplary UV chromatogram of an *in vitro* reaction containing SAS1, ATP and GTP. Retention times of different nucleotides are labelled by arrows. **B-C.** Correlation of measured UV signal intensity correlating with different concentrations of AMP in the injected sample.

Because of the lack of commercially available (p)ppGpp with suitable purity, the calibration curve accounting for the ratio of calculated peak area to analyte concentration was obtained using AMP in a concentration range between 2.5 and 5000 µM (**Figs. 19B** and **C**). Linear regression through all data points results in a good correlation between peak area and AMP concentration at ≥ 10 µM AMP. 5 µM AMP result in a peak area slightly below the slope of the regression curve while 2.5 µM AMP cannot be detected with the method. This allows to deduce the limit of detection and limit of quantification for the method to be 2.5 - 5 µM and 10 µM AMP, respectively. Although these values might not be directly applied to all other nucleotides, mainly (p)ppGpp, they allow for a rough estimation of the methods capabilities.

In vitro reactions probing the (p)ppGpp synthetase activity of SAS1 were prepared as described in the respective chapters and **6.2.6** except stated otherwise. Reactions were stopped by flash-freezing in liquid nitrogen and stored at - 20 °C until measurement conducted latest within three days. Before measurement, the samples were rapidly thawn and directly injected into the HPLC system.

3.2.4. SAS1 displays a highly cooperative behavior

In order to investigate the enzymatic properties of SAS1, kinetic analysis of SAS1's (p)ppGpp synthetase activity was performed. In brief, 2 µM SAS1 and 5 mM ATP were incubated in a modified SEC buffer (100 mM HEPES-Na, pH 7.5, 200 mM NaCl, 20 mM $MgCl_2$, 20 mM KCl) together with varying concentrations of GDP or GTP at 37 °C. After predefined time-points, aliquots were removed from the reaction, flash frozen in liquid nitrogen and stored at -20 °C until measurement. HPLC analysis was carried out as detailed in chapter **3.2.3**. In this experiment, ppGpp and pppGpp produced during the reactions were quantified by correlating the UV peak areas of (p)ppGpp with the UV peak areas of GDP or GTP obtained by measuring GDP/GTP samples of known concentration. This procedure is valid as the extinction coefficient

of (p)ppGpp solely depends on the presence of the nucleobase guanine while the ribose phosphate moieties are not contributing to UV absorption.

The initial velocities of (p)ppGpp synthesis by SAS1 were obtained from the slope of the linear regression of (p)ppGpp quantified at different time points (**Fig. 20**). Thereafter, the initial velocities were plotted against the concentration of GDP (GTP). Kinetic data analysis was carried out using GraphPad Prism version 6.04 for Windows (GraphPad Software, San Diego, California, USA). The values for K_m, V_{max} and the Hill coefficient (h) ± standard deviation were obtained from the sigmoidal fit of the v/S characteristic using the equation $v = V_{max} S^h/(K_m^h + S^h)$.

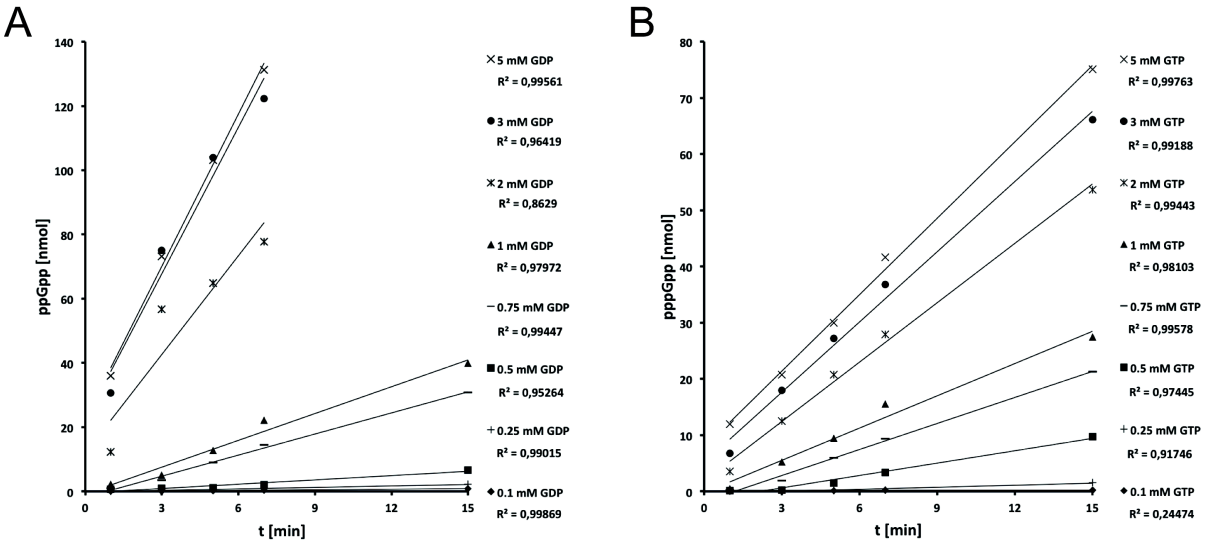

Figure 20. Progress curves of (p)ppGpp synthesis by SAS1. **A.** Progress curves of ppGpp production by SAS1 at differing GDP concentrations. For 2, 3, and 5 mM GDP, the 15-min data point was excluded because substrate limitation was reached. **B.** Progress curves of pppGpp production by SAS1 at differing GTP concentrations. **A-B.** GDP or GTP were used in concentrations of 0.1, 0.25, 0.5, 0.75, 1, 2, 3, 5 mM while ATP was used with 5 mM. For each GDP/GTP concentration, five different time points (i.e. 1, 3, 5, 7 and 15 min) were measured. The R^2 values for each progress curve are indicated. The figure originates from ref. (151).

SAS1 displays a cooperative behaviour for the synthesis of ppGpp and pppGpp reflected by the Hill coefficients of 3.0 ± 0.3 and 2.0 ± 0.1, respectively (**Fig. 21**). The K_m values differ only slightly (i.e. 1.7 ± 0.1 for GDP and 1.2 ± 0.1 for GTP), however the maximal velocity (V_{max}) shows an approximately 3.5-fold difference between both reactions. This preferential synthesis of ppGpp over pppGpp is in agreement with

earlier observations from this work (**Fig. 18A**) and reports on SAS1 orthologs from *B. subtilis*, *S. aureus* and *E. faecalis* (40, 57, 71). However, the kinetic description of SAS1 does not allow for the determination of an influence of allosterically bound pppGpp on SAS1 (compare to **3.1.6**). At first glance, the possibility of an effect of pppGpp on the enzymatic activity of SAS1, e.g. as an allosteric activator or inhibitor, must be rejected. In this case major deviations in the progress curves of pppGpp synthesis by SAS1 would have been expected (**Fig. 20**). Nevertheless, the conformational changes of SAS1 in presence of pppGpp render an effectuation of SAS1 by allosteric pppGpp a plausible hypothesis and require further attention.

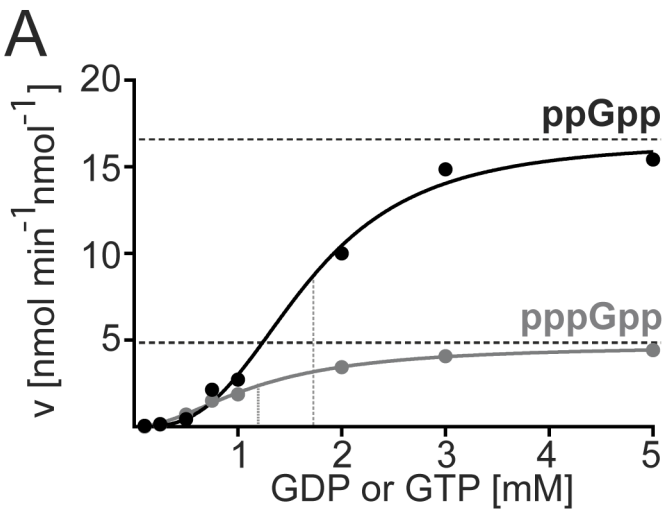

B

SAS1 (p)ppGpp-synthesis

	ppGpp	pppGpp
K_m	1.7 ± 0.1	1.2 ± 0.1
V_{max}	16.9 ± 0.8	4.9 ± 0.3
h	3.0 ± 0.3	2.0 ± 0.1

Figure 21. (p)ppGpp synthesis by SAS1. **A.** v/S characteristic of ppGpp (black) and pppGpp (grey) synthesis by SAS1. The approximate K_m and V_{max} values are indicated by dashed lines. **B.** Kinetic parameters of (p)ppGpp synthesis by SAS1 obtained from **A**. Figure 21A was adapted from ref. (151).

3.2.5. Development of a method for the production of (p)ppGpp in biochemical qualities and quantities

An examination of the influence of pppGpp and ppGpp on the activity of SAS1 requires availability of these nucleotides in biochemical quality and quantity. Unfortunately, while ppGpp was commercially available although with a rather low purity of 85% (TriLink Biotechnologies), pppGpp could not be purchased at all. This necessitated the development or adaptation of a method to produce and purify ppGpp and pppGpp.

To do so, a previously described method for purification of (p)ppGpp was adapted (112). In brief, 5 µM SAS1 were incubated with 10 mM ATP and 10 mM GDP or GTP to produce ppGpp or pppGpp, respectively. Thereafter, SAS1 was removed by precipitation with chloroform and the aqueous phase containing the nucleotides subjected to anion-exchange chromatography (ResourceQ, 6-ml, GE Healthcare). A gradient of NaCl was used for separation of the nucleotides, which elute in increasing order of their number of phosphate moieties allowing for a good separation of ppGpp and pppGpp from all other components in the injected sample, mainly AMP (**Fig. 22**). Although ppGpp and pppGpp elute at different NaCl concentrations of 200 and 220 mM, respectively, both nucleotides are not completely separated. The desired nucleotides were precipitated from the eluted fractions by addition of lithium chloride to a final concentration of 1 M followed by the addition of 4 volume parts of ethanol. The suspension was then incubated at -20 °C for 20 min and centrifuged (5000 x *g*, 20 min, 4 °C). The resulting pellets were washed twice with absolute ethanol, dried and stored at -20 °C. Quality of the so-prepared alarmones was controlled by analytical HPLC and typically yielded ppGpp and pppGpp in purities of 98% and 95%, respectively. The major source of contaminating ppGpp in pppGpp-preparations originates from GDP impurities in the GTP substrate used for synthesis. *Vice versa*, the presence of contaminating GTP in the GDP substrate results in low amounts of contaminating pppGpp in preparations of ppGpp.

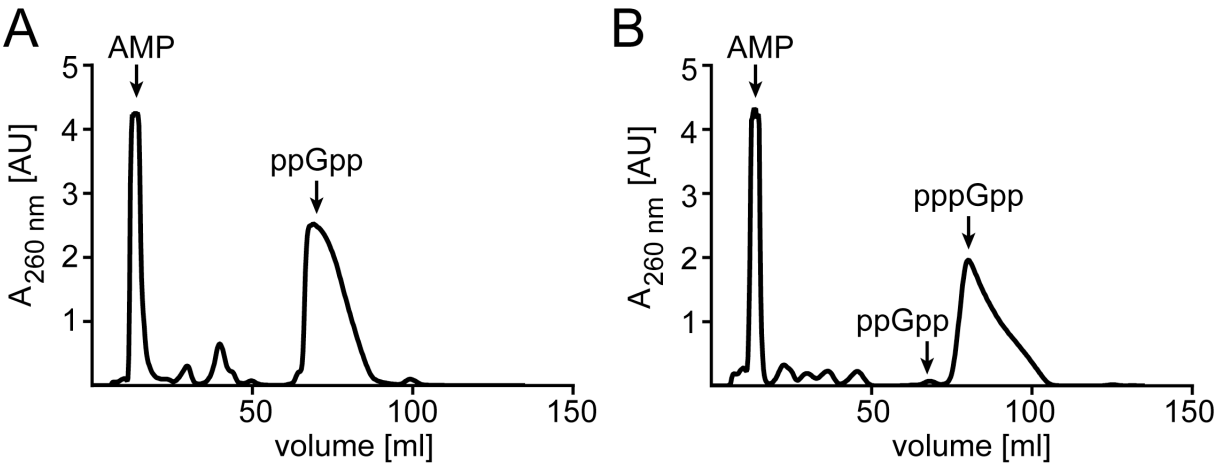

Figure 22. Purification of (p)ppGpp. **A-B.** Exemplary UV chromatograms of the purification of ppGpp (**A**) and pppGpp (**B**) from *in vitro* reactions containing SAS1 and the corresponding substrates. The reaction products of (p)ppGpp synthesis are indicated by arrows.

3.2.6. SAS1 is allosterically regulated by pppGpp but not ppGpp

The presence of pppGpp bound to an allosteric site in the central cleft of the SAS1 homotetramer obscures its functional role. To probe whether pppGpp or ppGpp would effect SAS1, its (p)ppGpp synthetase activity was determined in dependence of increasing amounts of pppGpp or ppGpp (**Fig. 23**). To discriminate between (p)ppGpp produced during the reaction and exogenously added (p)ppGpp, the amount of AMP released equimolar to the alarmone product was quantified. Moreover, the assays were carried out in presence of 0.25 mM GDP or GTP and 5 mM ATP at which (p)ppGpp synthesis by SAS1 proceeds considerably slow (compare to **Fig. 21**) to minimize a possible autoregulatory effect of (p)ppGpp synthesized during the reaction. The synthesis of both alarmones is affected by ppGpp and pppGpp (**Figs. 23A** and **B**). However, while pppGpp does already stimulate the activity of SAS1 by approximately 10-fold at a concentration as low as 12.5 µM, only a mild stimulation is observed in presence of 12.5 µM ppGpp. Even in presence of 250 µM, ppGpp fails to promote a similar stimulatory effect on SAS1's activity as pppGpp (**Fig. 23**).

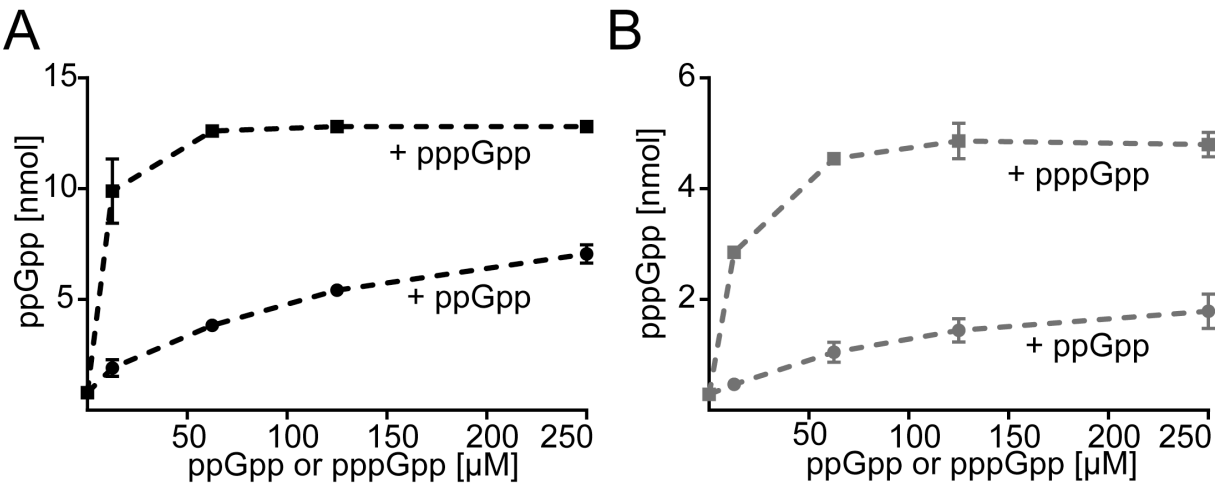

Figure 23. Dose-dependent effect of ppGpp and pppGpp on the (p)ppGpp synthetase activity of SAS1. **A.** The ppGpp synthetic activity of SAS1 is efficiently stimulated by pppGpp (black squares) and moderately stimulated by ppGpp (black circles). **B.** The pppGpp synthetic activity of SAS1 is efficiently stimulated by pppGpp (grey squares) and only moderately stimulated by ppGpp (grey circles). For both experiments, 2 µM SAS1 were incubated with 5 mM ATP, 0.25 mM GDP/GTP and (p)ppGpp as incidated in the figures for 5 min at 37 °C. Data represent the mean ± standard deviation of three independent measurements. The figure originates from ref. (151).

If binding of pppGpp to SAS1 stimulates its (p)ppGpp synthetic activity, it is however not clear whether pppGpp residing in the central cleft of SAS1 does effectuate SAS1 or if pppGpp binding into one of the four active sites of the homotetramer does effect the other active sites. To investigate the influence of pppGpp bound within the central allosteric cleft of SAS1, I measured the (p)ppGpp synthesis of SAS1 variants that should be incapable of pppGpp coordination (i.e. K25A, F42A and N148G, compare to **Fig. 13A**). Although all three variants still form homotetramers (not shown), they are unaffected by the addition of 12.5 µM pppGpp at which the activity of wild type SAS1 is significantly increased (**Fig. 24**). This demonstrates that pppGpp bound into the central cleft of the SAS1 homotetramer serves as an allosteric stimulator of SAS1's activity.

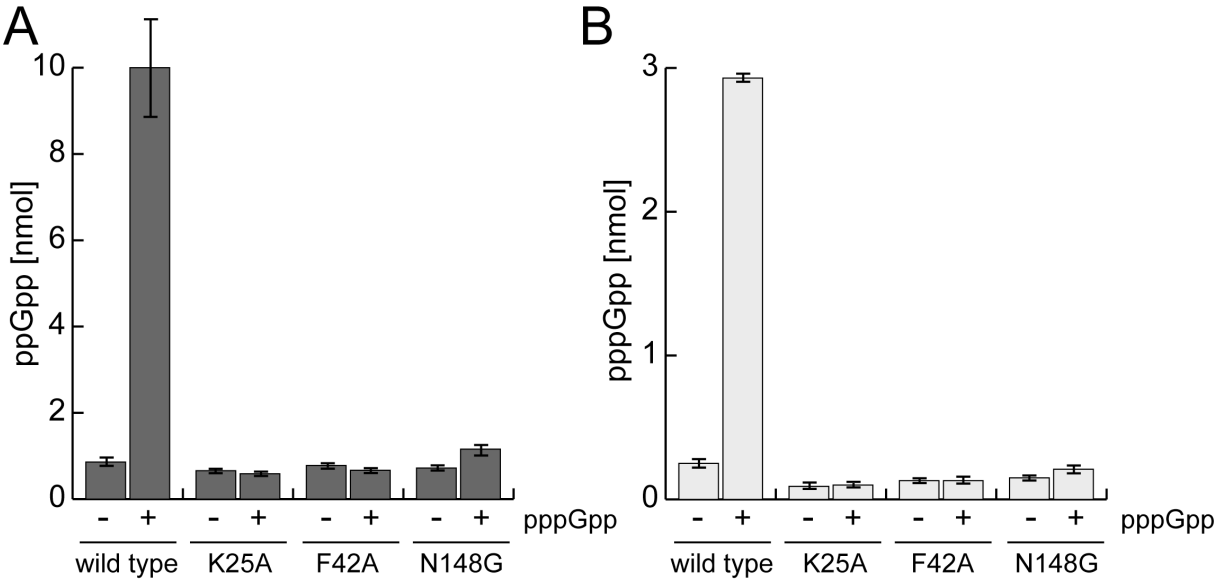

Figure 24. Variations in the allosteric cleft abolish stimulation by pppGpp. **A-B.** Stimulation of ppGpp (**A**) and pppGpp (**B**) synthetase activity of SAS1 and its variants in the presence of pppGpp. For both experiments, 2 µM SAS1 were incubated with 5 mM ATP, 0.25 mM GDP/GTP and 12.5 µM pppGpp where indicated for 5 min at 37 °C. Data represent the mean ± standard deviation of three independent measurements. The figure originates from ref. (151).

The different dose-dependency of ppGpp and pppGpp for stimulation of the (p)ppGpp synthetase activity of SAS1 raises the question why both alarmones differ in their ability to allosterically regulate SAS1. Analysis of pppGpp bound within the allosteric site of SAS1 revealed lysine and arginine residues from two opposing

subunits coordinating the phosphate moieties of pppGpp (compare to **Fig. 13A**). In this, the γ-phosphate moiety of pppGpp establishes contacts with Lys21 and Lys25 of one subunit. Therefore, the absence of a γ-phosphate moiety in ppGpp should allow for weaker binding of ppGpp compared to pppGpp. To investigate the binding of ppGpp and pppGpp to SAS1, I performed an HDX experiment in which the alarmones where added to SAS1 in a concentration of 12.5 µM. At this concentration, only pppGpp was able to efficiently stimulate SAS1 while ppGpp was not (compare to **Fig. 23**). Consistently, reduced hydrogen-deuterium exchange in regions comprising residues involved in coordination of allosteric pppGpp could only be observed in the presence of pppGpp but not in presence of ppGpp (**Fig. 25A**). The disparity in HDX between the pppGpp-bound state of SAS1 and the ppGpp-bound or apo-state even after prolonged deuteration supports the idea that pppGpp in contrast to ppGpp is stronlgy coordinated by SAS1 (**Figs. 25B-D**).

Taken together, these experiments demonstrate that pppGpp acts as a positive effector of SAS1's (p)ppGpp synthetase activity due to its ability to bind the regulatory cleft of the SAS1 homotetramer. The alarmone ppGpp however, although very similar to pppGpp, fails to exert the same regulatory role on the activity of SAS1.

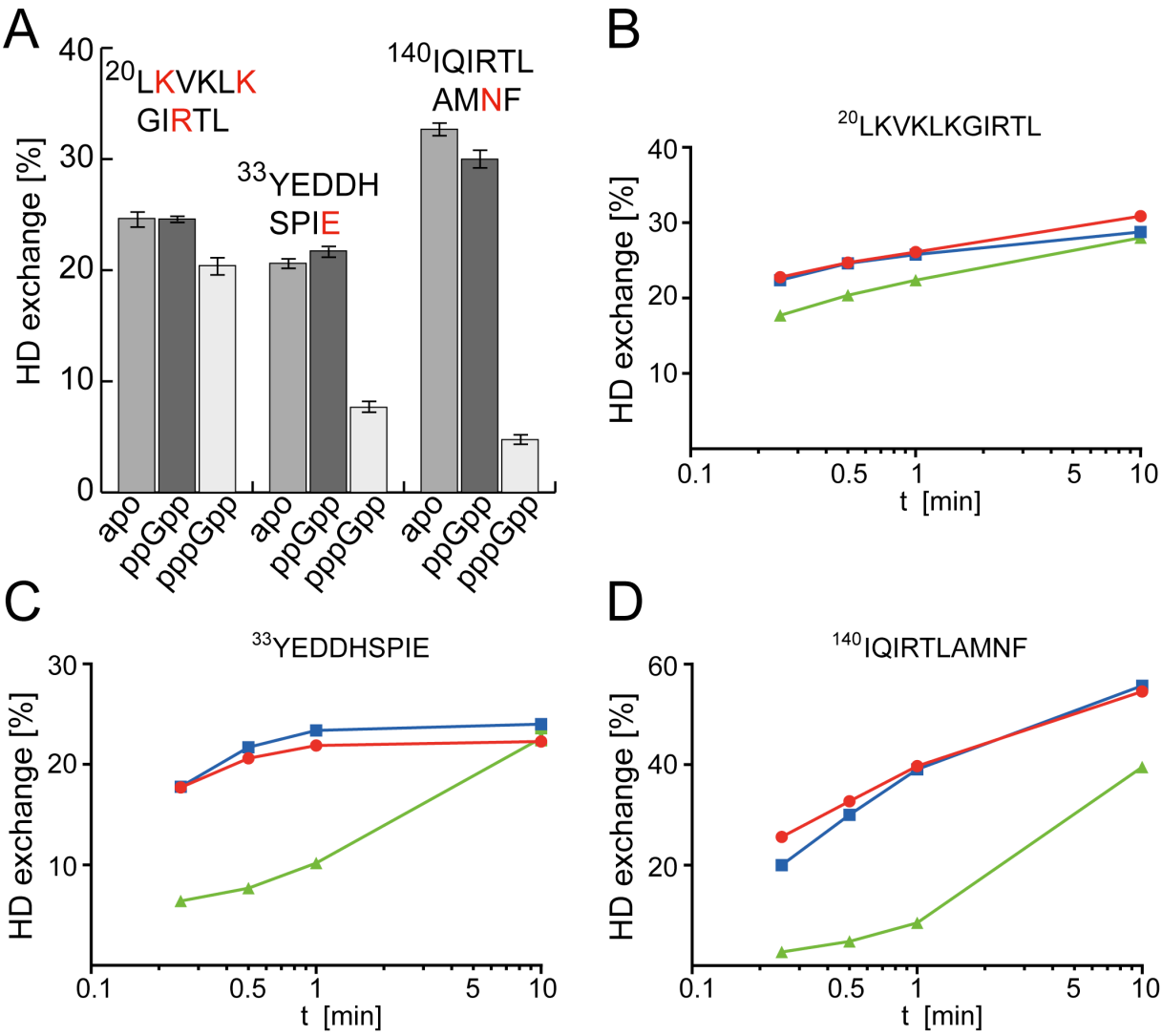

Figure 25. Allosteric binding of pppGpp to SAS1. **A.** Different response of SAS1 to the presence of ppGpp (dark grey bars) and pppGpp (light grey bars) compared to the apo-state (medium grey bars) in HDX after 30 s of deuteration. HD exchange of three representative peptides constituting the allosteric cleft of SAS1 is given in percent. Amino acids conferring binding of pppGpp to SAS1 are shown in red. **B-D.** HDX time course of three representative peptides of SAS1 without nucleotides (red) or in the presence of ppGpp (blue) or pppGpp (green). Data represent the mean ± standard deviation of three independent measurements. Figure 25A originates from ref. (151).

3.2.7 Effect of allosteric regulation by pppGpp on enzyme kinetics of SAS1

The function of pppGpp and to a certain degree also ppGpp as an allosteric stimulator of SAS1 substantiates the possibility that the initial kinetic description of the (p)ppGpp synthetase activity of SAS1 was biased by production of stimulating

(p)ppGpp during the course of the reaction (compare to **Fig. 21**). To further elaborate on this, the ppGpp synthetase activity of an SAS1 variant incapable of pppGpp-binding to its allosteric site (i.e. K25A/F42A) was determined. This variant was drastically impaired in synthesis of ppGpp (**Fig. 26A**) although ppGpp was shown to only mildly stimulate the activity of SAS1. Although SAS1 K25A/F42A was seemingly not disturbed in the assembly of homotetramers (not shown), however, the possibility could not be entirely excluded that this variant was negatively affected in its activity *per se*. Therefore, I determined the ppGpp synthesis of wild type SAS1 in presence of 12.5 µM pppGpp (**Fig. 26A**). While the K_m value is seemingly not altered, the maximal velocity V_{max} is increased ~ 1.5-fold. Moreover, the Hill coefficient (h) of ppGpp synthesis by SAS1 in presence of pppGpp is only 1.8 ± 0.3 in contrast to 3.0 ± 0.1 in the absence of pppGpp (**Fig. 26B**). This suggests that the Hill coefficient and therefore the degree of positive cooperativity of SAS1 was initially slightly overestimated. Nevertheless, even in presence of its allosteric stimulator pppGpp SAS1 - and by this minimizing the influence of stimulating ppGpp generated during the course of the reaction - still seems to display a positive cooperative behavior. The reason for the observed increase of V_{max} in presence of pppGpp is obscure. A plausible hypothesis might rely on the altered location of helix α2 in presence of pppGpp, which might confer a higher enzymatic activity of SAS1 through an increased binding affinity of the substrate ATP to SAS1 (compare to **Figs. 10** and **15**). Finally, although the K_m value of ppGpp synthesis seems to be unaffected by addition of pppGpp, a significant increase in the initial velocities at GDP concentrations below 0.5 mM is apparent (**Fig. 26A**). If binding of GDP would be the rate limiting step of ppGpp synthesis as hinted by the sequential order of substrate binding to SAS1 in presence of 100 µM AMPCPP and/or GDP (compare to **Fig. 16**), then the presence of allosteric pppGpp might stimulate SAS1 activity by simply improving GDP binding through alterations within the G-loop.

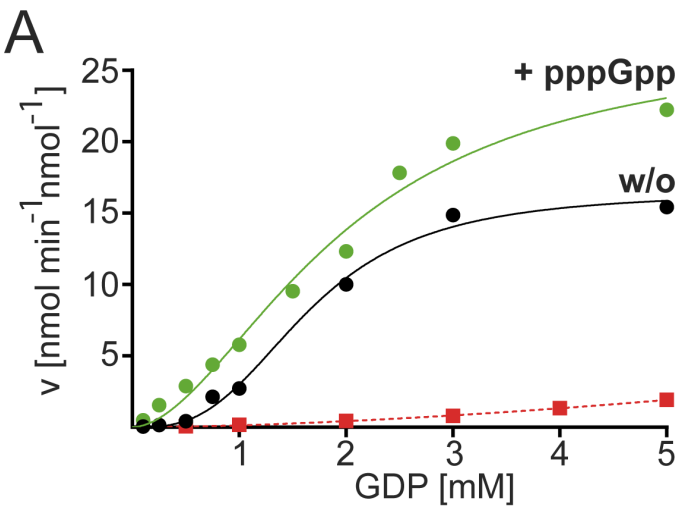

B

SAS1 ppGpp-synthesis

	w/o	+ pppGpp
K_m	1.7 ± 0.1	1.9 ± 0.3
V_{max}	16.9 ± 0.8	27.9 ± 3.1
h	3.0 ± 0.1	1.8 ± 0.3

Figure 26. Influence of allosteric stimulation of SAS1 by pppGpp on kinetics of ppGpp synthesis. **A.** v/S characteristic of ppGpp synthesis by SAS1 in the absence (black solid line) or presence (green solid line) of 12.5 µM pppGpp. ppGpp synthesis by the SAS1 variant K25A/F42A is shown as a red dashed line. **B.** Kinetic parameters of ppGpp synthesis by SAS1 obtained from **A**.

This hypothesis is further evidenced by a significant reduction in hydrogen-deuterium exchange of amino acids in helix α5 (i.e. peptide 'RLQRASE') that reside in close proximity to the G-loop (**Figs. 27A** and **B**). This decrease in HDX is only observable in presence of pppGpp but not ppGpp. Although no reduction in HDX can be observed for the G-loop (i.e. peptide 'YIAEHKESGYRSYHL', **Fig. 27A**), the close proximity of amino acid side chains from α5 and the G-loop is likely to establish interactions between both elements. By these interactions, the G-loop should become more rigid. Noteworthy, the G-loop of SAS2 proteins typically contains one or two proline residues (Fig. 28A) while SAS1 does not. Although these proline residues are not strictly conserved among SAS2 proteins, I tested whether the introduction of proline into the G-loop of SAS1 (i.e. variant H111P, compare to **Fig. 32B**) might affect its (p)ppGpp synthetase activity. Indeed, the H111P variant of SAS1 exhibited a significantly increased production of ppGpp even in the absence of allosterically stimulating pppGpp (**Fig. 27C**).

Taken together this demonstrates that allosteric binding of pppGpp to SAS1 induces major conformational changes affecting the activity of SAS1.

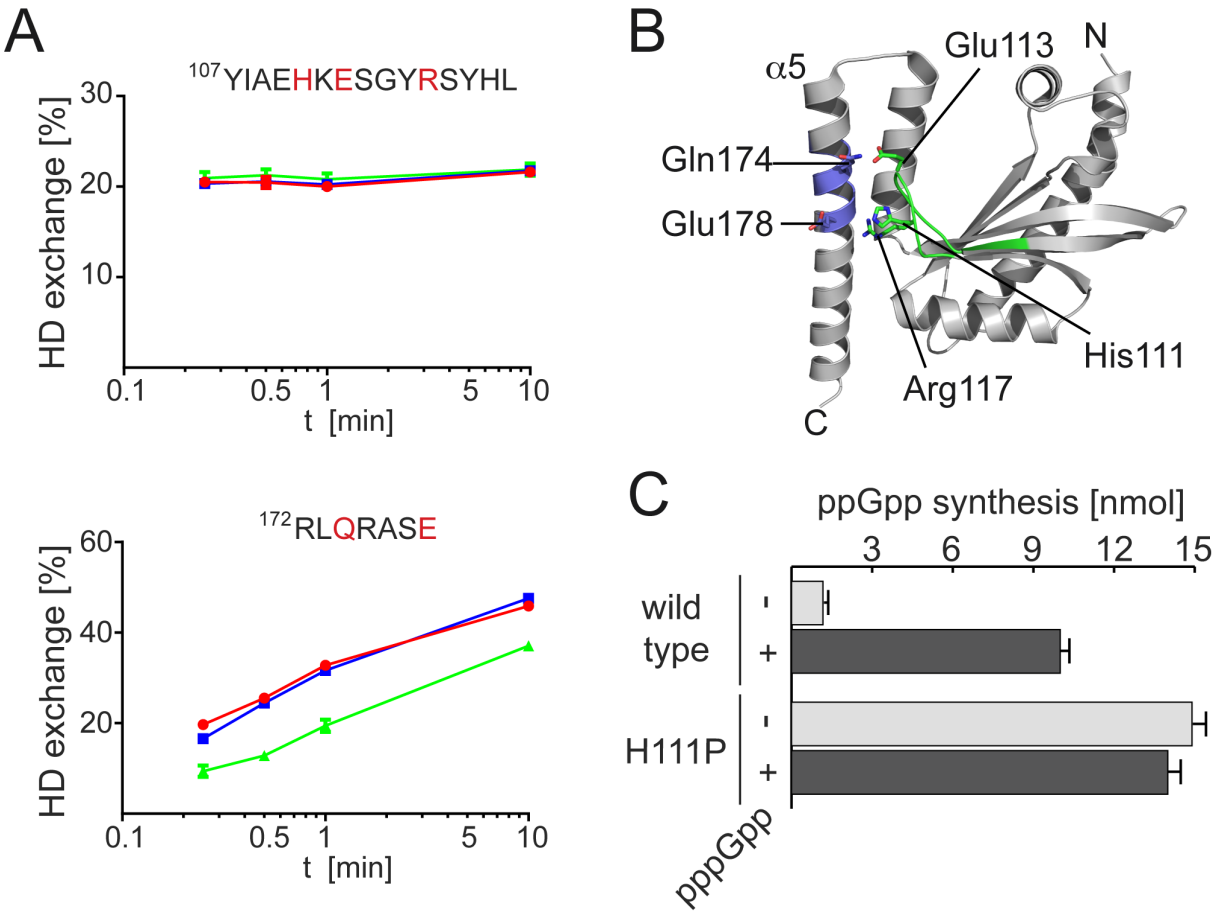

Figure 27. Rigidity of the G-loop influences the activity of SAS1. **A.** HDX time course of two representative peptides of SAS1 in absence (red) or in presence of 12.5 µM ppGpp (blue) or pppGpp (green). Data represent the mean ± standard deviation of three independent measurements. Amino acids appearing in **B** are colored in red. **B.** Location of the peptides in the crystal structure of a SAS1-pppGpp monomer. Amino acids that might mediate interactions between α5 and the G-loop are shown as sticks. **C.** ppGpp synthetase activity of SAS1 and its H111P variant in the absence (grey) and presence (black) of pppGpp. 2 µM SAS1 were incubated with 5 mM ATP, 5 mM GDP and 12.5 µM pppGpp where incidated for 10 min at 37 °C. Data represent the mean ± standard deviation of three independent measurements.

3.3 Structural analysis of SAS2

3.3.1 SAS2 from *S. aureus* forms homotetramers

The presence of two small alarmone synthetases (i.e. SAS1 and SAS2) in members of the firmicutes phylum e.g. *B. subtilis*, *S. aureus* or *L. monocytogenes* raises the question about a possibly disparate physiological relevance for the microorganism.

Although SAS1 and SAS2 homologues often share amino acid identities of 30-40% (**Fig. 28A**) they seem to exhibit different functional roles in the cell (71). For example, transcription of *Bs*SAS1 peaks during logarithmic growth in rich medium while *Bs*SAS2 is mainly transcribed at the transition to stationary phase (57, 72). Moreover, SAS2 but not SAS1 seems to play an important role during ribosome hibernation in both *B. subtilis* and *S. aureus* (72). However, it remained widely unadressed whether these discrepancies are solely based on different transcription and/or translation of the SAS proteins or if also differences in their enzymatic activities would exist.

To gain further insight into the functional properties of SAS2 and compare it with SAS1, the SAS2 orthologs from *B. subtilis* and *S. aureus* were cloned carrying an N-terminal hexa-histidine tag in-frame with the coding sequence of the proteins and heterologously produced in *E. coli* BL21 (DE3) using auto-induction medium. However, while *Sa*SAS2 could be readily obtained after purification using Ni-NTA affinity chromatography, *Bs*SAS2 was completely insoluble after elution from the Ni-NTA matrix under different buffer conditions including e.g. the addition of glycerol and different pH values of the buffers. Therefore, only SaSAS2 could be further purified employing size-exclusion chromatography (SEC). On SEC, SAS2 similarly to SAS1 had an apparent mass corresponding to the size of a homotetramer (**Fig. 28B**). This suggests that the formation of homotetrameric complexes is a common property of SAS1 and SAS2 homologs.

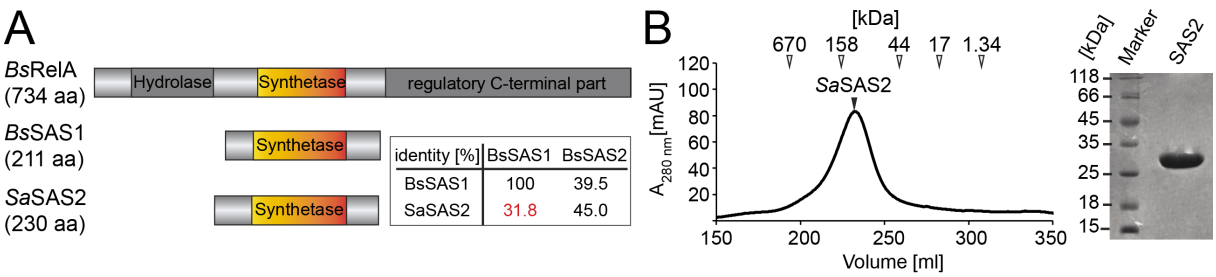

Figure 28. SAS2 from *S. aureus* form homotetramers. **A.** Domain architecture of *Bs*RelA, *Bs*SAS1 and *Sa*SAS2. The (p)ppGpp synthetase domain shared by all three proteins is shown in colors. **B.** Left: Size-exclusion chromatography profile of SAS2. Arrows indicate the molecular mass of the size standard. Right: Coomassie-stained SDS-PAGE of the peak fraction containing SAS2.

3.3.2 Crystal structure of the apo-state of SAS2

Determination of the crystal structure of SAS2 in the apo-state at 2.25 Å resolution (**Table S2**) proofs the suggestion of a tetrameric assembly of SAS2 (**Fig. 29**). SAS2 forms an oval-shaped tetramer with a prominent central cleft. Helices α5 and α6 establish the lateral sides of the homotetramer interface with a buried surface area of ~1200 Å^2, consisting mainly of polar contacts. The medial sides of the homotetramer interface of ~1200 Å^2 is stabilized only by helix α1 via hydrogen bonds and salt bridges. Interestingly, triethylene glycol (PGE) is bound within all four active sites of SAS2 (**Fig. 29**). This PGE molecule should originate from the crystallization condition from which the crystals of SAS2 were obtained (i.e. 0.1 M CHES, pH 9.5 and 40% (w/v) PEG600) and might mark the position of a substrate within the (p)ppGpp synthetase active site of SAS2 (see below).

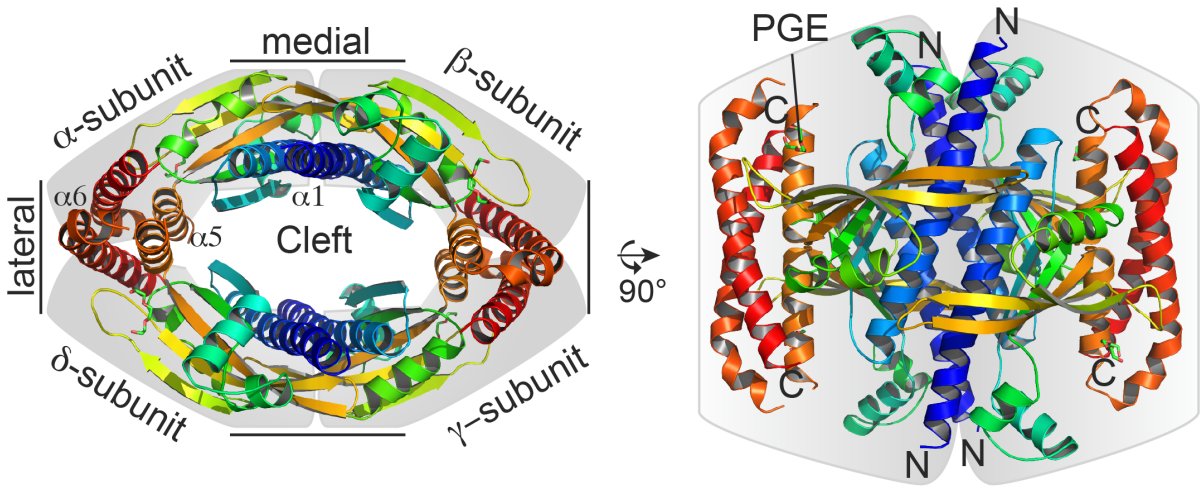

Figure 29. Crystal structure of the tetrameric alarmone synthetase SAS2 in the apo-state. Each monomer (α to δ, indicated by a grey shadow) of SAS2 is shown in cartoon representation colored in rainbow from N- to C-terminus, indicated by 'N' and 'C', respectively. Interfaces on the lateral and medial sides of the complex are indicated by brackets. PGE denotes triethylene glycol residing in the four active sites of SAS2.

At first glance, SAS2 seems to closely resemble the crystal structure of SAS1 (compare to **Fig. 8B**). Shortly, the (p)ppGpp synthetase domain of SAS2 consists of a mixed β-sheet build by five β-strands which is coated by six α-helices. However, close inspection of monomeric subunits as well as the topology of the homotetramer of SAS2 reveals significant differences to SAS1 (**Figs. 30A** and **B**). In SAS2, the G-

loop comprising Tyr151 (Tyr116 in SAS1) and conferring binding of the guanosine substrate within the active site is well-ordered in contrast to the disordered G-loop found in SAS1 (**Fig. 30A,** I). Furthermore, helix α2 comprising residues involved in ATP coordination to SAS proteins is shifted by ~2 Å away from the (p)ppGpp synthetase active site (**Fig. 30A,** II). This movement might at least be partially invoked by the presence of the additional short helix α3 (**Fig. 30A,** III). α3 is able to contact α1 thereby displacing α2. In the context of the tetrameric assembly of SAS2, a slightly altered arrangement of helices α1 and α5/ α6 establishing the medial and lateral interfaces of the complex, respectively, becomes apparent (**Fig. 30B**). As a result, the central cleft of SAS2 is more opened than that of SAS1.

The similar but disparate topology of the single (p)ppGpp synthetase domains and the tetrameric assemblies of SAS2 and SAS1 might imply differences in their enzymatic activity. Indeed, the (p)ppGpp synthetase activity of SAS2 and SAS1 differ (**Fig. 30C**). However, while the synthesis of ppGpp by both enzymes is comparable, SAS2 displays an approximately 2-fold reduced production of pppGpp compared to SAS1 (see **3.2.6**). As SAS1 was shown to be efficiently stimulated by pppGpp, this might suggest that the activity of SAS2 is not stimulated by ppGpp or pppGpp. However, it might also be possible that differences in the active site architectures of both proteins in presence of substrates might result in the different enzymatic activities. Taken together, SAS1 and SAS2 share the same overall structural topology, yet subtle differences in the subunits and homotetrameric assembly might account for their different enzymatic properties and cellular functions and remain to be further elucidated.

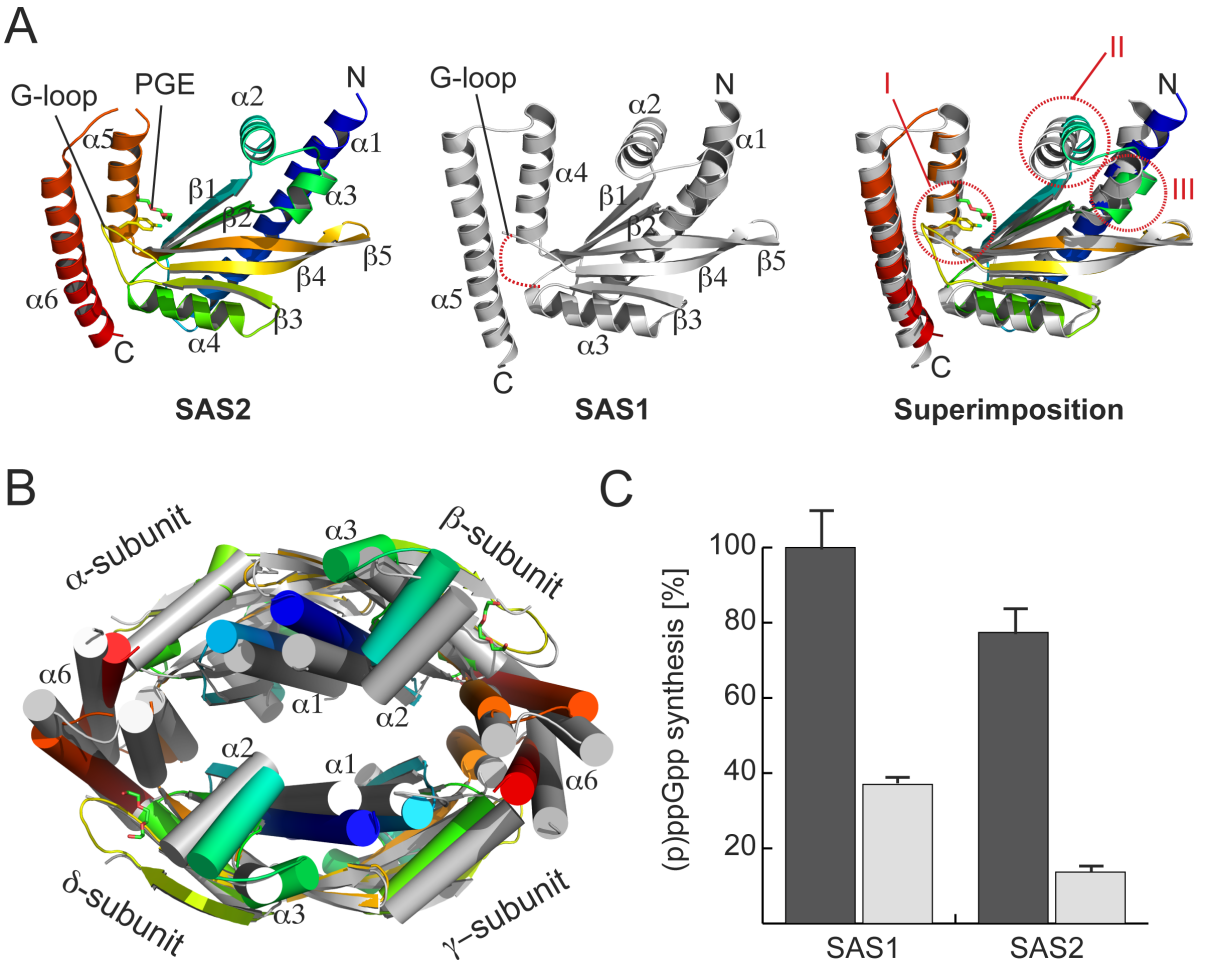

Figure 30. Structural comparison of SAS2 and SAS1 in their apo-states. **A.** Cartoon representation of the crystal structures of monomeric SAS2 (left), SAS1 (middle) and their superimposition (right). SAS2 is colored in rainbow from N- to C-terminus indicated by 'N' and 'C', respectively and SAS1 is shown in grey. Roman numbers depict significant differences between both structures and are further detailed in the text. **B.** Superimposition of the tetrameric assemblies of SAS2 (each monomer colored in rainbow from N- to C-terminus) and SAS1 (grey). **C.** Comparison of the ppGpp (black) and pppGpp (grey) synthetic activities of SAS1 and SAS2. 2 µM SAS1 or SAS2 were incubated with 5 mM ATP and 5 mM GDP/GTP for 10 min at 37 °C. Synthesis of ppGpp by SAS1 was set to 100%. Data represent the mean ± standard deviation of three independent measurements.

3.3.3 Crystal structure of the ATP-bound state of SAS2

SAS2 and SAS1 seem to exhibit differing activities for production of ppGpp and pppGpp (see above). This observation might be based on differences between SAS1 and SAS2 in e.g. binding of the substrates, catalysis or allosteric regulation by pppGpp or any other regulator. To examine whether differences in substrate binding

between both enzymes would occur, I aimed at determining the crystal structure in different substrate-bound states, i.e. ATP-bound (mimicked by AMPCPP) and GDP/GTP-bound state. To do so, SAS2 was incubated together with 5 mM AMPCPP, GDP, GTP or combinations thereof for 30 minutes at 4 °C prior to crystallization experiments. Although crystals for all putative substrate-bound states could be obtained, GDP/GTP-containing crystals only afforded for determination of the structure of SAS2 in the apo-state (see above). As this was also the case for SAS1, this might suggest that the substrates might bind in sequential order and moreover the guanosine substrate with lower affinity than ATP. Crystal for the ATP-bound state of SAS2 were obtained after 2 days from a crystallization condition containing 0.2 M lithium sulfate 0.1 M Tris, pH 8.5, 30% (w/v) PEG4000 and diffracted to 2.9 Å resolution (**Table S2**). Determination of the crystal structure employing apo-SAS2 as a search model for MR revealed the nucleotide AMPCPP bound within all four active sites of SAS2 (**Fig. 31A**). Binding of AMPCPP to the active site of SAS2 does only slightly alter the architecture of the active site (**Fig. 31B**). Differences confer α2, which is displaced by ~2 Å towards the (p)ppGpp synthetase active site. By this, the topology of the AMPCPP-bound state of SAS2 closely resembles that of SAS1 (compare to **Fig. 30A**). Coordination of AMPCPP by SAS2 is guided by π-stacking interactions of the adenine base with the arginine residues 78 and 112 (**Fig. 31C**). The ribose moiety of the adenosine is coordinated by hydrogen bonding via His190. Interactions with the phosphate moieties of AMPCPP are mainly established by lysine and arginine residues residing in β1 and α2 (i.e. Lys80, Lys88 and Arg91) and Ser84 contacting the 5' α–phosphate. The kinked conformation of the nucleotide is enforced by a magnesium ion coordinated by Asp107 and Glu154 (**Fig. 31C**).

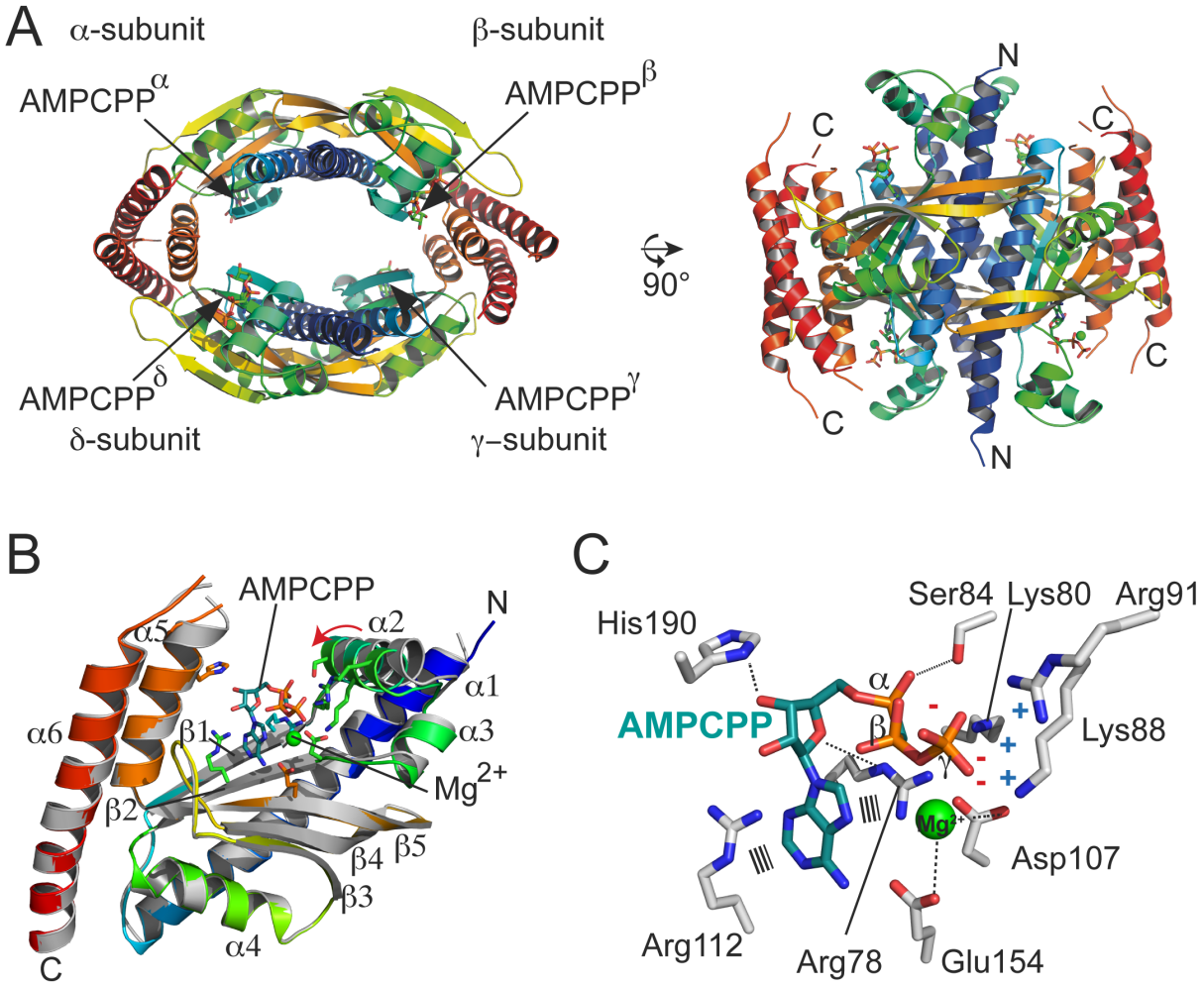

Figure 31. Crystal structure of SAS2 in the ATP-bound state. **A.** Crystal structure of SAS2-AMPCPP. Each monomer (α to δ) of SAS2 is shown in cartoon representation colored in rainbow from N- to C-terminus, indicated by 'N' and 'C', respectively. AMPCPP is shown as sticks. Magnesium is shown as sphere. **B.** Superimposition of a SAS2 monomer colored in rainbow from N- to C-terminus and bound to AMPCPP with apo-SAS2. 'N' and 'C' indicate the N- and C-termini, respectively. Amino acid residues coordinating AMPCPP are shown as sticks. **C.** ATP (mimicked by AMPCPP, deep teal) binds in a tense, U-shaped conformation in the active site of SAS2. Dashed lines indicate interactions between residues of SAS2 and AMPCPP. The magnesium ion is shown as a green sphere.

Identical amino acids shape the binding site for the ATP substrate and confer binding of the ATP-mimic AMPCPP to SAS2 and SAS1 (**Fig. 32A** and compare to **Fig. 10B**). An amino acid sequence alignment of SAS2 and SAS1 proteins from different bacterial species highlights the strict conservation of the ATP-binding site (**Fig. 32B**). Noteworthy, amino acids contributing to ATP coordination located within α2 and α5

of SAS2, i.e. Lys88/Arg91 and His190, respectively are also strictly conserved. These residues were so far not appreciated to contribute to the (p)ppGpp synthetic activity of (p)ppGpp synthetases as they seem to be restricted to SAS proteins and are absent in long RSH-type proteins (compare to **Fig. 8D**). Moreover, helix α2 of SAS1 and SAS2 differs in the relative orientation compared to its counterpart α13 found in long RSH-type protein Rel_{seq} by ~30 ° (compare to **Fig. 10**), thus further suggesting differences in the activities of SAS and long RSH-type proteins.

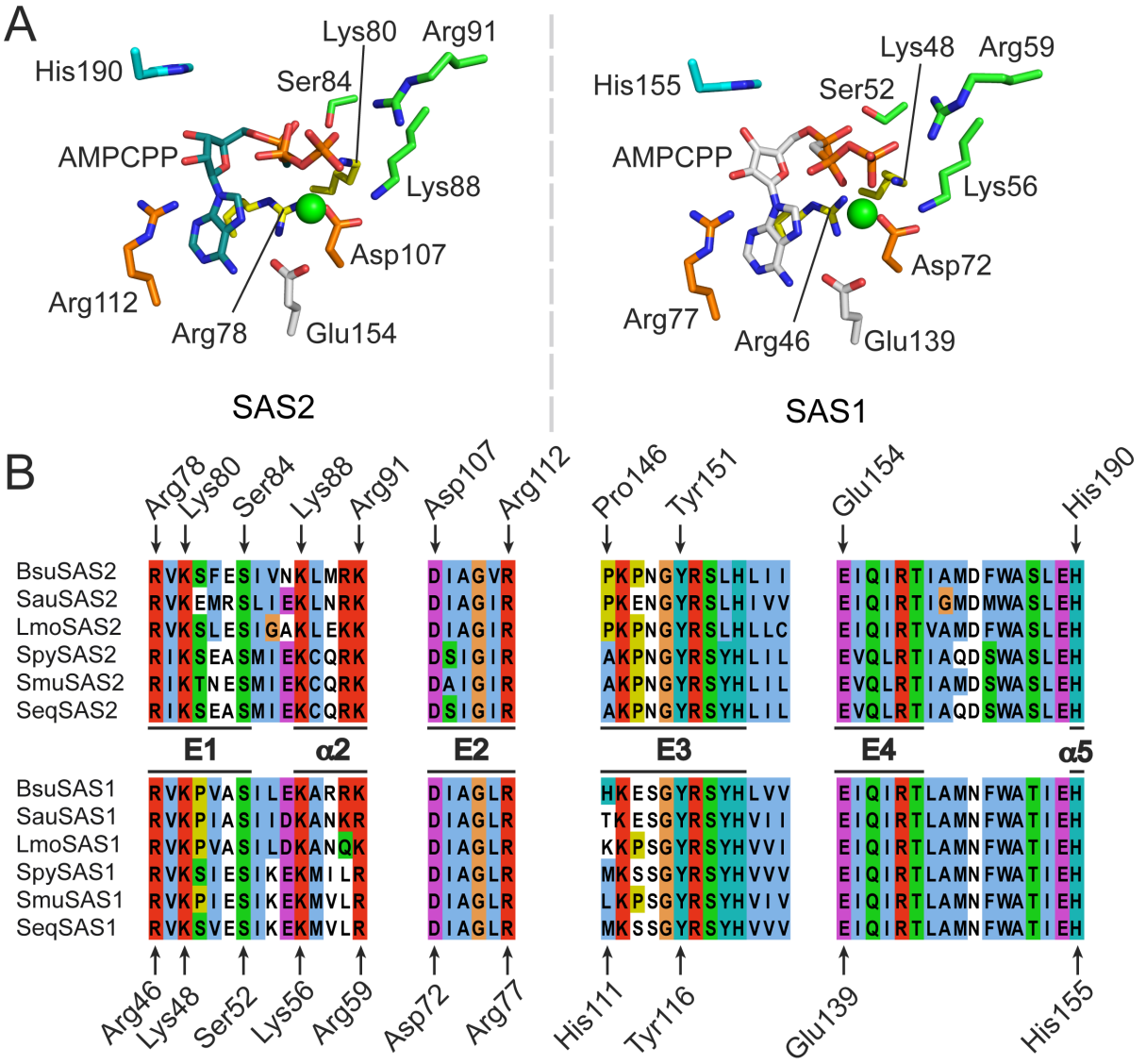

Figure 32. Conservation of ATP-binding to SAS2 and SAS1. **A.** Coordination of the ATP-mimic AMPCPP by SAS2 (left) and SAS1 (right). Amino acid side chains are shown as sticks and colored according to their affiliation to the following (p)ppGpp synthetase motifs: E1 (yellow), E2 (orange) and E4 (white). Residues residing in α2 and α5 of SAS2 are colored in green and cyan, respectively. **B.** Amino acid sequence alignment of SAS2 and SAS1

orthologs from *B. subtilis* (Bsu), *S. aureus* (Sau), *L. monocytogenes* (Lmo), *Streptococcus pyogenes* (Spy), *Streptococcus mutans* (Smu) and *Streptococcus dysgalactiae ssp. equisimilis* (Seq). E1-E4 indicate motifs essential for (p)ppGpp synthesis. Amino acids are numbered according to their position in *Sa*SAS2 and *Bs*SAS1 above and beneath the alignment, respectively.

3.3.4 Crystal structure of the pppGpp-bound state of SAS2

As the coordination of the ATP-substrate to SAS2 is almost identical to that observed in SAS1, the different enzymatic activities of both proteins might be related to variability in GDP/GTP-binding or the absence of allosteric regulation of SAS2 by pppGpp. In order to obtain the crystal structure of SAS2 bound to its product pppGpp, SAS2 was incubated together with 5 mM of ATP and GTP for 30 minutes at 4 °C prior to crystallization. Crystals of SAS2-pppGpp were obtained after 7 days from 0.2 M tri-potassium citrate and 20% (w/v) PEG 3350 and diffracted to 3.3 Å resolution (**Table S2**).

The crystal structure of SAS2-pppGpp reveals the alarmone bound to the four active sites of the homotetramer, however, additional density accounting for pppGpp bound within the central cleft is missing (**Figs. 33A** and **B**). The guanine base of the active site-bound pppGpp is coordinated by π-stacking interactions with Tyr151 and a hydrogen bond provided by Glu189 (**Fig. 33C**). Gln176 establishes contact to the ribose oxygen atom of pppGpp. The 3'-OH phosphate moieties of pppGpp (i.e. δ- and ε-phosphates) interact with the side chains of Arg78, Lys80 and His190. The 5'-OH phosphate groups are coordinated by lysine residues Lys88, Lys92, Lys138, Lys147 and His155. Summarized, this coordination of pppGpp within the active site of SAS2 closely resembles the one found in SAS1 (**Fig. 33C**, compare to **Fig. 12B**). The only difference in coordination of the alarmone product refers to the substitution of Arg105 found in SAS1 by Lys138 in SAS2 interacting with the β-phosphate moiety of pppGpp. It is not clear whether this single substitution can be held responsible for the different enzymatic activities of SAS2 and SAS1.

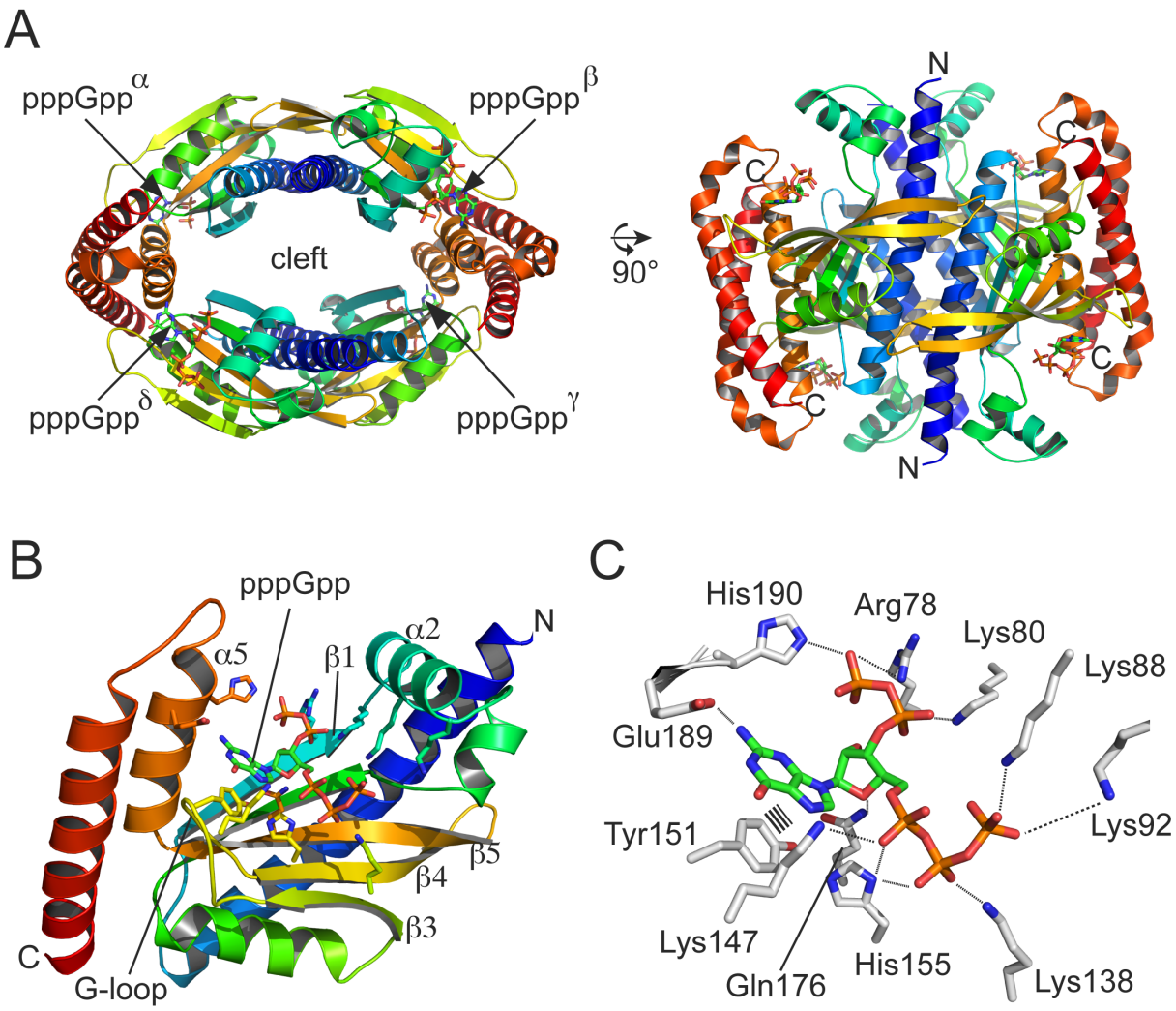

Figure 33. Crystal structure of SAS2 in the pppGpp-bound state. **A.** Crystal structure of SAS2-pppGpp. Each monomer (α to δ) of SAS2 is shown in cartoon representation colored in rainbow from N- to C-terminus, indicated by 'N' and 'C', respectively and pppGpp is shown as sticks. **B.** Cartoon representation of one monomer of SAS2 bound to pppGpp. Residues conferring coordination of pppGpp are shown as sticks. **C.** Coordination of pppGpp by amino acid residues within the active site of SAS2. Dashed lines indicate interactions between residues of SAS2 and pppGpp.

Although SAS2 forms homotetramers like SAS1, its central cleft remains unoccupied in the presence of pppGpp. Comparison of the pppGpp-bound with the apo-state of SAS2 reveals no dramatic conformational changes (**Fig. 34A**, left side). In this, only helix α2 is dislocated by ~ 2 Å towards the active site mainly guided by interaction of Lys88 and Lys92 with the active site-bound pppGpp (**Fig. 33B**). Overlay of the pppGpp-bound states of SAS2 and SAS1 reveals major rearrangements that are

most likely integrated by the allosteric pppGpp bound to SAS1 (**Fig. 34A**, right side). Binding of pppGpp tightened the central cleft of SAS1 by interactions with amino acid residues located in α1, β1 and α5; consequently similar alterations in these structural elements are not observed in SAS2-pppGpp. However, helix α6 of SAS2 (α5 in SAS1) seems to reside closer to the G-loop as its counterpart of SAS1 even in the absence of allosteric pppGpp (**Fig. 34A**). This suggests that SAS2 should more readily allow for binding of the GDP/GTP substrate through the well-ordered G-loop, which in SAS1 is facilitated or at least enforced by allosteric binding of pppGpp (compare to **Fig. 15**).

Inspection of the central cleft explains the inability of SAS2 to coordinate allosteric pppGpp (**Fig. 34B**). Mainly, basic amino acid residues essential for coordination of the 3' and 5' phosphate moieties of pppGpp to SAS1 are replaced in SAS2 (i.e. Ser53, Ser57 and Asp60 instead of Lys21, Lys25 and Arg28; compare to **Fig. 13B**). Moreover, a different set of amino acids is found in β1 (i.e. His73, His74 and Glu76) and α5 (i.e. Asp183) of SAS2 and would therefore preclude pppGpp binding by steric hindrance. To probe the inability of (p)ppGpp to bind to and stimulate SAS2, I determined (p)ppGpp synthesis by SAS2 in absence and presence of 100 µM ppGpp or pppGpp (**Fig. 34C**). Neither of the alarmones resulted in an increased synthesis of (p)ppGpp thereby verifying the inability of (p)ppGpp to bind to the central cleft provided by the SAS2 homotetramer.

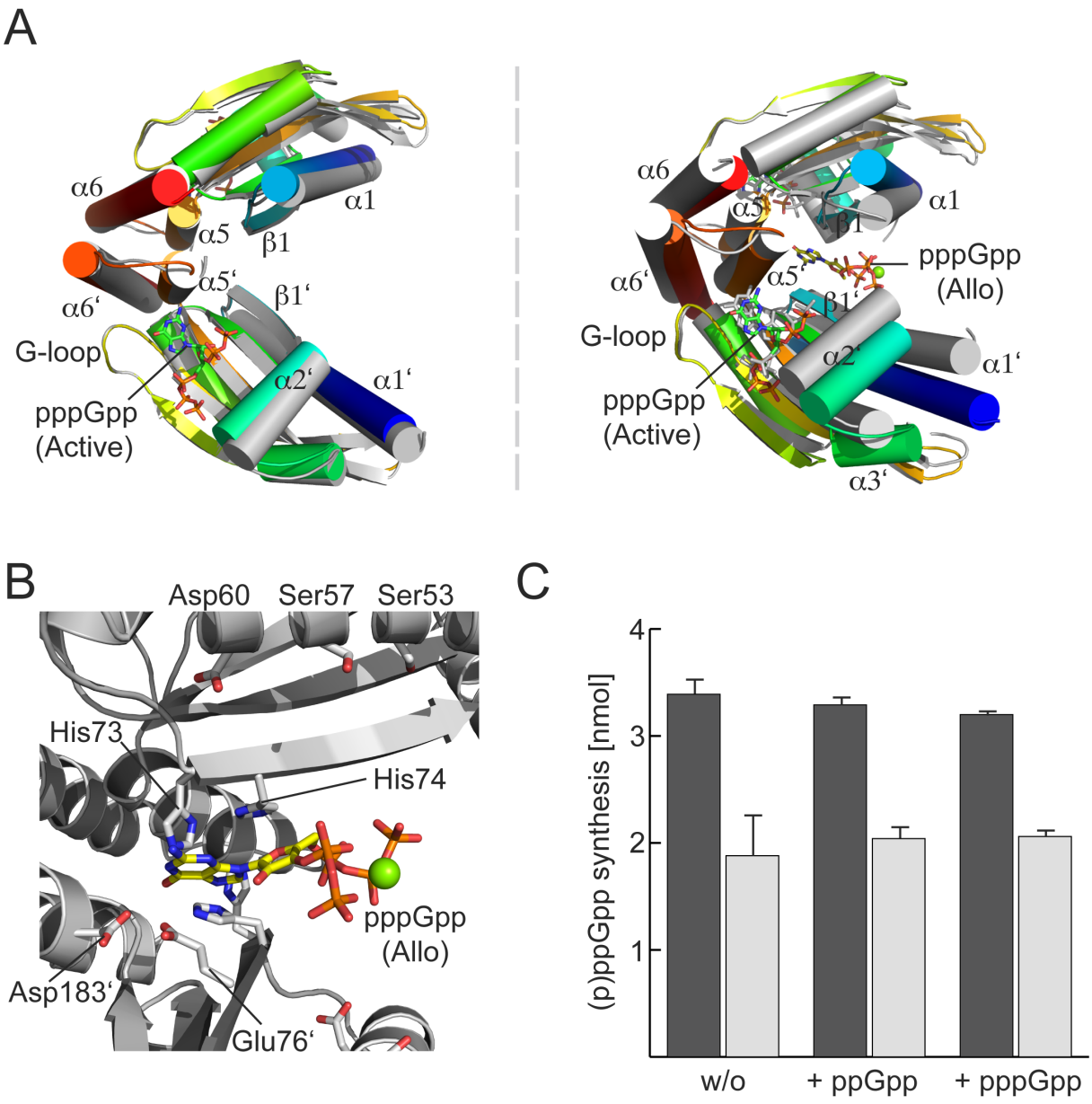

Figure 34. pppGpp does not bind to the central cleft present within the SAS2 homotetramer. **A.** Superimposition of one half of a SAS2-pppGpp homotetramer (each monomer colored in rainbow from N- to C-terminus) with apo-SAS2 (left) or SAS1-pppGpp (right) colored in grey. **B.** View into the central cleft of SAS2. Amino acids corresponding to residues conferring allosteric binding of pppGpp to SAS1 are shown as sticks. For illustration, allosterically-bound pppGpp was derived from a superimposition with the crystal structure of SAS1-pppGpp. **C.** Synthesis of ppGpp (black) or pppGpp (grey) by SAS2 in absence or presence ppGpp or pppGpp. 0.2 µM SAS2 were incubated with 5 mM ATP, 0.25 mM GDP/GTP and 12.5 µM ppGpp or pppGpp where indicated for 5 min at 37 °C. Data represent the mean ± standard deviation of three independent measurements.

3.3.5 Crystal structure of the pGpp-bound state of SAS2

In a recent study, synthesis of another alarmone pGpp by an SAS1 protein from *E. faecalis* was reported (40). Similarly to (p)ppGpp, this pGpp alarmone is synthesized by transfer of pyrophosphate from ATP onto the 3'-OH group of GMP. As (p)ppGpp, this pGpp alarmone mediates similar adaptative processes in the bacterial cell (40).

Therefore, I aimed at elucidate whether also SAS2 would be able to produce pGpp. Moreover, knowing the coordination of pGpp within the active site of SAS2 would allow for a better understanding of the basis for different synthesis of alarmones by SAS proteins. SAS2 was incubated together with 5 mM of ATP and 5 mM GMP at 4 °C for 30 minutes prior to crystallization. Crystals of SAS2-pGpp were obtained after three days from 0.2 M tri-potassium citrate and 20% (w/v) PEG 3350 and the crystal structure solved by MR employing apo-SAS2 at a resolution of 3.23 Å (**Table S2**).

In this structure, the alarmone occupied all four active sites of SAS2 thereby demonstrating that SAS2 is able to synthesize pGpp (**Fig. 35A**). pGpp was found in the same location within the (p)ppGpp synthetase active site of one SAS2 monomer as the pppGpp alarmone (**Fig. 35B**, compare to **Fig. 33B**) and the same amino acid residues of SAS2 are conferring pGpp coordination (**Fig. 35C**, compare to **Fig. 33C**). However, due to the absence of the 5'-OH β- and γ-phosphate moieties in pGpp, lysine residues 88, 92 and 138 due not contribute to coordination of pGpp (**Fig. 35C**). This suggests that the pGpp alarmone should bind with weaker affinity to SAS2 than pppGpp. However, also the GMP substrate should therefore bind less affine to SAS2 than GTP. It can therefore not be inferred from the crystal structure alone, whether synthesis of pGpp from GMP or pppGpp from GTP would be preferred or if both reactions are catalysed with equal efficiency. Nevertheless, that SAS2 - as previously shown for SAS1 - is an active pGpp synthetase is evidenced from the presence of the alarmone in the crystal structure.

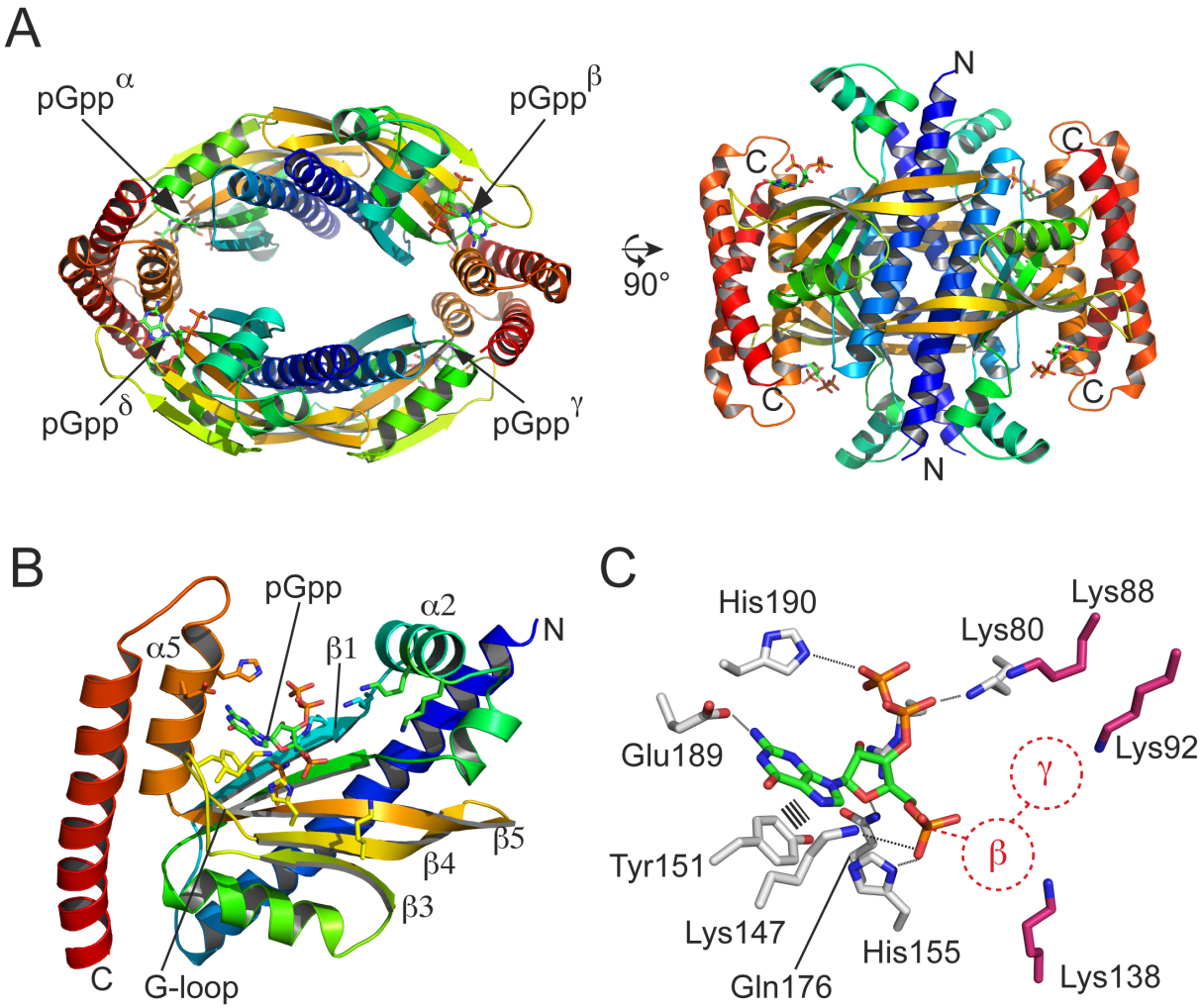

Figure 35. Crystal structure of SAS2 in the pGpp-bound state. **A.** Crystal structure of SAS2-pGpp. Each monomer (α to δ) of SAS2 is shown in cartoon representation colored in rainbow from N- to C-terminus, indicated by 'N' and 'C', respectively and pGpp is shown as sticks. **B.** Cartoon representation of one monomer of SAS2 bound to pGpp. Residues conferring coordination ofppGpp are shown as sticks. **C.** Coordination of pGpp by amino acid residues within the active site of SAS2. Dashed lines indicate interactions between residues of SAS2 and pGpp. 'β' and 'γ' denote the location of 5'-OH β– and γ-phosphate moieties absent in pGpp. Lysine residues that would coordinate the β– and γ-phosphates are colored in violet.

3.4 Catalytic mechanism and regulation of SAS2

3.4.1 Enzyme kinetic analysis of SAS2

Comparison of the crystal structures of SAS2 and SAS1 in different nucleotide-bound states revealed similarities but also highlighted critical differences between both proteins. Mainly, while the mode of ATP coordination to both proteins seems to be identical differences in conformation of the GDP/GTP-coordinating G-loop are apparent (compare to **Figs. 32** and **30A**). Moreover, SAS2 in contrast to SAS1 does not bind pppGpp within the central cleft of the homotetramer. These structural differences might translate into different kinetics of ppGpp and pppGpp synthesis by SAS2 and SAS1.

Kinetic analysis of SAS2's (p)ppGpp synthetase activity was carried out similar to SAS1 (compare to and chapters **3.2.3** and **3.2.4**) with two modifications: *i.*) The higher velocity of SAS2 at low GDP/GTP concentrations necessitated to use only 0.2 µM SAS2 in contrast to 2 µM SAS1 (see chapter **3.2.4**) in order to obtain the activity under substrate-saturating conditions and *ii.*) The enzymatic reactions were stopped by the combined use of chloroform and heat treatment to inactivate the protein (see below). In brief, 0.2 µM SAS2 were incubated together with 5 mM ATP and varying concentrations of GDP or GTP in modified SEC buffer (100 mM HEPES-Na, pH 7.5, 200 mM NaCl, 20 mM $MgCl_2$, 20 mM KCl) at 37 °C. Samples were taken after 2/4/6/8/10 min and mixed with two volume parts of chloroform for 30 s. This mixture was subsequently kept at 95 °C for 30 s before freezing in liquid nitrogen. While thawing, the mixture was centrifuged (17300 x *g*, 30 min, 4 °C) and the aqueous phase containing the nucleotides analyzed by RP-HPLC. The extraction and heating step results in an efficient removal of the protein yet does not affect the nucleotides present in the sample.

The velocities of (p)ppGpp synthesis by SAS2 were obtained from the slope of the linear regression of (p)ppGpp quantified at different time points and plotted against the concentration of GDP/GTP (**Fig. 36A**). The resulting v/S curve was obtained using the equation $v = V_{max} S^h/(K_m^h + S^h)$.

As SAS1, SAS2 preferentially synthesizes ppGpp more efficient than pppGpp as evidenced from an approximately 4-fold difference in the V_{max} values (i.e. 17.9 ± 1.1 and 4.5 ± 0.3 nmol min^{-1} $nmol^{-1}$ SAS2 for ppGpp and pppGpp, respectively) (**Fig. 36B**). SAS2 might exhibit a low degree of positive cooperativity exemplified by Hill coefficients of 1.3 ± 0.4 and 1.9 ± 0.5 for production of ppGpp and pppGpp, respectively, which is much less pronounced than in SAS1 (compare to **Fig. 21B**). In comparison the SAS1, the K_m values of SAS2 for both reactions are significantly lower (i.e. 0.4 ± 0.1 for GDP and 0.1 ± 0.1 for GTP) (compare to **Fig. 21B**). This observation is in good agreement with the presumption that the different conformation of the G-loop found in SAS2 and SAS1 might relate to differences in GDP/GTP-coordination.

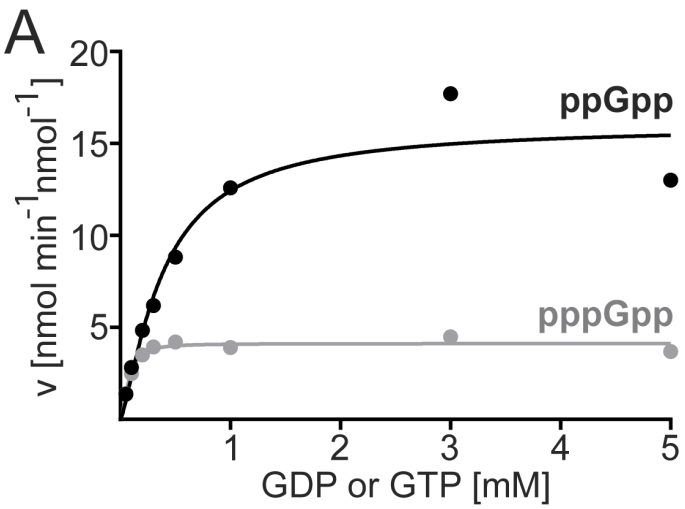

B

SAS2 (p)ppGpp-synthesis

	ppGpp	pppGpp
K_m	0.4 ± 0.1	0.1 ± 0.1
V_{max}	17.9 ± 1.1	4.5 ± 0.3
h	1.3 ± 0.4	1.9 ± 0.5

Figure 36. (p)ppGpp synthesis by SAS2. **A.** v/S characteristic of ppGpp (black) and pppGpp (grey) synthesis by SAS2. **B.** Kinetic parameters of (p)ppGpp synthesis by SAS2 obtained from **A**.

The high velocity of product formation by SAS2 at low GDP/GTP concentrations necessitated the use of a lower enzyme concentration (i.e. 0.2 µM) in contrast to 2 µM applied for the kinetic description of SAS1. To directly compare the kinetic parameters of (p)ppGpp synthesis exhibited by SAS1 and SAS2, pppGpp synthesis by different amounts of SAS2 was examined. Between 0.2 and 2 µM SAS2, alarmone product formation correlates directly proportional with enzyme concentration (**Fig. 37**). Therefore, it is possible to note that the maximal velocities of ppGpp and pppGpp synthesis by SAS2 and SAS1 are similar. This might further suggest that (p)ppGpp synthesis by both proteins in principle proceeds in the same

manner and most differences observed in the crystal structures of both proteins relate to a disparity in allosteric regulation.

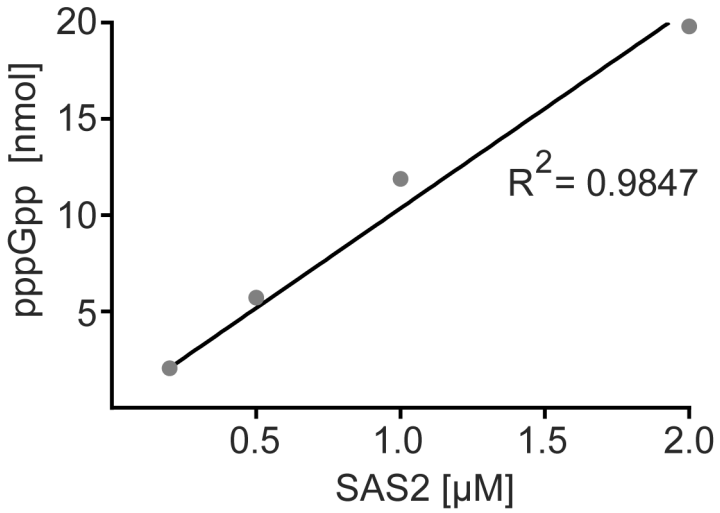

Figure 37. pppGpp synthesis by SAS2 is directly proportional to enzyme concentration between 0.2 and 2 µM SAS2. The R^2 value indicates the goodnees of the linear fit.

3.4.2 Regulation of SAS2 by various small molecules and metal ions

Based on the similar homotetrameric assembly of SAS2 and SAS1, I assumed that also SAS2 might be subject to regulation through allosteric binding of an effector within its central cleft. As SAS2 is thought to be involved in translating cell wall stress stimuli e.g. acidic and basic pH values, ethanol stress or cell wall-acting antibiotics into (p)ppGpp synthesis (57, 71, 73, 74), nucleotide second-messengers involved mediating cell wall stresses were plausible target molecules worth testing for their property to regulate the activity of SAS2. Additionally, I examined nucleotides involved in GTP biosynthesis via the salvage-pathway (compare to **Fig. 6**) for the same reason.

The effect of these target molecules was assessed by determining the pppGpp synthetase activity of SAS2 in presence of 100 µM of putative effector molecule. However, none of the molecules tested showed a pronounced effect on the activity of SAS2 (**Fig. 38**). Nevertheless, it cannot be ruled out than any other small molecule might regulate SAS2.

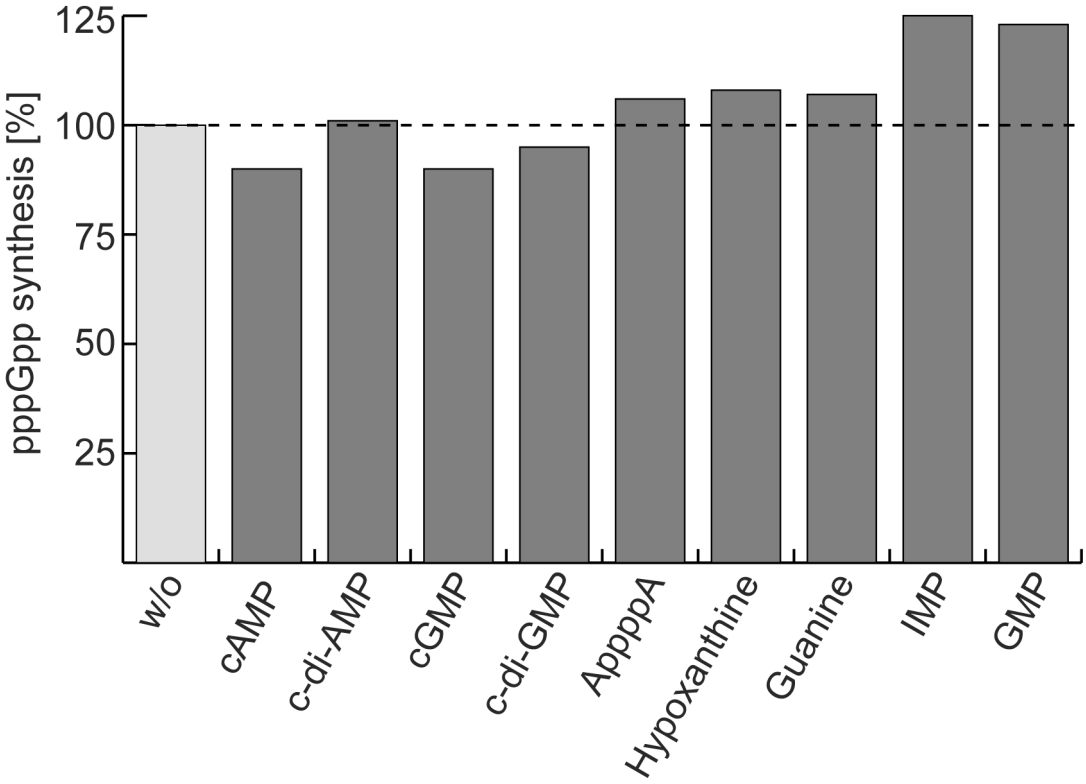

Figure 38. pppGpp synthesis by SAS2 is not affected by the presence of several nucleotide second-messengers and nucleotides. 2 µM SAS2 were incubated with 5 mM ATP, 5 mM GTP and 100 µM of the indicated effectors for 5 min at 37 °C. Synthesis of pppGpp by SAS2 in absence of an effector was set to 100%.

Closer inspection of the putative allosteric cleft of SAS2 revealed an eye-catching arrangement of histidine residues (i.e. His73 and His74) surrounded by two negatively charged amino acids (i.e. Glu76 and Asp183), which can seemingly only be established in the context of the SAS2 homotetramer (**Fig. 39A**). An amino acid sequence alignment of SAS2 and SAS1 orthologs revealed that these residues are partially conserved among SAS2 proteins (compare to **Fig. 13B**). In this, His74 and Asp183 of SAS2 relate to Phe42 and Asn148, which are essential for coordination of pppGpp to SAS1. As such pockets are typically found in metal-coordinating proteins (160), I tested an effect of the addition of various metal ions on the activity of SAS2. In the presence of 100 µM $ZnCl_2$ and $NiSO_4$ the pppGpp synthetase activity of SAS2 increased approximately 8-fold and 3-fold, respectively (**Fig. 39B**). The addition of $FeSO_4$, $FeCl_3$ and $MnCl_2$ failed to result in a similar stimulation. Therefore, zinc ions are the most likely allosteric regulator of the activity of SAS2.

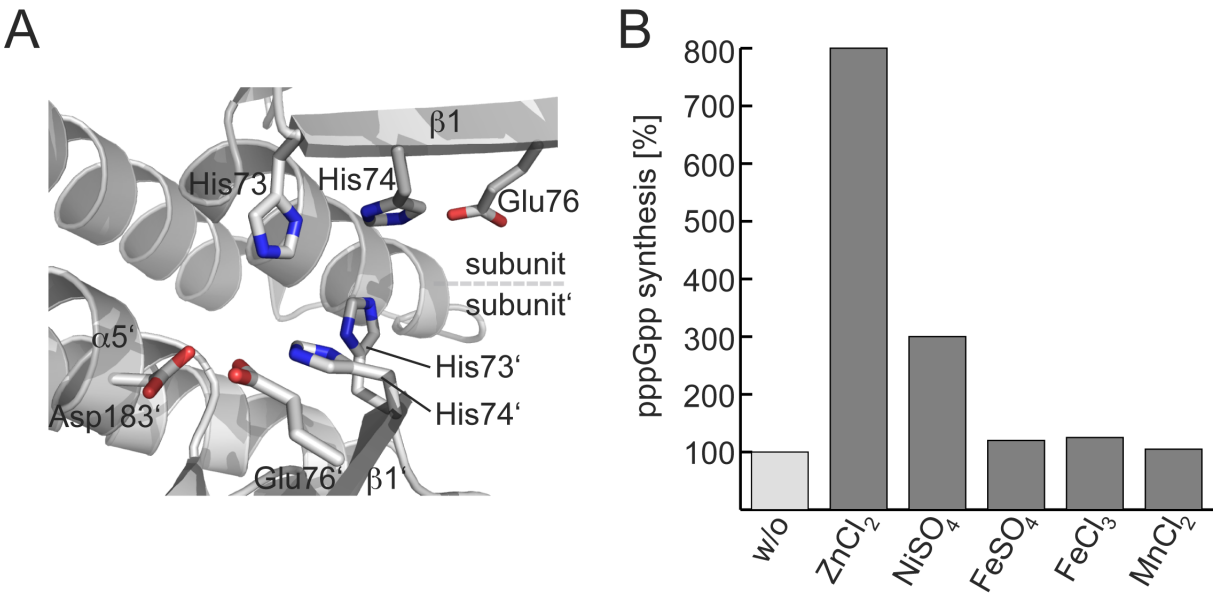

Figure 39. pppGpp synthesis by SAS2 is stimulated by presence of zinc and nickel ions. **A.** Residues from two subunits shape the central cleft of SAS2 and might provide a binding site for zinc. **B.** pppGpp synthesis by SAS2 in the presence of various metal ions in form of the indicated salts. 2 µM SAS2 were incubated with 5 mM ATP, 5 mM GTP and 100 µM of the indicated salts for 5 min at 37 °C. Synthesis of pppGpp by SAS2 in absence of ions was set to 100%.

3.4.3 SAS2 activity is regulated by Zn^{2+} in a dose-dependent manner

To further examinate the influence of zinc ions on the activity of SAS2 I measured the pppGpp and ppGpp synthetic activity of SAS2 in presence of increasing concentrations of $ZnCl_2$ (i.e. 0, 0.2, 2, 10, 25 µM). Interestingly, $ZnCl_2$ efficiently stimulated the production of pppGpp while synthesis of the ppGpp product was almost unaffected (**Fig. 40A**). To exclude the possibility that zinc ions might alter (p)ppGpp synthesis by SAS proteins *per se*, the same experiment was carried out employing SAS1 thereby serving as a negative control. In this, the (p)ppGpp synthetase activity of SAS1 was not stimulated by increasing concentrations of $ZnCl_2$ (**Fig. 40B**) thus substantiating the assumption that zinc ions stimulate the activity of SAS2. Noteworthy, however, seemingly only synthesis of pppGpp by SAS2 is stimulated upon addition of $ZnCl_2$ while production of ppGpp is not. This contrasts the stimulatory effect exhibited by pppGpp on the activity of SAS1 where the production of both ppGpp and pppGpp were efficiently stimulated by similar degree (compare to **Fig. 23**).

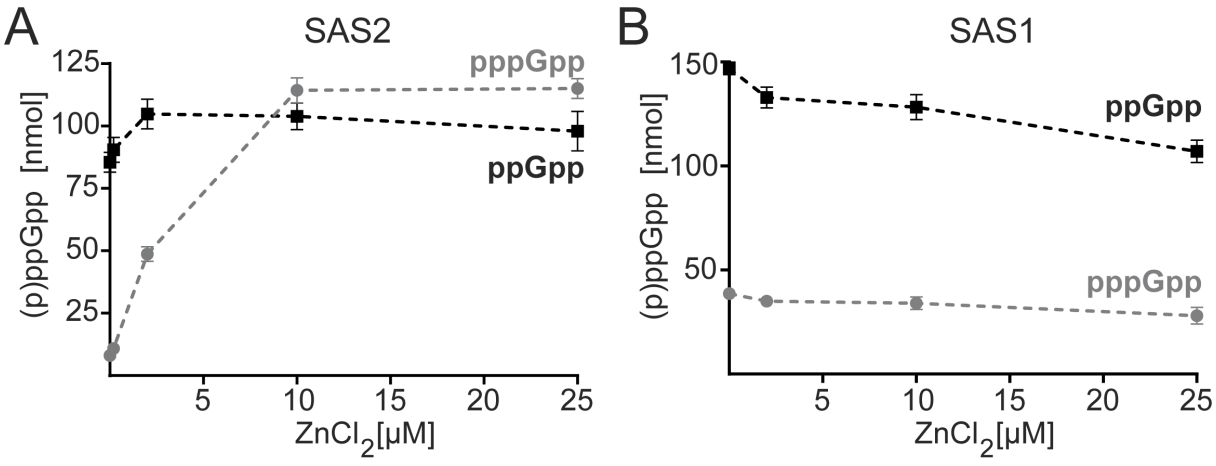

Figure 40. Zinc ions affect activity of SAS2 but not SAS1. **A.** The pppGpp synthetic activity of SAS2 (grey) is efficiently stimulated by $ZnCl_2$ in a dose-dependent manner while ppGpp synthesis (black) is unaffected **B.** The (p)ppGpp synthetic activity of SAS1 is not affected by zinc ions. For both experiments, 2 µM enzyme were incubated with 5 mM ATP, 5 mM GDP/GTP and $ZnCl_2$ as indicated for 5 min at 37 °C. Data represent the mean ± standard deviation of three independent measurements.

The experiments adhering to the dose-dependent stimulation of SAS2 by zinc ions were carried out in presence of 5 mM GTP (see above) at which pppGpp synthesis proceeds with maximal velocity (compare to **Fig. 36A**). This already suggests that Zn^{2+} should rather affect the V_{max} than K_m of pppGpp synthesis. An examination of the enzyme kinetics of ppGpp and pppGpp synthesis by SAS2 in presence of 20 µM $ZnCl_2$ provides proof for this assumption (**Fig. 41A**). The K_m values for both reactions are not altered by the addition of $ZnCl_2$ (**Fig. 41B**). Also, both v/S characteristics display similar Hill coefficients in absence and presence of $ZnCl_2$. However, the maximal velocities differ significantly for production of pppGpp (i.e. 4.5 ± 0.3 in absence versus 16.0 ± 0.6 in presence of $ZnCl_2$) and only slightly for production of ppGpp (i.e. 17.9 ± 1.1 in absence versus 19.2 ± 1.1 in presence of $ZnCl_2$ (**Fig. 41B**)). This substantiates that only pppGpp synthesis of SAS2 is affected by zinc ions.

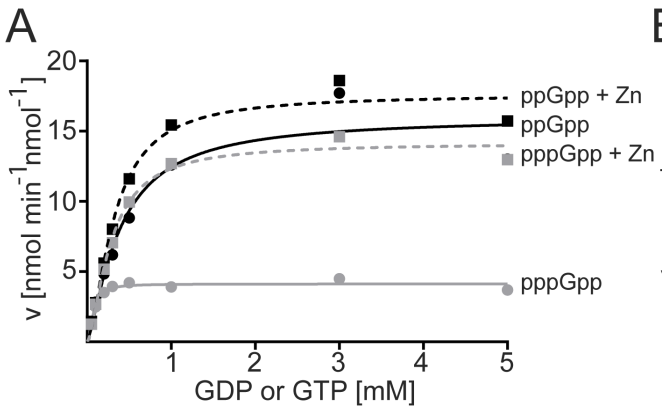

B

Zn-dependent SAS2 (p)ppGpp-synthesis

	ppGpp		pppGpp	
	w/o	+Zn^{2+}	w/o	+Zn^{2+}
K_m	0.4 ± 0.1	0.3 ± 0.1	0.1 ± 0.1	0.3 ± 0.1
V_{max}	17.9±1.1	19.2±1.1	4.5 ± 0.3	16.0 ± 0.6
h	1.3 ± 0.4	1.6 ± 0.3	1.9 ± 0.5	1.5 ± 0.2

Figure 41. Influence of zinc ions on (p)ppGpp synthesis by SAS2. **A.** v/S characteristic of ppGpp (black) and pppGpp (grey) synthesis by SAS2. Solid and dashed lines indicate velocities in absence and presence of $ZnCl_2$, respectively. **B.** Kinetic parameters of zinc-dependent (p)ppGpp synthesis by SAS2 obtained from **A**.

3.4.4 Attempts to identify the zinc-binding site on SAS2

To better understand how zinc ions stimulate the pppGpp synthetic activity of SAS2, I aimed at determining the zinc-binding site on the protein. At first, variants of SAS2 harboring mutations within the putative allosteric cleft of SAS2 (i.e. H73A, H74A, E76A and D183A, compare to **Fig. 39A**) were tested for their ability to be stimulated by $ZnCl_2$. All variants could be readily obtained and appeared as homotetramers on SEC (not shown), Nevertheless, determination of ppGpp synthesis by these variants served as negative control for their functionality.

The pppGpp synthetic activity of the H73A, H74A and D183A variant of SAS2 was not stimulated by the addition of 20 µM $ZnCl_2$ (**Fig. 42**). However, these variants were also drastically impaired in their ability to produce ppGpp. It therefore remains unclear whether the substituted amino acids contribute to zinc-binding. The E76A variant of SAS2 exhibited a similar activity as the wild type protein by this excluding a contribution of this residue for coordination of zinc ions to SAS2 (**Fig. 42**).

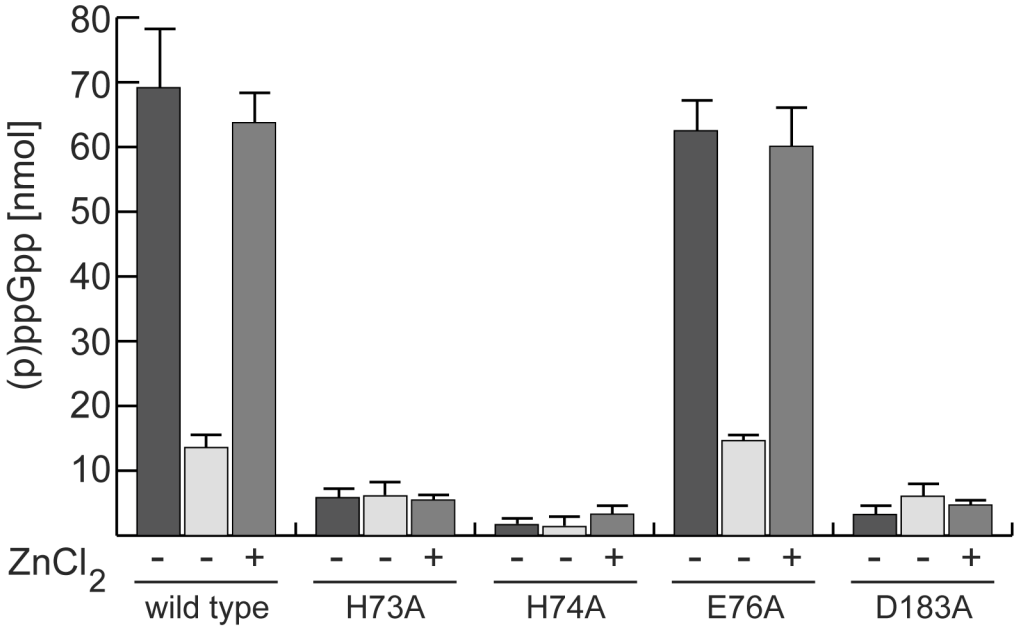

Figure 42. (p)ppGpp synthetic activity of SAS2 putative allosteric site variants. Production of ppGpp (dark grey) in absence of $ZnCl_2$ and production of pppGpp in absence (white) or presence of $ZnCl_2$ (light grey) are shown. 2 µM SAS2 or its variants were incubated with 5 mM ATP, 5 mM GDP/GTP and 20 µM $ZnCl_2$ where indicated for 5 min at 37 °C. Data represent the mean ± standard deviation of three independent measurements.

As the putative allosteric site located in the central cleft might possibly be uninvolved in coordination of the stimulating zinc ion (see above), more variants of SAS2 were investigated for their ability to be stimulated by $ZnCl_2$. The varied amino acids reside in α2 (i.e. Arg91 and Lys92), β3 (i.e. Lys138), the G-loop (i.e. Tyr142) and β4 (i.e. His155) and are involved in binding of or in close proximity to pppGpp residing in the active site of SAS2 (compare to **Fig. 33**). Even if these residues might not confer coordination of zinc to SAS2, they might provide an insight into the preferential stimulation of the synthesis of pppGpp.

None of the investigated variants was devoid of zinc-dependent stimulation of pppGpp synthesis (**Fig. 43**). However, the observed differences in the degree of stimulation might shed a light on the implication of Lys92 and His155 in mediation of the zinc-derived stimulation of SAS2. His155 coordinates the α- and β-phosphates of pppGpp in the active site of SAS2 while Lys92 and to very low degree also Arg91 only establish interactions with the γ-phosphate of pppGpp (**Fig. 33C**). As the presence of these residues is not a prerequisite for stimulation – and their absence rather enforces stimulation – possibly an interaction of Zn^{2+} with the substrate GTP or

the product pppGpp itself sets the stage for stimulation of SAS2's pppGpp synthetase activity.

This indirect mode of stimulation might be supported be the observation that neither cocrystallization experiments nor HDX employing SAS2 together with $ZnCl_2$ provided any insights into a zinc-coordination by the protein. However, both methods could also be hampered by a low binding affinity of Zn^{2+} to SAS2 or in case of HDX the small size of the ligand.

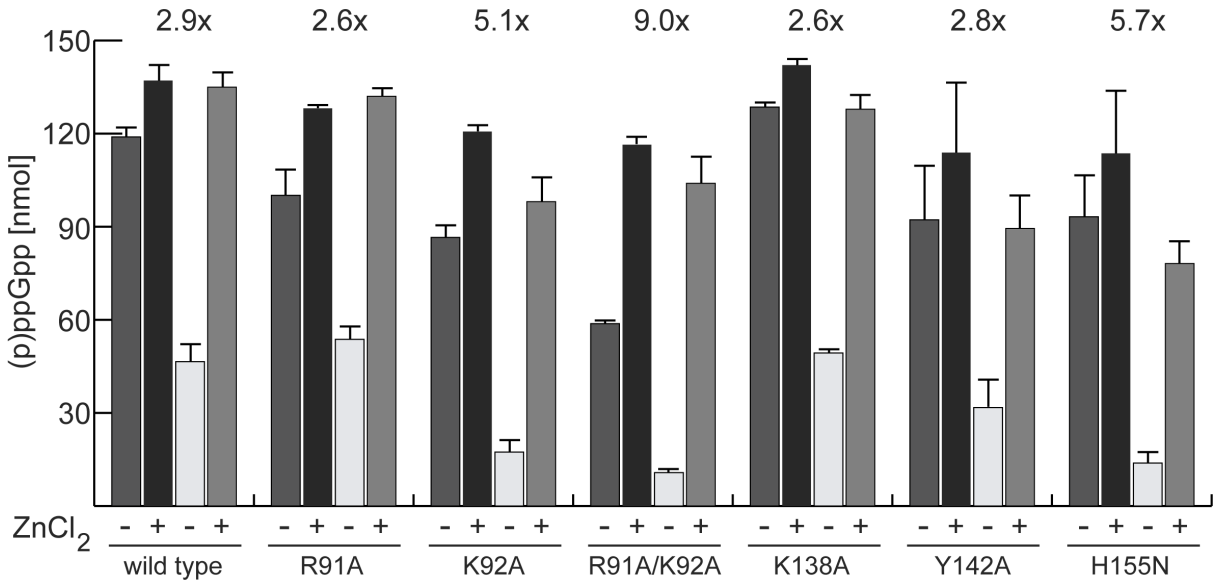

Figure 43. (p)ppGpp synthetic activity of SAS2 variants surrounding the active site. Production of ppGpp in absence (dark grey) or presence (black) and production of pppGpp in absence in absence (white) or presence (light grey) of $ZnCl_2$ are shown. Numbers above the bars indicate the relative differences between pppGpp synthesis in presence and absence of $ZnCl_2$, respectively. 2 µM SAS2 or its variants were incubated with 5 mM ATP, 5 mM GDP/GTP and 20 µM $ZnCl_2$ where indicated for 5 min at 37 °C. Data represent the mean ± standard deviation of three independent measurements.

In this regard remarkable is the observation that the degree of pppGpp synthesis stimulation by $ZnCl_2$ depends on the 'type' of the GTP molecule. Synthesis of pppGpp from ATP and GTP increases by approximately 2.5-fold in presence of $ZnCl_2$ (**Fig. 44** and see above). However, only a 1.4-fold stimulation of alarmone synthesis is observed when utilizing ATP together with the GTP-analog GMPPNP (i.e. guanosine-5'-[(β,γ)-imido]triphosphate). In GMPPNP, the oxygen atom linking the β- and γ-phosphates of GTP is substituted by an imido-group. Substitutions such as this

are thought to slightly but decidedly alter the binding angles between the phosphate moieties of nucleotidetriphosphates. This fact is also exemplified by the inability of SAS2 to produce a pppGpp-like alarmone from ATP and the GTP analog GMPPCP (i.e. guanosine-5'-[(β,γ)-methyleno]triphosphate) in which the same oxygen atom as in GMPPNP was replaced by a methyleno-group (**Fig. 44**). These results might support the hypothesis that the pppGpp synthetic activity of SAS2 is stimulated by zinc ions through interaction of Zn^{2+} with either GTP or pppGpp.

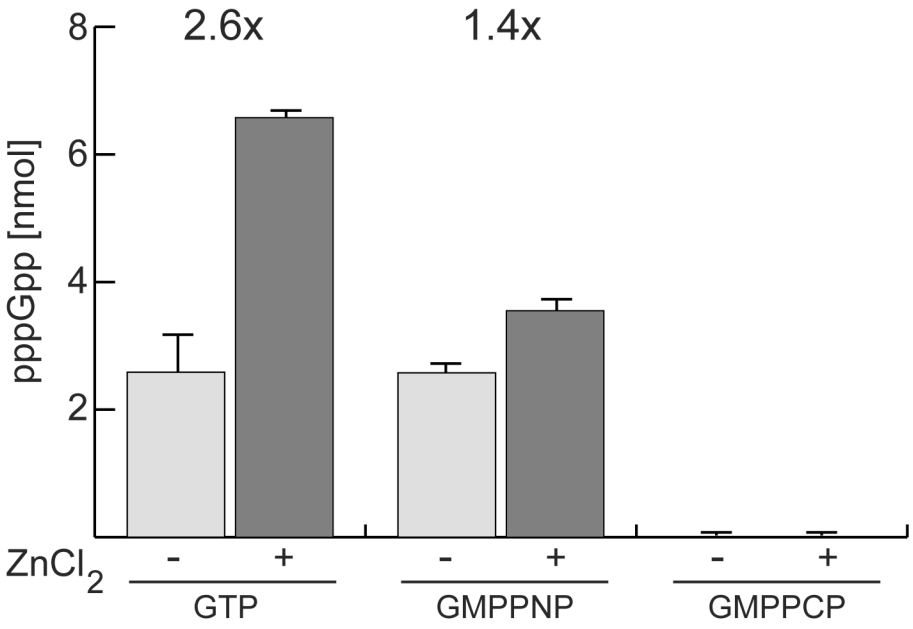

Figure 44. Conformation of the substrate GTP affects the grade of stimulation by $ZnCl_2$. (p)ppGpp synthetic activity SAS2 in absence (white) or presence (grey) of $ZnCl_2$ and GTP or its analogs. Numbers above the bars indicate the relative differences between pppGpp synthesis in presence and absence of $ZnCl_2$, respectively. 0.2 µM SAS2 were incubated with 1 mM GTP or its analogs and 5 mM ATP in absence or presence of 20 µM $ZnCl_2$ for 150 s at 37 °C. Data represent the mean ± standard deviation of three independent measurements.

3.4.5 pH-dependent stimulation of SAS2 (p)ppGpp synthesis by Zn^{2+}

In nucleotides, the pKa values of the phosphate moieties are not equal, but differ depending on their position (**Fig. 45**) (161, 162). Fully protonated (i.e. containing five protons) nucleoside triphosphates release their first two protons from the triphosphate chain at pH values below 1.5 (163, 164). The next proton is also abstracted from the 2-times deprotonated triphosphate with pKa values of approximately 1.4 ± 0.2 (162). Proton abstraction from the nucleobase (i.e. N7 of

GTP and N1 of ATP) occurs at pH values of ~ 2.9 and ~ 3.4 for GTP and ATP, respectively. Finally, a proton is released from the γ-phosphate moiety with a pKa value of ~ 6.5 (162). To my knowledge, no information is available on the pKa values of the 3'-OH phosphate moieties of alarmones. However, as all alarmones harbor a pyrophosphate at the 3'-OH position of the ribose, they are negligible in this consideration. The three alarmones pGpp, ppGpp and pppGpp should thereby differ in their number of deprotonated 5'-OH phosphate moieties, e.g. there is only one negative charge on the α-phosphate of pGpp while two negative charges would appear at the α- and β-phosphates of ppGpp at a pH of ~ 1.5 (**Fig. 45**).

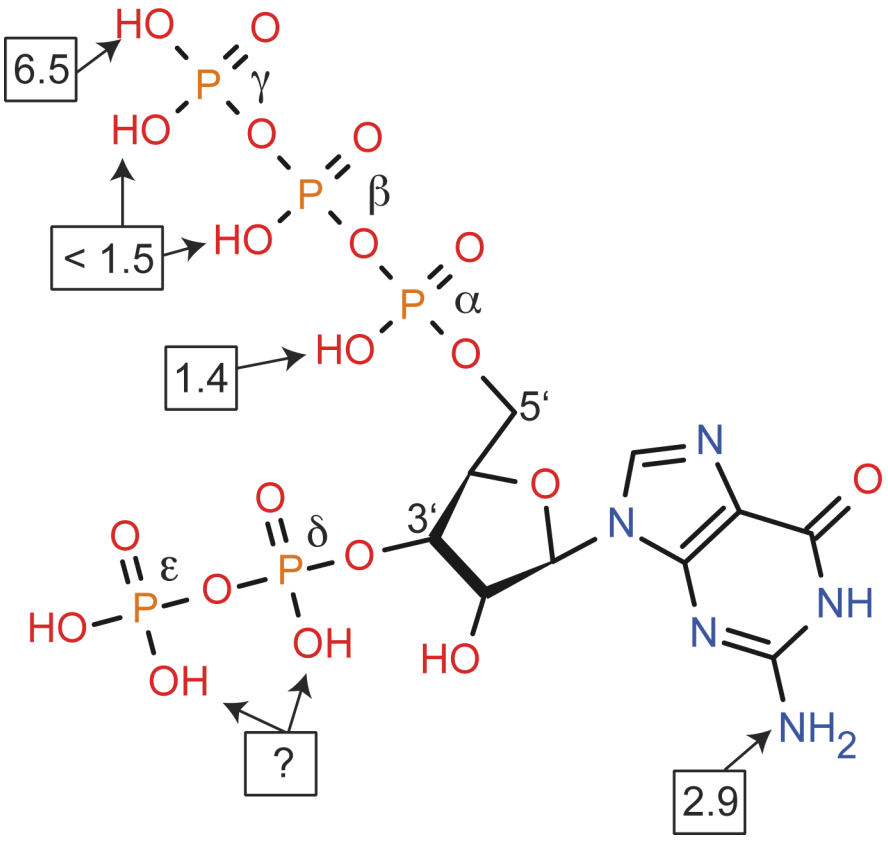

Figure 45. pKa values for deprotonation of pppGpp projected on the chemical structure of the alarmone.

If synthesis of pppGpp would be preferentially stimulated by Zn^{2+} compared to production of ppGpp or pGpp, then the pH value of the reaction conditions should influence this preference. This would be mainly based on the number of deprotonated phosphate moieties and their location at the 5' OH end of the ribose. While pppGpp would contain two deprotonated phosphates at the 5' position at any pH, protonation of the γ-phosphate would depend on the pH. For ppGpp, only the α-

phosphate would be permanently deprotonated and the β-phosphate subject to pH dependent deprotonation as this would be the terminal phosphate group with a pKa value in the physiological pH range.

Determination of the pH- and zinc-dependent (p)ppGpp synthetic activity of SAS2 was implemented by incubating 2 µM SAS2 together with 5 mM ATP and 5 mM GMP, GDP or GTP in absence of presence of 20 µM $ZnCl_2$ for 5 min at 37 °C and subsequent quantification of the alarmone products by RP-HPLC. Reactions were carried out in a buffer containing 200 mM NaCl, 20 mM $MgCl_2$, 20 mM KCl and either 100 mM MES-Na or Tris-HCl with a pH of 5.0-7.0 or 7.0-9.0, respectively.

Almost no alarmone synthesis is observed at a pH of 5 consistent with the proposed catalytic mechanism of (p)ppGpp synthesis, which relies on the abstraction of a proton from the 3'-OH group of the ribose to subsequently transfer the pyrophosphate moiety from ATP (**Fig. 46A**, compare to chapter **3.2.2**). Production of the alarmones from their respective substrates by SAS2 classifies as ppGpp > pppGpp > pGpp over the whole pH spectrum tested. This order is not altered by the addition of $ZnCl_2$ (**Fig. 46A**). Noteworthy, production of ppGpp is already significant at a pH of ~ 6.0 (**Fig. 46C**). Similar synthesis of pppGpp requires a pH value of ~ 6.25 (**Fig. 46B**), while production of pGpp reaches same levels not before a pH of approximately 7 (**Fig. 46D**). The hypothesis that zinc ions only stimulate the production of pppGpp by SAS2 seems to be falsified as also synthesis of ppGpp and pGpp is significantly stimulated (**Fig. 46A**). Noteworthy however, the degree of stimulation differs. Production of ppGpp is only mildly stimulated by Zn^{2+} with a higher grade of stimulation at low pH values where synthesis proceeds rather slow (**Fig. 46C**). As the basal activity (i.e. in absence of zinc ions) for production of pppGpp and pGpp is much lower than that for ppGpp, the stimulatory effect of $ZnCl_2$ becomes more apparent over the whole pH range (**Figs. 46B** and **D**).

Taken together, zinc ions stimulate the activity of SAS2 to synthesize alarmones. However, the pH-dependent grade of stimulation and different stimulatory effects on production of the different alarmones suggest that zinc ions do not affect SAS2 *per se* but rather act solely – or at least in concert with the protein - on the substrates or products of alarmone synthesis.

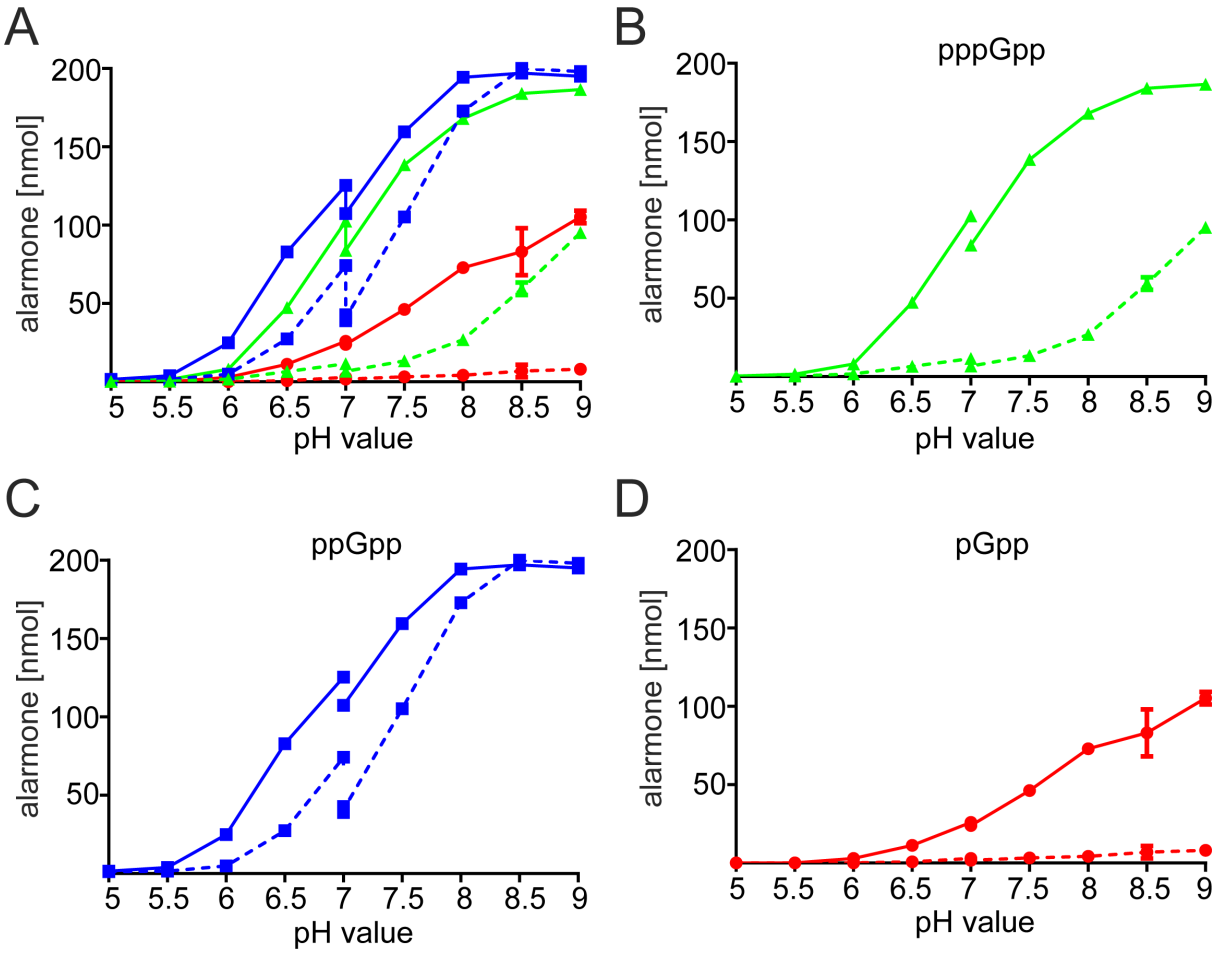

Figure 46. pH- and zinc-dependent synthesis of pGpp, ppGpp and pppGpp by SAS2. **A-D**. Synthesis of pGpp (red), ppGpp (blue) and pppGpp (green) by SAS2 in the absence (dashed line) or presence (solid line) of $ZnCl_2$. Alarmone synthesis at pH of 7.0 was determined for both buffer systems and therefore two values shown. 2 µM SAS2 were incubated with 5 mM ATP, 5 mM GMP/GDP/GTP and 20 µM $ZnCl_2$ as indicated for 5 min at 37 °C. Data represent the mean ± standard deviation of three independent measurements.

3.5 Mechanism of the bifunctional Rel enzyme from *B. subtilis*

The bifunctional Rel enzyme from *B. subtilis* belongs to the 'long' RSH-type family of (p)ppGpp synthetases. Long RSH-type (p)ppGpp synthetases are multi-domain proteins consisting of an N-terminal catalytic (NTD) and a C-terminal (CTD) regulatory part (compare to **Fig. 2A**). Rel from *B. subtilis* harbors an active (p)ppGpp hydrolase followed by a (p)ppGpp synthetase domain within its NTD rendering the protein bifunctional for these opposing catalytic activities.

The CTD of long RSH-type (p)ppGpp synthetases mediates binding of Rel to ribosomes stalled by uncharged tRNAs bound within the aminoacyl-acceptor site (A-site). Upon binding, the (p)ppGpp synthetase activity of Rel increases dramatically while (p)ppGpp hydrolysis is reduced (51-53, 58). However, it remained largely unadressed whether and to what extend the CTD might regulate the opposing activities of Rel in the absence of the ribosome.

3.5.1 Purification of Rel and its truncated variants

To investigate the influence of the CTD on the activity of Rel from *B. subtilis*, the full-length protein and a truncated variant harboring only the NTD (i.e. Rel-NTD, amino acids 1-395 of Rel) were fused to an N-terminal hexa-histidine tag and heterologously produced in *E. coli* BL21 (DE3) using auto-induction medium. Subsequently, Rel and Rel-NTD were purified by a two-step protocol employing Ni-NTA affinity chromatography and size-exclusion chromatography (see chapter **5.2.2**). For purification of Rel, all buffers included 500 mM NaCl to eliminate ribosomes that would otherwise remain bound to the protein. Moreover, Rel is prone to degrataion, which can be minimized by the increased ionic strength in the buffers (53, 91, 165). Nevertheless, only low amounts of Rel could be purified to homogeneity (**Fig. 47A**). Rel-NTD could be readily obtained in high amounts using the same buffers as already employed for the purification of SAS1 and SAS2 proteins (**Fig. 47B**).

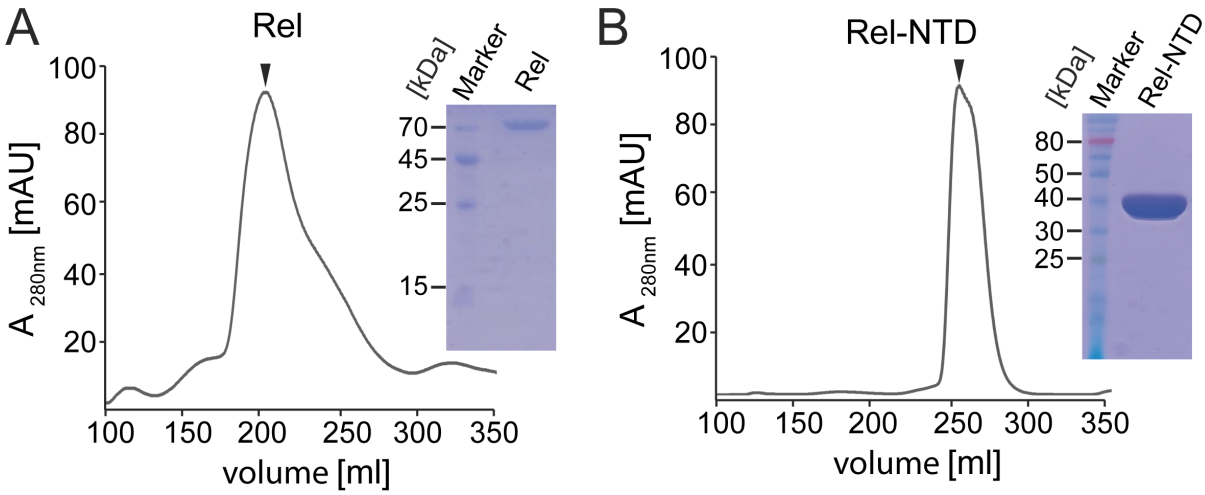

Figure 47. Purification of Rel and Rel-NTD. **A-B**. Size-exclusion chromatography profiles of Rel (**A**) and Rel-NTD (**B**). Coomassie-stained SDS-PAGE shows the peak fractions indicated by arrows in the profiles.

3.5.2 The C-terminus of Rel regulates its activity

To elucidate whether the CTD affects Rel's activities, the (p)ppGpp synthetic and hydrolytic activities of full-length Rel and Rel-NTD were assessed by RP-HPLC. In brief, (p)ppGpp synthesis was determined by incubation of 2 µM Rel or Rel-NTD together with 5 mM ATP and 5 mM GDP or GTP for 10 min at 37 °C. (p)ppGpp hydrolysis was evaluated similarly by incubation of 2 µM protein together with 1 mM of ppGpp or pppGpp.

Rel-NTD shows a ~3-fold increased ppGpp and ~6-fold increased pppGpp synthesis compared to full-length Rel (**Fig. 48A**). This implies that the CTD present in Rel but absent in Rel-NTD negatively affects Rel's (p)ppGpp synthesis. The (p)ppGpp hydrolysis by Rel on the other hand was positively affected by the presence of the CTD exemplified by an approximately 2-fold difference in hydrolysis between Rel and Rel-NTD (**Fig. 48B**). Noteworthy, (p)ppGpp hydrolysis surmounts (p)ppGpp synthesis in these experiments, i.e. in the absence of the ribosome. This is in agreement with the presumption that Rel should efficiently reduce (p)ppGpp levels in the bacterial cell under non-stringent conditions. Besides, both Rel variants preferentially produced pppGpp rather than ppGpp in contrast to SAS proteins (compare to **Figs. 21** and **36**) and also slightly differed in their potential to hydrolyse ppGpp and pppGpp.

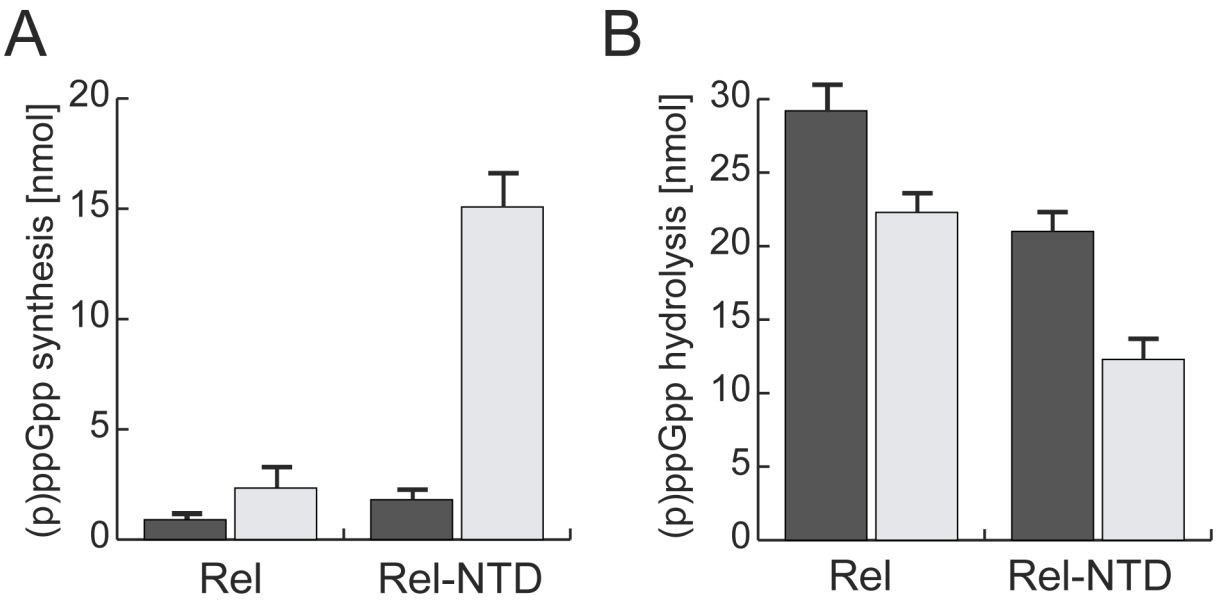

Figure 48. The C-terminus of Rel affects its (p)ppGpp synthetic and hydrolytic activity. **A.** Synthesis of ppGpp (black) and pppGpp (grey) by Rel and Rel-NTD. 2 µM enzyme were incubated with 1 mM ppGpp/pppGpp for 10 min at 37 °C. **B.** Hydrolysis of ppGpp (black) and pppGpp (grey) by Rel and Rel-NTD. 2 µM enzyme were incubated with 5 mM ATP and 5 mM GDP/GTP for 10 min at 37 °C. Data represent the mean ± standard deviation of three independent measurements.

To dissect which of the domains present within the CTD of Rel would be responsible for the inhibition of (p)ppGpp synthesis, two additional variants of Rel were probed for their activity to synthesize pppGpp. RelΔACT lacks the far C-terminal ACT domain of Rel while Rel-NTD+TGS additionally harbors the TGS domain adjacent of Rel-NTD (**Fig. 2A**). The presence of the TGS domain did not result in diminished pppGpp synthesis (**Fig. 48A**). However, truncation of the ACT domain resulted in an approximately 6-fold increase in Rel's activity (**Fig. 49**). This suggests that the ACT domain either alone or in concert with other motifs present within the CTD is involved in regulation of Rel's activity.

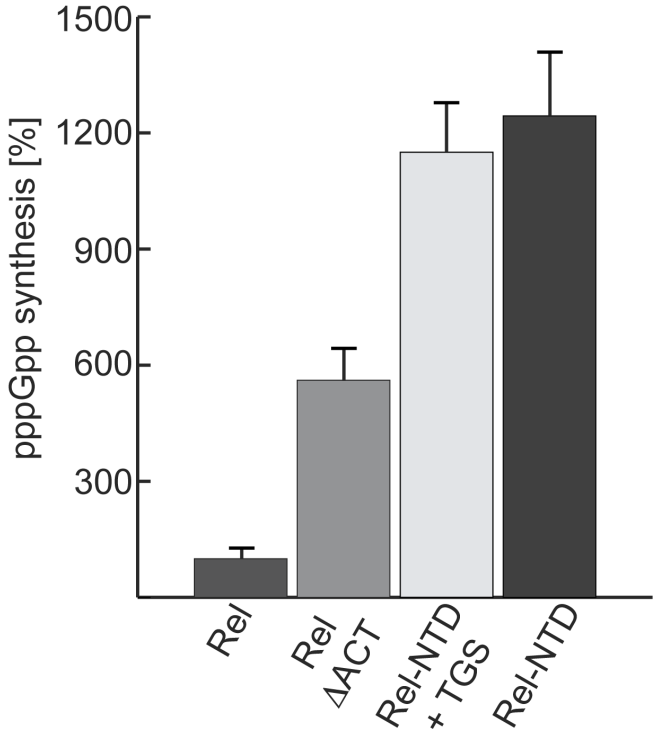

Figure 49. The ACT domain is primarily responsible for regulation of Rel's activities. 2 µM Rel or variants thereof were incubated with 5 mM ATP and 5 mM GTP for 10 min at 37 °C. Synthesis of pppGpp by Rel was set to 100%. Data represent the mean ± standard deviation of three independent measurements.

3.5.3 Catalytic properties of the Rel synthetase and hydrolase domains

To further illuminate the catalytic activities of Rel and the influence of the CTD, I performed a kinetic analysis of (p)ppGpp synthesis and hydrolysis for full-length Rel and Rel-NTD. In brief, (p)ppGpp synthesis was determined by incubation of 5 µM Rel or Rel-NTD together with 5 mM ATP and GDP/GTP at different concentrations at 37 °C. Linear regression of the amount of AMP released after 6/12/18/24/30 min yielded the velocity of (p)ppGpp formation at a given GDP/GTP substrate concentration. The so-obtained velocities were fitted according to the equation $v = V_{max}\ S^h/(K_m{}^h + S^h)$ (**Fig. 50A**).

The maximal velocities for production of ppGpp and pppGpp by Rel-NTD are 9.7 ± 1.4 and 23.7 ± 0.9, respectively (**Fig. 50B**) and by this 10-20-fold higher than those observed for full-length Rel (i.e. 0.5 ± 0.1 and 2.1 ± 0.1 for ppGpp and pppGpp synthesis, respectively). However, it must be noted that the V_{max} values for Rel-NTD are hard to estimate properly based on the current data. Nevertheless, the v/S characteristic of (p)ppGpp synthesis solidifies the observation that the CTD negatively affects (p)ppGpp production of Rel. Moreover, it is apparent now that pppGpp synthesis exceeds ppGpp synthesis independently of the presence of the CTD. This furthermore suggests that differences in the architectures of the (p)ppGpp synthetase domains of Rel and SAS proteins might relate to the different preference to either the ppGpp or pppGpp product.

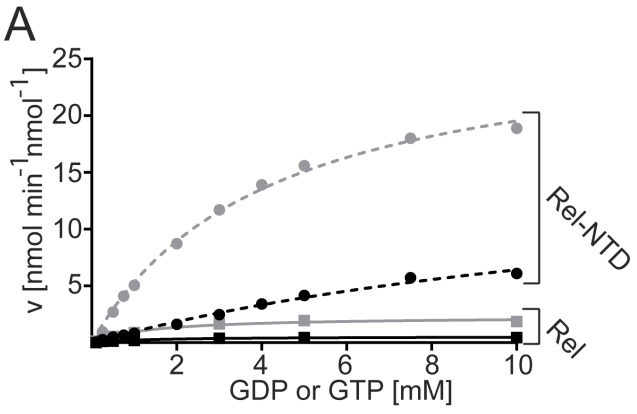

B

Rel (p)ppGpp synthesis

	Rel-NTD		Rel	
	ppGpp	pppGpp	ppGpp	pppGpp
K_m	6.3 ± 1.5	3.0 ± 0.2	1.2 ± 0.3	1.1 ± 0.2
V_{max}	9.7 ± 1.4	23.7 ± 0.9	0.5 ± 0.1	2.1 ± 0.1
h	1.3 ± 0.1	1.2 ± 0.1	1.2 ± 0.3	1.3 ± 0.2

Figure 50. (p)ppGpp synthesis by Rel-NTD and Rel. **A.** v/S characteristic of ppGpp (black) and pppGpp (grey) synthesis exhibited by Rel-NTD (dashed lines) and Rel (solid lines). **B.** Kinetic parameters of (p)ppGpp synthesis by Rel-NTD and Rel obtained from **A**.

(p)ppGpp hydrolysis by Rel was determined by incubation of 2 µM Rel or Rel-NTD together with varying concentrations of ppGpp or pppGpp at 37 °C. Linear regression of the amount of GDP or GTP released after 2/4/6/8/10 min yielded the velocity of ppGpp or pppGpp hydrolysis, respectively. The so-obtained velocities were fitted according to the equation $v = V_{max} S^h/(K_m{}^h + S^h)$ (**Fig. 51A**). The alarmone ppGpp seems to be preferred over pppGpp as substrate for hydrolysis as evidenced by a 2-3-fold difference in the maximal velocities. Presence of the CTD slightly influences (p)ppGpp hydrolysis in a positive manner as displayed by the higher velocity of hydrolysis exhibited by Rel. Surprisingly, (p)ppGpp hydrolysis by Rel seems to display a positive cooperative behaviour while hydrolysis by Rel-NTD does not (**Fig. 51B**). This observation might be either explained by the appearance of Rel as an oligomer (52, 101) although the behavior of the protein on SEC does not suggest so (**Fig. 47A**) or an effect of the GDP/GTP released during (p)ppGpp hydrolysis onto the active site of the hydrolase domain. Taken together, the CTD contributes to regulation of Rel's activities even in the absence of the ribosome.

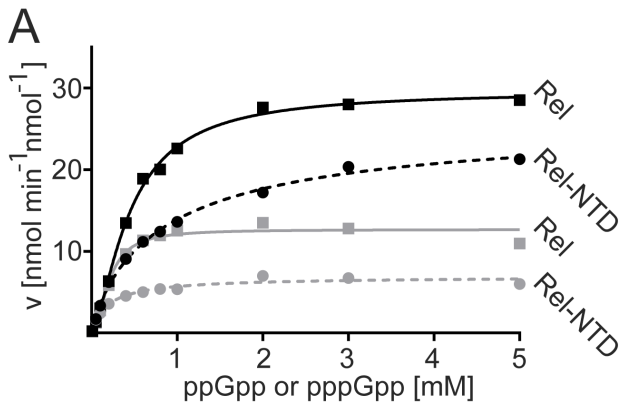

B

Rel (p)ppGpp hydrolysis

	Rel-NTD		Rel	
	ppGpp	pppGpp	ppGpp	pppGpp
K_m	0.9 ± 0.1	0.2 ± 0.1	0.5 ± 0.1	0.2 ± 0.1
V_{max}	26.3 ± 1.4	6.9 ± 0.5	29.6 ± 0.5	12.7 ± 0.4
h	0.9 ± 0.1	0.9 ± 0.2	1.5 ± 0.1	1.9 ± 0.3

Figure 51. (p)ppGpp hydrolysis by Rel-NTD and Rel. **A.** v/S characteristic of ppGpp (black) and pppGpp (grey) hydrolysis exhibited by Rel-NTD (dashed lines) and Rel (solid lines). **B.** Kinetic parameters of (p)ppGpp hydrolysis by Rel-NTD and Rel obtained from **A**.

3.5.4 Crystal structure of Rel-NTD from *B. subtilis*

In order to delineate the molecular mechanism of (p)ppGpp synthesis and hydrolysis by Rel from *B. subtilis* and to compare it with Rel from *S. equisimilis*, full-length Rel and Rel-NTD were purified ~500 µM protein concentration as described to in chapter **3.5.1** and crystals obtained after approximately three days (**Fig. 52**). Crystal obtained for Rel from 0.05 M lithium sulfate, 0.05 M sodium chloride, 0.05 M Tris-HCl, pH 8.5

and 30% (w/v) PEG400 were very small, only diffracted to ~7 Å resolution and did not allow for successful determination of the crystal structure. Unfortunately, the crystals could not be further optimized. Crystals for Rel-NTD were obtained from 0.2 M sodium chloride, 0.1 M imidazole, pH 8.0 and 1.0 M potassium/sodium tartrate that diffracted to ~3.5 Å resolution.

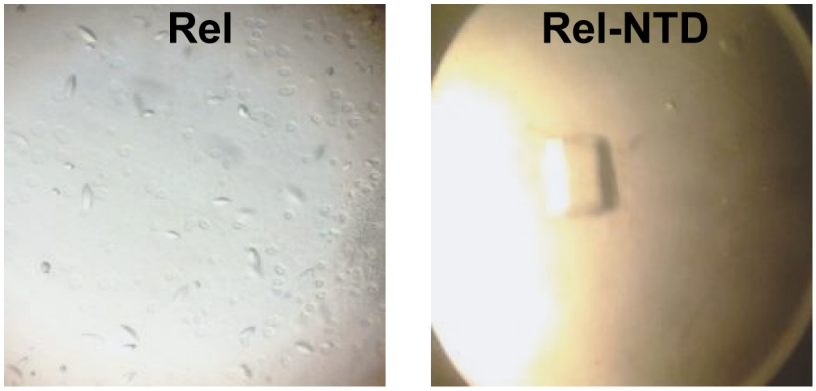

Figure 52. Crystals of Rel and Rel-NTD from *B. subtilis* after three days.

The crystal structure of Rel-NTD from *B. subtilis* was subsequently determined by MR employing Rel-NTD from *S. equisimilis* (Rel_{seq}) as a search model (PDB: 1VJ7, (54) and **Table S3**). The structure of Rel-NTD basically resembles the structure of its orthologue Rel_{seq} (**Fig. 53**). Rel-NTD comprises the HD and adjacent Syn domain. The cofactor manganese bound to Rel-NTD marks the active site of the HD domain. In contrast to Rel_{seq} to which GDP was bound, the (p)ppGpp synthetase active site is unoccupied in Rel-NTD (**Fig. 53**). This is somehow surprising as GDP was found in Rel_{seq} although the cofactor was never added to the crystallization condition and should therefore originate from the purification of the protein, thereby implying a high binding affinity (54). However, no major deviations in the Syn domains of both proteins can be identified that might relate to this observation.

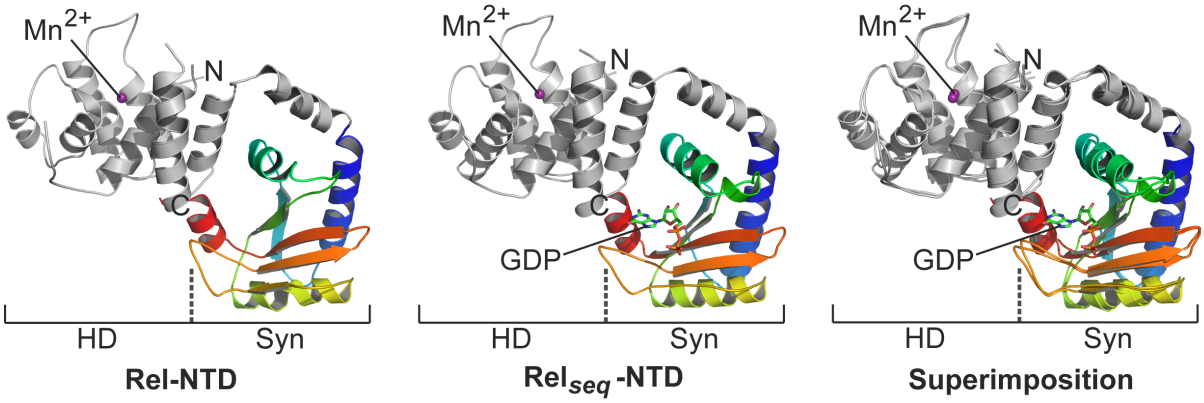

Figure 53. Crystal structure of Rel-NTD from *B. subtilis*. Cartoon representation of the crystal structures of Rel-NTD (left), Rel_{seq}-NTD (middle, PDB: 1VJ7 chain A; (54)) and the superimposition of both structures (right). The Syn domains are shown in rainbow colors from N- to C-termini.

3.5.5 Substrate-binding mechanism of the Rel synthetase

The absence of the nucleotide GDP in the crystal structure of Rel-NTD from *B. subtilis* – in contrast to the nucleotide bound to Rel from *S. equisimilis* – prompted me to investigate the binding modalities of GDP, GTP and ATP (mimicked by the non-hydrolyzable analog AMPCPP) to Rel-NTD by HDX.

In brief, 50 µM Rel-NTD were incubated in deuterated SEC-buffer containing no nucleotide or 1 mM of GDP, GTP or AMPCPP at 25 °C for 0.25/0.5/1/2/10 minutes. Subsequently, the reactions were quenched, digested with pepsin and the resulting peptic peptides analyzed by electrospray ionization mass spectrometry. Data analysis was carried out using PLGS and DynamX 3.0 (Waters) softwares as detailed in chapter **5.2.8**. Surprisingly and in contrast to SAS1 (compare to **Fig. 16**), no reduced HDX was observed in regions that confer residues involved in ATP coordination (i.e. R1 and R2) thus suggesting no binding of tha ATP-analog AMPCPP (**Figs. 54A-C**). However, binding of GDP and GTP to Rel-NTD could be demonstrated by a reduction of HDX in the regions R3 and R4 locating in close proximity of the GDP/GTP-binding site of Rel-NTD (**Figs. 54A, D** and **E**). This disparity of the substrate-binding modes of Rel-NTD and SAS1 (**Fig. 54G**, compare to **Fig. 16C**) might be explained by the different orientation of helix α13 (α2 in SAS1) mediating ATP coordination (**Fig. 10**). Minor reduction in HDX in presence of GDP

and GTP could also be observed for region R5 constituting the nucleotide-binding site of the (p)ppGpp hydrolase domain of Rel-NTD (**Figs. 54A** and **F**). This might suggest that GDP/GTP coordination affects binding of (p)ppGpp to the hydrolase domain thereby regulating Rel-NTD's reciprocal catalytic activites.

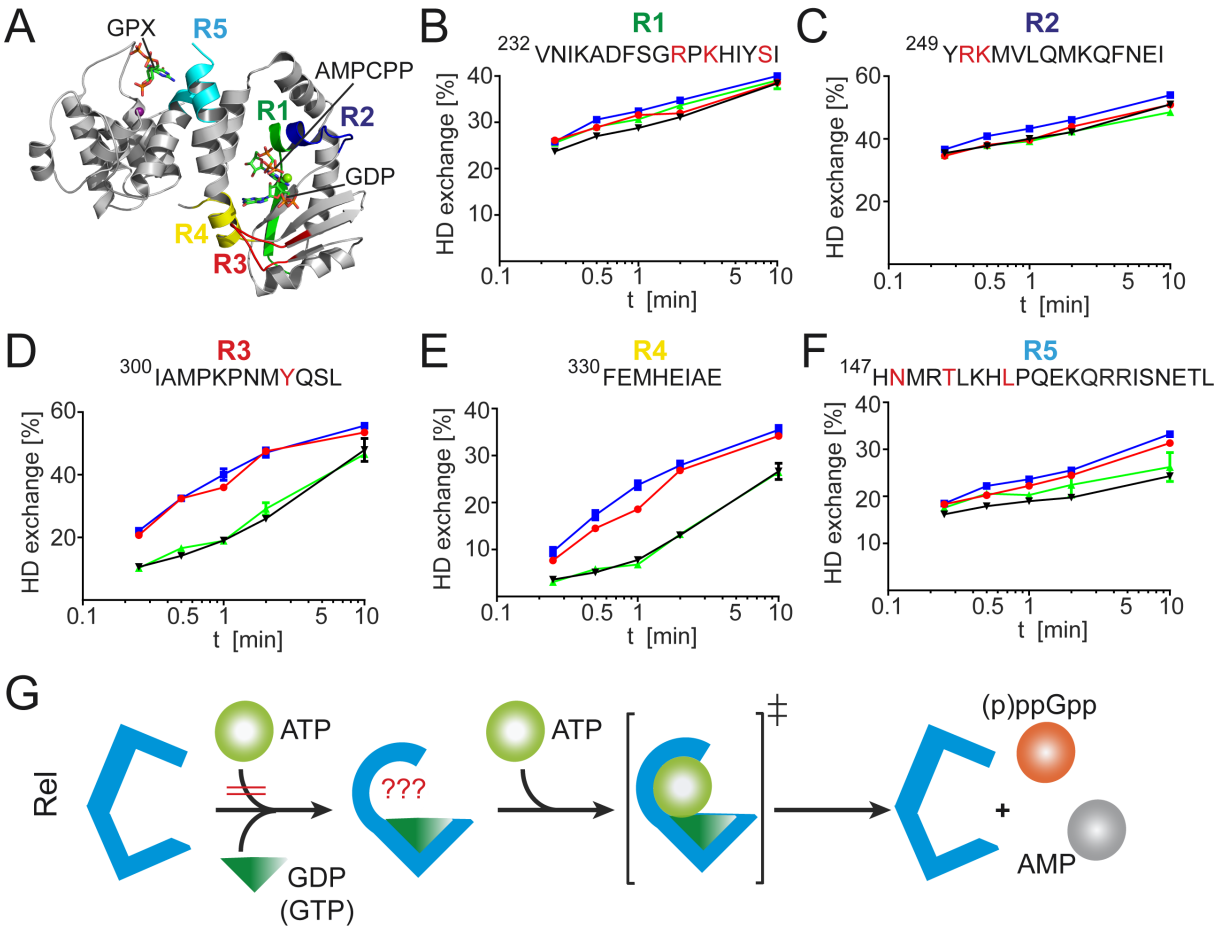

Figure 54. Substrate binding to Rel-NTD. **A.** Location of the peptides R1 (green), R2 (blue), R3 (red), R4 (yellow) and R5 (cyan) in the crystal structure of Rel-NTD. The nucleotides AMPCPP and GDP/GPX are derived from superimpositions of Rel-NTD with the crystal structures SAS2-AMPCPP and Rel_{seq} (PDB: 1VJ7 chain B (54)), respectively. **B-F.** HDX time course of five representative peptides of Rel-NTD without nucleotides (red) or in the presence of AMPCPP (blue), GDP (black) or GTP (green). Amino acids contributing to nucleotide-coordination are colored in red. Data represent the mean ± standard deviation of three independent measurements. **G.** The substrates GDP/GTP (dark green triangle) and ATP (pale green ball) bind to Rel (blue) in sequential order. Binding of the first substrate GDP/GTP should lead to a conformational change within Rel allowing binding of the second substrate ATP. The transition state of catalysis in indicated by a double dagger (‡). The reaction products (p)ppGpp and AMP are shown as orange and grey balls, respectively.

3.5.6 Structural basis for preferential pppGpp synthesis by bifunctional Rel

The bifunctional Rel from *B. subtilis* differentially utilizes GDP and GTP as substrates for synthesis of ppGpp and pppGpp, respectively in that pppGpp is the preferred product (**Fig. 49**). In contrast, the monofunctional (i.e. only (p)ppGpp synthetically active) RelA from *E. coli* prioritizes synthesis of ppGpp over pppGpp. This discrimination between both reactions was attributed by Prakash and coworkers to the presence of 'charge revearsal' in mono- and bifunctional Rel proteins (80, 81). In this, bifunctional Rel proteins from e.g. *B. subtilis* or *S. equisimilis* possess a 'RxKD' motif while monofunctional RelA from *E. coli* harbors a 'ExDD' motif instead correlating with preferred synthesis of pppGpp or ppGpp, respectively (**Fig. 55A**). The crystal structure of Rel-NTD reveals that Arg295 and Lys297 from the 'RxKD' residing in β3 are able to interact with the β- and γ-phosphate moieties of pppGpp or also GTP (**Fig. 55B**). It should be noted, that this interaction is not directly apparent as the nucleotide was not found in the crystal structure of Rel-NTD and its location is solely based on superimposition of Rel-NTD with SAS2-pppGpp. By this, the location of the amino acid side chains does not reflect the 'true' nucleotide-bound state for Rel-NTD (**Fig. 55B**). Nevertheless, in the 'ExDD'-containing Rel from *E. coli* where Glu306 and Asp308 replace Arg295 and Lys297, respectively, similar interactions would be impossible and rather repulsion of the β- and γ-phosphate moieties through the negatively charged amino acids would occur. By this, binding of GTP should be stronger negatively affected than GDP-binding rendering ppGpp synthesis preferred over pppGpp (**Fig. 55A**).

It however seems that the equivalent motifs in SAS1 and SAS2 do not result in similar discrimination between both products. In SAS1 from *B. subtilis*, Arg105 from the motif 'DxRD' coordinates the β-phosphate while Asp103 is too far away to exhibit any repulsive effect that might exlain SAS1's preference for ppGpp synthesis (**Figs. 55A** and **C**, compare to **Fig. 22**). SAS2 from S. aureus possesses a 'KxKD' motif that might resemble 'RxKD' found in bifunctional Rel enzymes (**Figs. 55A** and **D**). Nevertheless, also SAS2 similar to SAS1 prefers synthesis of ppGpp over pppGpp (compare to **Fig. 36**).

Taken together, the presence of a special ‘charge revearsal’ motif in a (p)ppGpp synthetase does not completely explain the preference of the enzyme for production of either the ppGpp or pppGpp alarmone.

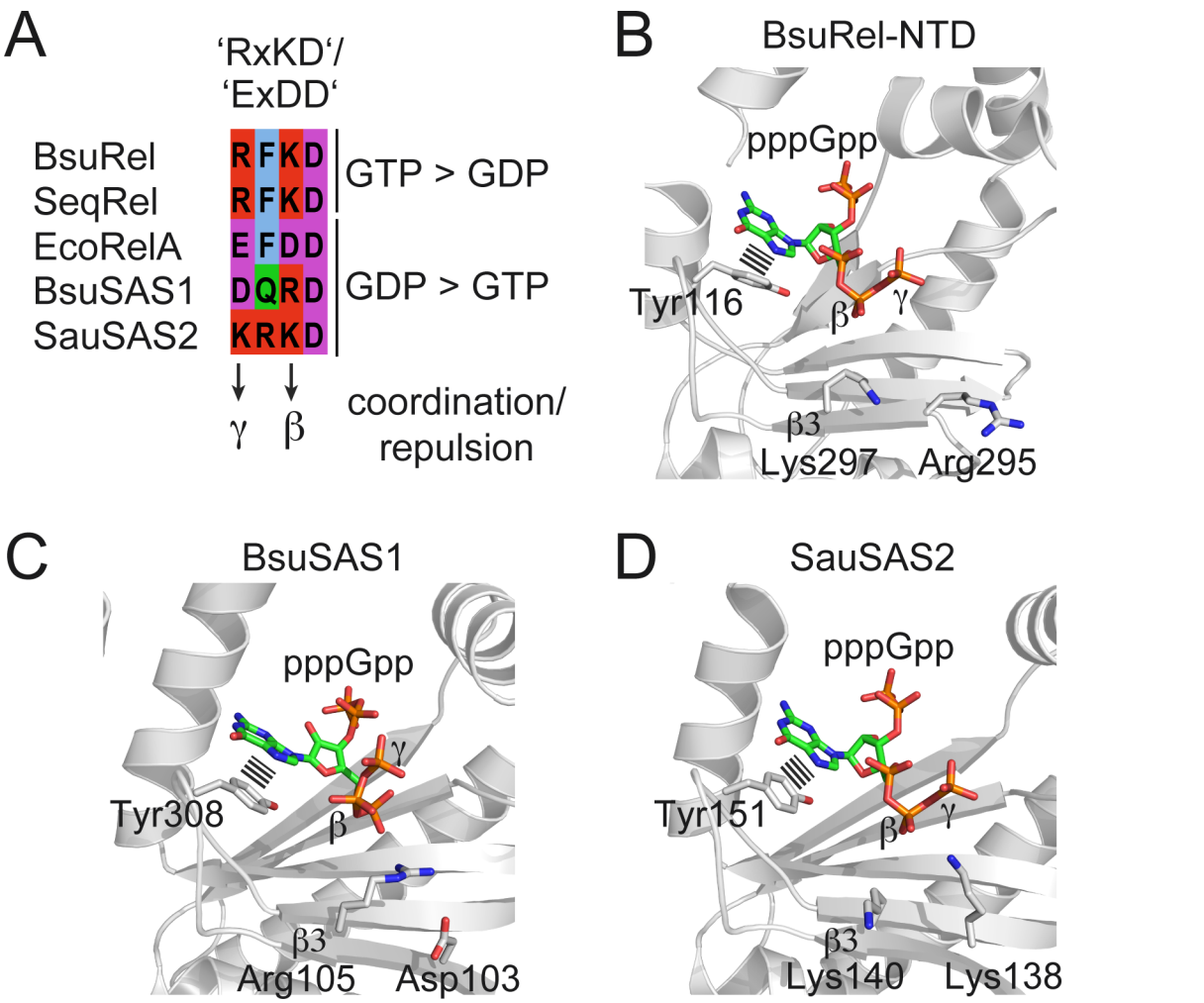

Figure 55. Structural basis for preferential pppGpp synthesis by bifunctional Rel. **A.** Amino acid sequence alignment of the ‘charge revearsal motif’ of Rel and SAS proteins from *B. subtilis* (Bsu), *Streptococcus dysgalactiae ssp. equisimilis* (Seq), *E. coli* (Eco) and *S. aureus* (Sau). Preferences for ppGpp or pppGpp synthesis exhibited by the proteins are incdicated. **B-D.** Crystal structures of BsuRel-NTD (**B**), BsuSAS1-pppGpp (**C**) and SauSAS2-pppGpp (**D**) with the amino acids from the ‘charge inversion motif’ and the catalytically essential tyrosine shown as sticks. The pppGpp in BsuRel-NTD originates from a superimposition with SauSAS2-pppGpp.

3.6 Physiological implications of alarmone synthetases in *B. subtilis*

The alarmones (p)ppGpp are well-known to promote a dormant state in bacteria, which is characterized by a reversible but substantial reduction of growth rate and metabolism rendering the microorganism more resistant to different environmental challenges (36, 166). For example, during prolonged phases of nutrient starvation by e.g. lack of amino acids, (p)ppGpp decreases anabolic processes while in turn amino acid biogenesis and uptake are elevated (15, 17). Nevertheless, (p)ppGpp also mediates adaptational processes of bacterial physiology in the absence of a concise stress stimulus. In this, (p)ppGpp plays a role in the development of virulence (29-31), biofilm and persister cell formation (32-37, 167) and development of cellular heterogeneity (38, 39). Taken together, alarmones are second messengers important in shaping the lifestyle of microorganisms.

3.6.1 Activity of SAS1 is important for growth of *B. subtilis* in minimal medium

The small alarmone synthetase SAS1 from *B. subtilis* exhibits a high activity synthesis of ppGpp and pppGpp, respectively (chapter **3.2.4**). Hence, SAS1 should be important for growth of *B. subtilis* under nutrient limitation but might also already be relevant under nutrient-rich conditions.

To study the influence of SAS1 on growth of *B. subtilis*, the *yjbM* gene encoding for SAS1 was replaced by *yjbM* harboring mutations within the active and allosteric site of SAS1 (i.e. SAS1-E139V and SAS1-K25A/F42A, respectively). This approach allows for a ‘markerless’ substitution and thereby excludes the possibility of polar effects on genes downstream of *yjbM* caused by a knockout (168). Also, any so far unanticipated protein-protein interactions that might be established by SAS1 should not be disrupted by this method.

Growth curves were obtained for SAS1-E139V, SAS1-K25A/F42A and the parenteral *B. subtilis* PY79 wild type strain at 37 °C under vigorous shaking in rich medium (i.e. lysogeny broth (LB)) and minimal medium (i.e. S7, (169)). All three strains grew almost identical in rich medium (**Fig. 56).** In minimal medium, however, SAS1-E139V exhibited slower growth than wild type and SAS1-K25A/F42A (**Fig. 56B**). This

suggests that (p)ppGpp provided by SAS1 is important for the adaptation to nutrient-limiting conditions.

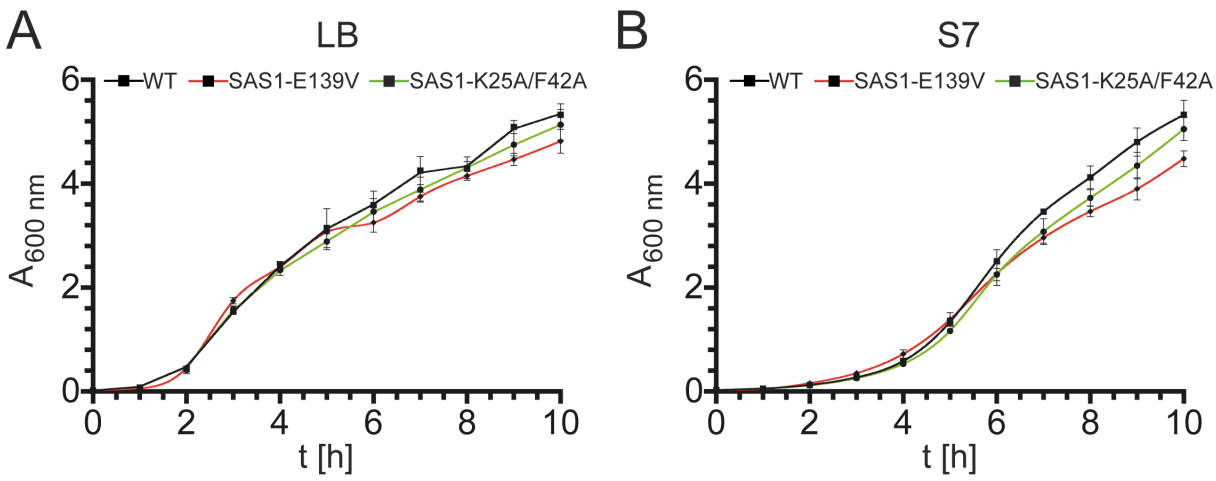

Figure 56. Influence of SAS1 on growth of *B. subtilis* in rich and minimal medium. **A.** Growth of *B. subtilis* PY79 wild type (black), SAS1-E139V (red) and SAS1-K25A/F42A (green) strains in rich medium (LB). Data represent the mean ± standard deviation of three independent measurements. **B.** Growth of *B. subtilis* PY79 wild type (black), SAS1-E139V (red) and SAS1-K25A/F42A (green) strains in minimal medium (S7). Data represent the mean ± standard deviation of three independent measurements.

The S7 minimal medium is composed of the buffer salt MOPS (3-(N-morpholino) propanesulfonic acid), trace elements and $(NH_4)_2SO_4$ and KH_2PO_4 as sources of inorganic nitrogen and phosphate, respectively. Additionally, S7 contains 1% (w/v) glucose, 0.1% (w/v) glutamate and 0.004% (w/v) casamino acids. I assumed that upon reduction of the glucose content or omission of glutamate and casamino acids any putative differences between the strains might me more pronounced in these modified minimal media. Moreover, reduction of the carbon source glucose should also enable displaying of the stationary phase and death phase of the bacterial growth.

Removal of casamino acids and glutamate from the S7 minimal medium leads to a delayed entering of SAS1-E139V and SAS1-K25A/F42A into the logarithmic growth phase (**Figs. 57A** and **B**). The same effect is also apparent when only 0.2% (w/v) glucose is added to the medium (**Fig. 57C**). Moreover, under these conditions it is obvious that both strains harboring amino acid substitutions within SAS1 reach lower cell densities in stationary phase than the wild type strain and enter death phase

earlier (**Fig. 57C**). Simultaneous omission of glutatame and reduction of glucose does not result in additive effects on the growth behaviour of the *B. subtilis* strains (**Fig. 57D**). These results indicate SAS1 is important under nitrogen- and carbon-limiting conditions. Moreover, the similar growth behaviour of catalytically inactive SAS1 (i.e. SAS1-E139V) and SAS1 disrupted for allosteric binding of pppGpp (i.e. SAS1-K25A/F42A) suggests that allosteric stimulation of SAS1 is an important feature of its functionality in the living cell. It might furthermore be suggested that, albeit no differences of growth between the three strains are apparent in rich medium (compare to **Fig. 56**), adaptational processes might also already be relayed by SAS1.

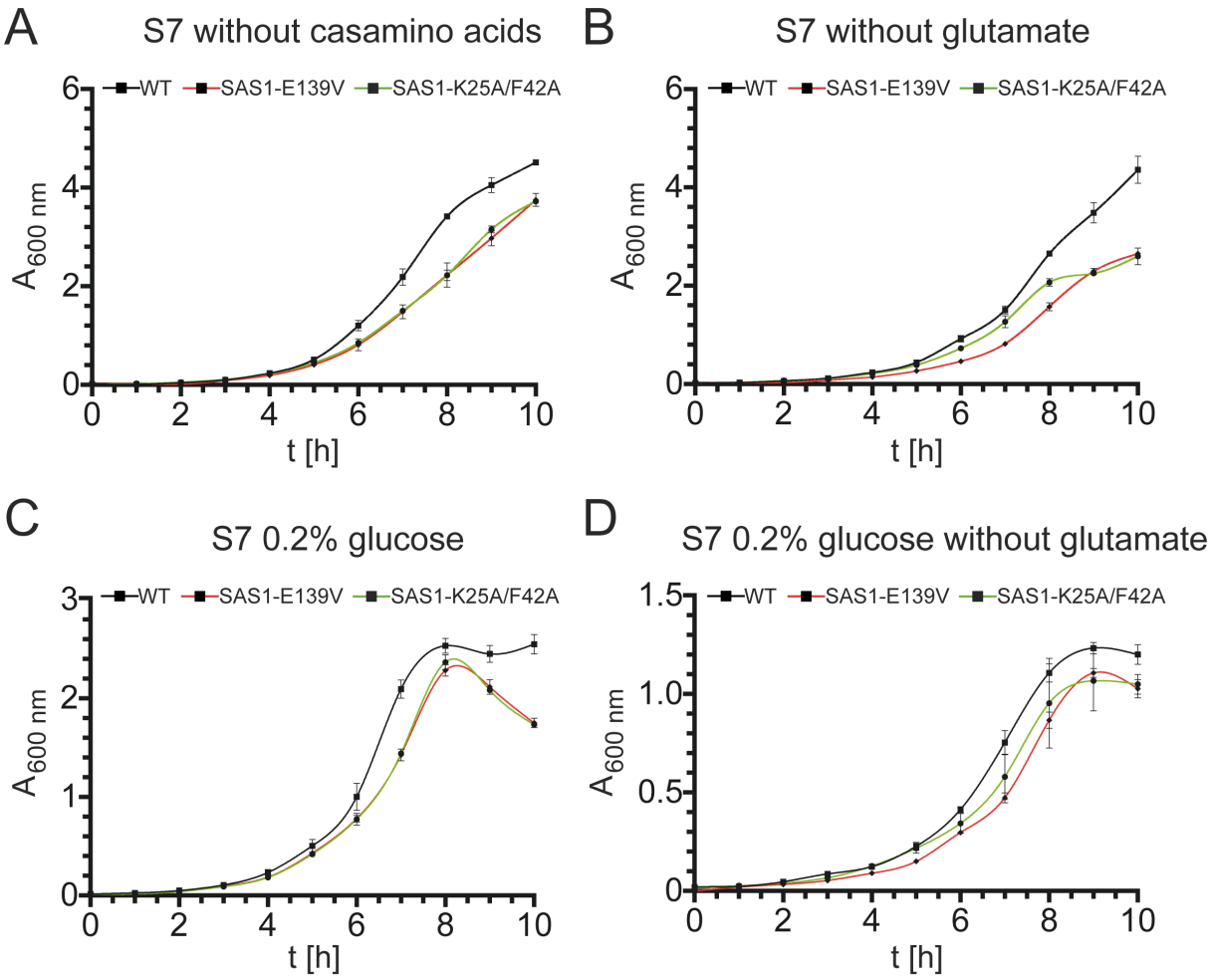

Figure 57. Activity of SAS1 is important for growth of *B. subtilis* in minimal medium. **A-D.** Growth of *B. subtilis* PY79 wild type (black), SAS1-E139V (red) and SAS1-K25A/F42A (green) strains in modified minimal medium (S7). Data represent the mean ± standard deviation of three independent measurements.

3.6.2 SAS1 impacts cellular heterogeneity of *B. subtilis*

Rapidly dividing populations of *B. subtilis* PY79 consist of either long, sessile chains that have completed cytokinesis but have not yet separated from each other or actively swimming singlets or duplets (170, 171). Typically, during logarithmic phase in full medium approximately 90% of the cells in a population appear as chains while 10% of the cells are non-chained (38, 170). Disruption of Rel's (p)ppGpp hydrolase activity results in 100% of the cells appearing in single cells or duplets (38). This suggests that artificially increased (p)ppGpp levels affect the cellular heterogeneity of *B. subtilis* PY79.

To test the influence of SAS1 on cellular heterogeneity of *B. subtilis* in presence of the intact bifunctional Rel protein, different *B. subtilis* PY79 strains were grown in rich medium (i.e. lysogeny broth (LB)) to an optical density of approximately 2 and analyzed for their distribution of chained/unchained cells by bright-field microscopy (see chapter **5.2.9.4**). The wild type strain showed a typical distribution of ~90/10% chained versus unchained cells (**Figs. 58A** and **B**). Overexpression of SAS1 from the ectopic *amyE* locus under the control of the xylose-inducible promotor P_{xyl} by addition of 0.001% (w/v) xylose altered the distribution to ~60/40% (**Figs. 58A** and **B**). This result is in agreement with the observation by Herman and coworkers that increased (p)ppGpp levels result in an elevated number of single cells (38). However, also disruption of the catalytic activity of SAS1 through substitution of the catalytically essential amino acid Glu139 (i.e. SAS1-E139V, compare to **Fig. 18A**) induces the appearance of the *B. subtilis* population as single cells (**Fig. 58B**). Moreover, disruption of amino residues conferring coordination of allosteric stimulator pppGpp to SAS1 (i.e. SAS1-K25A/F42A, compare to **Fig. 24**) had a similar effect as the complete inactivation of SAS1 activity (**Fig. 58B** and see above). These results demonstrate that reduced (p)ppGpp levels are likely to affect the cellular heterogeneity of *B. subtilis* PY79. Furthermore, they provide further evidence for the importance of the allosteric stimulation of SAS1 for the activity of the protein.

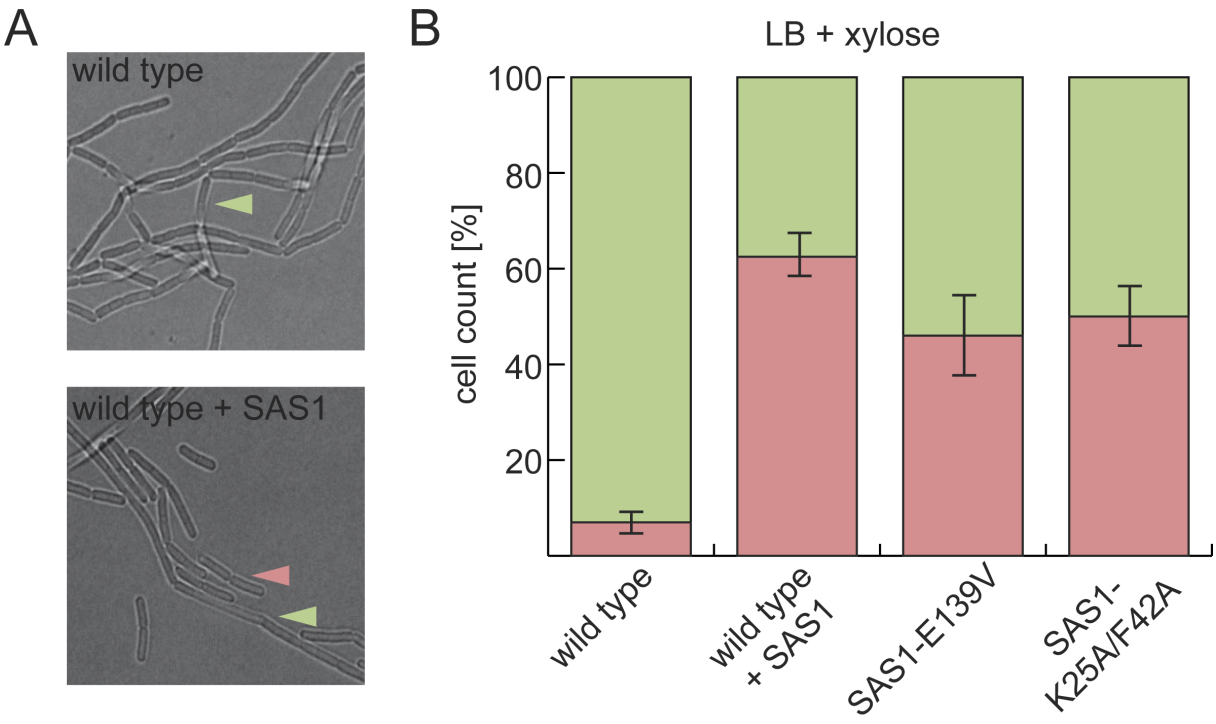

Figure 58. SAS1 is involved in generation of cellular heterogeneity of *B. subtilis*. **A.** Bright-field microscopic images of *B. subtilis* PY79 wild type (top) and *B. subtilis* PY79 overexpressing SAS1 (bottom). Chained and unchained cells of *B. subtilis* are marked with green and red arrows, respectively. **B.** Distribution of *B. subtilis* cells appearing in chains (green) or as unchained cells (red). The distribution was determined from cultures of *B. subtilis* grown in rich medium (LB) supplemented with 0.001% (w/v) xylose to an optical density of 2. Data represent the mean ± standard deviation of three independent measurements.

3.6.3 pppGpp seems primarily responsible in shaping cellular heterogeneity of *B. subtilis*

The increased amount of *B. subtilis* cells appearing as singlets or duplets rather than sessile chains in absence of catalytically active SAS1 might be implemented by either of the alarmones, ppGpp or pppGpp. At first, I tried to complement the phenotype of *B. subtilis* PY79 SAS1-E139V by overexpressing SAS1. The wild type situation of ~90/10% chained versus unchained cells could almost be reestablished by very mild overexpression of SAS1 from the ectopic *amyE* locus (**Fig. 59A**). In this, both the P_{xyl}-inducing xylose and P_{xyl}-repressing glucose had to be present, while addition of xylose alone to the medium led to presumably too strong overexpression of SAS1 (compare to **Fig. 58B**). To further assess which of the two alarmones is

primarily responsible for shaping the observed heterogeneity within the *B. subtilis* population, I introduced Rel-NTD-H77A/D78A into SAS1-E139V at the ectopic *amyE* locus under the control of P_{xyl}. Rel-NTD-H77A/D78A is devoid of any (p)ppGpp hydrolysis through substitution of the conserved and essential catalytic residues His77 and Asp78 (50, 54, 60). Moreover, this construct almost exclusively produces pppGpp at physiological GTP/GDP levels, i.e. 5 mM GTP and 0.5 mM GDP (**Fig. 59B**, (172)). Strikingly, mild overexpression of this Rel-NTD variant in SAS1-E139V phenocopied the mild overexpression of SAS1 in the same strain and almost reestablished the distribution ratio of chained/unchained cells found in wild type *B. subtilis* PY79 (**Fig. 59A**). This suggests that pppGpp is primarily responsible in shaping cellular heterogeneity of *B. subtilis*. However, no quantification of the amounts of overexpressed SAS1 and Rel-NTD was attempted by e.g. quantitative Westen-blotting and therefore it cannot be entirely ruled out that ppGpp synthesis by Rel-NTD might still contribute to complementation of the single-cell phenotype of SAS1-E139V.

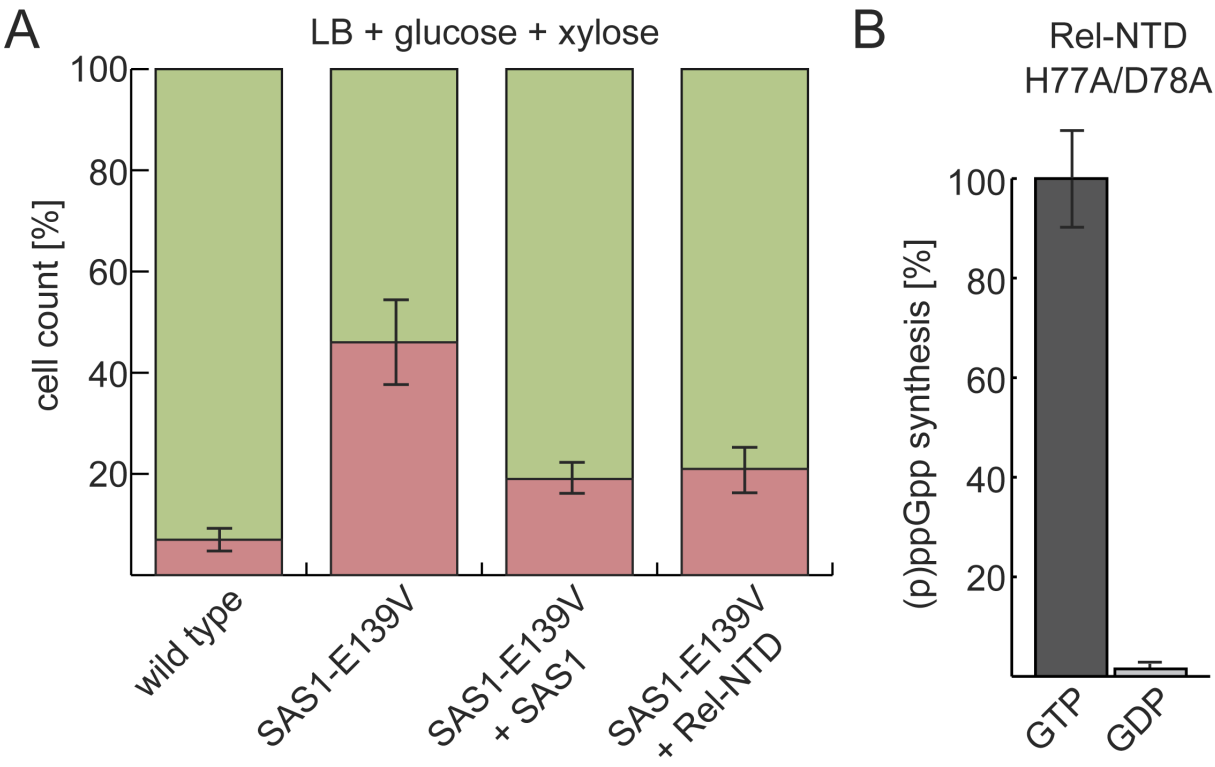

Figure 59. pppGpp is primarily responsible for generation of cellular heterogeneity of *B. subtilis*. **A.** Distribution of *B. subtilis* cells appearing in chains (green) or as unchained cells (red). The distribution was determined from cultures of *B. subtilis* grown in rich medium (LB) supplemented with 0.5% (w/v) glucose and 0.001% (w/v) xylose to an optical density of 2. Data represent the mean ± standard deviation of three independent measurements. **B.**

Synthesis of pppGpp (black) and ppGpp (grey) by Rel-NTD at intracellular levels of GTP/GDP. Data represent the mean ± standard deviation of three independent measurements.

3.6.4 SAS1 confers resistance to zinc stress in *B. subtilis*

Zinc ions were shown to stimulate the (p)ppGpp synthetase activity of SAS2 (compare to **Fig. 41**). Moreover, a recent study indicated that the addition of zinc oxide nanoparticles to *B. subtilis* growing in rich medium induced the expression of SAS2 by approximately 7-fold and led to an approximately 2-fold increase in intracellular (p)ppGpp levels (173). I therefore suspected that SAS2 should somehow be involved in sensing and/or transducing the zinc signal.

As the binding site for zinc could not be established on SAS2 and a selective disruption of zinc-dependent stimulation was therefore impossible, I constructed a strain in which similarly to SAS1 the essential Glu154 of SAS2 was replaced by valine (i.e. SAS2-E154V). The growth curve of *B. subtilis* PY79 SAS1-E139V, SAS2-E154V and the parenteral strain grown in LB medium supplemented with 0.3 mM $ZnCl_2$ suggests that SAS1 rather than SAS2 is important at high zinc concentrations present in the medium (**Fig. 60A**).

Investigation of the cellular heterogeneity of SAS1-E139V under these conditions reveals a slight decrase of cells appearing in chains compared to cultivation in LB medium without $ZnCl_2$ (i.e. 30% in presence versus 50% in absence of $ZnCl_2$, compare to **Figs. 58B** and **60A**). This might suggest that a functional SAS1 is even more important in the presence of $ZnCl_2$.

Noteworthy, also SAS2-E154V displays a high degree of single cells (i.e. 60%) although the growth behaviour was similar to the wild type strain (**Figs. 60A** and **B**). This demonstrates that (p)ppGpp from whatever source, either SAS1 or SAS2, is responsible in altering the cellular heterogeneity of chained and unchained cells in *B. subtilis*.

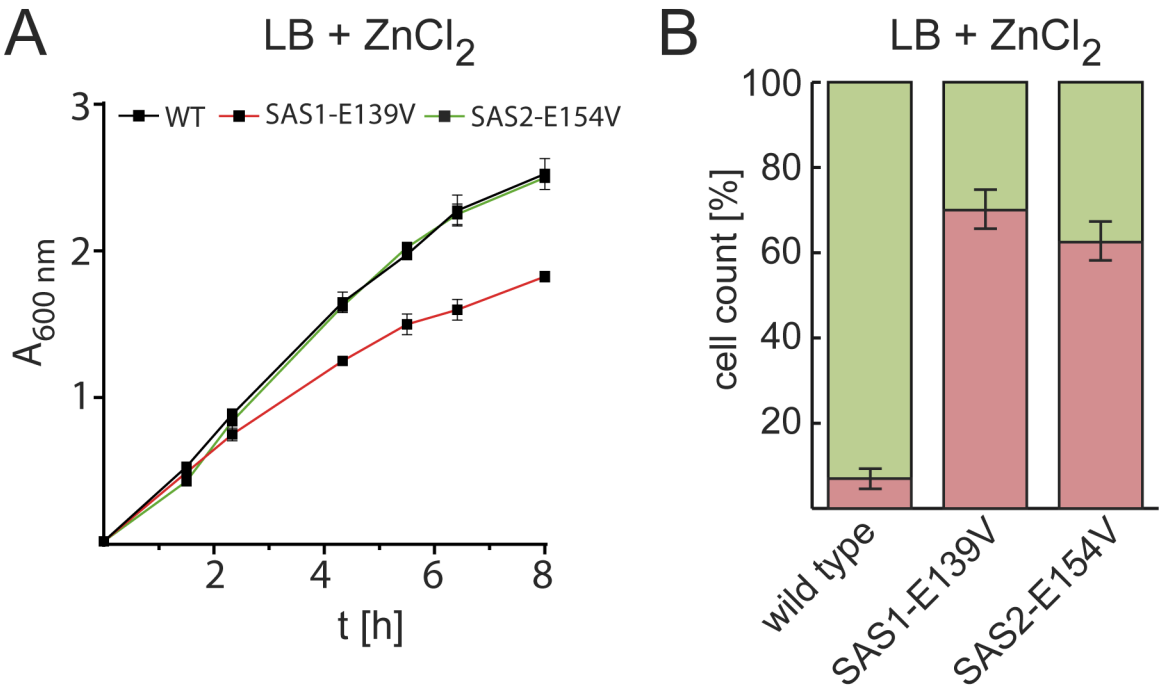

Figure 60. SAS1 confers resistance to elevated zinc levels in *B. subtilis.* **A.** Growth of *B. subtilis* PY79 wild type (black), SAS1-E139V (red) and SAS2-E154V (green) strains in rich medium (LB) supplemented with 0.3 mM $ZnCl_2$. Data represent the mean ± standard deviation of three independent measurements. **B.** Distribution of *B. subtilis* cells appearing in chains (green) or as unchained cells (red). The distribution was determined from cultures of *B. subtilis* grown in rich medium (LB) supplemented with 0.3 mM $ZnCl_2$ to an optical density of 1. Data represent the mean ± standard deviation of three independent measurements.

3.7 Structural comparison of alarmone binding to different cellular targets

The crystal structure of SAS1 in complex with pppGpp revealed an unusual conformation of the nucleotide bound within the allosteric site of the protein (compare to **Fig. 13**). In this, the 3' and 5' OH phosphate moieties wrapped around a magnesium ion in a ring-like arrangement. I asked whether (p)ppGpp would exhibit a similar conformation on any other target protein. To compare the binding modes of (p)ppGpp to its effector molecules, I searched the Protein Data Bank (PDB) for structures of (p)ppGpp bound to target proteins (**Fig. 61**).

Target	Organism	Ligand	PDB ID	Reference
BipA	*E. coli*	ppGpp/magnesium	4ZCM	(174)
BipA	*E. coli*	ppGpp	5A9Y	(175)
Obg	*B. subtilis*	ppGpp/magnesium	1LNZ	(69)
GMK	*S. aureus*	pppGpp/magnesium	4QRH	(18)
DnaG-RPD	*S. aureus*	ppGpp/manganese	4EDT	(127)
DnaG-RPD	*S. aureus*	pppGpp/manganese	4EDV	(127)
RNAP	*T. thermophilus*	ppGpp/magnesium	1SMY	(130)
RNAP	*E. coli*	ppGpp	4JKR	(133)
RNAP	*E. coli*	ppGpp	4JK1	(112)
RNAP	*E. coli*	pppGpp	4JK2	(112)
CadA/LdcI	*E. coli*	ppGpp	3N75	(148)
NatA	*Saccharomyces cerevisiae*	ppGpp	4HNX	unpublished
RF3	*Desulfovibrio vulgaris*	ppGpp	3VR1	(176)

Figure 61. Structures related to (p)ppGpp bound to cellular targets within the PDB. The figure contains parts of Table 1 from ref. (48).

Comparison of the configuration of the nucleotide adopted at its target proteins reveals three major orientations of the ligand: *i.*) (p)ppGpp adopts a 'stretched' conformation, in which the 3' and 5' OH phosphate moieties point away from each other (**Fig. 62A-D**). *ii.*) (p)ppGpp adopts a 'ring-like' arrangement, in which the 3' and 5' OH phosphate moieties wrap around one or two magnesium ions bound between the phosphates (**Fig. 62E-H**). *iii.*) (p)ppGpp adopts a 'ring-like' arrangements that is not aided by a metal ion cofactor (**Fig. 62I-L**). Strikingly, the binding and/or inhibitory constants exhibited by the bound alarmones seem to correlate with their binding mechanism. The 'stretched' conformation seems to confer only rather weak binding with K_i values above 100 µM. The 'ring-like' conformation of (p)ppGpp, however, allows for much stronger binding of the alarmones with Ki values ranging from approximately 1 µM (LdcI-ppGpp, **Fig. 62L**) to 30 µM (BipA-ppGpp, **Fig. 62I**). This stronger binding of 'ring-like' (p)ppGpp is observed regardless of the presence of a metal ion cofactor mediating this conformation. For example, in LdcI, an arginine residue seems to provide the basis for the wrapping of the 3' and 5' OH phosphate moieties (**Fig. 62L**). This example also illustrates, that residues from two opposing subunits can establish the binding site of the alarmone molecule.

Taken together, (p)ppGpp possesses an enormous conformational flexibility mainly conferred through its ribose moiety that allows interaction with a plethora of cellular targets (**Figs. 61** and **62**).

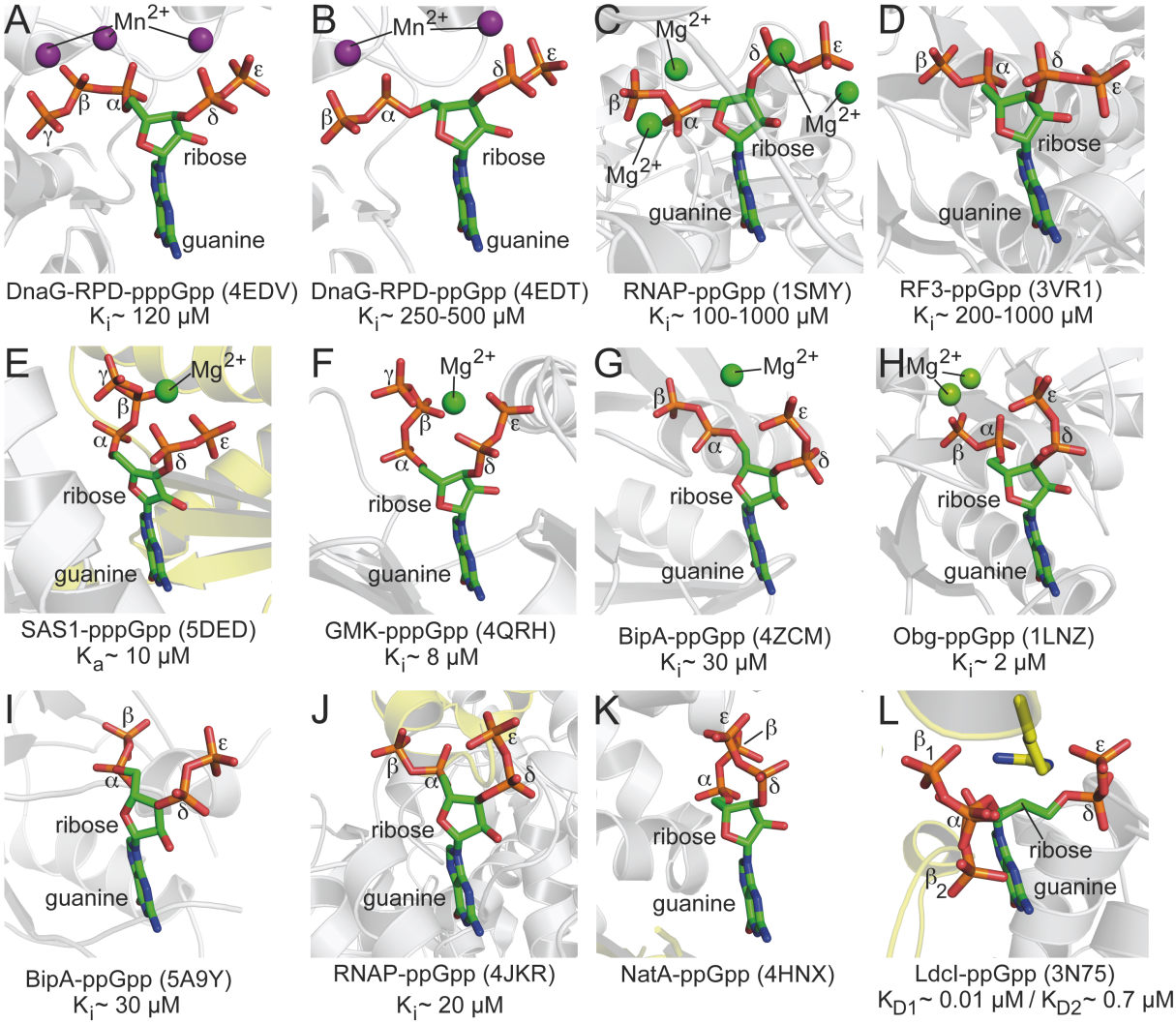

Figure 62. Stretched and ring-like conformations adopted by (p)ppGpp. Alarmones (shown as sticks) were superimposed based on their guanosine moiety. Carbon, nitrogen, oxygen and phosphate atoms are colored in green, blue, red and orange, respectively. Cellular target, PDB ID and binding, inhibitory or stimulatory constants of the alarmone-bound target are given where available. **A-D.** Stretched conformation of (p)ppGpp. **E-H.** Ring-like conformation of (p)ppGpp aided by magnesium ion(s). **I-L.** Ring-like conformation of (p)ppGpp without the aid of metal ion cofactors. Images were obtained from the structure listed in Fig. 61. The figure is rearranged from ref. (48).

Discussion

4.1 Structural and functional characterization of small alarmone synthetases

The alarmones ppGpp and pppGpp are the mediators of the stringent response in bacteria and are synthesized by proteins of the RSH-type family. Two homologs of this protein family have been identified in *E. coli*, RelA and SpoT (50, 177). While RelA proteins are essential for the adaptation of bacteria to amino acid limiting conditions (8, 9, 91), SpoT is implicated to confer resistance to carbon starvation (65, 66). However, two additional RSH-type proteins, the small alarmone synthetases (SAS) SAS1 and SAS2 have been discovered recently (56, 57, 70). SAS proteins differ from RelA/SpoT in length and domain architecture. Mainly, they lack the C-terminal regulatory part present in RelA/SpoT that mediates their interaction with stalled ribosomes and the acyl carrier protein, respectively (**Fig. 2A**). Also, SAS protein are only present in the firmicutes phylum but absent in e.g. γ-proteobacteria obscuring their role during the stringent response.

4.1.1 SAS1 integrates cellular energy imbalances into the stringent response

The structural and functional characterization of SAS1 from *B. subtilis* revealed two major features of the protein: *i.*) SAS1 synthesizes ppGpp and pppGpp with different efficiencies (**Fig. 21A**). *ii.*) Synthesis of ppGpp and pppGpp by SAS1 is stimulated through binding of the product pppGpp to an allosteric cleft provided by the SAS1 homotetramer (**Figs. 11** and **23**). These distinct features allow bacteria to convert different stress types into (p)ppGpp levels via SAS1 (**Fig. 63**). Under nutrient-rich conditions, the RelA/SpoT homolog Rel would remain absent from the ribosome and be in its hydrolytically active state (**Fig. 63,** I). Cellular alarmone levels should then be low and insufficient to allosterically stimulate SAS1. In this synthetically less active form, synthesis of ppGpp and pppGpp by SAS1 would solely depend on the intracellular concentrations of GDP and GTP, which are estimated to be

approximately 0.5 and 5 mM, respectively (172). Simply because GTP is in large excess over GDP, pppGpp should be the primary alarmone product. This preference is negated when the intracellular GTP/GDP ratio is altered towards higher GDP levels (**Fig. 63, *II***). While the total alarmone pool would reach similar levels as in the previous scenario (see above), the ratio between the ppGpp and pppGpp alarmone should differ. Indeed, few studies report disparate roles of both alarmones on bacterial physiology. In *E. coli*, pppGpp is less potent than ppGpp with respect to growth rate regulation and transcription from the ribosomal P1 promoter (2, 112). Conversely, the DNA-dependent RNA polymerase DnaG from *B. subtilis* seems more susceptible to inhibition by pppGpp than ppGpp (10). Nevertheless, SAS1 is a rather inefficient (p)ppGpp synthetase in the absence of stimulating pppGpp and only mildly affeces intracellular alarmone levels (**Fig. 63,** I and II). Under nutrient limiting conditions (i.e. amino acid starvation) however, Rel senses the presence of uncharged tRNAs at the ribosome (91). Detection of the so-stalled ribosomes leads to synthesis of alarmones by Rel and inactivation of their hydrolysis as both activities of Rel are mutually exclusive (53, 54). Because of the preference of Rel for pppGpp synthesis and the excess of intracellular GTP over GDP, pppGpp would be the major product of (p)ppGpp synthesis by Rel (**Fig. 50**, (80, 81, 155)). The intracellular concentration of pppGpp would exceed a certain threshold allowing for allosteric stimulation of SAS1. In this scenario, SAS1 would serve as an amplifier of the signal provided by Rel (**Fig. 63,** III).

Although the three scenarios are unlikely to occur independently, cells would be able to integrate different stress types (i.e. imbalances in GTP/GDP levels via SAS1 and amino acid starvation via Rel/SAS1) at the level of ppGpp and pppGpp. This notion is supported by the observation that (p)ppGpp levels appear to be linked to the cellular energy state as decreased GTP levels render *B. subtilis* more capable of surviving amino acid starvation (15, 17). Moreover, the low basal activity (i.e. allosterically stimulating pppGpp below certain threshold) of SAS1 might provide a mechanism that allows for control of GTP levels in the absence of nutrient-limiting conditions as ppGpp and pppGpp are also able to inhibit multiple enzymes for GTP biosynthesis (15-18, 143).

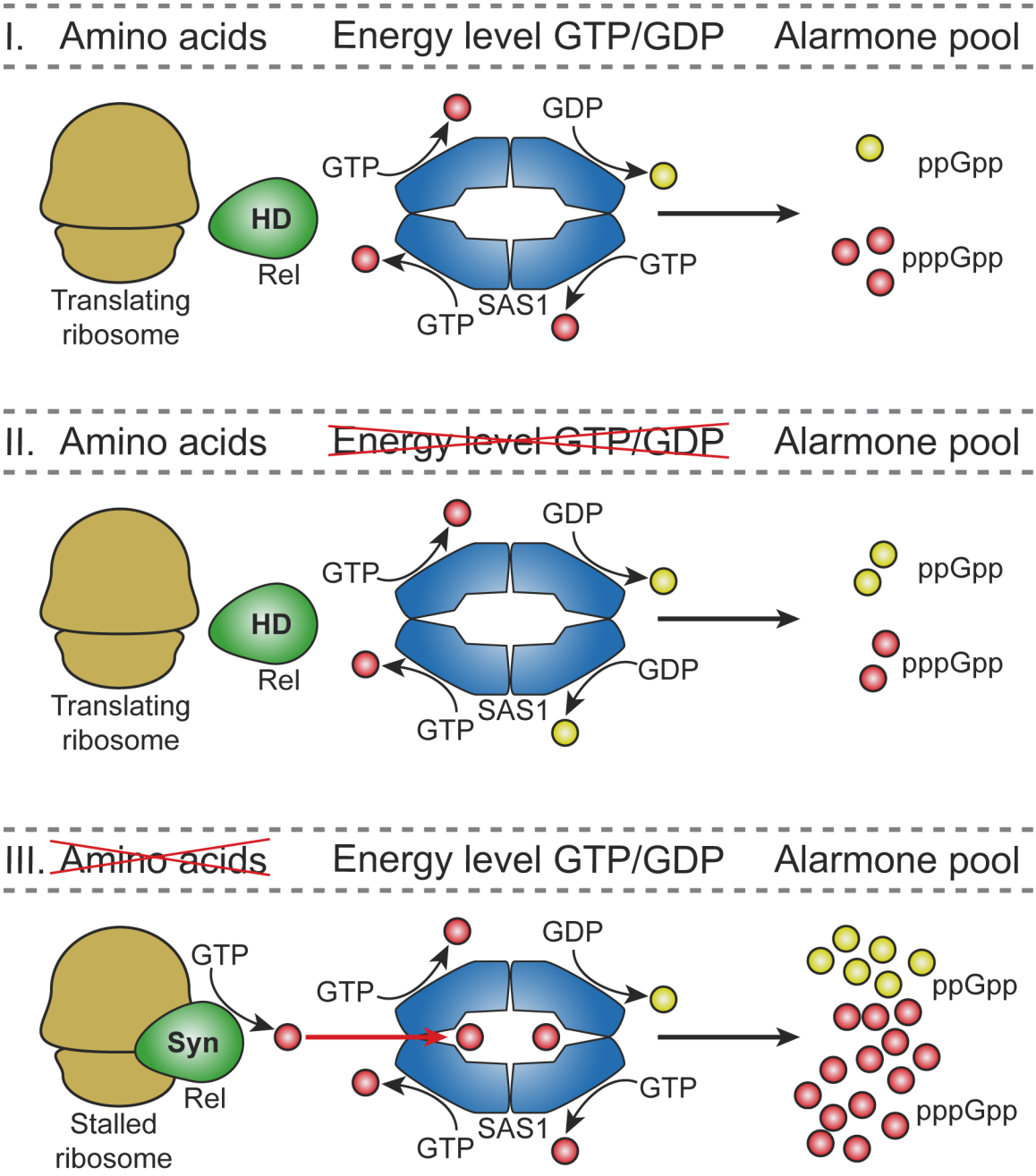

Figure 63. Influence of SAS1 on alarmone levels in *B. subtilis*. Sections I-III depict three different scenarios of how SAS1 contributes to alarmone levels in *B. subtilis*. Further details are given in the text.

4.1.2 Role of SAS2 in mediation of zinc-depleted stress

The topology of SAS2 is highly reminiscent to SAS1 (**Fig. 30**). Nevertheless, both proteins decisively differ in their susceptibility to allosteric regulation (**Figs. 34** and **39**). At first hand, it seems mysterious where from the SAS2-stimulating Zn^{2+} might originate.

Zinc is an enormously important cofactor in bacteria, as approximately 6% of the total proteome are estimated to coordinate zinc ions. Although most of these proteins (i.e. ~80%) are enzymes, zinc is also found as cofactor in transcription factors or ribosomal proteins (160, 178, 179). In order to acquire sufficient amounts of zinc, bacteria developed intricate regulatory circuits ensuring its availability. The transcription factor Zur belongs to the class of metal-sensing transcription factors whose DNA-binding activity is regulated by the reversible binding of zinc (180). When bound to zinc, Zur represses the transcription of the *znuABC* operon encoding for the high-affinity Zn^{2+} ABC transporter uptake system ZnuABC (180). Under zinc limitation, Zur-dependent repression is relieved allowing for increased zinc uptake into the bacterial cell.

Bacteria face zinc limitation e.g. during host infection caused by uptake of free extracellular into macrophages that deliver the ion into their phagocytes and other intracellular vesicles to activate antimicrobial responses including direct zinc toxicity (181). Moreover, the cell wall antibiotic vancomycin induces zinc starvation in bacteria by direct interaction with Zn^{2+} (182) and through sensing by the VraRS two-component system (183-185). Strikingly, the transcription of SAS2 from *B. subtilis* and *S. aureus* is upregulated in presence of various stress conditions including ethanol, high salt, acidic or alkalic pH and various cell wall antibiotics including vancomycin (57, 71, 73-75, 185). This allows to propose a model of how allosteric stimulation of SAS2 by zinc ions might confer resistance to vancomycin stress (**Fig. 64**). The presence of vancomycin is sensed by the extracellular domain of VraS (**Fig. 64,** step 1). The cytosolic domain of VraS is autophosphorylated under consumption of ATP and the phosphate subsequently transferred onto the response regulator VraR (**Fig. 64,** step 2). In this activated form, VraR induces transcription of the *ywaC* gene encoding for SAS2 (**Fig. 64,** step 3). Simultaneously, vancomycin reduces the

concentration of free extracellular Zn^{2+} by chelation (**Fig. 64,** step 4) resulting in a reduced availability of the ion within the microorganism. By this, the repressor of zinc uptake Zur is inactivated (**Fig. 64,** step 5) resulting in increased transcription of znuABC (**Fig. 64,** step 6). ZnuABC, most likely in concert with the zinc scavenging lipoprotein ZinT (186-188), provides an increased influx of Zn^{2+} (**Fig. 64,** step 7) subsequently resulting in increased (p)ppGpp levels through allosteric stimulation of SAS2 (**Fig. 64,** step 8). It is unclear so far how other environmental stress signals acting on the bacterial cell wall (see above) are sensed and translated into the stringent response network.

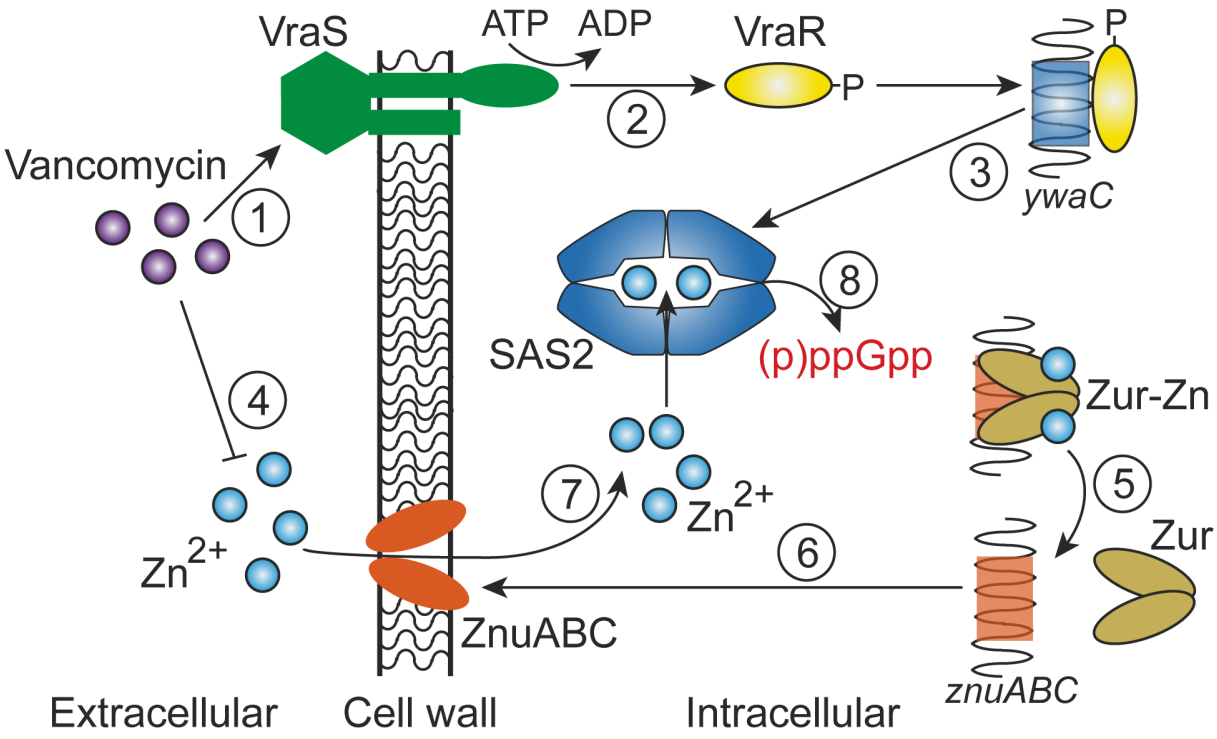

Figure 64. Model depicting the zinc-dependent stimulation of the stringent response via SAS2. Further details are given in the text.

The zinc ions for allosteric stimulation of SAS2 might however also originiate from other sources. Zn^{2+} is a cofactor of many ribosomal proteins (189). Therefore, during unstressed conditions zinc ions are consumed during ribosomal assembly (**Fig. 65**). The GTPases RbgA, HflX, RsgA and Era involved in assembly of mature ribosomes from the 30S and 50S ribosomal subunits are subject to inhibition by ppGpp under stringent response conditions (**Fig. 65B**, (14)). This ppGpp might originate from

either Rel or SAS1. Reduced ribosomal biogenesis results in a decreased consumption of Zn^{2+} and elevated intracellular levels that might cause allosteric stimulation of SAS2 (**Fig. 65**). Moreover, zinc-independent homologs of the ribosomal proteins S14, L31 and L33 were identified in *B. subtilis* that are expressed during zinc deprivation and can replace their zinc-dependent counterparts (180, 189, 190).

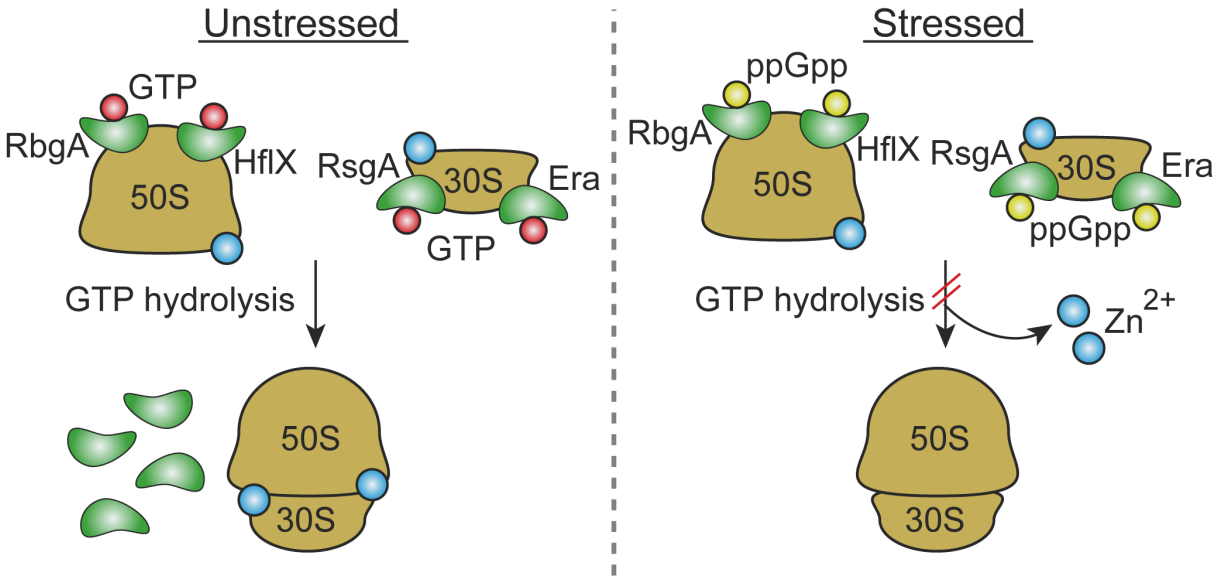

Figure 65. Inhibition of ribosome biogenesis through ppGpp might free up Zn^{2+} for SAS2. The GTPases RbgA, HflX, RsgA and Era (green) are involved in assembly of mature ribosomes (ochre) relying on hydrolysis of GTP (red). Inhibition of the GTPases by ppGpp (yellow) under stressed conditions frees up Zn^{2+} (blue) that might serve as stimulator for SAS2. The image was adapted from ref. (14).

In a recent study, the addition of zinc oxide nanoparticles or zinc sulfate to *B. subtilis* led to a strong overexpression of the *ywaC* gene while an increased expression of *yjbM* could not be observed (173). An indirect effect of the nanoparticles was ruled out as titanium oxide nanoparticles failed to result in similar effects on the transcriptome. Conversely, in my studies *B. subtilis* PY79 carrying an inactive SAS1 variant was severely impaired in growth in the presence of zinc ions contrasted to a strain harboring an inactive SAS2 variant that behaved like the parenteral strain (**Fig. 60**). It is therefore unclear how elevated zinc levels contribute to the stringent response via an increased activity of SAS2.

4.1.3 SAS1 and SAS2 are 'tailored' for their role during the stringent response

Besides differences in allosteric regulation, SAS1 and SAS2 displayed a different v/S characteristic of (p)ppGpp synthesis (**Figs. 21** and **36**). The maximal velocities of (p)ppGpp synthesis by SAS1 and SAS2 are comparable. However, the K_m values of below 0.5 mM for (p)ppGpp synthesis exhibited by SAS2 are much smaller than the K_m values of 1.7 and 1.2 for synthesis of ppGpp and pppGpp, respectively, featured by SAS1. Differences in the G-Loop conferring coordination of the GDP/GTP substrate provide the structural basis for this disparity. Hence, SAS2 synthesizes (p)ppGpp much more efficiently at low GDP/GTP concentrations than SAS1.

These differences in enzymatic activitiy of both proteins are in agreement with their different transcriptional profile during growth of *B. subtilis* (**Fig. 66**). While the transcript of *yjbM* encoding for SAS1 is mainly present during logarithmic growth, transcripts of *ywaC* encoding for SAS2 are only observed in the stationary phase (57, 72). Although the presence of transcripts does not necessarily have to correlate with protein levels, this observation seems to be in agreement with the different functional roles of SAS1 and SAS2. In principle, no stringent response caused by e.g. amino acid starvation should occur during logarithmic growth as nutrients are abundant. Nevertheless, the presence of SAS1 influences the transition between sessile, non-flagellated cells appearing in chains and flagellated single cells or duplets (**Fig. 66**, compare to **Fig. 58**). Despite this heterogeneity in the cell population of *B. subtilis*, no impact on the growth behavior of the culture was evident (**Fig. 56**). This suggest that (p)ppGpp levels are still as low as to not lead to growth inhibition of *B. subtilis* yet are sufficient to cause alterations in the cellular metabolism exemplified by the heterogenous cell population. In contrast, SAS2 has been reported to mediate hibernation of ribosomes. In this, two ribosomes are hold together at their small ribosomal subunits by the hibernation factor YvyD only present in the firmicutes (191). Noteworthy, only overexpression of SAS2 but not SAS1 in *B. subtilis* causes this effect (72). However, the appearance of 100S ribosomes was also observed to be dependent on the presence of *relA* in *E. coli*, which lacks SAS1/SAS2 (192) thus suggesting that (p)ppGpp and not SAS2 *per se* promotes ribosome hibernation. Anyhow, the high enzymatic activity of SAS2 already at low GDP/GTP concentrations even in the absence of stimulating Zn^{2+} would allow for a rapid increase of

intracellular (p)ppGpp in turn realizing adaptational processes within the microorganism (**Fig. 66**).

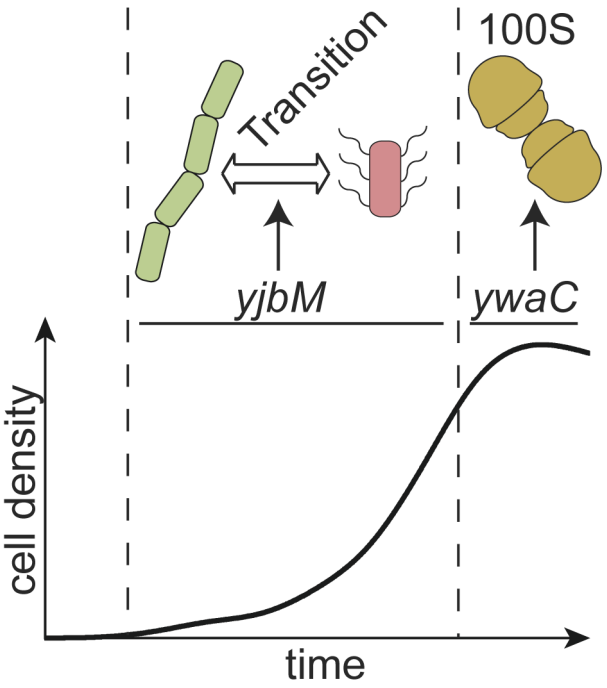

Figure 66. SAS1 and SAS2 are tailored for their functional role in the bacterial cell. Transcription of *yjbM* (encoding for SAS1) and *ywaC* (encoding for SAS2) distinctly differs during growth of *B. subtilis* (indicates by black bars). SAS1 does influence the transition between sessile (green) and motile (red) cell types. SAS2 is involved in mediation of the formation of translational inactive 100S ribosomes (ochre).

4.2 The stringent response can be solely mediated by SAS1 and SAS2

So far, the bifunctional Rel protein and the (p)ppGpp synthetases SAS1 and SAS2 are the only contributors to (p)ppGpp metabolism in *B. subtilis* (50, 57). The elucidation of their enzymatic properties therefore allows for a preliminary model of (p)ppGpp metabolism (**Fig. 67**). In the absence of amino acid starvation, the bifunctional Rel protein predominantly exhibits (p)ppGpp hydrolytic activity (**Figs. 50** and **51**). In presence of 1 mM of alarmones, Rel hydrolyzes approximately 22 or 11 nmol * min^{-1} * nmol Rel^{-1} ppGpp or pppGpp, respectively (**Fig. 51**). Thereby, (p)ppGpp hydrolysis by Rel surmounts (p)ppGpp synthesis provided by SAS1 and SAS2 (**Fig. 67A**, compare to **Figs. 21** and **36**). It must be noted that intracellular levels of 1 mM (p)ppGpp are typically only reached during amino acid starvation (193). Nevertheless, basal levels of (p)ppGpp are estimated to be below 10 µM

evidencing that (p)ppGpp hydrolysis by Rel is indeed more efficient than synthesis by SAS1 and SAS2 under these non-stringent conditions. In the presence of allosteric stimulators of SAS proteins (i.e. pppGpp and Zn^{2+}), however, (p)ppGpp synthesis surmounts (p)ppGpp hydrolysis by Rel (**Fig. 67B**). Regulatory proteins that inhibit Rel's hydrolytic activity might aid in the subsequent increase of intracellular alarmone levels. The membrane associated ATPase ComGA involved in the development of genetic competence of *B. subtilis* is implicated to exhibit this function through direct interaction with Rel (194). These considerations are based on the assumption that the intracellular concentration of Rel, SAS1 and SAS2 are comparable. The number of Rel molecules can be estimated to be approximately 250 given a ratio of one moleculre Rel per 200 ribosomes and ~50000 ribosomes per cell (165). However, no quantitative measurement of SAS1 and SAS2 molecules per cell is available so far.

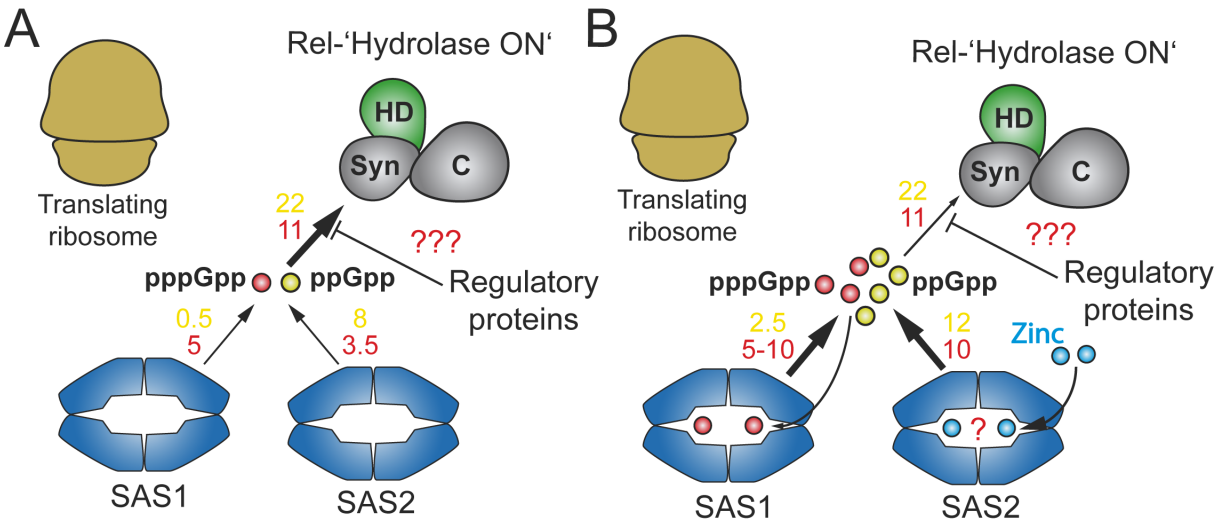

Figure 67. Model of stringent response in the absence of amino acid starvation. SAS1 and SAS2 (blue) establish the ppGpp (yellow balls) and pppGpp (red balls) pools in *B. subtilis*. These are efficiently cleared by the Rel hydrolase (HD, green) in the absence of amino acid starvation (**A**). In the presence of elevated pppGpp and/or zinc levels, (p)ppGpp synthesis by SAS1 and SAS2 surmounts (p)ppGpp hydrolysis by the Rel hydrolase (**B**). Unknown regulatory proteins might permit or assist in increasing (p)ppGpp levels by inhibition of the Rel hydrolase. Yellow and red numbers indicate the rates of ppGpp (yellow) and pppGpp (red) synthesis by SAS1/2 and hydrolysis by Rel in nmol * min^{-1} * nmol $protein^{-1}$. Rates of synthesis are given for 0.5 mM and 5 mM GDP and GTP, respectively. Rates of hydrolysis are given for 1 mM ppGpp or pppGpp.

4.3 Regulation of Rel's opposing activities in the absence of the ribosome

Recent cryo-EM structures provided detailed insights in the conformation of Rel when bound to stalled ribosomes (61, 95, 96). However, the domain topology of Rel in the absence of the ribosome is largely unknown so far. In this study, full-length Rel and a truncated variant lacking the regulatory CTD of Rel (**Fig. 68A**) were biochemically characterized.

The CTD of Rel was so far mainly appreciated for mediating binding of Rel to stalled ribosomes leading to a rapid accumulation of intracellular (p)ppGpp (30, 82, 90). Nevertheless, one study by Cashel and coworkers provided evidence for a regulation of Rel's activites by the CTD in the absence of the ribosome (53). In this, the presence of the CTD negatively affected (p)ppGpp synthesis while in turn (p)ppGpp hydrolysis was stimulated. Moreover, a hexa-histidine tag fused C-terminally to the protein mildly stimulated (p)ppGpp synthesis and almost completely abrogated (p)ppGpp hydrolysis similar to the complete lack of the CTD (53).

The contribution of domains present in Rel's CTD could be refined in this study. Mainly the far C-terminal ACT domain confers diminished (p)ppGpp synthesis of non-ribosomally associated *B. subtilis* Rel (**Fig. 49**) and stands in contrast to an earlier study on *M. tubercolusis* Rel where truncation of the ACT domain did not result in increasing (p)ppGpp synthesis (101). Neverthelss, the results from this study allow to deduce a model of Rel's domain topology albeit structural information is lacking (**Fig. 68B**). Binding of Rel to stalled ribosomes mediated by the CTD lures the ACT away from the Syn domain thereby relieving inhibition of (p)ppGpp synthesis. At the same time (p)ppGpp hydrolysis should be reduced (**Fig. 51**). How the (p)ppGpp synthetic activity of Rel is further enhanced by binding to ribosomes remains elusive as the limited resolution of the cryo-EM structures do not allow for inspection of conformational changes within the Rel-NTD.

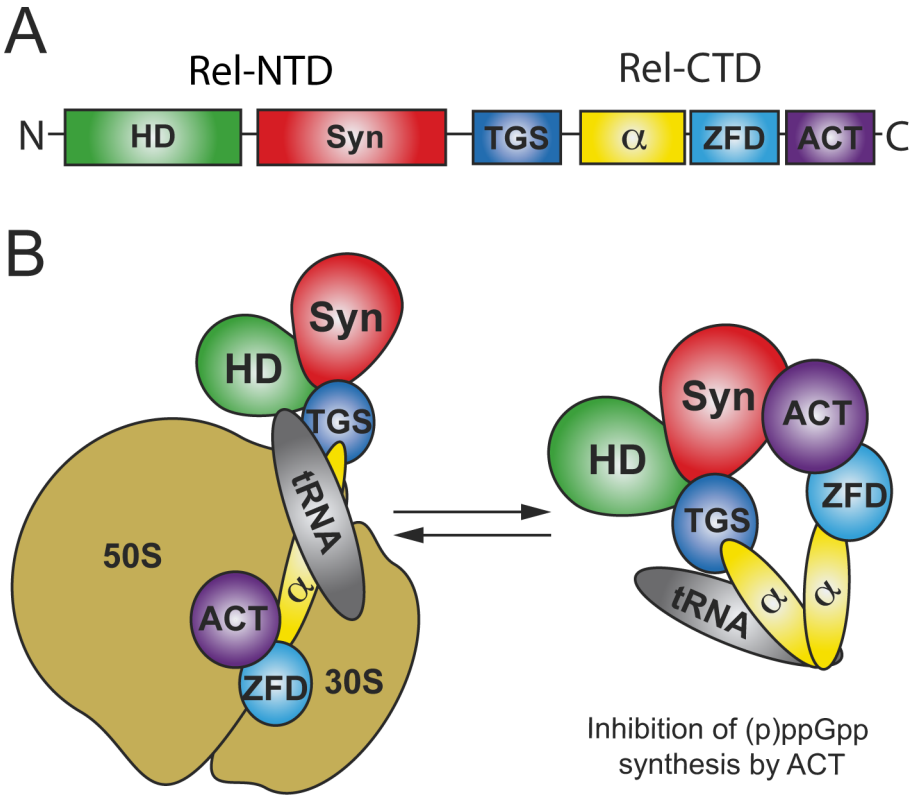

Figure 68. Domain topology of Rel. **A.** Domain architecture of Rel. **B.** Model depicting the domain topology of Rel adapopted in the presence and absence of the ribosome. Domains of Rel are colored as in (**A**).

The presence of uncharged tRNA within the ribosomal A-site is generally considered as the primary agent for binding of Rel to and stimulation by the so-stalled ribosome (83). However, it is only evident that the activity of Rel is stimulated in the presence of uncharged tRNA within the ribosomal A-site (58, 87, 91, 195, 196) and not where this tRNA originates. In fact, an interaction between Rel and tRNA has already been observed in the absence of the ribosome (51, 52, 101). *Vice versa*, Rel is able to bind to ribosomes in the absence of tRNA but its (p)ppGpp synthesis is only minorly stimulated (195). It is therefore not surprising that the Rel protein retained significant amounts of tRNA during purification of the protein (personal communication: Patrick Pausch). Taken together, further structural and functional studies are required to finally decipher the molecular details of the stringent factor Rel.

4.4 Disparate effects of ppGpp and pppGpp on bacterial lifestlye

The alarmones ppGpp and pppGpp are most often collectively referred to as (p)ppGpp. Although both alarmones mediate similar adaptational processes in their host microorganism, there is also growing evidence that they affect the same targets to different extent (10, 112).

Experiments performed in the course of this work support this notion. Substitution of SAS1 by the catalytically inactive variant SAS1-E139V in the genome of *B. subtilis* PY79 resulted in an increased percentage of the population appearing as flagellated single cells. An ectopically integrated copy of SAS1 restored the situation present in wild type *B. subtilis* PY79 (**Fig. 59A**). However, also ectopic introduction of Rel-NTD, which almost exclusively produces pppGpp, into *B. subtilis* PY79-E139V reestablished the ratio of flagellatet versus non-flagellated cells present in wild type (**Figs. 59A** and **B**). This observation does not rule out the possibility that also a lack of intracellular ppGpp (caused by inactivation of SAS1) might have contributed to the observed phenotype. Nevertheless, pppGpp was able to restore the wild type condition. It might therefore also be possible that ppGpp was not present at all under the experimental conditions so that only the lack of pppGpp – and subsequently its replenishment through ectopic expression of Rel-NTD – resulted in the cellular heterogeneity. The kinetic parameters of (p)ppGpp synthesis by SAS1, SAS2 and Rel also seemingly favor this idea as all three proteins primarily synthesize pppGpp at physiological GDP/GTP levels. Conversely, Rel exhibits a higher rate of ppGpp degradation compared to pppGpp (**Fig. 67**). How might the ability to synthesize and degrade (p)ppGpp relate to specific bacterial lifestyles? Two prototypic ‘stringent response networks’ do exist in bacteria that are restricted to bacterial clades (**Fig. 69**).

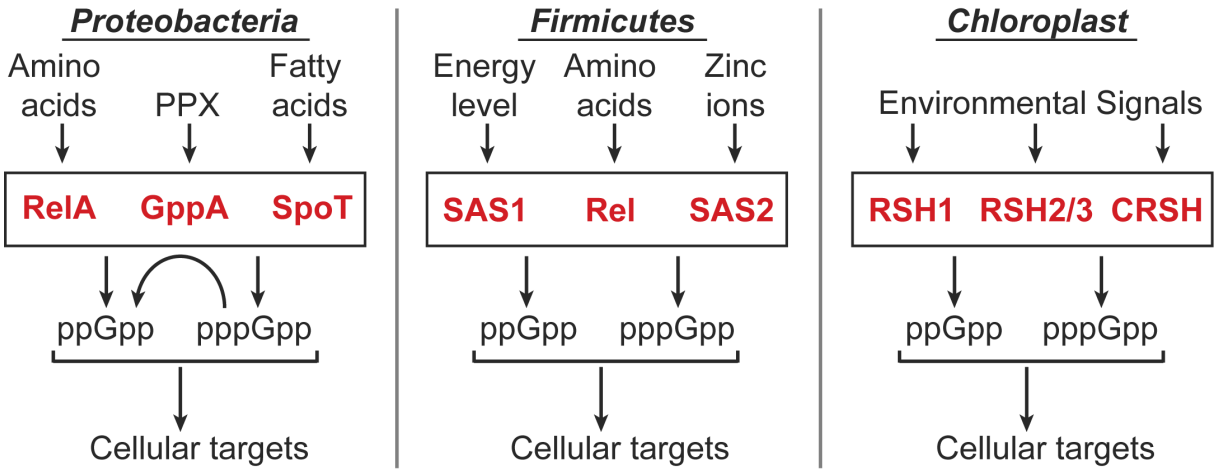

Figure 69. Scheme of prototypic 'stringent response networks' found in bacteria and plant chloroplasts.

In proteobacteria, the two monofunctional long RSH-type proteins RelA and SpoT do exist. Additionally, proteobacteria possess the protein GppA able to degrade pppGpp to ppGpp by removal of the 5' OH γ-phosphate (43). Firmicutes, however, only harbor one monofunctional long RSH-type protein and the two small alarmone synthetases SAS1 and SAS2 but lack the GppA enzyme (**Fig. 69**). Based on the kinetic properties of (p)ppGpp synthesis and hydrolysis exhibited by those enzymes, it might be suspected that each network results in the primary production of either ppGpp or pppGpp. The monofunctional RelA from *E. coli* favors synthesis of ppGpp over pppGpp. Moreover, the GppA protein converts pppGpp directly into ppGpp. In this, mainly ppGpp should be the mediator of the stringent response in proteobacteria, which is exemplified by the observation that ppGpp has a stronger impact on growth rate control and reduction in rRNA synthesis in *E. coli* (112). In firmicutes, pppGpp should be the predominant alarmone based on its higher synthesis through by the three (p)ppGpp synthetases present, the slower degradation by Rel and the absence of an interconverting enzyme similar to GppA. This notion is supported by the observation made in this study that synthesis of pppGpp by introduction of Rel-NTD into a *B. subtilis* strain lacking catalytically active SAS1 was able to restore cellular heterogeneity (**Fig. 59**).

Noteworthy, BLAST analysis in firmicutes revealed the presence of an ortholog of GppA in *M. tuberculosis* (**Fig. 70**), which is has not been described so far (50). Besides, *M. tuberculosis* harbors the Rel and SAS1/2 proteins typical for firmicutes.

The contribution of this GppA to the (p)ppGpp pools iand how this might be related to the lifestyle of *M. tuberculosis* is not yet clear.

Plant chloroplasts heavily differ in their enzymes from bacteria (**Fig. 69**). This and the lack of kinetic data for these enzymes do not allow to deduce any prioritization of ppGpp or pppGpp as mediatos of the stringent response.

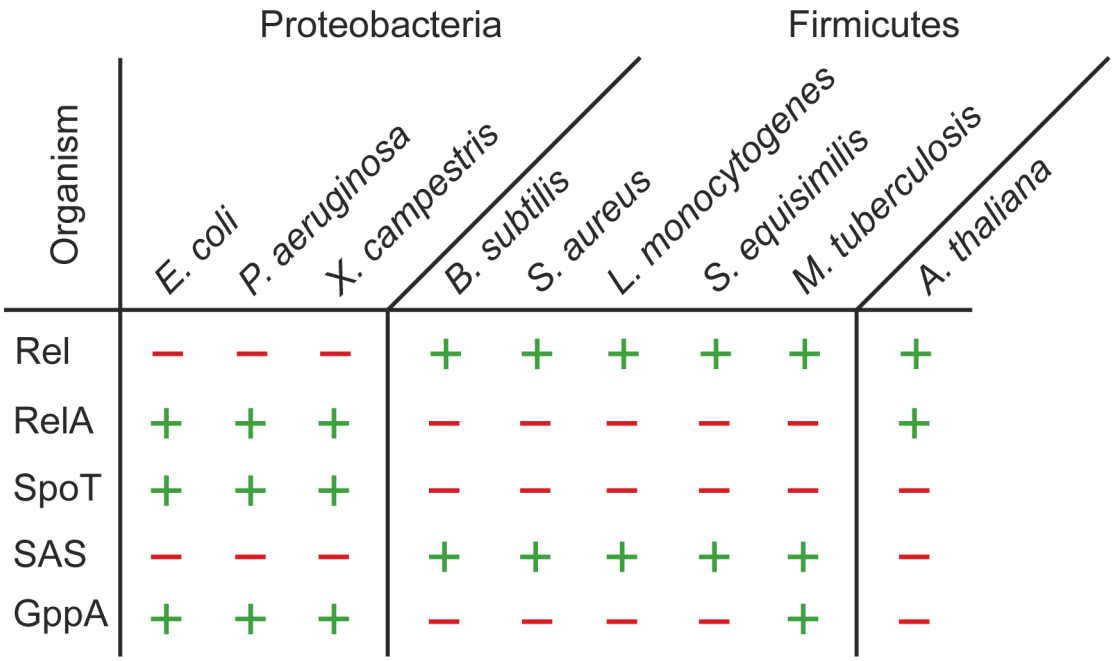

Figure 70. Presence of enzymes involved in (p)ppGpp metabolism in selected bacterial and plant species. The annotation is primarily based on ref. (50).

4.5 Alarmones gradually adapt microorganisms to environmental cues

Alarmone levels range between 1-10 µM under non-stringent response conditions and reach approximately 1 mM during the stringent response caused by e.g. amino acid starvation (193). The alarmones ppGpp and pppGpp exhibit different inhibitory constants for regulation of the activity of their respective cellular target (**Figs. 61** and **62**), that might be as low as 1 µM.

Ordering the cellular targets by increasing inhibitory constants reveals a gradual effect of (p)ppGpp on the dogmatic cellular processes (**Fig. 71**). Enzymes involved in amino acid (i.e. *Ec*LdcI) and nucleotide metabolism (i.e. *Bs*GMK and *Bs*SAS1) are already targeted by (p)ppGpp at basal levels of the alarmones. With increasing (p)ppGpp concentrations, translational GTPases are inhibited. Inhibition of DNA

replication and transcription by binding to DnaG and RNAP, respectively, should be the last adaptational processes mediated at very high (p)ppGpp levels (**Fig. 71**). This ordering exemplifies that the bacterial stringent reponse adapts the host microorganism gradually to environmental stresses integrated via (p)ppGpp. Nevertheless, this also solidifies the assumption that (p)ppGpp already plays fundamental roles under non-stressed or only mild stress conditions in preparation of even harsher environmental conditions and/or stresses.

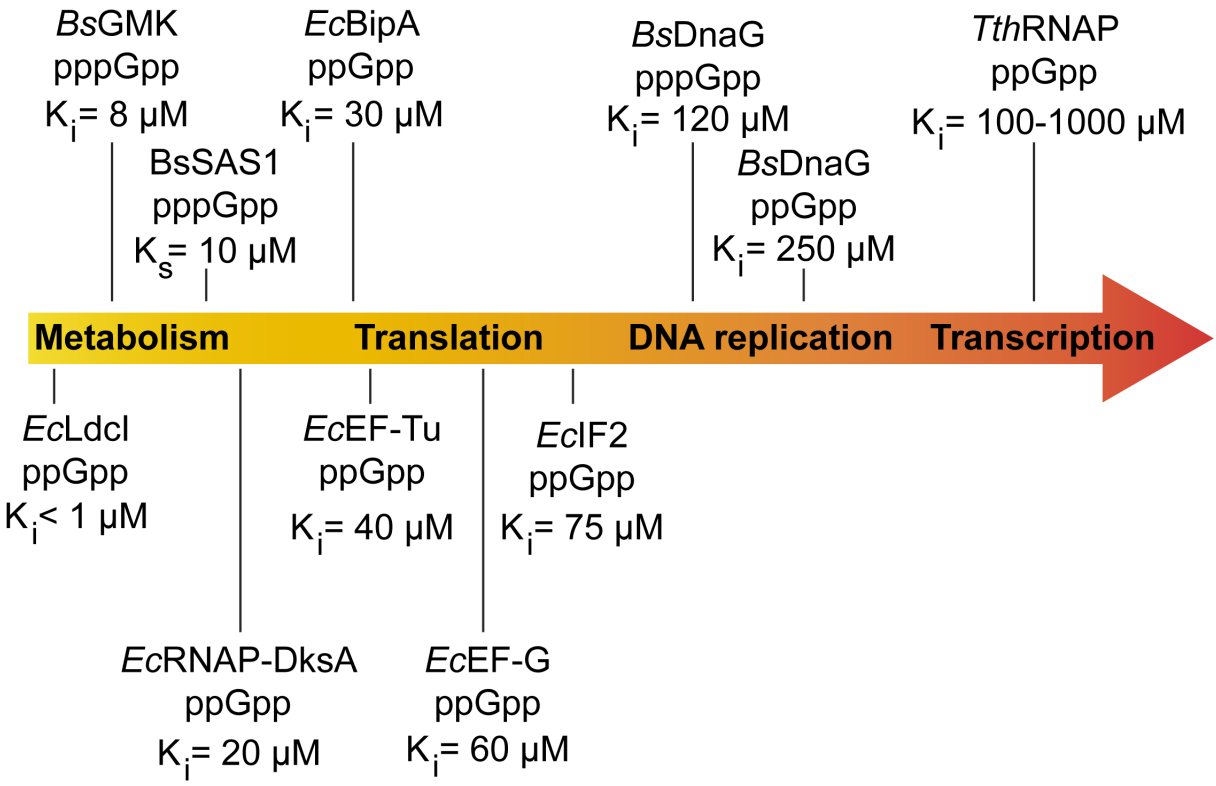

Figure 71. The alarmones (p)ppGpp gradually affect cellular targets. The references for the K values are: *Ec*LdcI-ppGpp (148), *Bs*GMK-pppGpp (18), *Bs*SAS1-pppGpp (151), *Ec*RNAP-DksA-ppGpp (135), *Ec*BipA-ppGpp (174), *Ec*EF-Tu-ppGpp and *Ec*EF-G-ppGpp (197), *Ec*IF2-ppGpp (198), *Bs*DnaG-pppGpp and *Bs*DnaG-ppGpp (127) and *Tth*RNAP-ppGpp (131).

4.6 The bacterial stringent response as a target for antibiotic treatment

Given the fundamental role of alarmones as second messengers in microorganismic metabolism and the fact that they are seemingly restricted to bacteria and plant chloroplasts, an inhibition of (p)ppGpp synthesis and hydrolysis as the basis for future antimicrobial treatment seems possible.

In this respect, Ben-Yehuda and coworkers reported a the (p)ppGpp analogous compound relacin as an inhibitor of (p)ppGpp synthesis by Rel (**Fig. 72**, (199)). Unfortunately, relacin displays only moderate inhibition of Rel. In relacin, the 3' and 5' OH phosphate moieties were replaced by glycil-glycine dipeptides linked to the ribose by carbamate bridges. Although this substitution should confer stability against hydrolysis of the phosphates, it impedes the conformational flexibility of the phosphates (or its stereoisomeric analogs in relacin) that seems essential for the establishment of high-affinity interactions with its target (**Fig. 62**).

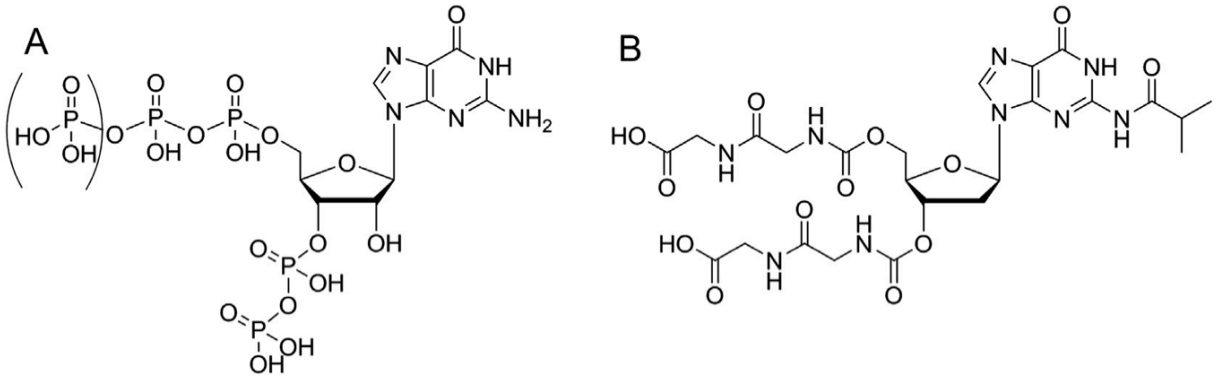

Figure 72. The antibiotic Relacin targeting the (p)ppGpp synthetase Rel. Chemical formulas of (p)ppGpp (**A**) and Relacin (**B**).

An attractive alternative to inhibition of (p)ppGpp synthesis by compounds targeting the active site of (p)ppGpp synthetases seems to be offered by the allosteric site of SAS1. The possibility of allosteric stimulation through coordination of pppGpp is essential for SAS1's activity. This is exemplified by the observation that a strain with a disrupted allosteric binding site displayed similar cellular heterogeneity phenotypes as a strain harboring a catalytically inactive variant of SAS1 (**Fig. 58**). As many human-pathogenic bacteria are members of the firmicutes harboring SAS proteins, this knowledge might guide the development of future antibiotics. In this regard, these antibiotics would also already interefere with (p)ppGpp adaptation at its earliest stage, i.e. adaptational changes in nucleotide metabolism (**Fig. 71**).

Materials and Methods

5.1 Materials

5.1.1 Chemicals and consumables

Chemicals were purchased from Sigma Aldrich, Carl Roth, AppliChem or Acros in biochemical grades unless otherwise stated. Eluents for HPLC (gradient grade) were from VWR. Nucleotides were purchased from Sigma Aldrich or Jena Bioscience in highest available grade. Consumable plastic ware (reaction tubes, falcon tubes, pipette tips, syringes) was from Sarstedt and Braun. HPLC vials and caps were from Macherey-Nagel.

5.1.2 Enzymes and cloning equipment

Q5 High-Fidelity DNA Polymerase, restriction enzymes and T4 DNA Ligase with their corresponding buffers were purchased from New England Biolabs (NEB). Desoxynucleoside triphosphates (dNTPs, 100 mM of each dNTP) were from Fermentas. Purification of DNA and preparation of plasmids from *E. coli* cells were carried out using the QIAquick Gel Extraction Kit and QIAprep Spin Miniprep Kit, respectively (both Qiagen) according to the manufacturer's manuals. Agarose gels for analysis of DNA were prepared in TBE-buffer according to the experimental requirements. GeneRuler 1kb (Thermo Scientific) served as size standard for agarose gel electrophoresis.

5.1.3 Bacterial strains and plasmids

5.1.3.1 Oligonucleotides

Oligonucleotides were purchased from Sigma Aldrich or Eurofins Genomics in the purity 'salt free'. All oligonucleotides used in this study are listed in **Table S4**.

5.1.3.2 Plasmids

For overproduction of hexa-histidine tagged proteins in *E. coli*, the vector pET24d(+) (Novagen) was employed. For integration of DNA into *B. subtilis*, the vectors pMAD (200) and pSG1154 (201) were utilized.

All plasmids used in this study are listed in **Table S5**. Plasmids were obtained using techniques deschribed in chapter **6.2.1**.

5.1.3.3 Strains

For plasmid amplification, chemically competent *E. coli* DH5α cells (Thermo Scientific) were employed. Proteins were produced in chemically competent *E. coli* BL21 (DE3) cells (Thermo Scientific). Strains of *B. subtilis* were generated as described under 6.2.2 and are listed in **Table S6**.

5.1.4 Growth media and buffers

5.1.4.1 Growth media

Lysogeny broth (LB) medium was purchased as a premix from Roth and sterilized (121 °C, 20 min) before use. For preparation of LB medium for cultivation of *E. coli* and *B. subtilis*, 20 or 25 g/l of LB premix were used, respectively. S7 minimal medium for cultivation of *B. subtilis* was prepared as described previously (169). Shortly, stock solutions of buffer salts (10x), trace elements (100x), glucose (50x), K-glutamate (100x) and casamino acids (250x) were sterilized by filtration through a 0.2 µM filter under aseptic conditions and mixed with sterilized (121 °C, 20 min) destilled water to obtain the desired final concentrations in the medium.

S7 minimal medium		
Stock solution	**Component**	**Final concentration**
Buffer salts, pH 7.0 with KOH	MOPS	50 mM
	$(NH_4)_2SO_4$	10 mM
	KH_2PO_4	5 mM
Trace elements	$MgCl_2$	2 mM
	$CaCl_2$	0.7 mM
	$MnCl_2$	50 µM
	$FeCl_3$	5 µM
	$ZnCl_2$	1 µM
	Thiamine-HCl	1 µg/ml
	HCl	20 µM
Glucose	Glucose	1% (w/v)
Glutamate	Monopotassium glutamate	0.1% (w/v)
Casamino acids	Casamino acids	0.004% (w/v)

5.1.4.2 Antibiotics

All antibiotics were purchased from Carl Roth and Sigma Aldrich. 1000x concentrated stock solutions were prepared by dissolving the antibiotic in the appropriate solvent and filtrated through a 0.2 µM filter under aseptic conditions. Antibiotic stock solutions were stored at -20 °C until use. Antibiotics were used in the following final concentrations:

Organism	Antibiotic	Final concentration	Solvent
B. subtilis	Spectinomycin	100 µg/ml	ddH_2O
	Erythromycin	1 µg/ml	70% (v/v) ethanol
	Lincomycin	25 µg/ml	ddH_2O
E. coli	Ampicillin	100 µg/ml	ddH_2O
	Kanamycine	50 µg/ml	ddH_2O

5.1.4.3 Buffers for protein purification

Proteins were purified by a two-step protocol employing Ni-NTA affinity chromatography and size-exclusion chromatography (SEC). Buffers in the left column were used for purification of SAS1, SAS2 and Rel-NTD. Buffers in the right column were used for purification of Rel. PMSF was added to the Rel lysis buffer as a 100x concentrated stock solution prepared by dissolving PMSF in isopropanol.

SAS1/SAS2/Rel-NTD	
Ni-NTA Lysis buffer	
HEPES	20 mM
$MgCl_2$	20 mM
KCl	20 mM
NaCl	250 mM
Imidazole	40 mM
pH 8.0 with NaOH	

Rel	
Ni-NTA Lysis buffer	
Tris	50 mM
NaCl	500 mM
Imidazole	40 mM
PMSF	1 mM
pH 8.0 with NaOH	

Ni-NTA Elution buffer	
HEPES	20 mM
$MgCl_2$	20 mM
KCl	20 mM
NaCl	250 mM
Imidazole	500 mM
pH 8.0 with NaOH	

Ni-NTA Elution buffer	
Tris	50 mM
NaCl	500 mM
Imidazole	500 mM
pH 8.0 with NaOH	

SEC buffer	
HEPES	20 mM
$MgCl_2$	20 mM
KCl	20 mM
NaCl	200 mM
pH 8.0 with NaOH	

SEC buffer	
Tris	50 mM
NaCl	500 mM
pH 8.0 with NaOH	

5.1.4.4 Buffers for HDX

D_2O-containing SEC buffer for deuteration of SAS1 and Rel during HDX experiments (see chapter **5.2.8**) was prepared by dissolving the solid components in deuterium oxide 99.9% (Sigma Aldrich). The pD value of the solution was adjusted to 7.5 using 10 M NaOD obtained by dissolving NaOH in deuterium oxide 99.9%. During determination of the pD value of deuterated SEC buffer with a pH electrode calibrated for H_2O, the differing dissociation constants of H_2O and D_2O were taken into account (202). Peptides were separated during HDX employing HDX buffer A and B. The quench buffer for stopping the HDX reaction and the wash solution for cleaning the columns used in the HDX setup were prepared as follows:

HDX quench buffer	
KH_2PO_4/H_3PO_4	400 mM
pH 2.2 with H_3PO_4	

HDX column wash solution	
Acetonitrile	4% (v/v)
Guanidine-HCl	500 mM

HDX buffer A	
ddH_2O	
Formic acid	0.1 % (v/v)

HDX buffer B	
Acetonitrile	
Formic acid	0.1 % (v/v)

5.1.4.5 Buffers for HPLC

For separation and elution of nucleotides during HPLC analysis, the following buffers were employed:

HPLC buffer A	
KH_2PO_4	50 mM
K_2HPO_4	50 mM
TPAB	10 mM
Acetonitrile	15% (v/v)

HPLC buffer B	
Acetonitrile	100% (v/v)

5.1.4.6 Buffers for AX chromatography

For separation and elution of nucleotides during AX chromatography, the following buffers were employed:

AX buffer A	
Tris	20 mM
pH 8.0 with HCl	

AX buffer B	
Tris	20 mM
NaCl	1 M
pH 8.0 with HCl	

5.1.4.7 Buffers for agarose gel electrophoresis

Agarose gels were prepared by dissolving agarose in TBE buffer. For visualization of nucleic acids, ethidium bromide was directly added to the gels in a final concentration of approximately 0.00005% (w/v). The following buffers were used for agarose gel electrophoresis:

TBE buffer	
Tris	90 mM
Boric acid	90 mM
EDTA	2 mM

pH 8.3 with NaOH

6x DNA loading dye	
TBE buffer	1x concentrated
Glycerole	20% (v/v)
Bromophenol blue	0.25% (w/v)

5.1.4.8 Buffers for SDS-PAGE

Gels for sodium dodecyl sulfate polyacrylamide gel electrophoresis (SDS-PAGE) were prepared using a Mini-PROTEAN 3 Multi-Casting Chamber (Biorad) and stored at 4 °C until use. The stacking and separation gels had the following composition:

Component	Stacking gel	Separation gel
Acrylamide/Bisacrylamide (37.5/1)	4.5% (w/v)	15% (w/v)
Tris	125 mM	375 mM
SDS	0.1% (w/v)	0.1% (w/v)
APS	0.1% (w/v)	0.1% (w/v)
TEMED	0.1% (v/v)	0.1% (v/v)
Final pH adjusted with HCl	6.8	8.8

For loading and running of SDS-PAGE gels and visualization of proteins, the following buffers were employed:

SDS running buffer	
Tris	25 mM
Glycine	192 mM
SDS	0.1% (w/v)

5x SDS loading dye	
Tris-HCl pH 6.8	300 mM
SDS	10% (w/v)
β-mercaptoethanol	25% (v/v)
Glycerine	25% (v/v)
Bromophenol blue	0.05% (w/v)

SDS staining solution	
Comassie R250	0.36% (w/v)
Ethanol 99%	45.5% (v/v)
Acetic acid 99%	9% (v/v)

SDS destaining solution	
Ethanol 99%	30% (v/v)
Acetic acid 99%	10% (v/v)

5.1.4.9 Nucleotides

Nucleotides were typically employed as ~50-100 mM concentrated stock solutions in ddH_2O and were adjusted in pH to 7.5 using NaOH. Concentrations of stock solutions were determined by spectrophotometric measurement applying extinction coefficients of ε = 15400 $M^{-1} * cm^{-1}$ and ε = 11500 $M^{-1} * cm^{-1}$ at 260 nm for ATP and guanosine nucleoside (GDP, GTP, ppGpp and pppGpp), respectively (203).

5.1.5 Protein biochemistry

Prepacked columns (HisTrap FF, 1 ml) for purification of hexa-histidine tagged proteins were purchased from GE Healthcare. Purified proteins were concentrated using Amicon Ultra-15 centrifugal filter units (Merck Millipore) with molecular weight cut-offs of 10 kDa. PageRuler unstained protein ladder (Thermo Scientific) and Pierce unstained protein MW marker (Thermo Scientific) served as standards for molecular weight estamination on SDS-PAGE gels.

5.1.6 Crystallization and Data collection

Crystallization screens were carried out by the sitting-drop method in SWISSCI MRC 2-well or SWISSCI MRC 3-well plates (Jena Bioscience) using the JCSG Core Suites (Qiagen) with 96 conditions on each plate. Crystals were looped with equipment sourced from Hampton Research (CrystalCap Spine HT, CrystalCap SPINE Vial and CrystalWand Magnetic). Diffraction data of crystals were collected at the European Synchrotron Radiation Facility (ESRF) in Grenoble, France at beamlines ID23-1, ID23-2 and ID29.

5.1.7 Laboratory equipment

Equipment	Supplier
Centrifuges	
Sorvall LYNX 6000	Thermo Scientific
A27-8 x 50 Fixed Angle Rotor	Thermo Scientific
Fiberlite F9-6 x 1000 LEX Fixed Angle Rotor	Thermo Scientific
Heraeus Megafure 40R	Thermo Scientific
Heraeus Fresco 21 Centrifuge	Thermo Scientific
Heraeus Pico 21 Centrifuge	Thermo Scientific
Columns for protein purification	
HiLoad 26/600 Superdex S200 pg	GE Healthcare
HiLoad 26/600 Superdex S75 pg	GE Healthcare
HisTrap FF, 1 ml	GE Healthcare
FPLC systems	
ÄKTApurifier	GE Healthcare
ÄKTAprime	GE Healthcare
HDX equipment	
ACQUITY UPLC M-Class system with HDX technology	Waters

Two-arm robotic autosampler	LEAP Technologies
Enzymate BEH Pepsin column 2.1 x 30 mm	Waters
ACQUITY UPLC BEH C18 1.7 µm 1.0 x 100 mm column	Waters
AQUITY UPLC BEH C18 1.7 µm 2.1 x 5 mm VanGuard	Waters
SYNAPT G2-Si	Waters
HPLC equipment	
Agilent 1100 Series	Agilent Technologies
G1311A Quaternary Pump	Agilent Technologies
G1313A Autosampler	Agilent Technologies
G1314A Variable wavelength detector (VWD)	Agilent Technologies
G1316A Column Compartment	Agilent Technologies
G1379A Degasser	Agilent Technologies
EC 250/4.6 NUCLEODUR C18 HTec, 3 µm	Macherey-Nagel
Agilent ChemStation B.04.03	Agilent Technologies
Microscopes	
SZM-2	Optika Microscopes
AX70 Research System Microscope	Olympus
UPlanSApo 100x/1.40 objective	Olympus
Photometrics CoolSnap ES^2 CCD camera	Visitron Systems
Incubators	
WiseCube	Wisd Laboratory Instruments
Ecotron	Infors HT
Incucell	MMM Medcenter Einrichtungen GmbH

Weights	
Präzisionswaage PCB, d = 0.1g	Kern
S-203, d = 0.001 g	Denver Instrument
SI-203, d = 0.1 mg	Denver Instrument
Miscellaneous	
SDS-PAGE equipment	Biorad
Agarose gel equipment	Cleaver Scientific
Ultrospec 10 Cell Density Meter	Amersham
T100^{TM} Thermal cycler	Biorad
M-110L Microfluidizer	Microfluidics
Gel iX20 Imager	Intas
Crystal Gryphon LCP	ARI - Art Robbins Instruments
Peristaltic pump	Gilson
NanoDrop Lite	Thermo Scientific
HI-2211 Bench Top pH & mV meter	Hanna Instruments

5.2 Methods

5.2.1 Molecular cloning

Genes encoding for *Bs*SAS1, *Bs*SAS2, *Bs*Rel and *Sa*SAS2 were amplified from genomic DNA of *B. subtilis* PY79 and *S. aureus* SA113 by polymerase chain reaction (PCR) using Q5 High-Fidelity DNA Polymerase (NEB) according to the manufacturer's manual. Oligonucleotide primers (see **Table S4**) were designed according to the following gene annotations: BSU11600 (*Bs*SAS1), BSU38480 (*Bs*SAS2), BSU27600 (*Bs*Rel) and SA2297 (*Sa*SAS2). A hexa-histidine tag was encoded by the *forward* primer in-frame with the sequence of the cloned genes (see **Table S4**). Protein variants were generated by overlapping PCR. In brief, two fragments of the genes were generated by PCR that overlapped at the mutation site.

These fragments were fused and the resulting mutated gene amplified in a second round of PCR. PCR fragments and vectors were digested at the introduced restriction enzyme sites according to the manufacturer's manual (NEB). Ligations were carried out employing T4 DNA Ligase (NEB) according to the manufacturer's manual and typically contained an approximately 3-fold excess of insert over vector.

DNA was separated and visualized by agarose gel electrophoresis employing TBE as buffer. Purification of DNA and preparation of plasmids from *E. coli* DH5α cells were carried out using the QIAquick Gel Extraction Kit and QIAprep Spin Miniprep Kit, respectively (both Qiagen) according to the manufacturer's manuals.

5.2.2 Purification of recombinant proteins

SAS1, SAS2, Rel and variants thereof were purified by the same procedure with the buffers stated in chapter **6.1.4.3**. *E. coli* BL21(DE3) cells carrying the expression plasmid were grown in LB medium supplemented with 50 µg/ml kanamycine and 12.5 g/l D(+)-lactose-monohydrate for 16 h at 30 °C and shaking at 150 rpm (WiseCube). Cells were harvested (3500 x *g*, 20 min, 4 °C), resuspended in lysis buffer and lysed using a pressure of 18,000 psi through the M-110L Microfluidizer (Microfluidics). After centrifugation (47850 x *g*, 20 min, 4 °C), the clarified supernatant was loaded on a 1-ml HisTrap column equilibrated with 10 column volumes (CV) of lysis buffer. After washing with 15 CV lysis buffer, the protein was eluted with 5 CV elution buffer. The protein was concentrated to ~25 mg/ml using an Amicon Ultracel-10K (Millipore) and applied to size-exclusion chromatography (HiLoad 26/600 Superdex S200 pg) equilibrated in SEC buffer. Fractions containing the pure protein were pooled and concentrated according to the experimental requirements. Protein concentration was determined spectrophotometrically (NanoDrop Lite).

5.2.3 SDS-PAGE

Prior to SDS-PAGE analysis, protein samples were mixed with 5x SDS loading dye in a volume ratio of 5:1. Electrophoresis was performed in a Mini-PROTEAN Tetra cell (Biorad) at 260 V for 35 min. The gels were stained for approximately 30 min using SDS staining solution. After removal of the staining solution, the gels were destained using SDS destaining solution until the protein bands were clearly distinguishable from the background.

5.2.4 Structural biology

5.2.4.1 Crystallization

Crystallization screens were carried out at room temperature by the sitting-drop method in SWISSCI MRC 2-well or SWISSCI MRC 3-well plates (Jena Bioscience) using the JCSG Core Suites (Qiagen). The reservoir volume was 50 µl and the drop volume typically 1 µl containing a 1:1 mixture of protein and crystallization solution.

Crystals of *Bs*SAS1 were obtained from a 20 mg/ml solution after 1 day in 0.1 M MES, pH 5.0, 20% (w/v) PEG 6000. For crystallization of nucleotide-bound states of SAS1, the protein was incubated together with 1 mM of the respective nucleotides (AMPCPP and ATP+GTP yielding pppGpp) for 1 h on ice prior to crystallization. Crystals of *Bs*SAS1-AMPCPP were obtained at 11.5 mg/ml protein concentration after 1 week in 0.2 M KSCN, 20% (w/v) PEG3350. Crystals of *Bs*SAS1-pppGpp were obtained at 11.5 mg/ml protein concentration after 1 week in 0.1 M Citric acid, pH 4.0, 5% (w/v) PEG 6000.

Crystals of *Sa*SAS2 were obtained from a 15 mg/ml solution after 1 week in 0.1 M CHES, pH 9.5, 40% (w/v) PEG600. For crystallization of nucleotide-bound states of SAS2, a 15 mg/ml concentrated solution of the protein was incubated together with 5 mM of the respective nucleotides (AMPCPP, ATP+GTP yielding pppGpp and ATP+GMP yielding pGpp) for 30 min on ice prior to crystallization. Crystals of *Sa*SAS2-AMPCPP were obtained after 2 days from 0.1 M Tris, pH 8.5, 0.2 M lithium sulfate, 30% (w/v) PEG4000. Crystals of *Sa*SAS2-pppGpp were obtained after 7 days from 0.2 M tri-potassium citrate, 20% (w/v) PEG 3350. Crystals of *Sa*SAS2-

pGpp were obtained after three days from 0.2 M tri-potassium citrate, 20% (w/v) PEG 3350.

5.2.4.2 Data collection

Prior to data collection, 0.5 µl of a cryo-protecting solution containing mother liquor supplemented with 20% (v/v) glycerol were added to the crystallization drops. Subsequently, the crystals were looped and flash frozen in liquid nitrogen. Diffraction data of crystals were collected at the European Synchrotron Radiation Facility (ESRF) in Grenoble, France at beamlines ID23-1, ID23-2 and ID29 under laminar nitrogen flow at 100 K (Oxford Cryosystems 700 Series) with a DECTRIS PILATUS 6M detector.

5.2.4.3 Data processing and refinement

Diffraction data were processed with XDS (204) and the CCP4-implemented program SCALA (205). The crystal structure of apo-*Bs*SAS1 was determined by molecular replacement (102) using the CCP4-implemented program PHASER (206) and employing a truncated structure of Rel_{seq} (PDB: 1VJ7, chain A, amino acids 200-340; (54)) as a search model. The nucleotide-bound structures of *Bs*SAS1 and apo-*Sa*SAS2 were determined employing the structure of apo-*Bs*SAS1 (this study) as a search model for MR. The nucleotide-bound structures of *Sa*SAS2 were determined by MR using the structure of apo-*Sa*SAS2 (this study) as search model for MR. Structures were built in COOT (207) and refined with PHENIX refined (208). Figures were prepared with PyMOL (www.pymol.org).

5.2.5 HPLC-based assay for characterization of enzyme kinetics of (p)ppGpp synthetases and hydrolases

All reactions for characterization of enzyme kinetics of (p)ppGpp synthetases and hydrolases were carried out in a total volume of 50 µl in a buffer containing 100 mM HEPES-Na, pH 7.5, 20 mM $MgCl_2$, 20 mM KCl and 200 mM NaCl. The enzyme concentration in the assays and the sampled time points differed between the proteins according to the experimental requirements.

Enzyme kinetics of (p)ppGpp synthesis by SAS1 were determined by incubating 2 µM enzyme together with 5 mM ATP and varying concentrations of GDP or GTP (i.e. 0.1, 0.25, 0.5, 0.75, 1, 2, 3 and 5 mM) at 37 °C. Samples were taken after five different time points (i.e. 1, 3, 5, 7 and 15 min), flash frozen in liquid nitrogen and stored at -20 °C until measurement. HPLC measurements were performed with an Agilent 1100 Series system (Agilent Technologies) and a C18 column (EC 250/4.6 Nucleodur HTec 3 µm; Macherey-Nagel). The frozen samples were rapidly thawn and directly injected into the HPLC system. After running 30 min with HPLC buffer A, a linear gradient up to 90% HPLC buffer B over 20 min was applied at 0.8 ml/min flow rate. The reaction products ppGpp and pppGpp were detected at a wavelength of 260.8 nm and quantified by peak area using ChemStation version B.04.03 (Agilent Technologies).

Enzyme kinetics of (p)ppGpp synthesis by SAS2 were determined by incubating 0.2 µM enzyme together with 5 mM ATP and varying concentrations of GDP or GTP (i.e. 0.05, 0.1, 0.2, 0.3, 0.5, 1, 3 and 5 mM) at 37 °C. Samples were taken after five different time points (i.e. 2, 4, 6, 8 and 10 min). The enzymatic reactions were stopped as follows: Two volume parts chloroform were added to the sample followed by thorough mixing for 30 s. After heat treatment for 30 s at 95 °C, the samples were flash frozen in liquid nitrogen. Subsequently, samples were centrifuged (17300 x *g*, 30 min, 4 °C) while thawing and the aqueous phase containing the nucleotides analyzed by HPLC as described for SAS1 (see above). The reaction products ppGpp and pppGpp were detected at a wavelength of 260.8 nm and quantified by peak area using ChemStation version B.04.03 (Agilent Technologies).

Enzyme kinetics of (p)ppGpp synthesis by Rel and Rel-NTD were determined by incubating 5 µM enzyme together with 5 mM ATP and varying concentrations of GDP or GTP (i.e. 0.1, 0.25, 0.5, 0.75, 1, 2, 3, 4, 5, 7.5 and 10 mM) at 37 °C. Samples were taken after five different time points (i.e. 6, 12, 18, 24 and 30 min). The reactions were stopped and analyzed as described for SAS2 (see above). The reaction product AMP released equimolar to (p)ppGpp was detected at a wavelength of 260.8 nm and quantified by peak area using ChemStation version B.04.03 (Agilent Technologies).

Enzyme kinetics of (p)ppGpp hydrolysis by Rel and Rel-NTD were determined by incubating 2 µM enzyme together with varying concentrations of ppGpp or pppGpp

(i.e. 0.05, 0.1, 0.2, 0.4, 0.6, 0.8, 1, 2, 3 and 5 mM) at 37 °C. Samples were taken after five different time points (i.e. 2, 4, 6, 8 and 10 min). The reactions were stopped and analyzed as described for SAS2 (see above). The amount of GDP or GTP released during hydrolysis of ppGpp or pppGpp, respectively, was determined at a wavelength of 260.8 nm and quantified by peak area using ChemStation version B.04.03 (Agilent Technologies).

The initial velocities of (p)ppGpp synthesis or hydrolysis were obtained from the slope of the linear regression of the amount of reaction product quantified at different incubation times. The so-obtained initial velocities were plotted against the concentration of reaction substrate, i.e. GDP, GTP, ppGpp or pppGpp. Values of K_m, V_{max} and the Hill coefficient (h) ± standard deviation were obtained from the sigmoidal fit of the v/S characteristic using the equation $v = V_{max} S^h/(K_m{}^h + S^h)$. All analysis of kinetic data were carried out using GraphPad Prism version 6.04 for Windows (GraphPad Software, San Diego, California, USA).

5.2.6 Production and purification of (p)ppGpp

For production of ppGpp, 5 µM SAS1 were incubated in SEC buffer together with 10 mM ATP and 10 mM GDP for 30 min at 37 °C. For production of pppGpp, 5 µM SAS1 were incubated in SEC buffer together with 10 mM ATP and 10 mM GTP for 2h at 37 °C. Thereafter, the reaction mixture was thoroughly mixed with one volume part chloroform and centrifuged (17300 x *g*, 5 min, 4 °C). The aqueous phase was removed, the organic phase thoroughly mixed with one volume part ddH_2O and centrifuged (17300 x *g*, 5 min, 4 °C). The combined aqueous phases were subjected to anion-exchange chromatography using a ResourceQ 6-ml column (column volume (CV) = 6 ml) at a flow rate of 6 ml/min. A gradient of NaCl was used for separation of nucleotides established by employing AX buffer A and AX buffer B. In brief, the gradient employed was as follows: 0% B (0-4 CV), 0-18% B (4-9 CV), 18-30% B (9-21 CV), 30-100% B (21-22 CV), 100% B (22-23 CV), 100-0% B (23-24 CV), 0% B (24-27 CV). The alarmones ppGpp and pppGpp typically eluted after 20 and 22% B, corresponding to 200 and 220 mM NaCl, respectively. Fractions containing the desired nucleotides were pooled and lithium chloride added to a final concentration of 1 M followed by the addition of four volume parts ethanol. The suspension was then incubated at -20 °C for 20 min and centrifuged (5000 x *g*, 20 min, 4 °C). The resulting

pellets were washed twice with absolute ethanol, dried and stored at -20 °C. Quality of the so-prepared alarmones was controlled by analytical HPLC and typically yielded ppGpp and pppGpp in purities of 98% and 95%, respectively.

5.2.7 Allosteric regulation of SAS1 and SAS2 by various ligands

The effect of various ligands on (p)ppGpp synthetase activity of SAS1 and SAS2 was basically determined as described in chapter **6.2.6**. In brief, proteins were incubated in a buffer containing 100 mM HEPES-Na, pH 7.5, 20 mM $MgCl_2$, 20 mM KCl and 200 mM NaCl at 37 °C and the reactions stopped by flash freezing in liquid nitrogen. Protein concentration, incubation time and concentrations of substrates and ligands were adjusted to the experimental requirements and are stated in the figures and/or text. HPLC analysis was carried out as described in chapter **6.2.6**, however, a buffer containing 50 mM KH_2PO_4, 50 mM K_2HPO_4, 25% (v/v) acetonitrile and 10 mM TPAB was employed. Mainly to discriminate between (p)ppGpp added to the reaction and newly synthesized (p)ppGpp, the amount of AMP released equimolar to (p)ppGpp during the reaction was quantified in agreement with standards at a wavelength of 260.8 nm. The amount of AMP present as contamination in the ATP substrate was quantified by triplicate measurement of ATP in each experiment.

5.2.8 Hydrogen-Deuterium Exchange Mass Spectrometry (HDXMS)

5.2.8.1 Data acquisition

For HDX analysis of SAS1, 200 pmol (4 µl of 50 µM solution) SAS1 were incubated without or in the presence of nucleotides for 5 min at 37 °C prior to H/D exchange. Nucleotides were added to SAS1 in concentrations of 125 µM (ppGpp and pppGpp) or 1 mM (AMPCPP, GDP or GTP). The mixtures were diluted 10-fold in D_2O-containing SEC buffer to start the H/D exchange and incubated at 37 °C. The reactions were stopped after different incubation times (i.e. 15, 30, 60, 600 sec) through addition of an equal volume of ice-cold quench buffer and directly injected into an ACQUITY UPLC M-class system with HDX technology (Waters). SAS1 was digested online using an Enzymate BEH Pepsin column 2.1 x 30 mm (Waters) at a flow rate of 100 µl/min ddH_2O + 0.1 % (v/v) formic acid at 11 °C and the resulting peptic peptides trapped for 3 min using an AQUITY UPLC BEH C18 1.7 µm 2.1 x 5

mm VanGuard Pre-column (Waters) kept at 0.5 °C (209). Thereafter, the trap column was placed in line with an ACQUITY UPLC BEH C18 1.7 µm 1.0 x 100 mm column (Waters) and the peptides eluted at 0.5 °C using a gradient of water + 0.1 % formic acid (Hdx buffer A) and acetonitrile + 0.1 % formic acid (HDX buffer B) at 40 µl/min flow rate: 5% B (0 min), 5-35% B (0-7 min), 35-85% B (7-8 min), 85% B (8-10 min), 85-95% B (10-10.1 min), 95% B (10.1-11 min), 95-5% B (11-11.1 min), 5% B (11.1-16 min). Mass spectra were acquired in positive ion mode using a SYNAPT G2-Si mass spectrometer equipped with an electrospray ionization source (Waters). Deuterated peptides were detected in High Definition MS (HDMS, (210)) mode including ion mobility separation (IMS). Lock mass spectra were obtained every 30-45 s using [Glu1]-Fibrinopeptide B standard (Waters). Undeuterated peptides of SAS1 were obtained similar as described above by 10-fold dilution of SAS1 in H_2O-containing SEC buffer and detected in Enhanced High Definition MS ($HDMS^E$) mode including IMS of precursor ions within the gas phase and alternating high and low energies applied to the transfer cell (Waters). All measurements were performed in triplicates. Blank runs were performed between each sample to avoid peptide carry-over.

Preparation of samples during HDX analysis of Rel-NTD was aided by a two-arm robotic autosampler (LEAP Technologies) embedded in the same HDX setup as used for SAS1. For each replicate, 6.8 µl of a 50 µM solution of Rel-NTD were mixed with 61.8 µl of D_2O-containing SEC buffer to start the H/D exchange and incubated at 25 °C. Nucleotides (GDP, GTP, AMPCPP and combinations thereof) were present in the SEC buffer at a concentration of 1.1 mM, yielding 1 mM in the final HDX reaction. The reactions were stopped after different incubation times (i.e. 15, 30, 60, 120, 600 sec) by transfer of 55 µl HDX reaction into an equal volume of quench buffer kept at 0.5 °C. 95 µl of the quenched solution were injected into an ACQUITY UPLC M-class system with HDX technology (Waters). LCMS analysis was carried out as described for SAS1 with the exception that a flow rate of 30 µl/min was employed during chromatographic separation of Rel-NTD peptic peptides. All measurements were performed in triplicates. Blank runs were performed between each sample to avoid peptide carry-over. Also, the pepsin column was washed by 3 times injection of 80 µL HDX column wash solution during LCMS of Rel-NTD.

5.2.8.2 Data analysis

Analysis of HDX data was aided by the softwares Protein LynX Global Server (PLGS) and DynamX 3.0 (both Waters). Identification of undeuterated peptides was performed using PLGS with custom-created databases and the setting 'no enzyme'. Only peptides identified in at least two replicates of each nucleotide-bound state were used for assignment of deuterium incorporation in DynamX 3.0. Thresholds of 0.5 min and 25 ppm for retention time and *m/z* values, respectively, were applied for assignment of the deuterated peptides to their undeuterated counterparts. Deuterium incorporation into each peptide was calculated by subtracting the centroid of the isotope distribution of the undeuterated from the deuterated peptides. Relative deuteration was calculated as the quotient between absolute deuteration and the number of backbone amide hydrogens of the peptide (211).

5.2.9 Growth behaviour and cellular heterogeneity of *B. subtilis* strains

5.2.9.1 Generation of *B. subtilis* PY79 strains encoding mutated SAS1 or SAS2

Strains of *B. subtilis* carrying mutations in *yjbM* or *ywaC* encoding for varied SAS1 and SAS2, respectively, were generated using the pMAD-protocol for markerless allelic replacement (200). In brief, *yjbM*$^{K25A/F42A}$, *yjbM*^{E139V} *and ywaC*^{E154V} (where the elevations denote the respective amino acid substitutions in the translated proteins SAS1 and SAS2) were obtained by overlapping PCR as described in chapter **6.2.1**. Additionally, two fragments of ~500 base pairs flanking *yjbM* in the genome were generated by PCR using the primers SAS1-flk1-EcoRI-F and SAS1-flk1-R (flank 1) and SAS1-flk2-F and SAS1-flk2-NcoI-R (flank 2) (**Table S4**). For *ywaC*, only one flank downstream of the gene was generated by PCR employing the oligonucleotides BsSAS2-EcoRI-F and BsSAS2+fla-NcoI-R (**Table S4**). Subsequently, the mutated *yjbM* and *ywaC* genes were fused with their respective flanks by overlapping PCR and cloned into the shuttle vector pMAD via EcoRI/NcoI restriction sites. The so-obtained plasmids were integrated into the *B. subtilis* PY79 genome by homologous recombination (200). Correct replacement of the native *yjbM* and *ywaC* alleles was verifed by DNA sequencing.

5.2.9.2 Generation of *B. subtilis* PY79 strains harboring ectopic integrations

Plasmids for ectopic integration of SAS1 and Rel-NTD H77A/D78A were obtained using the same methods as described in chapter **5.2.1**. The so-obtained plasmids were integrated into the *B. subtilis* PY79 genome by homologous recombination (200). Correct genomic integration into the *amyE* locus was verified by deficiency of the resulting strains to degrade starch and DNA sequencing.

5.2.9.3 Investigation of growth behaviour of *Bacillus subtilis* PY79

B. subtilis PY79 strains were grown on LB agar plates, solidified with 1.5% agar, for 16 h at 37°C. Cells were resuspended in LB medium and further grown for approximately 1 h under vigorous shaking at 37°C. These precultures were used to inoculate 50 ml medium (composition as stated in figures and text) to an OD_{600nm} of 0.02. Cells were further grown under vigorous shaking at 37°C and the OD_{600nm} of the culture determined after regular time intervals (Ultrospec 10 Cell Density Meter, Amersham).

5.2.9.4 Investigation of cellular heterogeneity of *Bacillus subtilis* PY79

B. subtilis PY79 strains were grown on LB agar plates, solidified with 1.5% agar, for 16 h at 37°C. Cells were resuspended in LB medium or LB medium supplemented with 0.5% (w/v) glucose, when glucose was also added to the main culture. These precultures were used to inoculate 50 ml medium eventually supplemented with 0.5% (w/v) glucose and/or 0.001% (w/v) xylose as stated in figures and text, to an OD_{600nm} of 0.02. Cells were then grown under vigorous shaking at 37°C. Samples for light microscopy were taken at an OD_{600nm} of 2.0 ± 0.2 (1.0 ± 0.1 in presence of $ZnCl_2$) and immobilized on an agarose pad, consisting of the respective medium supplemented with 1% (w/v) agarose. Light microscopy was carried out using an AX70 microscope (Olympus) equipped with a UPlanSApo 100x objective (Olympus) with a numerical aperture of 1.40 and a Photometrics CoolSnap ES^2 CCD camera (Visitron Systems). Images were recorded using VisiView Version 1.5.8 software (Visitron Systems). At least 10^3 cells were counted manually for each replicate of the experiment. All experiments were performed in biologically independent triplicates.

For data analysis, > 4 cells connected were considered as long, sessile chains while ≤ 4 connected cells were considered as unchained.

Literature

1. Boutte CC & Crosson S (2013) Bacterial lifestyle shapes stringent response activation. *Trends in microbiology* 21(4):174-180.
2. Potrykus K, Murphy H, Philippe N, & Cashel M (2011) ppGpp is the major source of growth rate control in E. coli. *Environmental microbiology* 13(3):563-575.
3. Liu K, Bittner AN, & Wang JD (2015) Diversity in (p)ppGpp metabolism and effectors. *Current opinion in microbiology* 24:72-79.
4. Takahashi K, Kasai K, & Ochi K (2004) Identification of the bacterial alarmone guanosine 5'-diphosphate 3'-diphosphate (ppGpp) in plants. *Proceedings of the National Academy of Sciences of the United States of America* 101(12):4320-4324.
5. van der Biezen EA, Sun J, Coleman MJ, Bibb MJ, & Jones JD (2000) Arabidopsis RelA/SpoT homologs implicate (p)ppGpp in plant signaling. *Proceedings of the National Academy of Sciences of the United States of America* 97(7):3747-3752.
6. Masuda S*, et al.* (2008) The bacterial stringent response, conserved in chloroplasts, controls plant fertilization. *Plant & cell physiology* 49(2):135-141.
7. Masuda S, Tozawa Y, & Ohta H (2008) Possible targets of "magic spots" in plant signalling. *Plant signaling & behavior* 3(11):1021-1023.
8. Stent GS & Brenner S (1961) A genetic locus for the regulation of ribonucleic acid synthesis. *Proceedings of the National Academy of Sciences of the United States of America* 47:2005-2014.
9. Cashel M (1969) The control of ribonucleic acid synthesis in Escherichia coli. IV. Relevance of unusual phosphorylated compounds from amino acid-starved stringent strains. *The Journal of biological chemistry* 244(12):3133-3141.
10. Wang JD, Sanders GM, & Grossman AD (2007) Nutritional control of elongation of DNA replication by (p)ppGpp. *Cell* 128(5):865-875.
11. Denapoli J, Tehranchi AK, & Wang JD (2013) Dose-dependent reduction of replication elongation rate by (p)ppGpp in Escherichia coli and Bacillus subtilis. *Molecular microbiology* 88(1):93-104.
12. Kastle B*, et al.* (2015) rRNA regulation during growth and under stringent conditions in Staphylococcus aureus. *Environmental microbiology* 17(11):4394-4405.
13. Barker MM, Gaal T, Josaitis CA, & Gourse RL (2001) Mechanism of regulation of transcription initiation by ppGpp. I. Effects of ppGpp on transcription initiation in vivo and in vitro. *Journal of molecular biology* 305(4):673-688.
14. Corrigan RM, Bellows LE, Wood A, & Grundling A (2016) ppGpp negatively impacts ribosome assembly affecting growth and antimicrobial tolerance in Gram-positive bacteria. *Proceedings of the National Academy of Sciences of the United States of America* 113(12):E1710-1719.
15. Bittner AN, Kriel A, & Wang JD (2014) Lowering GTP level increases survival of amino acid starvation but slows growth rate for Bacillus subtilis cells lacking (p)ppGpp. *Journal of bacteriology* 196(11):2067-2076.
16. Kriel A*, et al.* (2012) Direct regulation of GTP homeostasis by (p)ppGpp: a critical component of viability and stress resistance. *Molecular cell* 48(2):231-241.
17. Kriel A*, et al.* (2014) GTP dysregulation in Bacillus subtilis cells lacking (p)ppGpp results in phenotypic amino acid auxotrophy and failure to adapt to

nutrient downshift and regulate biosynthesis genes. *Journal of bacteriology* 196(1):189-201.
18. Liu K*, et al.* (2015) Molecular mechanism and evolution of guanylate kinase regulation by (p)ppGpp. *Molecular cell* 57(4):735-749.
19. Gaca AO, Colomer-Winter C, & Lemos JA (2015) Many means to a common end: the intricacies of (p)ppGpp metabolism and its control of bacterial homeostasis. *Journal of bacteriology* 197(7):1146-1156.
20. Samarrai W*, et al.* (2011) Differential responses of Bacillus subtilis rRNA promoters to nutritional stress. *Journal of bacteriology* 193(3):723-733.
21. Dalebroux ZD & Swanson MS (2012) ppGpp: magic beyond RNA polymerase. *Nature reviews. Microbiology* 10(3):203-212.
22. Wolz C, Geiger T, & Goerke C (2010) The synthesis and function of the alarmone (p)ppGpp in firmicutes. *International journal of medical microbiology : IJMM* 300(2-3):142-147.
23. Chang DE, Smalley DJ, & Conway T (2002) Gene expression profiling of Escherichia coli growth transitions: an expanded stringent response model. *Molecular microbiology* 45(2):289-306.
24. Yang X & Ishiguro EE (2003) Temperature-sensitive growth and decreased thermotolerance associated with relA mutations in Escherichia coli. *Journal of bacteriology* 185(19):5765-5771.
25. Tedin K & Norel F (2001) Comparison of DeltarelA strains of Escherichia coli and Salmonella enterica serovar Typhimurium suggests a role for ppGpp in attenuation regulation of branched-chain amino acid biosynthesis. *Journal of bacteriology* 183(21):6184-6196.
26. Magnusson LU, Farewell A, & Nystrom T (2005) ppGpp: a global regulator in Escherichia coli. *Trends in microbiology* 13(5):236-242.
27. Paul BJ*, et al.* (2004) DksA: a critical component of the transcription initiation machinery that potentiates the regulation of rRNA promoters by ppGpp and the initiating NTP. *Cell* 118(3):311-322.
28. Paul BJ, Berkmen MB, & Gourse RL (2005) DksA potentiates direct activation of amino acid promoters by ppGpp. *Proceedings of the National Academy of Sciences of the United States of America* 102(22):7823-7828.
29. Chatnaparat T, Li Z, Korban SS, & Zhao Y (2015) The Stringent Response Mediated by (p)ppGpp Is Required for Virulence of Pseudomonas syringae pv. tomato and Its Survival on Tomato. *Molecular plant-microbe interactions : MPMI* 28(7):776-789.
30. Geiger T*, et al.* (2010) Role of the (p)ppGpp synthase RSH, a RelA/SpoT homolog, in stringent response and virulence of Staphylococcus aureus. *Infection and immunity* 78(5):1873-1883.
31. Haralalka S, Nandi S, & Bhadra RK (2003) Mutation in the relA gene of Vibrio cholerae affects in vitro and in vivo expression of virulence factors. *Journal of bacteriology* 185(16):4672-4682.
32. Chavez de Paz LE, Lemos JA, Wickstrom C, & Sedgley CM (2012) Role of (p)ppGpp in biofilm formation by Enterococcus faecalis. *Applied and environmental microbiology* 78(5):1627-1630.
33. He H, Cooper JN, Mishra A, & Raskin DM (2012) Stringent response regulation of biofilm formation in Vibrio cholerae. *Journal of bacteriology* 194(11):2962-2972.
34. Gerdes K & Maisonneuve E (2015) Remarkable Functional Convergence: Alarmone ppGpp Mediates Persistence by Activating Type I and II Toxin-Antitoxins. *Molecular cell* 59(1):1-3.

35. Maisonneuve E, Castro-Camargo M, & Gerdes K (2013) (p)ppGpp controls bacterial persistence by stochastic induction of toxin-antitoxin activity. *Cell* 154(5):1140-1150.
36. Maisonneuve E & Gerdes K (2014) Molecular mechanisms underlying bacterial persisters. *Cell* 157(3):539-548.
37. Weiss LA & Stallings CL (2013) Essential roles for Mycobacterium tuberculosis Rel beyond the production of (p)ppGpp. *Journal of bacteriology* 195(24):5629-5638.
38. Ababneh QO & Herman JK (2015) RelA inhibits Bacillus subtilis motility and chaining. *Journal of bacteriology* 197(1):128-137.
39. Ababneh QO & Herman JK (2015) CodY Regulates SigD Levels and Activity by Binding to Three Sites in the fla/che Operon. *Journal of bacteriology* 197(18):2999-3006.
40. Gaca AO*, et al.* (2015) From (p)ppGpp to (pp)pGpp: Characterization of Regulatory Effects of pGpp Synthesized by the Small Alarmone Synthetase of Enterococcus faecalis. *Journal of bacteriology* 197(18):2908-2919.
41. Hara A & Sy J (1983) Guanosine 5'-triphosphate, 3'-diphosphate 5'-phosphohydrolase. Purification and substrate specificity. *The Journal of biological chemistry* 258(3):1678-1683.
42. Keasling JD, Bertsch L, & Kornberg A (1993) Guanosine pentaphosphate phosphohydrolase of Escherichia coli is a long-chain exopolyphosphatase. *Proceedings of the National Academy of Sciences of the United States of America* 90(15):7029-7033.
43. Kristensen O, Ross B, & Gajhede M (2008) Structure of the PPX/GPPA phosphatase from Aquifex aeolicus in complex with the alarmone ppGpp. *Journal of molecular biology* 375(5):1469-1476.
44. Ooga T*, et al.* (2009) Degradation of ppGpp by nudix pyrophosphatase modulates the transition of growth phase in the bacterium Thermus thermophilus. *The Journal of biological chemistry* 284(23):15549-15556.
45. Ito D*, et al.* (2012) Enzymatic and molecular characterization of Arabidopsis ppGpp pyrophosphohydrolase, AtNUDX26. *Bioscience, biotechnology, and biochemistry* 76(12):2236-2241.
46. Tanaka H*, et al.* (2015) Identification and characterization of Arabidopsis AtNUDX9 as a GDP-d-mannose pyrophosphohydrolase: its involvement in root growth inhibition in response to ammonium. *Journal of experimental botany* 66(19):5797-5808.
47. McLennan AG (2013) Substrate ambiguity among the nudix hydrolases: biologically significant, evolutionary remnant, or both? *Cellular and molecular life sciences : CMLS* 70(3):373-385.
48. Steinchen W & Bange G (2016) The magic dance of the alarmones (p)ppGpp. *Molecular microbiology* 101(4):531-544.
49. Mittenhuber G (2001) Comparative genomics and evolution of genes encoding bacterial (p)ppGpp synthetases/hydrolases (the Rel, RelA and SpoT proteins). *Journal of molecular microbiology and biotechnology* 3(4):585-600.
50. Atkinson GC, Tenson T, & Hauryliuk V (2011) The RelA/SpoT homolog (RSH) superfamily: distribution and functional evolution of ppGpp synthetases and hydrolases across the tree of life. *PloS one* 6(8):e23479.
51. Avarbock D, Avarbock A, & Rubin H (2000) Differential regulation of opposing RelMtb activities by the aminoacylation state of a tRNA.ribosome.mRNA.RelMtb complex. *Biochemistry* 39(38):11640-11648.

52. Avarbock A*, et al.* (2005) Functional regulation of the opposing (p)ppGpp synthetase/hydrolase activities of RelMtb from Mycobacterium tuberculosis. *Biochemistry* 44(29):9913-9923.
53. Mechold U, Murphy H, Brown L, & Cashel M (2002) Intramolecular regulation of the opposing (p)ppGpp catalytic activities of Rel(Seq), the Rel/Spo enzyme from Streptococcus equisimilis. *Journal of bacteriology* 184(11):2878-2888.
54. Hogg T, Mechold U, Malke H, Cashel M, & Hilgenfeld R (2004) Conformational antagonism between opposing active sites in a bifunctional RelA/SpoT homolog modulates (p)ppGpp metabolism during the stringent response [corrected]. *Cell* 117(1):57-68.
55. Bag S, Das B, Dasgupta S, & Bhadra RK (2014) Mutational analysis of the (p)ppGpp synthetase activity of the Rel enzyme of Mycobacterium tuberculosis. *Archives of microbiology* 196(8):575-588.
56. Lemos JA, Lin VK, Nascimento MM, Abranches J, & Burne RA (2007) Three gene products govern (p)ppGpp production by Streptococcus mutans. *Molecular microbiology* 65(6):1568-1581.
57. Nanamiya H*, et al.* (2008) Identification and functional analysis of novel (p)ppGpp synthetase genes in Bacillus subtilis. *Molecular microbiology* 67(2):291-304.
58. Sprinzl M & Richter D (1976) Free 3'-OH group of the terminal adenosine of the tRNA molecule is essential for the synthesis in vitro of guanosine tetraphosphate and pentaphosphate in a ribosomal system from Escherichia coli. *European journal of biochemistry* 71(1):171-176.
59. Kuchta K, Knizewski L, Wyrwicz LS, Rychlewski L, & Ginalski K (2009) Comprehensive classification of nucleotidyltransferase fold proteins: identification of novel families and their representatives in human. *Nucleic acids research* 37(22):7701-7714.
60. Sun D*, et al.* (2010) A metazoan ortholog of SpoT hydrolyzes ppGpp and functions in starvation responses. *Nature structural & molecular biology* 17(10):1188-1194.
61. Brown A, Fernandez IS, Gordiyenko Y, & Ramakrishnan V (2016) Ribosome-dependent activation of stringent control. *Nature* 534(7606):277-280.
62. Seyfzadeh M, Keener J, & Nomura M (1993) spoT-dependent accumulation of guanosine tetraphosphate in response to fatty acid starvation in Escherichia coli. *Proceedings of the National Academy of Sciences of the United States of America* 90(23):11004-11008.
63. Vinella D, Albrecht C, Cashel M, & D'Ari R (2005) Iron limitation induces SpoT-dependent accumulation of ppGpp in Escherichia coli. *Molecular microbiology* 56(4):958-970.
64. Xiao H*, et al.* (1991) Residual guanosine 3',5'-bispyrophosphate synthetic activity of relA null mutants can be eliminated by spoT null mutations. *The Journal of biological chemistry* 266(9):5980-5990.
65. Battesti A & Bouveret E (2006) Acyl carrier protein/SpoT interaction, the switch linking SpoT-dependent stress response to fatty acid metabolism. *Molecular microbiology* 62(4):1048-1063.
66. Battesti A & Bouveret E (2009) Bacteria possessing two RelA/SpoT-like proteins have evolved a specific stringent response involving the acyl carrier protein-SpoT interaction. *Journal of bacteriology* 191(2):616-624.
67. Angelini S, My L, & Bouveret E (2012) Disrupting the Acyl Carrier Protein/SpoT interaction in vivo: identification of ACP residues involved in the interaction and consequence on growth. *PloS one* 7(4):e36111.

68. Raskin DM, Judson N, & Mekalanos JJ (2007) Regulation of the stringent response is the essential function of the conserved bacterial G protein CgtA in Vibrio cholerae. *Proceedings of the National Academy of Sciences of the United States of America* 104(11):4636-4641.
69. Buglino J, Shen V, Hakimian P, & Lima CD (2002) Structural and biochemical analysis of the Obg GTP binding protein. *Structure* 10(11):1581-1592.
70. Srivatsan A*, et al.* (2008) High-precision, whole-genome sequencing of laboratory strains facilitates genetic studies. *PLoS genetics* 4(8):e1000139.
71. Geiger T, Kastle B, Gratani FL, Goerke C, & Wolz C (2014) Two small (p)ppGpp synthases in Staphylococcus aureus mediate tolerance against cell envelope stress conditions. *Journal of bacteriology* 196(4):894-902.
72. Tagami K*, et al.* (2012) Expression of a small (p)ppGpp synthetase, YwaC, in the (p)ppGpp(0) mutant of Bacillus subtilis triggers YvyD-dependent dimerization of ribosome. *MicrobiologyOpen* 1(2):115-134.
73. Anderson KL*, et al.* (2010) Characterizing the effects of inorganic acid and alkaline shock on the Staphylococcus aureus transcriptome and messenger RNA turnover. *FEMS immunology and medical microbiology* 60(3):208-250.
74. Thackray PD & Moir A (2003) SigM, an extracytoplasmic function sigma factor of Bacillus subtilis, is activated in response to cell wall antibiotics, ethanol, heat, acid, and superoxide stress. *Journal of bacteriology* 185(12):3491-3498.
75. Eiamphungporn W & Helmann JD (2008) The Bacillus subtilis sigma(M) regulon and its contribution to cell envelope stress responses. *Molecular microbiology* 67(4):830-848.
76. Petrackova D, Semberova L, Halada P, Svoboda P, & Svobodova J (2010) Stress proteins in the cytoplasmic membrane fraction of Bacillus subtilis. *Folia microbiologica* 55(5):427-434.
77. Das B, Pal RR, Bag S, & Bhadra RK (2009) Stringent response in Vibrio cholerae: genetic analysis of spoT gene function and identification of a novel (p)ppGpp synthetase gene. *Molecular microbiology* 72(2):380-398.
78. Oh YT, Lee KM, Bari W, Raskin DM, & Yoon SS (2015) (p)ppGpp, a Small Nucleotide Regulator, Directs the Metabolic Fate of Glucose in Vibrio cholerae. *The Journal of biological chemistry* 290(21):13178-13190.
79. Dasgupta S, Basu P, Pal RR, Bag S, & Bhadra RK (2014) Genetic and mutational characterization of the small alarmone synthetase gene relV of Vibrio cholerae. *Microbiology* 160(Pt 9):1855-1866.
80. Sajish M, Tiwari D, Rananaware D, Nandicoori VK, & Prakash B (2007) A charge reversal differentiates (p)ppGpp synthesis by monofunctional and bifunctional Rel proteins. *The Journal of biological chemistry* 282(48):34977-34983.
81. Sajish M, Kalayil S, Verma SK, Nandicoori VK, & Prakash B (2009) The significance of EXDD and RXKD motif conservation in Rel proteins. *The Journal of biological chemistry* 284(14):9115-9123.
82. Shyp V*, et al.* (2012) Positive allosteric feedback regulation of the stringent response enzyme RelA by its product. *EMBO reports* 13(9):835-839.
83. Hauryliuk V, Atkinson GC, Murakami KS, Tenson T, & Gerdes K (2015) Recent functional insights into the role of (p)ppGpp in bacterial physiology. *Nature reviews. Microbiology* 13(5):298-309.
84. Tozawa Y & Nomura Y (2011) Signalling by the global regulatory molecule ppGpp in bacteria and chloroplasts of land plants. *Plant biology* 13(5):699-709.

85. Silverman RH & Atherly AG (1979) The search for guanosine tetraphosphate (ppGpp) and other unusual nucleotides in eucaryotes. *Microbiological reviews* 43(1):27-41.
86. Yegian CD, Stent GS, & Martin EM (1966) Intracellular condition of Escherichia coli transfer RNA. *Proceedings of the National Academy of Sciences of the United States of America* 55(4):839-846.
87. Haseltine WA & Block R (1973) Synthesis of guanosine tetra- and pentaphosphate requires the presence of a codon-specific, uncharged transfer ribonucleic acid in the acceptor site of ribosomes. *Proceedings of the National Academy of Sciences of the United States of America* 70(5):1564-1568.
88. Richter D (1976) Stringent factor from Escherichia coli directs ribosomal binding and release of uncharged tRNA. *Proceedings of the National Academy of Sciences of the United States of America* 73(3):707-711.
89. Richter D (1976) The stringent control mechanism. Binding of uncharged tRNA and stringent factor to Escherichia coli ribosomes. *Archivos de biologia y medicina experimentales* 10(1-3):85-91.
90. Sy J & Lipmann F (1973) Identification of the synthesis of guanosine tetraphosphate (MS I) as insertion of a pyrophosphoryl group into the 3'-position in guanosine 5'-diphosphate. *Proceedings of the National Academy of Sciences of the United States of America* 70(2):306-309.
91. Wendrich TM, Blaha G, Wilson DN, Marahiel MA, & Nierhaus KH (2002) Dissection of the mechanism for the stringent factor RelA. *Molecular cell* 10(4):779-788.
92. Schreiber G*, et al.* (1991) Overexpression of the relA gene in Escherichia coli. *The Journal of biological chemistry* 266(6):3760-3767.
93. Gropp M, Strausz Y, Gross M, & Glaser G (2001) Regulation of Escherichia coli RelA requires oligomerization of the C-terminal domain. *Journal of bacteriology* 183(2):570-579.
94. Agirrezabala X*, et al.* (2013) The ribosome triggers the stringent response by RelA via a highly distorted tRNA. *EMBO reports* 14(9):811-816.
95. Arenz S*, et al.* (2016) The stringent factor RelA adopts an open conformation on the ribosome to stimulate ppGpp synthesis. *Nucleic acids research* 44(13):6471-6481.
96. Loveland AB*, et al.* (2016) Ribosome*RelA structures reveal the mechanism of stringent response activation. *eLife* 5.
97. Schmeing TM*, et al.* (2009) The crystal structure of the ribosome bound to EF-Tu and aminoacyl-tRNA. *Science* 326(5953):688-694.
98. Schuette JC*, et al.* (2009) GTPase activation of elongation factor EF-Tu by the ribosome during decoding. *The EMBO journal* 28(6):755-765.
99. Fischer N*, et al.* (2015) Structure of the E. coli ribosome-EF-Tu complex at <3 A resolution by Cs-corrected cryo-EM. *Nature* 520(7548):567-570.
100. Friesen JD, Fiil NP, Parker JM, & Haseltine WA (1974) A new relaxed mutant of Escherichia coli with an altered 50S ribosomal subunit. *Proceedings of the National Academy of Sciences of the United States of America* 71(9):3465-3469.
101. Jain V, Saleem-Batcha R, China A, & Chatterji D (2006) Molecular dissection of the mycobacterial stringent response protein Rel. *Protein science : a publication of the Protein Society* 15(6):1449-1464.
102. English BP*, et al.* (2011) Single-molecule investigations of the stringent response machinery in living bacterial cells. *Proceedings of the National Academy of Sciences of the United States of America* 108(31):E365-373.

103. Li W*, et al.* (2016) Effects of amino acid starvation on RelA diffusive behavior in live Escherichia coli. *Molecular microbiology* 99(3):571-585.
104. Tozawa Y*, et al.* (2007) Calcium-activated (p)ppGpp synthetase in chloroplasts of land plants. *The Journal of biological chemistry* 282(49):35536-35545.
105. Mizusawa K, Masuda S, & Ohta H (2008) Expression profiling of four RelA/SpoT-like proteins, homologues of bacterial stringent factors, in Arabidopsis thaliana. *Planta* 228(4):553-562.
106. Kuroda A, Murphy H, Cashel M, & Kornberg A (1997) Guanosine tetra- and pentaphosphate promote accumulation of inorganic polyphosphate in Escherichia coli. *The Journal of biological chemistry* 272(34):21240-21243.
107. Kuroda A*, et al.* (2001) Role of inorganic polyphosphate in promoting ribosomal protein degradation by the Lon protease in E. coli. *Science* 293(5530):705-708.
108. Ryals J, Little R, & Bremer H (1982) Control of rRNA and tRNA syntheses in Escherichia coli by guanosine tetraphosphate. *Journal of bacteriology* 151(3):1261-1268.
109. Baracchini E & Bremer H (1988) Stringent and growth control of rRNA synthesis in Escherichia coli are both mediated by ppGpp. *The Journal of biological chemistry* 263(6):2597-2602.
110. Baracchini E, Glass R, & Bremer H (1988) Studies in vivo on Escherichia coli RNA polymerase mutants altered in the stringent response. *Molecular & general genetics : MGG* 213(2-3):379-387.
111. Ehrenberg M, Bremer H, & Dennis PP (2013) Medium-dependent control of the bacterial growth rate. *Biochimie* 95(4):643-658.
112. Mechold U, Potrykus K, Murphy H, Murakami KS, & Cashel M (2013) Differential regulation by ppGpp versus pppGpp in Escherichia coli. *Nucleic acids research* 41(12):6175-6189.
113. Deckert G*, et al.* (1998) The complete genome of the hyperthermophilic bacterium Aquifex aeolicus. *Nature* 392(6674):353-358.
114. Alvarado J*, et al.* (2006) Origin of exopolyphosphatase processivity: Fusion of an ASKHA phosphotransferase and a cyclic nucleotide phosphodiesterase homolog. *Structure* 14(8):1263-1272.
115. Rangarajan ES*, et al.* (2006) The structure of the exopolyphosphatase (PPX) from Escherichia coli O157:H7 suggests a binding mode for long polyphosphate chains. *Journal of molecular biology* 359(5):1249-1260.
116. Aravind L & Koonin EV (1998) The HD domain defines a new superfamily of metal-dependent phosphohydrolases. *Trends in biochemical sciences* 23(12):469-472.
117. Akiyama M, Crooke E, & Kornberg A (1993) An exopolyphosphatase of Escherichia coli. The enzyme and its ppx gene in a polyphosphate operon. *The Journal of biological chemistry* 268(1):633-639.
118. Bolesch DG & Keasling JD (2000) Polyphosphate binding and chain length recognition of Escherichia coli exopolyphosphatase. *The Journal of biological chemistry* 275(43):33814-33819.
119. Bolesch DG & Keasling JD (2000) The effect of monovalent ions on polyphosphate binding to Escherichia coli exopolyphosphatase. *Biochemical and biophysical research communications* 274(1):236-241.
120. Kanjee U, Ogata K, & Houry WA (2012) Direct binding targets of the stringent response alarmone (p)ppGpp. *Molecular microbiology* 85(6):1029-1043.

121. Levine A, Vannier F, Dehbi M, Henckes G, & Seror SJ (1991) The stringent response blocks DNA replication outside the ori region in Bacillus subtilis and at the origin in Escherichia coli. *Journal of molecular biology* 219(4):605-613.
122. Schreiber G, Ron EZ, & Glaser G (1995) ppGpp-mediated regulation of DNA replication and cell division in Escherichia coli. *Current microbiology* 30(1):27-32.
123. Frick DN & Richardson CC (2001) DNA primases. *Annual review of biochemistry* 70:39-80.
124. Kuchta RD & Stengel G (2010) Mechanism and evolution of DNA primases. *Biochimica et biophysica acta* 1804(5):1180-1189.
125. Maciag M, Kochanowska M, Lyzen R, Wegrzyn G, & Szalewska-Palasz A (2010) ppGpp inhibits the activity of Escherichia coli DnaG primase. *Plasmid* 63(1):61-67.
126. Maciag-Dorszynska M, Szalewska-Palasz A, & Wegrzyn G (2013) Different effects of ppGpp on Escherichia coli DNA replication in vivo and in vitro. *FEBS open bio* 3:161-164.
127. Rymer RU*, et al.* (2012) Binding mechanism of metalNTP substrates and stringent-response alarmones to bacterial DnaG-type primases. *Structure* 20(9):1478-1489.
128. Haugen SP, Ross W, Manrique M, & Gourse RL (2008) Fine structure of the promoter-sigma region 1.2 interaction. *Proceedings of the National Academy of Sciences of the United States of America* 105(9):3292-3297.
129. Durfee T, Hansen AM, Zhi H, Blattner FR, & Jin DJ (2008) Transcription profiling of the stringent response in Escherichia coli. *Journal of bacteriology* 190(3):1084-1096.
130. Artsimovitch I*, et al.* (2004) Structural basis for transcription regulation by alarmone ppGpp. *Cell* 117(3):299-310.
131. Jores L & Wagner R (2003) Essential steps in the ppGpp-dependent regulation of bacterial ribosomal RNA promoters can be explained by substrate competition. *The Journal of biological chemistry* 278(19):16834-16843.
132. Vrentas CE*, et al.* (2008) Still looking for the magic spot: the crystallographically defined binding site for ppGpp on RNA polymerase is unlikely to be responsible for rRNA transcription regulation. *Journal of molecular biology* 377(2):551-564.
133. Zuo Y, Wang Y, & Steitz TA (2013) The mechanism of E. coli RNA polymerase regulation by ppGpp is suggested by the structure of their complex. *Molecular cell* 50(3):430-436.
134. Ross W, Vrentas CE, Sanchez-Vazquez P, Gaal T, & Gourse RL (2013) The magic spot: a ppGpp binding site on E. coli RNA polymerase responsible for regulation of transcription initiation. *Molecular cell* 50(3):420-429.
135. Ross W*, et al.* (2016) ppGpp Binding to a Site at the RNAP-DksA Interface Accounts for Its Dramatic Effects on Transcription Initiation during the Stringent Response. *Molecular cell* 62(6):811-823.
136. Perederina A*, et al.* (2004) Regulation through the secondary channel--structural framework for ppGpp-DksA synergism during transcription. *Cell* 118(3):297-309.
137. Lennon CW*, et al.* (2012) Direct interactions between the coiled-coil tip of DksA and the trigger loop of RNA polymerase mediate transcriptional regulation. *Genes & development* 26(23):2634-2646.

138. Lemke JJ, Durfee T, & Gourse RL (2009) DksA and ppGpp directly regulate transcription of the Escherichia coli flagellar cascade. *Molecular microbiology* 74(6):1368-1379.
139. Lemke JJ*, et al.* (2011) Direct regulation of Escherichia coli ribosomal protein promoters by the transcription factors ppGpp and DksA. *Proceedings of the National Academy of Sciences of the United States of America* 108(14):5712-5717.
140. Blaby-Haas CE, Furman R, Rodionov DA, Artsimovitch I, & de Crecy-Lagard V (2011) Role of a Zn-independent DksA in Zn homeostasis and stringent response. *Molecular microbiology* 79(3):700-715.
141. Krasny L & Gourse RL (2004) An alternative strategy for bacterial ribosome synthesis: Bacillus subtilis rRNA transcription regulation. *The EMBO journal* 23(22):4473-4483.
142. Kasai K*, et al.* (2006) Physiological analysis of the stringent response elicited in an extreme thermophilic bacterium, Thermus thermophilus. *Journal of bacteriology* 188(20):7111-7122.
143. Gallant J, Irr J, & Cashel M (1971) The mechanism of amino acid control of guanylate and adenylate biosynthesis. *The Journal of biological chemistry* 246(18):5812-5816.
144. Pao CC & Dyess BT (1981) Effect of unusual guanosine nucleotides on the activities of some Escherichia coli cellular enzymes. *Biochimica et biophysica acta* 677(3-4):358-362.
145. Hochstadt-Ozer J & Cashel M (1972) The regulation of purine utilization in bacteria. V. Inhibition of purine phosphoribosyltransferase activities and purine uptake in isolated membrane vesicles by guanosine tetraphosphate. *The Journal of biological chemistry* 247(21):7067-7072.
146. Beaman TC*, et al.* (1983) Specificity and control of uptake of purines and other compounds in Bacillus subtilis. *Journal of bacteriology* 156(3):1107-1117.
147. Stayton MM & Fromm HJ (1979) Guanosine 5'-diphosphate-3'-diphosphate inhibition of adenylosuccinate synthetase. *The Journal of biological chemistry* 254(8):2579-2581.
148. Kanjee U*, et al.* (2011) Linkage between the bacterial acid stress and stringent responses: the structure of the inducible lysine decarboxylase. *The EMBO journal* 30(5):931-944.
149. Kanjee U, Gutsche I, Ramachandran S, & Houry WA (2011) The enzymatic activities of the Escherichia coli basic aliphatic amino acid decarboxylases exhibit a pH zone of inhibition. *Biochemistry* 50(43):9388-9398.
150. Rao F*, et al.* (2010) YybT is a signaling protein that contains a cyclic dinucleotide phosphodiesterase domain and a GGDEF domain with ATPase activity. *The Journal of biological chemistry* 285(1):473-482.
151. Steinchen W*, et al.* (2015) Catalytic mechanism and allosteric regulation of an oligomeric (p)ppGpp synthetase by an alarmone. *Proceedings of the National Academy of Sciences of the United States of America* 112(43):13348-13353.
152. Traxler MF*, et al.* (2008) The global, ppGpp-mediated stringent response to amino acid starvation in Escherichia coli. *Molecular microbiology* 68(5):1128-1148.
153. Cashel M, Lazzarini RA, & Kalbacher B (1969) An improved method for thin-layer chromatography of nucleotide mixtures containing 32P-labelled orthophosphate. *Journal of chromatography* 40(1):103-109.

154. Cordell RL, Hill SJ, Ortori CA, & Barrett DA (2008) Quantitative profiling of nucleotides and related phosphate-containing metabolites in cultured mammalian cells by liquid chromatography tandem electrospray mass spectrometry. *Journal of chromatography. B, Analytical technologies in the biomedical and life sciences* 871(1):115-124.
155. Wilkinson RC, Batten LE, Wells NJ, Oyston PC, & Roach PL (2015) Biochemical studies on Francisella tularensis RelA in (p)ppGpp biosynthesis. *Bioscience reports* 35(6).
156. Rao F*, et al.* (2009) Enzymatic synthesis of c-di-GMP using a thermophilic diguanylate cyclase. *Analytical biochemistry* 389(2):138-142.
157. Neubauer P, Ahman M, Tornkvist M, Larsson G, & Enfors SO (1995) Response of guanosine tetraphosphate to glucose fluctuations in fed-batch cultivations of Escherichia coli. *Journal of biotechnology* 43(3):195-204.
158. Meyer S, Noisommit-Rizzi N, Reuss M, & Neubauer P (1999) Optimized analysis of intracellular adenosine and guanosine phosphates in Escherichia coli. *Analytical biochemistry* 271(1):43-52.
159. Gong L (2015) Comparing ion-pairing reagents and counter anions for ion-pair reversed-phase liquid chromatography/electrospray ionization mass spectrometry analysis of synthetic oligonucleotides. *Rapid communications in mass spectrometry : RCM* 29(24):2402-2410.
160. Waldron KJ & Robinson NJ (2009) How do bacterial cells ensure that metalloproteins get the correct metal? *Nature reviews. Microbiology* 7(1):25-35.
161. Corfu NA & Sigel H (1991) Acid-base properties of nucleosides and nucleotides as a function of concentration. Comparison of the proton affinity of the nucleic base residues in the monomeric and self-associated, oligomeric 5'-triphosphates of inosine (ITP), guanosine (GTP), and adenosine (ATP). *European journal of biochemistry* 199(3):659-669.
162. Corfu NA, Tribolet R, & Sigel H (1990) Comparison of the self-association properties of the 5'-triphosphates of inosine (ITP), guanosine (GTP), and adenosine (ATP). Further evidence for ionic interactions in the highly stable dimeric [H2(ATP)]2(4-) stack. *European journal of biochemistry* 191(3):721-735.
163. Tribolet R & Sigel H (1987) Self-association of adenosine 5'-monophosphate (5'-AMP) as a function of pH and in comparison with adenosine, 2'-AMP and 3'-AMP. *Biophysical chemistry* 27(2):119-130.
164. Tribolet R & Sigel H (1988) Influence of the protonation degree on the self-association properties of adenosine 5'-triphosphate (ATP). *European journal of biochemistry* 170(3):617-626.
165. Pedersen FS & Kjeldgaard NO (1977) Analysis of the relA gene product of Escherichia coli. *European journal of biochemistry* 76(1):91-97.
166. Lewis K (2010) Persister cells. *Annual review of microbiology* 64:357-372.
167. Germain E, Roghanian M, Gerdes K, & Maisonneuve E (2015) Stochastic induction of persister cells by HipA through (p)ppGpp-mediated activation of mRNA endonucleases. *Proceedings of the National Academy of Sciences of the United States of America* 112(16):5171-5176.
168. Cozy LM & Kearns DB (2010) Gene position in a long operon governs motility development in Bacillus subtilis. *Molecular microbiology* 76(2):273-285.
169. Jaacks KJ, Healy J, Losick R, & Grossman AD (1989) Identification and characterization of genes controlled by the sporulation-regulatory gene spo0H in Bacillus subtilis. *Journal of bacteriology* 171(8):4121-4129.

170. Kearns DB & Losick R (2005) Cell population heterogeneity during growth of Bacillus subtilis. *Genes & development* 19(24):3083-3094.
171. Dubnau D & Losick R (2006) Bistability in bacteria. *Molecular microbiology* 61(3):564-572.
172. Bennett BD*, et al.* (2009) Absolute metabolite concentrations and implied enzyme active site occupancy in Escherichia coli. *Nature chemical biology* 5(8):593-599.
173. Luche S*, et al.* (2016) Zinc oxide induces the stringent response and major reorientations in the central metabolism of Bacillus subtilis. *Journal of proteomics* 135:170-180.
174. Fan H, Hahm J, Diggs S, Perry JJ, & Blaha G (2015) Structural and Functional Analysis of BipA, a Regulator of Virulence in Enteropathogenic Escherichia coli. *The Journal of biological chemistry* 290(34):20856-20864.
175. Kumar V*, et al.* (2015) Structure of BipA in GTP form bound to the ratcheted ribosome. *Proceedings of the National Academy of Sciences of the United States of America* 112(35):10944-10949.
176. Kihira K*, et al.* (2012) Crystal structure analysis of the translation factor RF3 (release factor 3). *FEBS letters* 586(20):3705-3709.
177. Mechold U, Cashel M, Steiner K, Gentry D, & Malke H (1996) Functional analysis of a relA/spoT gene homolog from Streptococcus equisimilis. *Journal of bacteriology* 178(5):1401-1411.
178. Andreini C, Banci L, Bertini I, & Rosato A (2006) Zinc through the three domains of life. *Journal of proteome research* 5(11):3173-3178.
179. Andreini C, Bertini I, & Rosato A (2009) Metalloproteomes: a bioinformatic approach. *Accounts of chemical research* 42(10):1471-1479.
180. Shin JH & Helmann JD (2016) Molecular logic of the Zur-regulated zinc deprivation response in Bacillus subtilis. *Nature communications* 7:12612.
181. Stafford SL*, et al.* (2013) Metal ions in macrophage antimicrobial pathways: emerging roles for zinc and copper. *Bioscience reports* 33(4).
182. Zarkan A, Macklyne HR, Truman AW, Hesketh AR, & Hong HJ (2016) The frontline antibiotic vancomycin induces a zinc starvation response in bacteria by binding to Zn(II). *Scientific reports* 6:19602.
183. Kuroda M*, et al.* (2003) Two-component system VraSR positively modulates the regulation of cell-wall biosynthesis pathway in Staphylococcus aureus. *Molecular microbiology* 49(3):807-821.
184. Hesketh A*, et al.* (2011) Genome-wide dynamics of a bacterial response to antibiotics that target the cell envelope. *BMC genomics* 12:226.
185. Hessling B*, et al.* (2013) Global proteome analysis of vancomycin stress in Staphylococcus aureus. *International journal of medical microbiology : IJMM* 303(8):624-634.
186. Graham AI*, et al.* (2009) Severe zinc depletion of Escherichia coli: roles for high affinity zinc binding by ZinT, zinc transport and zinc-independent proteins. *The Journal of biological chemistry* 284(27):18377-18389.
187. Kershaw CJ, Brown NL, & Hobman JL (2007) Zinc dependence of zinT (yodA) mutants and binding of zinc, cadmium and mercury by ZinT. *Biochemical and biophysical research communications* 364(1):66-71.
188. Petrarca P, Ammendola S, Pasquali P, & Battistoni A (2010) The Zur-regulated ZinT protein is an auxiliary component of the high-affinity ZnuABC zinc transporter that facilitates metal recruitment during severe zinc shortage. *Journal of bacteriology* 192(6):1553-1564.

189. Natori Y*, et al.* (2007) A fail-safe system for the ribosome under zinc-limiting conditions in Bacillus subtilis. *Molecular microbiology* 63(1):294-307.
190. Nanamiya H, Kawamura F, & Kosono S (2006) Proteomic study of the Bacillus subtilis ribosome: Finding of zinc-dependent replacement for ribosomal protein L31 paralogues. *The Journal of general and applied microbiology* 52(5):249-258.
191. Yoshida H & Wada A (2014) The 100S ribosome: ribosomal hibernation induced by stress. *Wiley interdisciplinary reviews. RNA* 5(5):723-732.
192. Izutsu K, Wada A, & Wada C (2001) Expression of ribosome modulation factor (RMF) in Escherichia coli requires ppGpp. *Genes to cells : devoted to molecular & cellular mechanisms* 6(8):665-676.
193. Balsalobre C (2011) Concentration matters!! ppGpp, from a whispering to a strident alarmone. *Molecular microbiology* 79(4):827-829.
194. Hahn J, Tanner AW, Carabetta VJ, Cristea IM, & Dubnau D (2015) ComGA-RelA interaction and persistence in the Bacillus subtilis K-state. *Molecular microbiology* 97(3):454-471.
195. Payoe R & Fahlman RP (2011) Dependence of RelA-mediated (p)ppGpp formation on tRNA identity. *Biochemistry* 50(15):3075-3083.
196. Jenvert RM & Schiavone LH (2007) The flexible N-terminal domain of ribosomal protein L11 from Escherichia coli is necessary for the activation of stringent factor. *Journal of molecular biology* 365(3):764-772.
197. Rojas AM, Ehrenberg M, Andersson SG, & Kurland CG (1984) ppGpp inhibition of elongation factors Tu, G and Ts during polypeptide synthesis. *Molecular & general genetics : MGG* 197(1):36-45.
198. Milon P*, et al.* (2006) The nucleotide-binding site of bacterial translation initiation factor 2 (IF2) as a metabolic sensor. *Proceedings of the National Academy of Sciences of the United States of America* 103(38):13962-13967.
199. Wexselblatt E, Kaspy I, Glaser G, Katzhendler J, & Yavin E (2013) Design, synthesis and structure-activity relationship of novel Relacin analogs as inhibitors of Rel proteins. *European journal of medicinal chemistry* 70:497-504.
200. Arnaud M, Chastanet A, & Debarbouille M (2004) New vector for efficient allelic replacement in naturally nontransformable, low-GC-content, gram-positive bacteria. *Applied and environmental microbiology* 70(11):6887-6891.
201. Lewis PJ & Marston AL (1999) GFP vectors for controlled expression and dual labelling of protein fusions in Bacillus subtilis. *Gene* 227(1):101-110.
202. Krezel A & Bal W (2004) A formula for correlating pKa values determined in D2O and H2O. *Journal of inorganic biochemistry* 98(1):161-166.
203. Zhu J, Zhang L, Zhou Z, Dong S, & Wang E (2014) Molecular aptamer beacon tuned DNA strand displacement to transform small molecules into DNA logic outputs. *Chemical communications* 50(25):3321-3323.
204. Kabsch W (2010) Xds. *Acta crystallographica. Section D, Biological crystallography* 66(Pt 2):125-132.
205. Winn MD*, et al.* (2011) Overview of the CCP4 suite and current developments. *Acta crystallographica. Section D, Biological crystallography* 67(Pt 4):235-242.
206. McCoy AJ*, et al.* (2007) Phaser crystallographic software. *Journal of applied crystallography* 40(Pt 4):658-674.
207. Emsley P & Cowtan K (2004) Coot: model-building tools for molecular graphics. *Acta crystallographica. Section D, Biological crystallography* 60(Pt 12 Pt 1):2126-2132.

208. Adams PD*, et al.* (2010) PHENIX: a comprehensive Python-based system for macromolecular structure solution. *Acta crystallographica. Section D, Biological crystallography* 66(Pt 2):213-221.
209. Wales TE, Fadgen KE, Gerhardt GC, & Engen JR (2008) High-speed and high-resolution UPLC separation at zero degrees Celsius. *Analytical chemistry* 80(17):6815-6820.
210. Li GZ*, et al.* (2009) Database searching and accounting of multiplexed precursor and product ion spectra from the data independent analysis of simple and complex peptide mixtures. *Proteomics* 9(6):1696-1719.
211. Zhang Z & Smith DL (1993) Determination of amide hydrogen exchange by mass spectrometry: a new tool for protein structure elucidation. *Protein science : a publication of the Protein Society* 2(4):522-531.
212. Zeigler DR*, et al.* (2008) The origins of 168, W23, and other Bacillus subtilis legacy strains. *Journal of bacteriology* 190(21):6983-6995.

Appendix

Supplementary tables

Table S1. Crystallographic data collection and refinement statistics for *B. subtilis* SAS1 in different nucleotide-bound states.

	***Bs*SAS1**	***Bs*SAS1-AMPCPP**	***Bs*SAS1-pppGpp**
Data collection			
Space group	P 2_1	P 2_1	C 2
Cell dimensions			
a, *b*, *c* (Å)	78.13	116.67	197.87
	77.69	103.63	113.49
	81.61	138.29	139.85
α, β, γ (°)	90.00	90.00	90.00
	90.40	104.84	127.17
	90.00	90.00	90.00
Energy (keV)	12.6616		
Resolution (Å)	56.63 – 1.86	48.31 – 2.80	50.57 – 2.94
	(1.96 – 1.86)	(2.95 – 2.80)	(3.10 – 2.94)
R_{merge}	0.083 (0.46)	0.090 (0.48)	0.103 (0.273)
$I / \sigma I$	7.4 (2.5)	10.6 (2.8)	12.1 (5.8)
Completeness (%)	97.7 (98.1)	100 (100)	99.3 (96.1)
Redundancy	3.4 (3.5)	3.8 (3.9)	6.8 (6.4)
Refinement			
Resolution (Å)	56.6 – 2.00	48.3 – 2.8	50.6 – 2.94
No. reflections	64368	78505	51454
R_{work}/ R_{free}	19.4/23.8	19.6/25.7	18.1/24.5
No. atoms	6542	18586	13016
R.m.s deviations			
Bond lengths (Å)	0.010	0.013	0.014
Bond angles (°)	1.25	1.242	1.441

*Values for the highest-resolution shell are given in parentheses.

Table S2. Crystallographic data collection and refinement statistics for *S. aureus* SAS2 in different nucleotide-bound states.

	***Sa*SAS2**	***Sa*SAS2-AMPCPP**	***Sa*SAS2-pppGpp**	***Sa*SAS2-pGpp**
Data collection				
Space group	$P4_32_12$	$I4_122$	$P6_1$	$I4_122$
Resolution (Å)	49.06 - 2.25 (2.33 - 2.25)	46.46-2.90 (3.00-2.90)	47.97-3.30 (3.42-3.30)	44.56 - 3.23 (3.34 - 3.23)
Unit cell parameters				
a, *b*, *c* (Å)	71.80, 71.80, 190.82	125.86, 125.86, 217.88	127.84, 127.84 290.32	126.029, 126.029, 217.912
α, *β*, *γ* (°)	90, 90, 90	90, 90, 90	90, 90, 120	90, 90, 90
R_{merge}	0.0364 (0.580)	0.178 (1.234)	0.052 (0.315)	0.01501 (0.3236)
CC½ (%)	1 (0.85)	99.7 (79.7)	99.7 (82.1)	1 (0.69)
$I / \sigma I$	20.37 (2.22)	14.65 (2.19)	10.35 (2.2)	22.82 (2.55)
No. of total reflections	103930 (10417)	231522 (22086)	77531 (7672)	28736 (2670)
Redundancy	4.3 (4.4)	11.7 (11.4)	1.9 (1.9)	2.0 (2.0)
Refinement				
Completeness (%)	99.0 (100.0)	100.0 (100.0)	99.0 (100.0)	99.4 (100.0)
R_{work}/R_{free} (%)	0.199 / 0.248	19.9/23.4 (32.4/34.5)	21.7/27.0 (29.0/33.9)	20.81/25.05 (35.37/43.85)
No. of atoms				
Overall	3314	3328	13352	3322
Protein	3261	3211	13032	3258
Ligands	20	64	320	64
Water	33	53	0	0
Average *B*-factors (Å^2)				
Overall	72.00	32.26	42.74	81.38
Protein	72.12	31.23	42.51	80.33
Ligands	87.05	69.31	52.39	134.54
Water	50.71	49.70	0.00	0.00
Root-mean-square deviation				
Bond lengths (Å)	0.010	0.009	0.013	0.009
Bond angles (°)	1.26	1.36	1.27	1.47
Ramachandran plot (%)				
Favored	98.74	98.00	96.05	96.89
Allowed	1.00	1.80	3.50	2.60
Outliers	0.26	0.20	0.45	0.51

*Values for the highest-resolution shell are given in parentheses.

Table S3. Crystallographic data collection and refinement statistics for *B. subtilis* Rel-NTD.

	*Bs*Rel-NTD
Data collection	
Space group	$P4_322$
Cell dimensions	
a, *b*, *c* (Å)	80.662
	80.662
	125.596
a, b, g (°)	90.00
	90.00
	90.00
Energy (keV)	12.6616
Resolution (Å)	37.15 – 3.70
	(3.83 – 3.70)
R_{merge}	0.052 (0.901)
$I / \sigma I$	23.7 (2.2)
Completeness (%)	99.7 (98.1)
Redundancy	8.3 (8.0)
Refinement	
Resolution (Å)	37.15 – 3.70
No. reflections	11903
$R_{work/}$ R_{free}	27.9
	32.7
No. atoms	2160
Protein	2160
Ligand	0
Water	0
R.m.s deviations	
Bond lengths (Å)	0.013
Bond angles (°)	1.57
Ramachandran (%)	
Preferred	94.72
Allowed	5.28
Outliers	0.00

*Values for the highest-resolution shell are given in parentheses.

Table S4. List of oligonucleotides.

Oligonucleotide	Org	Sequence (5' to 3')	Amplificate
SAS1-Nco-6H-F	*Bs*	ttaaccatgggccaccatcaccatcaccatgatgacaaacaat gggagc	SAS1
SAS1-Xho-R	*Bs*	ttaactcgagttattgttgctcgcttccttttttc	
BsSAS1-R46G-F	*Bs*	gaatttgtgacccgaggcgtcaagcctgtcg	SAS1
BsSAS1-R46G-R	*Bs*	ccacaggcttgacgcctccggtcacaaattc	R46G
BsSAS1-E139V-F	*Bs*	gaaaagcatgttctcgtagtaatacagatccgtacac	SAS1
BsSAS1-E139V-R	*Bs*	gtgtacggatctgtattactacgagaacatgcttttc	E139V
RelP-K25A-F	*Bs*	gtgaagctcgcggggatccgcacac	SAS1
RelP-K25A-R	*Bs*	gtgtgcggatccccgcgagcttcac	K25A
RelP-F42A-F	*Bs*	ccgatcgaagctgtgaccggacgcg	SAS1
RelP-F42A-R	*Bs*	cgcgtccggtcacagcttcgatcgg	F42A
RelP-N148G-F	*Bs*	ctggcgatgggtttttgggcgac	SAS1
RelP-N148G-R	*Bs*	gtcgcccaaaaacccatcgccag	N148G
BsSAS1-H111P-F	*Bs*	gcggaacctaaagagagc	SAS1
BsSAS1-H111P-R	*Bs*	gctctctttaggttccgc	H111P
SAS2-Nco-6H-F	*Bs*	ttaaccatgggccaccatcaccatcaccatgatttatctgtaaca	SAS2
SAS2-Xho-R	*Bs*	ttaactcgagttaatccacttctttcttaatcc	
Sau-RelQ-Nco6H-F	*Sa*	ttaaccatgggccaccatcaccatcaccattatgtagatcgaa aacca	SAS2
Sau-RelQ-Xho-R	*Sa*	ttaactcgagctactctgttatttc	
SaSAS2-H73A-F	*Sa*	ctatagctcatatggagc	SAS2
SaSAS2-H73A-R	*Sa*	gctccatatgagctatag	H73A
SaSAS2-H74A-F	*Sa*	ctatacatgctatggagc	SAS2
SaSAS2-H74A-R	*Sa*	gctccatagcatgtatag	H74A
SaSAS2-E76A-F	*Sa*	catcatatggcgcgacgtg	SAS2
SaSAS2-E76A-R	*Sa*	cacgtcgcgccatatgatg	E76A
SaSAS2-D183A-F	*Sa*	ggtatggctatgtgggc	SAS2
SaSAS2-D183A-R	*Sa*	gcccacatagccatacc	D183A
SaSAS2-R91A-F	*Sa*	cttaatgctaaaggattac	SAS2
SaSAS2-R91A-R	*Sa*	gtaatcctttagcattaag	R91A
SaSAS2-K92A-F	*Sa*	cttaatcgtgcaggattac	SAS2
SaSAS2-K92A-R	*Sa*	gtaatcctgcacgattaag	K92A
SaSAS2-R91A-K92A-F	*Sa*	cttaatgctgcaggattac	SAS2

SaSAS2-R91A-K92A-R	*Sa*	gtaatcctgcagcattaag	R91A/K92A
SaSAS2-K138A-F	*Sa*	caattgatagcacgtaaag	SAS2
SaSAS2-K138A-R	*Sa*	ctttacgtgctatcaattg	K138A
SaSAS2-Y142F-F	*Sa*	gtaaagattttattcag	SAS2
SaSAS2-Y142F-R	*Sa*	ctgaataaaatctttac	Y142F
SaSAS2-H155N-F	*Sa*	cagtttaaatatcgttg	SAS2
SaSAS2-H155N-R	*Sa*	caacgatatttaaactg	H155N
RelA-Nco-6H-F	*Bs*	ttaaccatgggccaccatcaccatcaccataacgaacaagtat	Rel
RelA-Xho-R	*Bs*	ttaactcgagttagttcatgacgcggcgcacag	
RelA-Nco-6H-F	*Bs*	ttaaccatgggccaccatcaccatcaccataacgaacaagtat	Rel-NTD
RelA-NT-XhoI-R	*Bs*	ttaactcgagttaatacaccatgtcagagaa	
SAS1-flk1-EcoRI-F	*Bs*	ttaagaattcccgccctgtaaatcttattt	SAS1 genomic integration
SAS1-flk1-R	*Bs*	tcccattgtttgtcatccatcatacatcccccaattccga	
SAS1-flk2-F	*Bs*	aaggaagcgagcaacaataggtaaaggggaagaagagca	
SAS1-flk2-NcoI-R	*Bs*	aattccatgggtgctgcctgatggagttga	
BsSAS2-EcoRI-F	*Bs*	ttaagaattcatggatttatctgtaacac	SAS2 genomic integration
BsSAS2+fla-NcoI-R	*Bs*	ttaaccatggaatccagccgtacggctgc	
BsSAS2-E154V-F	*Bs*	gtcaaagcagtaattc	SAS2 E154V
BsSAS2-E154V-R	*Bs*	gaattactgctttgac	
RelP_amyup_ApaI	*Bs*	ttaagggcccatggatgacaaacaatgg	SAS1 amyE
RelP_ClaI_R	*Bs*	ttaaatcgatttattgttgctcgcttcc	integration
RelA-KpnI-F	*Bs*	ttaaggtaccatggcgaacgaacaagtattgac	Rel-NTD amyE integration
RelA-NT-XhoI-R	*Bs*	ttaactcgagttaatacaccatgtcagagaa	
RelANT-HDmut-F	*Bs*	gatttttggccgctgtcgtggaagatac	Rel-NTD
RelANT-HDmut-R	*Bs*	gtatcttccacgacagcggccaaaaatc	H77A/D78A

'Org' denotes the originating microbial origins *B. subtilis* (*Bs*) or *S. aureus* (*Sa*).

Table S5. List of plasmids.

Vector	Insert	Organism	Affinity tag	Cloning sites
pET-24d(+)	SAS1	*B. subtilis*	N-His_6	NcoI/XhoI
pET-24d(+)	SAS1 R46G	*B. subtilis*	N-His_6	NcoI/XhoI
pET-24d(+)	SAS1 E139V	*B. subtilis*	N-His_6	NcoI/XhoI
pET-24d(+)	SAS1 K25A	*B. subtilis*	N-His_6	NcoI/XhoI
pET-24d(+)	SAS1 F42A	*B. subtilis*	N-His_6	NcoI/XhoI
pET-24d(+)	SAS1 N148G	*B. subtilis*	N-His_6	NcoI/XhoI
pET-24d(+)	SAS1 H111P	*B. subtilis*	N-His_6	NcoI/XhoI
pET-24d(+)	SAS2	*B. subtilis*	N-His_6	NcoI/XhoI
pET-24d(+)	SAS2	*S. aureus*	N-His_6	NcoI/XhoI
pET-24d(+)	SAS2 H73A	*S. aureus*	N-His_6	NcoI/XhoI
pET-24d(+)	SAS2 H74A	*S. aureus*	N-His_6	NcoI/XhoI
pET-24d(+)	SAS2 E76A	*S. aureus*	N-His_6	NcoI/XhoI
pET-24d(+)	SAS2 D183A	*S. aureus*	N-His_6	NcoI/XhoI
pET-24d(+)	SAS2 R91A	*S. aureus*	N-His_6	NcoI/XhoI
pET-24d(+)	SAS2 K92A	*S. aureus*	N-His_6	NcoI/XhoI
pET-24d(+)	SAS2 R91A/K92A	*S. aureus*	N-His_6	NcoI/XhoI
pET-24d(+)	SAS2 K138A	*S. aureus*	N-His_6	NcoI/XhoI
pET-24d(+)	SAS2 Y142A	*S. aureus*	N-His_6	NcoI/XhoI
pET-24d(+)	SAS2 H155N	*S. aureus*	N-His_6	NcoI/XhoI
pET-24d(+)	Rel	*B. subtilis*	N-His_6	NcoI/XhoI
pET-24d(+)	Rel-NTD (aa 1-395)	*B. subtilis*	N-His_6	NcoI/XhoI
pET-24d(+)	Rel-NTD (aa 1-395) H77A/D78A	*B. subtilis*	N-His_6	NcoI/XhoI
pMAD	SAS1 E139V	*B. subtilis*	-	EcoRI/NcoI
pMAD	SAS1 K25A/F42A	*B. subtilis*	-	EcoRI/NcoI
pMAD	SAS2 E154V	*B. subtilis*	-	EcoRI/NcoI
pSG1154	SAS1	*B. subtilis*	-	ApaI/ClaI
pSG1154	Rel-NTD (aa 1-395) H77A/D78A	*B. subtilis*	-	KpnI/XhoI

Table S6. List of *Bacillus subtilis* strains.

Strain	Description	Integrated plasmid	Reference
PY79	wild type	-	(212)
SAS1-E139V	*yjbM* substituted by *yjbM*^{E139V}	pMAD:SAS1 E139V	This work
SAS1-K25A/F42A	*yjbM* substituted by *yjbM*$^{K25A/F42A}$	pMAD:SAS1 K25A/F42A	This work
PY79 + SAS1	Integration of *yjbM* into the *amyE* locus of PY79	pSG1154:SAS1	This work
SAS1-E139V + SAS1	Integration of *yjbM* into the *amyE* locus of SAS1-E139V	pMAD:SAS1 E139V + pSG1154:SAS1	This work
SAS1-E139V + Rel-NTD H77A/D78A	Integration of a gene encoding for Rel-NTD H77A/D78A into the *amyE* locus of SAS1-E139V	pMAD:SAS1 E139V + pSG1154:Rel-NTD H77A/D78A	This work